UNIVERSITY OF SOUTHAMPTON

FACULTY OF MEDICINE, HEALTH AND LIFE SCIENCES

School of Medicine

The Intra-Articular Synovial Folds of the Lateral Atlanto-Axial Joints. An Anatomic and Magnetic Resonance Imaging Study

by

Alexandra Louise Webb

Thesis for the degree of Doctor of Philosophy

September 2007

UNIVERSITY OF SOUTHAMPTON

ABSTRACT
FACULTY OF MEDICINE, HEALTH AND LIFE SCIENCES
SCHOOL OF MEDICINE

Doctor of Philosophy

THE INTRA-ARTICULAR SYNOVIAL FOLDS OF THE LATERAL ATLANTO-AXIAL JOINTS. AN ANATOMIC AND MAGNETIC RESONANCE IMAGING STUDY

by Alexandra Louise Webb

This thesis reports on methods developed to identify and quantify the normal morphology of the intra-articular synovial folds of the lateral atlanto-axial joints to aid in the identification and quantification of injury to these structures in patients. A system of naming and classifying the synovial folds was developed to remove the ambiguity surrounding the various terminologies applied to these structures. A comprehensive critical review of the literature revealed that the potential role of the synovial folds in the generation of neck pain and disability is poorly understood, primarily because of the limited techniques available to identify the synovial folds and to quantify their dimensions. New anatomical methods to quantify objectively the morphology of the synovial folds *in vitro* were developed. The precision and accuracy of these methods were established through a series of validation experiments and a robust statistical analysis of the results. To address the current difficulty in visualising and quantifying the synovial folds *in vivo* new methods of magnetic resonance (MR) imaging were developed and validated for precision and accuracy through statistically viable experiments. This is the first study to develop an MR imaging protocol that enables the synovial folds of the lateral atlanto-axial joints to be visualised *in vivo*. The statistical approaches commonly used in similar research for the determination of measurement precision were critically reviewed and their strengths and limitations discussed. Using these newly developed anatomical and imaging methods, the normal morphology of the synovial folds of the lateral atlanto-axial joints was determined and the results are presented. Future developments and applications of this work, including applications to investigations of pain and disability affecting the cervical spine, are discussed.

Contents

ii

List of Tables

List of Figures

xvi

xix

ACKNOWLEDGEMENTS

Chapter 1

Introduction

1.1   Neck pain

Neck pain is common in the adult population with a reported lifetime prevalence of approximately 70% (Makela et al., 1991; Cote et al., 1998) and a point prevalence of 15 to 20% (Andersson et al., 1993; Cote et al., 1998). Neck pain is second only to low back pain as the most common musculoskeletal disorder in population surveys (Cassidy et al., 1998; Cote et al., 1998; Ferrari and Russell, 2003). Like low back pain, neck pain greatly affects a person's quality of life and is a financial burden to society due to substantial costs related to medical care and absenteeism from work (Borghouts et al., 1999; Suissa et al., 2001). In the Netherlands in 1996, the total cost of neck pain was estimated to be US$686 million with the total number of sick days related to neck pain estimated to be 1.4 million days, at a cost of US$185.4 million (Borghouts et al., 1999).

The International Association for the Study of Pain (IASP) lists some 60 causes of neck pain (Merskey and Bogduk, 1994). Pathologies, such as fractures, tumours and infections, largely diagnosed by medical imaging, are recognised causes of neck pain but are uncommon (Heller et al., 1983; McNamara et al., 1988; Bogduk, 2003). The determination of sources and causes of common, uncomplicated neck pain that is idiopathic in nature or the result of trauma (e.g. whiplash) is more of a diagnostic challenge (Bogduk, 1999; Bogduk, 2003). The intra-articular synovial folds of the lateral atlanto-axial joints are considered to be potential sources of such neck pain and numerous theories have been generated to explain their potential pathoanatomy and pathophysiology (Giles, 1986; Yu et al., 1987; Mercer and Bogduk, 1993; Inami et al., 2000).

1

1.2   The problem and the purpose

The ability objectively to describe the morphology of the synovial folds in an asymptomatic population would provide baseline data against which future investigations of pathological morphological changes in the synovial folds could be evaluated and their relationships to symptoms in patients with neck pain and disability discerned. The hypothesis of this study may therefore be stated as follows: It is possible to quantify the morphology of the synovial folds *in vitro* and *in vivo* with adequate precision and accuracy that allows changes to these synovial folds to be detected and quantified. The purpose of this project was therefore to develop the means of assessing the morphology of the synovial folds of the lateral atlanto-axial joints and to establish the normal morphometry of the synovial folds. This was thought to permit investigation of the synovial folds in selected patient groups that suffer from disorders of and injuries to the cervical spine.

1.3   Aims

In order to achieve the above purpose, a number of distinct aims were identified for this work:

1. To review the current knowledge of the synovial folds of the cervical spine

2. To develop a new unambiguous system for naming and classifying the synovial folds

3. To develop new methods of visualising the synovial folds and quantifying their morphology using an *in vitro* anatomic cadaver-based method and an *in vivo* magnetic resonance imaging method

4. To review, analyse and evaluate the statistical tests commonly used for the determination of measurement precision

5. To evaluate the precision and accuracy of the newly developed anatomic and magnetic resonance imaging methods

6. To describe and quantify the normal morphology of the synovial folds using the developed methods

Figure 1.1 illustrates the plan of the project.
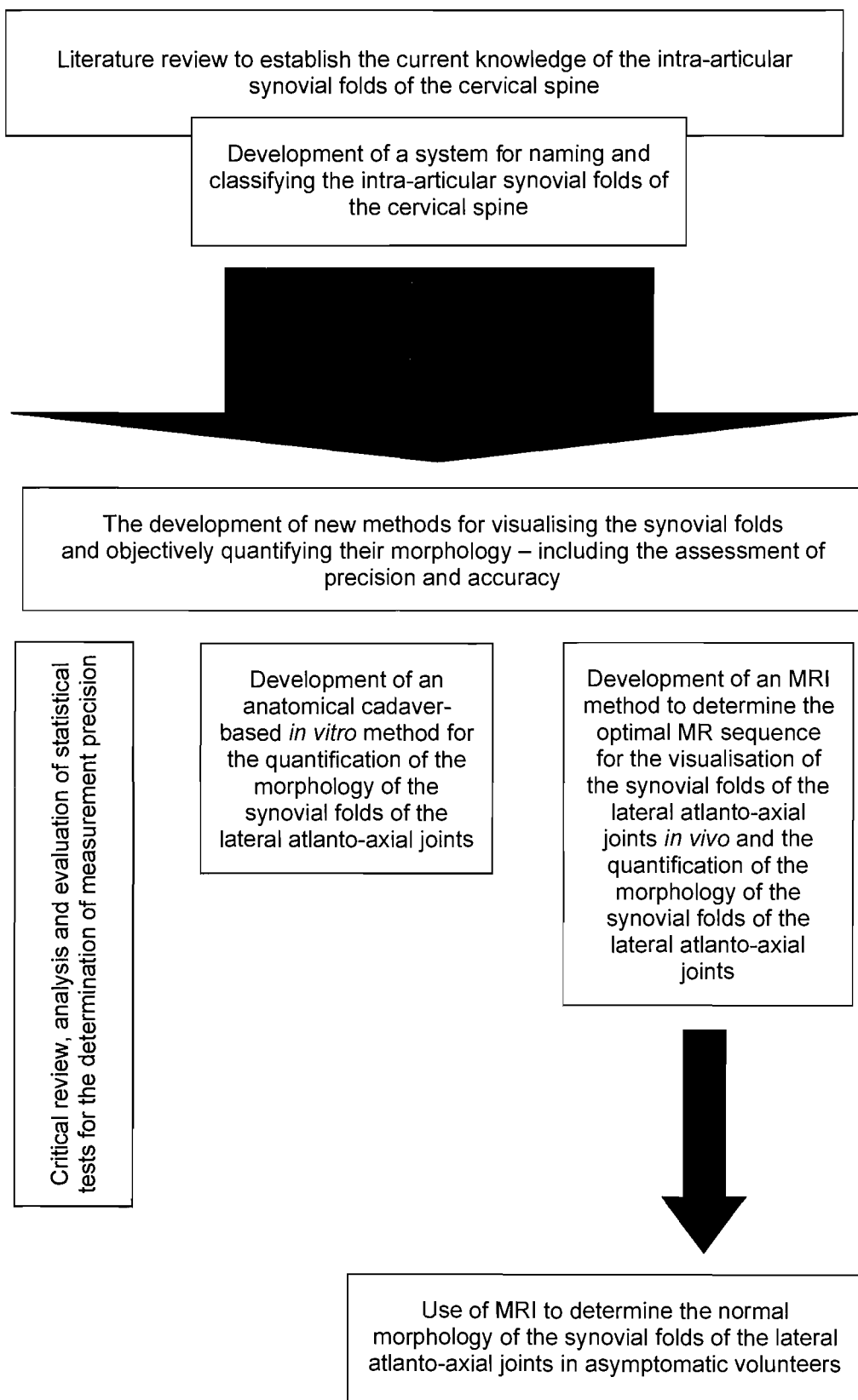
Figure 1.1. The plan and organisation of the present study designed to determine the normal morphology of the synovial folds of the lateral atlanto-axial joints as a basis for the investigation of their potential role in the production of neck pain and disability.

Chapter 2

Review of the literature

2.1 Introduction

The earliest description of intra-articular synovial folds in the vertebral column is attributed to Henle in 1855 (Dorr, 1958). European studies in the early 20th Century (Schmincke and Santo, 1932; Tondury, 1940; Zaccheo and Reale, 1956; Dorr, 1958; De Marchi, 1963) confirmed the presence of synovial folds in the atlanto-occipital, atlanto-axial and zygapophysial joints of the vertebral column in all age groups and documented the existence of synovial fold sub-types. These studies were predominantly based upon examination of the whole cadaver spine and provided limited information regarding the detailed morphology, disposition and prevalence of the synovial folds of the lateral atlanto-axial joints. Apart from two publications in the 1960s (Hadley, 1961; Lewin et al., 1962), it was not until the 1980s that the synovial folds received attention in the English language literature. 19 studies investigating the morphology and innervation of the synovial folds of the cervical spine have been published since 1932 (Table A1.1., Appendix 1), 15 of these have included the lateral atlanto-axial joints. 23 studies have documented the synovial folds of the lumbar spine. All published studies, with the exception of one conference abstract that described the synovial folds in the lumbar spine of the rat (Ginsburg et al., 2000), have been undertaken on the human vertebral column.

Of the 15 publications that have studied the synovial folds of the lateral atlanto-axial joints, few have published detailed descriptions of the morphology of the synovial folds. The most comprehensive descriptions of the gross appearance and histology of the lateral atlanto-axial synovial folds have been reported by Ibattulin et al. (1987), Yu et al. (1987), Chang et al. (1992), Mercer and Bogduk (1993), Schonstrom et al. (1993), Kos et al. (2002) and Tang et al. (2007). Despite the use of different anatomical techniques,

4

the results of these studies are generally in good agreement. One study has investigated the potential of imaging the lateral atlanto-axial synovial folds of cadavers using MRI (Yu et al., 1987) and two studies have examined the lateral atlanto-axial synovial folds of whiplash victims at postmortem (Schonstrom et al., 1993, Taylor and Taylor, 1996).

The aim of this literature review was critically to appraise previously published literature regarding the intra-articular synovial folds located within the lateral atlanto-axial articulations to:

1. devise a system for naming and classifying the synovial folds that can be applied to all regions of the vertebral column
2. establish the morphology of the synovial folds of the lateral atlanto-axial joints including their gross anatomy, histology, development and innervation
3. critically review the proposed functions of the synovial folds
4. critically review the proposed theories surrounding the clinical significance of the synovial folds in the generation of neck pain and disability with a particular focus on their potential role in whiplash injury
5. propose new methods for evaluating the synovial folds and investigating their clinical significance

Attention is naturally focused on investigations of the synovial folds of the lateral atlanto-axial joints but studies of the synovial folds of other spinal and peripheral articulations are considered where the information is thought to be of interest or information specific to the lateral atlanto-axial synovial folds is not available.

2.2 Naming and classification of the synovial folds

A diverse array of names has been assigned to the synovial folds of the vertebral column by different authors (Table 2.1). These names predominantly reflect the macroscopic appearance and/or histology of the synovial folds.

'*Synovialfalten*' (German translation: synovial fold) was the original name adopted by Henle in 1855 (Dorr, 1958; De Marchi, 1963) to describe these structures. Unfortunately, later workers used terms such as 'meniscus' or 'meniscoid'. The term meniscus (from μηνίκος [Greek]: a crescent; a diminutive of μήνη [Greek]: the moon (Skinner, 1961)) appears to have been adopted due to the macroscopic resemblance of the synovial folds to the crescent-shaped menisci of the knee joint. Despite the fact that

synovial folds are composed of synovium whilst menisci are formed of fibrocartilage that is not covered by synovial membrane (Standring, 2005). Use of the term 'meniscus' to describe the synovial folds thus is inaccurate and is likely to cause confusion with fibrocartilaginous articular discs/mensici found in the temporomandibular, sternoclavicular, acromioclavicular, radiocarpal and knee joints. It is recommended that its use be discontinued.

Table 2.1. Different terminology used for the synovial folds of the vertebral column.

Name	Study
Synovial folds	Tondury, 1940; Tondury, 1972; Giles, 1986; Giles and Taylor, 1987a; Giles and Harvey, 1987; Giles and Taylor, 1987b; Giles, 1988; Kawabe et al., 1989; Singer et al., 1990; Chang et al., 1992; Schonstrom et al., 1993; Taylor and Taylor, 1996; Erwin et al., 2000; Inami et al., 2000; Inami et al., 2001; Tang et al., 2007
Capsular folds ("Kapselfalten")	Fick, 1904
Synovial protrusions	Giles and Taylor, 1982
Synovial plicae	Konttinen et al., 1990; Gronblad et al., 1991
Meniscus/menisci	Schmincke and Santo, 1932; Zaccheo and Reale, 1956; Dorr, 1958; Hadley, 1961; Lewin et al., 1962; De Marchi, 1963; Engel and Bogduk, 1982; Yu et al., 1987; Bland and Boushey, 1990
Meniscoids	Kos, 1969; Emminger, 1972; Benini, 1979; Ibattulin et al., 1987; Jones et al., 1989; Kos et al., 2002 ; Friedrich et al., 2007
Fat pads/synovial fat pads/adipose tissue pads	Lewin et al., 1962; McFadden and Taylor, 1990; Taylor and McCormick, 1991
Intra-articular inclusions	Mercer and Bogduk, 1993

Meniscoid (from μηνίκος [Greek]: a crescent plus είδος [Greek]: like (Skinner, 1961)) refers to a crescent-like or crescent-shaped structure. The term was proposed by Kos and Wolf (1972) and broadly accepted by a number of authors. Although an improvement on meniscus, meniscoid is also likely to cause confusion due to its similarity to the term meniscus. 'Synovial fold' or 'synovial plica/plica synovialis' (from plicare [Latin]: to fold (Skinner, 1961) are the specified terms for these structures (Terminologia Anatomica, 1998) and make clear their morphology. Whilst the term synovial plica is typically used in the peripheral joint literature (Awaya et al., 2001, Deutsch et al., 1981, Garcia-Valtuille et al., 2002), synovial fold has been more frequently adopted in the vertebral column literature and accordingly is the designation of choice in this study. It is recommended that the term synovial fold be readily adopted to replace previously used names as the wide use of different names has led to some confusion and controversy in the literature. Interestingly the retention of some misleading and inappropriate terms still persists in recent literature.

A variety of different classification systems have been devised by researchers to describe different sub-types of synovial fold observed within spinal articulations (Table 2.2). These classification systems are predominantly based upon the histological composition of the synovial fold or a combination of the synovial fold histology, gross morphology and disposition.

Table 2.2. Classification systems used to describe sub-types of the synovial folds of the vertebral column.

Study	Spinal region	Name	Classification terms used	Basis of classification
Giles, 1986	Cervical	Synovial fold	Adipose synovial fold Fibro-adipose synovial fold	Histological composition
Zaccheo and Reale, 1956	Cervical Thoracic Lumbar	Menisci	Synovio-adipose foliform meniscus Linguiform fibrous meniscus Annular fibrocartilaginous meniscus	Gross morphology, histological composition & disposition
Engel and Bogduk, 1982	Lumbar	Menisci	Adipose tissue pad Fibro-adipose meniscoid Connective tissue rim	Histological composition & disposition
Yu et al., 1987	Cervical	Menisci	Types 1, 2, 3 & 4	Gross morphology
Mercer and Bogduk, 1993	Cervical	Intra-articular inclusions	Adipose tissue pad Fibro-adipose meniscoid Connective tissue rim	Gross morphology & histological composition
Inami et al., 2000	Cervical	Synovial fold	Types 1, 2, & 3	Gross morphology & histological composition
Kos et al., 2002	Cervical Thoracic Lumbar	Meniscoid	Synovial meniscoid Fibrous meniscoid Fat pad	Gross morphology & histological composition
Friedrich et al., 2007	Cervical	Meniscoid	Types 1, 2, & 3	Based on Inami et al. (2000)
Tang et al., 2007	Upper cervical	Synovial fold	Types 1, 2, & 3	Histological composition Based on Inami et al. (2000)

A classification system based upon the anatomic site of the synovial fold within the articulation, similar to that used for the synovial plicae/folds of the knee joint and elbow joint (Kim and Choe, 1997; Kosarek and Helms, 1999; Awaya et al., 2001; Isogai et al., 2001; Garcia-Valtuille et al., 2002), would be a simpler method for classifying synovial folds. The synovial folds of the lateral atlanto-axial joints would thus be described as the ventral, ventrolateral, dorsal or dorsomedial synovial folds. This could be simplified to the ventral and dorsal synovial folds. Ventral and dorsal being the most appropriate terms to use, rather than anterior and posterior, to prevent disorientation between animal, embryo and human studies (Collins, 1999). A similar system of classification could be easily applied to the synovial folds of other vertebral regions. The system of naming and classifying the synovial folds proposed in the present study would reduce

7

the confusion surrounding the morphology of these structures and promote comparisons between studies and between different regions of the spine.

2.3   Morphology of the synovial folds

The intra-articular synovial folds are formed by folds of the synovial membrane (synovium) (Figure 2.1).
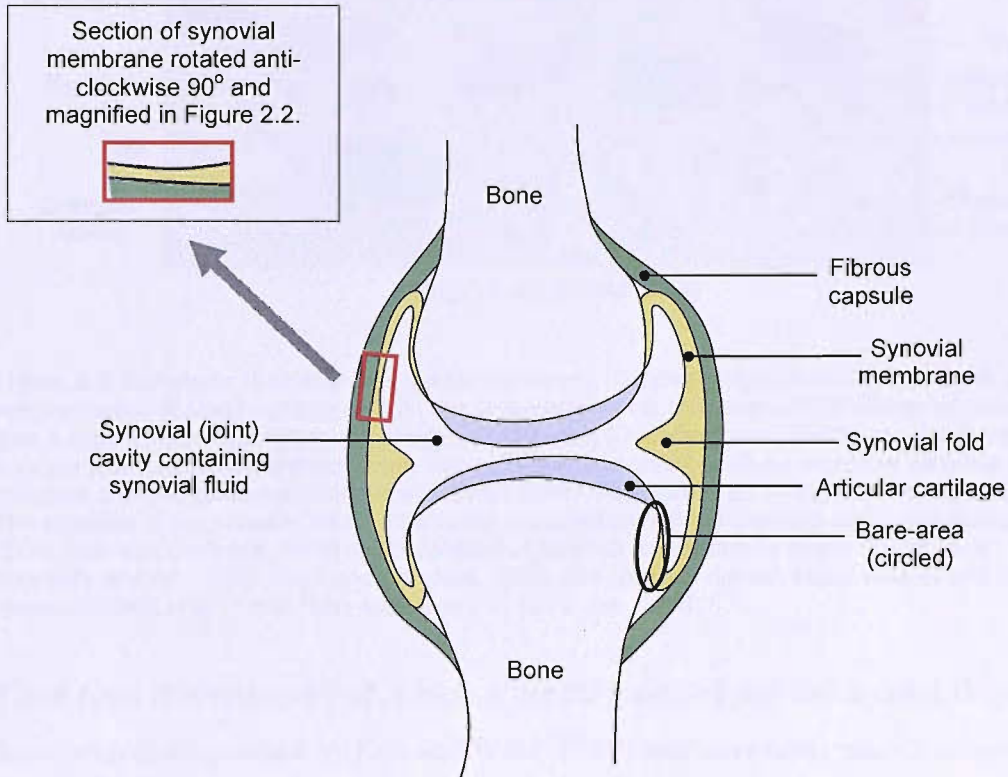
Figure 2.1. Coronal section of a synovial joint. At synovial joints, the surfaces of articulating bones are covered by hyaline articular cartilage. Synovial membrane lines the inner surface of the fibrous capsule and a small region of bone between the cartilage and fibrous capsule insertion, referred to as the 'bare-area' (Barnett et al., 1961; Sommer et al., 2005).

Synovial membrane consists of two layers, the synovial intimal (lining) layer and the subintimal (subsynovial) layer (Paget and Bullough, 1980; Giles et al., 1986; Giles, 1989) (Figure 2.2). Synovial folds consist of a central core of subintimal tissue covered by upper and lower layers of synovial intima (Giles et al., 1986). Following the classification of Key (1928) it has been customary to name the type of synovium according to the nature of the subintimal tissue (Hasselbacher, 1981). In the adipose-type of synovial membrane the subintimal tissue consists of adipocytes interspersed with collagen fibres covered by two to three layers of type A and B synoviocytes (Ham and Cormack, 1979; Jee, 1988; Burkitt et al., 1993). The fibrous-type of synovium is less vascular than the adipose-type and characterised by abundant bundles of collagen fibres covered by a single layer of widely spaced type A and B synoviocytes (Davies

and Edwards, 1948; Ham and Cormack, 1979; Jee, 1988). The subsynovial tissue also contains a network of fine elastic fibres (Davies, 1946; Ghadially and Roy, 1969).

SYNOVIAL JOINT CAVITY CONTAINING SYNOVIAL FLUID

FIBROUS JOINT CAPSULE
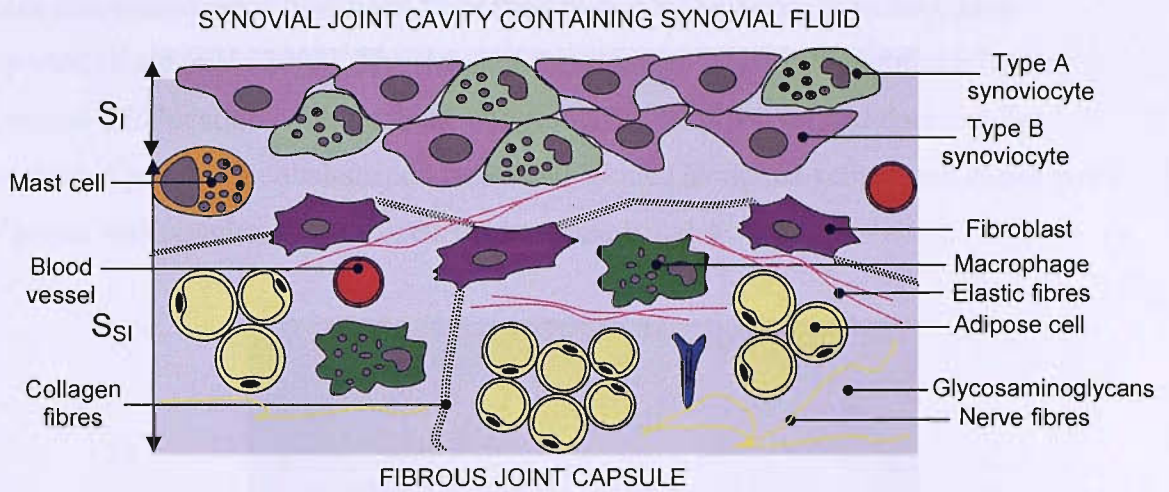
Figure 2.2. Schematic illustration of synovial membrane. Synovial membrane consists of two layers, the synovial intima (S_I) and subintima (S_{SI}). The synovial intima is characterised by a layer of macrophage-like type A synoviocytes that function in phagocytic activities (Cochrane et al., 1965) and fibroblast-like type B synoviocytes that have a predominantly secretory role and possibly act as receptors sensitive to local chemical and/or mechanical changes in the joint cavity (Kitamura et al., 1999; Vandenabeele et al., 2001). The structure of the synovial intima reflects the composition of the underlying subintimal tissue (Davies, 1950; Ham and Cormack, 1979) which consists of adipose and/or fibrous tissue (Burkitt et al., 1993; Ghadially and Roy, 1969; Ham and Cormack, 1979) and contains nerves, blood vessels and lymphatic vessels (Burkitt et al., 1993; Ham and Cormack, 1979; Jee, 1988).

Three parts of a synovial fold, a base, a central (middle) part and an apex (Figure 2.3), have been distinguished by Kos and Wolf (1969) and have been readily adopted in the literature. The thick peripheral base extends from the fibrous capsule and tapers to form a thin apex that projects between the articular surfaces (Engel and Bogduk, 1982; Mercer and Bogduk, 1993). This terminology is useful for describing individual synovial folds and will be used throughout the present study.
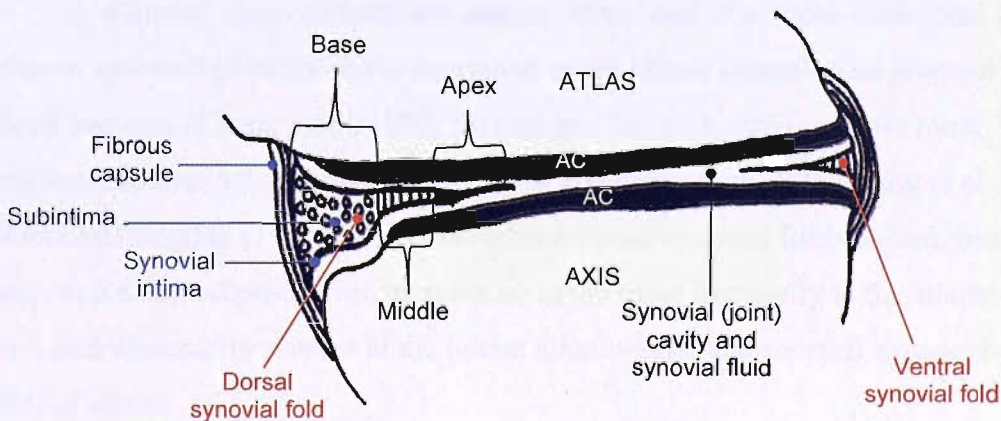
Figure 2.3. Sagittal section of a right lateral atlanto-axial joint (lateral view): schematic illustration of a synovial fold. AC – hyaline articular cartilage.

At the lateral atlanto-axial joints (Figure 2.4), the synovial folds extend between the articular surfaces for distances ranging from 1-5mm (Chang et al., 1992; Mercer and Bogduk, 1993), covering up to 50% of the articular surface (Yu et al., 1987). Synovial folds that extend more than 5mm from their base into the joint cavity have been reported (Tang et al., 2007). The shape of the articular facets is thought to influence synovial fold location, with folds located along the ventrolateral and dorsomedial margins of joints with oval-shaped facets and located along the ventral and dorsal poles of joints with circular-shaped facets (Mercer and Bogduk, 1993).
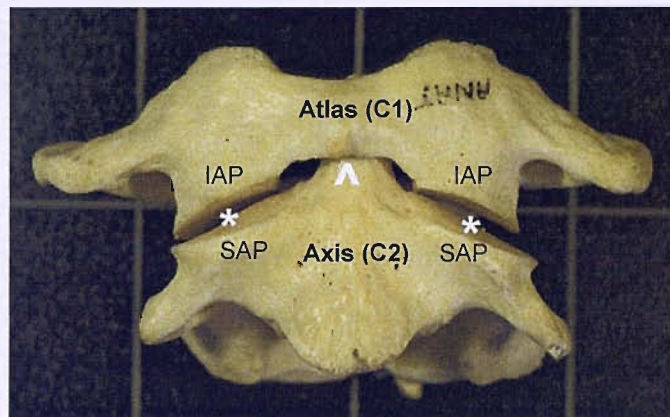
Figure 2.4. Anterior view of the atlas and axis vertebrae. The paired lateral atlanto-axial joints (*) are formed by the facets on the inferior articular processes (IAP) of the atlas (1st cervical vertebra, C1) and superior articular processes (SAP) of the axis (2nd cervical vertebra, C2). The median atlanto-axial joint (^) is formed by the anterior arch of the atlas, the dens of the axis and the transverse ligament. Adapted from Taylor (2001), with permission.

On analysis of the literature it is evident that, based on the histology of the synovial folds, there are three different possible tissue arrangements. In this study they will be referred to as adipose, fibro-adipose and fibrous synovial folds and can be summarised as follows:

a. Adipose synovial folds are entirely composed of adipose subintimal tissue. Adipose synovial folds are rarely described in the lateral atlanto-axial joints of adult and elderly subjects (Chang et al., 1992; Mercer and Bogduk, 1993) and are more commonly found in the joints of children (Schonstrom et al., 1993; Tang et al., 2007). Mercer and Bogduk (1993), who referred to adipose synovial folds as 'adipose tissue pads', noted that adipose synovial folds occurred most frequently at the atlanto-occipital joints and were rarely present at the lateral atlanto-axial and cervical zygapophysial joints of adults.

b. Fibro-adipose synovial folds consist of a base composed of adipose tissue, covered by adipose-type synovial intima, and an apex of fibrous subintimal tissue covered by fibrous-type synovial intima. The middle part may consist of adipose tissue or fibrous tissue or a combination of the two. This is the most common type of synovial fold reported to be found in adult lateral atlanto-axial joints (Mercer and Bogduk, 1993; Schonstrom et al., 1993; Yu et al., 1987). The histological composition of the 'typical synovial folds' and 'synovial meniscoids' reported by Chang et al. (1992) and Kos et al. (2002), respectively, were not clearly described but appear to correspond to the fibro-adipose synovial folds defined in the current literature review. Ibattulin et al. (1987) and Tang et al. (2007) also described synovial folds composed of variable quantities of fibrous and adipose tissue.

c. Fibrous synovial folds, entirely composed of fibrous tissue and covered by fibrous-type synovial intima, have not been frequently described at the lateral atlanto-axial joints. Mercer and Bogduk (1993) determined the prevalence of adipose and fibro-adipose synovial folds at all cervical articulations but did not distinguish between fibrous and fibro-adipose synovial folds. In a study of the cervical zygapophysial joints, Inami et al. (2000) documented the prevalence of adipose, fibro-adipose and fibrous synovial folds and found that fibro-adipose and fibrous synovial folds were equally common. Tang et al. (2007) reported a greater number of fibrous synovial folds in the upper cervical articulations of adults compared to children but did not distinguish between atlanto-occipital and atlanto-axial joints. Further investigations are required to determine the prevalence of fibrous synovial folds at the lateral atlanto-axial joints.

The synovial folds of the lateral atlanto-axial joints contain an abundant vascular network (Ibatullin et al., 1987; Chang et al., 1992; Mercer and Bogduk, 1993; Schonstrom et al., 1993). Blood vessels are reported to be more plentiful in dorsal compared to ventral synovial folds (Schonstrom et al., 1993) and in adipose compared to fibrous synovial folds (Kos et al., 2002; Tang et al., 2007). The subintimal tissue of lumbosacral synovial folds has a high elastic fibre content and it has been suggested that this may be important in preventing the synovial folds from becoming impinged between the articular surfaces during normal joint motion (Giles, 1988). To date, no studies have documented the presence of elastic fibres within the synovial folds of the cervical spine.

2.3.1 Development and ageing of the synovial folds

Various explanations have been proposed in the literature to account for the three different histological types of synovial fold observed within adult spinal articulations. These are based upon the development of the synovial fold, its exposure to mechanical forces during life and the effects of increasing age/articular degeneration.

The development of the synovial folds of the vertebral column has not been comprehensively studied. Engel and Bogduk (1982) proposed that the different histological types of synovial fold described in the literature are variants of a single embryonic precursor. This is supported by the presence of one mesenchymal intra-articular (interzonal) plate between the primitive chondral articular processes of embryonic spinal articulations (Engel and Bogduk, 1982). Engel and Bogduk (1982) studied a small number of embryonic lumbar zygapophysial joints and noted that the central portion of the intra-articular plate disappeared as development progressed leaving a circumferential lip of mesenchyme projecting from the internal aspect of the future adult fibrous capsule (Engel and Bogduk, 1982). The mesenchyme then appeared to regress to varying extents leaving peripheral wedges of tissue in positions analogous to the location of adult synovial folds (Engel and Bogduk, 1982). These observations are supported by early European studies of embryonic, fetal and newborn vertebral columns (Tondury, 1940; Lewin et al., 1962; De Marchi, 1963; Kos, 1969) and studies of embryonic and fetal knee and elbow joints (Ogata and Uhthoff, 1990; Dupont, 1997; Issogai et al., 2001; Duparc et al., 2002). The variable extent of mesenchymal regression ensures that each individual joint gets mesenchyme left behind in positions appropriate for each joint and is thought to explain the inconsistent presence, size and shape of the synovial folds observed in adult articulations. The extent of mesenchymal regression may be related to motion of the fetal joints *in utero* (Dupont, 1997).

Tondury (1940) proposed that the adipose synovial folds observed in adults were degenerative forms of initially fibrous structures, however, the presence of predominantly adipose synovial folds in neonatal, infant and child spinal articulations has negated this view (Lewin et al., 1962; Tang et al., 2007). It is most likely that the mesenchyme of the intra-articular plate differentiates into adipose tissue that, depending on the synovial fold size and location, may differentiate into fibrous tissue to varying extents as a result of repeated mechanical stress (Engel and Bogduk, 1982; Giles and Taylor, 1982; Inami et al., 2000). This hypothesis is supported by studies comparing the

12

synovial folds of children and adults. In children aged 2 to 11 years, Tang et al. (2007) found that the majority of synovial folds were adipose or fibro-adipose types whilst in adults, aged 42 to 80 years, most were fibro-adipose or fibrous. Thus it appears that with increasing age, synovial folds differentiate from originally adipose structures into increasingly fibrous structures. The adipose synovial folds found in young subjects have been observed to be more flexible and less stiff than the fibro-adipose and fibrous synovial folds of older subjects (Schonstrom et al., 1993).

No clear association between synovial fold size and age is evident from the literature. Yu et al. (1987) and Inami et al. (2000) have proposed that the synovial folds undergo regressive changes with increasing age whilst Kos et al. (2002) and Taylor and Twomey (1986) have suggested that the synovial folds become larger and "more complicated" with increasing age and articular degeneration. In a recent study, Tang et al. (2007) observed a greater number of large synovial folds in the lateral atlanto-axial joints of children compared to adults. To date there have been no objective studies of the relationship between synovial fold dimensions and age. Furthermore, differences in synovial fold morphology due to gender, physical dimensions, range of motion or activity levels in life have not been explored.

Repeated mechanical impingement between the articular surfaces and/or inflammatory reactions over time are thought to cause the originally adipose synovial folds to undergo varying degrees of fibrous change with increasing age (Engel and Bogduk, 1982; Giles and Taylor, 1982; Inami et al., 2000). The retention of the adipose type of synovial fold in adult atlanto-occipital joints, in which the synovial folds do not project between the cartilage surfaces and are unlikely to be exposed to mechanical stresses, supports this (Mercer and Bogduk, 1993). In comparison, the fibro-adipose synovial folds of the zygapophysial joints project further into the joint cavity (Engel and Bogduk, 1982) and are located along the principal line of joint motion (Engel and Bogduk, 1982; Inami et al., 2000). Inami et al. (2000) reported that, in the cervical zygapophysial joints, adipose synovial folds were predominantly located at the ventral aspect of the joint and fibrous synovial folds at the dorsal aspect, which invites speculation regarding the mechanical stress distribution in these articulations. A comparison between the ventral and dorsal synovial fold morphology of the lateral atlanto-axial joints has not previously been conducted.

Mechanical loading is of pivotal importance to the development, function and repair of all tissues in the musculoskeletal system and regulates fundamental processes such as cell division and differentiation and the determination of tissue form in a process referred to as 'mechanical morphogenesis' (Benjamin and Hillen, 2003). The physiologic adaptation of soft connective tissues, such as ligaments and synovial folds, to a specific mechanical environment is thought to be reflected in their molecular composition (Milz et al., 2001). Tendons and ligaments subject to compression forces adapt to the mechanical stimulus by forming fibrocartilage (Vogel, 1996; Benjamin and Ralphs, 1998; Benjamin and McGonagle, 2001). It is thought that the extent of metaplasia of fibroblasts to fibrocartilage cells is dependent upon the degree of mechanical stimulation which suggests that tendons and ligaments are capable of detecting changes in mechanical load and responding appropriately (Benjamin and McGonagle, 2001). A similar process of mechanical morphogenesis as a result of mechanical impingement and compression forces may explain the differentiation from adipose to fibrous tissue in the synovial folds and may also account for the presence of fibrocartilage and signs of calcification observed in some synovial folds (Chang et al., 1992; Jones et al., 1989; Kos, 1969; Yu et al., 1987). Another explanation for the presence of cartilage within the synovial folds is the presence of progenitor cell populations in the synovial membrane that have the potential to differentiate into cartilage. Mesenchymal stem cells derived from both fibrous and adipose-synovium have demonstrated a greater potential for proliferation and chondrogenesis than stem cells derived from bone marrow, periosteum, muscle and subcutaneous adipose tissue (Mochizuki et al., 2006).

The replacement of adipose tissue with fibrous tissue may be the consequence of a prior inflammatory reaction that could be related to tissue damage caused by mechanical compression or impingement. Collagen-producing, activated fibroblasts, not typically present in normal resting connective tissue, have been observed within lumbar synovial folds and it has been suggested that this may indicate evidence of previous inflammation and repair (Konttinen et al., 1990). In the knee joint, symptomatic synovial folds (plicae) are thickened and fibrotic (Garcia-Valtuille et al., 2002). This is thought to result from trauma or repetition/overuse that causes inflammation of the synovial plica (Biedert et al., 2002) followed by fibrous repair or chronic inflammation (Bogdan 1985; Garcia-Valtuille et al., 2002).

2.3.2 Innervation of the synovial folds

"For a structure to be a potential source of pain, it must be innervated" (Bogduk, 2003). The innervated tissues of the cervical spine that theoretically have the potential to cause neck pain include the atlanto-occipital and lateral atlanto-axial joints, innervated by the C1 and C2 ventral rami respectively, and the cervical zygapophysial joints supplied by the cervical dorsal rami (Table 2.3) (Lazorthes and Gaubert, 1956; Bogduk, 1982; Bogduk et al., 1985). Within the synovial articulations of the cervical spine, the innervated tissues with the potential to produce pain include the fibrous capsule, synovial membrane, synovial folds and bone (Beaman et al., 1993; McLain, 1994; Inami et al., 2001; Ohtori et al., 2001; Kallakuri et al., 2004).

Table 2.3. Possible sources of neck pain and referred pain to the head and shoulder, listed according to innervation.

C1-C3 ventral rami	C1-C3 sinuvertebral nerves	C1-C3 dorsal rami
Atlanto-occipital joint	Median atlanto-axial joint	C2/C3 & C3/C4 zygapophysial joints
Lateral atlanto-axial joint	Transverse ligament	
Longus capitis	Alar ligaments	Suboccipital muscles
Longus cervicis	Dura mater of the spinal cord	Semispinalis capitis
Rectus capitis anterior	C2/C3 intervertebral disc	Semispinalis cervicis
Rectus capitis lateralis	Posterior longitudinal ligament	Multifidus
Trapezius		Longissimus capitis
Sternocleidomastoid		Splenius capitis
Dura mater of posterior fossa		
Vertebral artery		
C4-C8 ventral rami	**C4-C8 sinuvertebral nerves**	**C4-C8 dorsal rami**
Longus capitis	Dura mater of the spinal cord	Zygapophysial joints
Longus cervicis	Intervertebral disc	Semispinalis capitis
Trapezius	Posterior longitudinal ligament	Semispinalis cervicis
Sternocleidomastoid		Multifidus
Dura mater of posterior fossa		Longissimus capitis
Vertebral artery		Splenius capitis
		Splenius cervicis

Early research identified nerve fibres and endings in the posterolateral fibrous capsule but not the synovium or synovial folds of spinal articulations (Wyke, 1979; Wyke, 1981). More recently, impregnation techniques, transmission electron microscopy and immunohistochemistry have demonstrated the presence of nerve fibres and endings within the synovial membrane (Mapp, 1995) and synovial folds of human zygapophysial joints (Giles and Harvey, 1987; Giles and Taylor, 1987a; Giles and Taylor, 1987b; Giles, 1988; Gronblad et al., 1991; Inami et al., 2001).

Giles and Taylor (1987a; 1987b) were the first to demonstrate the presence of nerve fibres in the synovial intima and subintimal tissue of lumbar synovial folds. Using silver

and gold chloride impregnation techniques they discovered nerve fibres (0.2-12.0μm in diameter) located both alongside blood vessels (paravascular) and independent of blood vessels. Based on nerve fibre diameter (Guyton, 2006), these nerve fibres could include myelinated afferent proprioceptive fibres (Aβ or II fibres, 5-12μm diameter), myelinated afferent pain fibres (Aδ or III fibres, 1-5μm diameter), and unmyelinated afferent pain fibres or unmyelinated sympathetic postganglionic fibres (C or IV fibres, <2μm in diameter). The small nerve fibres independent of blood vessels are possibly nociceptive and those located alongside blood vessels probably have a vasomotor function. The presence of medium-sized myelinated proprioceptive fibres within the synovial fold is explained by the existence of mechanoreceptors at the junction between the fibrous capsule and subsynovial tissue in zygapophysial joints (Giles and Taylor, 1987b; McLain, 1994; McLain and Pickar, 1998).

More recently, heavy metal impregnation methods have been replaced by immunohistochemical techniques. Immunoreactivity to PGP 9.5, a general neuronal marker, has confirmed the existence of numerous nerve fibres (measuring ≤5μm and ≤1.5μm in diameter), located both close to and distant from blood vessels, within the synovial folds of cervical and lumbar zygapophysial joints (Gronblad et al., 1991; Inami et al., 2001). Substance-P (SP)-like and calcitonin gene-related protein (CGRP)-like immunoreactivity has been demonstrated in cervical, thoracic and lumbar synovial folds, however, there is disagreement as to whether these nerve fibres are paravascular or independent of blood vessels or both, which has led to some controversy regarding their potential function (Gronblad et al., 1991; Inami et al., 2001; Erwin et al., 2000; Giles and Harvey, 1987). SP and CGRP are neurotransmitters of nociceptive sensation thus the presence of SP-like and CGRP-like immunoreactivity provides further support to the suggestion that the synovial folds are potential sources of pain. SP and CGRP also have roles in plasma extravasation and vasodilation and thus may also contribute to neurogenic inflammation, vasoregulation and tissue repair (Erwin et al., 2000).

The atlanto-occipital, atlanto-axial and zygapophysial joints, intervertebral discs and suboccipital muscles have been subjected to formal experimental studies to verify their role in the generation of neck pain (Cyriax, 1938; Cloward, 1959; Aprill et al., 1990; Dwyer et al., 1990; Dreyfuss et al., 1994; Grubb and Kelly, 2000; Aprill et al., 2002). Many other tissues theoretically proposed as potential pain sources (Table 2.3) based on their innervation alone have not. Noxious stimulation, using intra-articular injections, of

the articulations of the cervical spine in normal volunteers has been shown to produce local neck pain in addition to pain referred to the head, shoulder girdle and upper limb (Figure 2.5.A) (Busch and Wilson, 1989; Dwyer et al., 1990; Dreyfuss et al., 1994). The lateral atlanto-axial joints can refer pain to the head producing what is referred to as a 'cervicogenic headache', i.e. "pain perceived as arising in the head but whose actual source lies not in the head but in the cervical spine" (Bogduk, 1992; Dreyfuss et al., 1994). The neuroanatomical basis for cervicogenic headache is illustrated in Figure 2.5.B. Any cervical spine structure innervated by the 1st, 2nd and 3rd cervical spinal nerves has the potential to cause cervicogenic headache (Table 2.3).
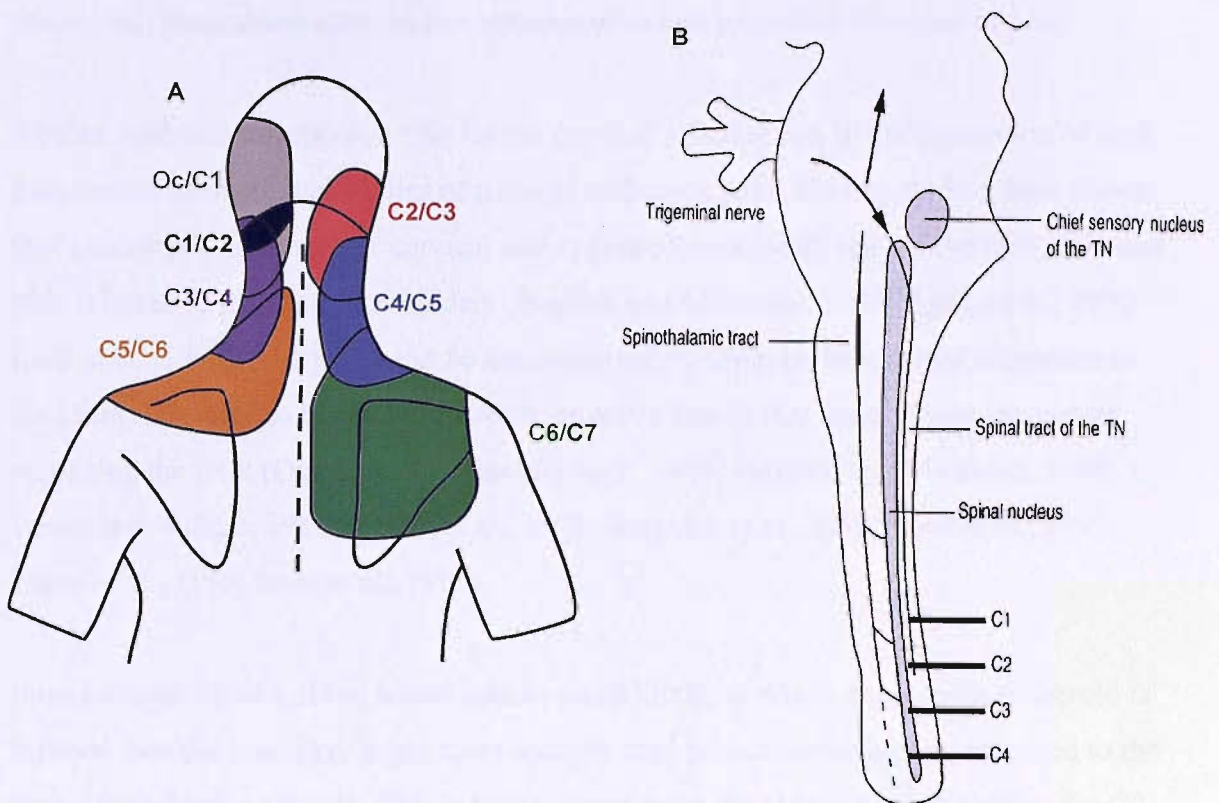
Figure 2.5.A. Posterior view of the head, neck and thorax. Referred pain patterns from the atlanto-occipital (Oc/C1), lateral atlanto-axial (C1/C2) and cervical zygapophysial joints (C2/C3 to C6/C7). Based on data from Dwyer et al. (1990) and Dreyfuss et al. (1994). **B.** The neuroanatomical basis for cervicogenic headache is the convergence of trigeminal and C1-C3 cervical afferents (from the head and cervical spine) on the trigeminocervical nucleus in the dorsal grey column of the C1-C3 segments of the spinal cord (Escolar, 1948; Kerr, 1961; Bogduk, 1992). Cervicogenic headache arises when structures supplied by the C1-C3 cervical afferents are injured (e.g. following trauma such as whiplash) and the axons supplying these structures converge upon axons innervating the occipital region in the trigeminocervical nucleus (Bogduk, 1992; Bogduk, 2001). The nociceptive information is relayed to the brain and is interpreted as arising from the head rather than the cervical spine thus resulting in the production of referred pain to the head (i.e. headache) (Bogduk, 1992; Bogduk, 2001). From Jull and Niere (2004), with permission.

It is not known whether the pain generating event following noxious stimulation of a joint is mechanical as a result of distension of the fibrous capsule or chemical due to synovial irritation from the injected stimulant. Dreyfuss et al. (1994) injected into the lateral atlanto-axial joints a contrast medium thought to be less noxious than hypertonic saline (Mooney and Robertson, 1976; McCall et al., 1979). Pain was not elicited until

distension of the fibrous capsule was perceived by the injectionist (Dwyer et al., 1990; Dreyfuss et al., 1994; Bogduk, 2001) which would suggest the ensuing pain was the result of mechanical stimulation of the fibrous capsule. Presumably distension of the fibrous capsule would be accompanied by distension of the synovial membrane and its associated synovial folds thus the resulting pain could be from mechanical stimulation of both the fibrous capsule and its related synovial structures. It is not known whether the contrast agent used by Dreyfuss et al. (1994) had the potential to irritate the synovial membrane and folds chemically or whether the passage of the needle through the fibrous capsule, synovial fold and synovial membrane to enter the joint cavity may have caused mechanical irritation and/or inflammation and provoked the onset of pain.

Further evidence to support a role for the cervical articulations in the generation of neck pain comes from clinical studies of patients with neck pain. Several studies have shown that anaesthetising the upper cervical and zygapophysial joints can relieve neck pain and pain referred to the head or shoulders (Bogduk and Marsland, 1988; Aprill et al., 1990; Lord et al., 1996). The joints can be anaesthetised by articular blocks that anaesthetise the joint(s) thought to be the pain source, or nerve blocks that anaesthetise the nerves supplying the joint (Okada, 1981; Sjaastad et al., 1986; Bogduk and Marsland, 1988; Busch and Wilson, 1989; Bovim et al., 1992; Barnsley et al., 1995; Lord et al., 1995; Fukui et al., 1996; Lord et al., 1996).

Intra-articular blocks of the lateral atlanto-axial joints, in which anaesthetic or steroid is injected into the joint cavity, are more specific than peri-articular blocks delivered to the back of the fibrous capsule. This is because peri-articular blocks may also affect the C2 spinal nerve that crosses the posterior aspect of the joint or other surrounding structures (Mooney and Robertson, 1976; McCall et al., 1979; Dreyfuss et al., 1994). Intra-articular blocks will selectively anaesthetise the intended joint provided that the injectate does not escape from within the fibrous capsule (Dreyfuss et al., 1994). Intra-articular blocks are typically delivered to the posterior or lateral aspect of the joint and usually pass through the synovial folds, sometimes drawing blood from the fold upon aspiration prior to injection (Aprill et al., 2002). Based on the anatomy of the lateral atlanto-axial joints, intra-articular structures that may be anaesthetised by an intra-articular block include the synovial membrane and folds. This adds further support to the suggestion that the synovial folds are pain-producing structures. There is some debate regarding whether nerve blocks are as specific as intra-articular blocks because

nerve blocks do not identify the actual source of pain and only indicate that the pain is mediated by the anaesthetised nerve. Because the synovial folds are innervated by the same nerves supplying the joint, a nerve block presumably anaesthetises the synovial folds.

There is thus considerable evidence to suggest that synovial folds may be a source of pain originating from the spinal articulations, in particular the lateral atlanto-axial joints, that results in the production of neck pain and headache. However, the exact mechanisms of pain generation from the synovial folds are currently not clear. Research into the normal morphology of the synovial folds is needed in order to understand the pathoanatomy and mechanisms of pain generation of the synovial folds.

2.3.3 Extracapsular communications of the synovial folds

Tondury (1940) observed that the synovial folds of the lumbar zygapophysial joints communicate with an extracapsular recess located outside the fibrous capsule (Figure 2.6). A number of authors since have described the presence of a foramen in the inferomedial fibrous capsule that enables adipose tissue in the extracapsular recess to become continuous with the intracapsular synovial fold in the lumbar spine (Engel and Bogduk, 1982; Giles, 1989; Lewin et al., 1962; Taylor and McCormick, 1991). Kos (2002) has disputed the existence of such a communication and claimed that the fibrous capsule completely encloses the synovial folds of all spinal regions.

During passive flexion and extension movements of non-fixed postmortem lumbar spines, the adipose tissue of the extracapsular recess has been observed to move freely in and out of the zygapophysial joint cavity through the hole in the inferomedial fibrous capsule (McFadden and Taylor, 1990). This occurs when the articular processes encroach upon the synovial folds as the joint moves (McFadden and Taylor, 1990). During arthrography of the lumbar zygapophysial joints, the leakage of contrast medium outside the joint cavity may be explained by the presence of this hole in the fibrous capsule, although, this could also be explained by rupture of the fibrous capsule caused by injecting too much contrast medium (Dory, 1981; Giles, 1984; McCormick et al., 1989).
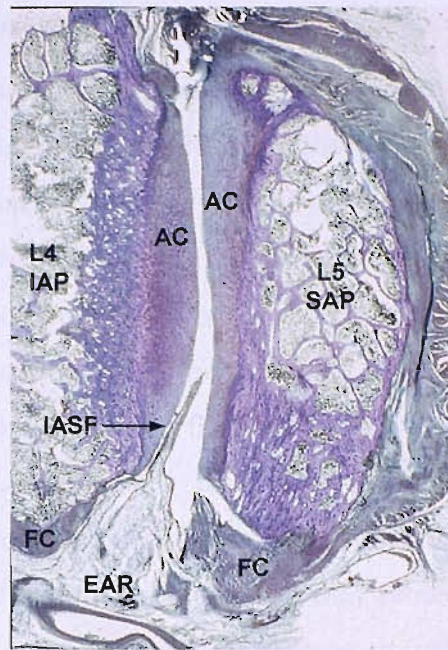
Figure 2.6. Sagittal section of a L4/L5 zygapophysial joint formed by the hyaline articular cartilage (AC) covering the facets of the L4 inferior articular process (IAP) and L5 superior articular process (SAP). The adipose tissue of the intra-articular synovial fold (IASF) communicates with the adipose tissue in the extracapsular articular recess (EAR) via an opening in the fibrous capsule (FC). Adapted from Taylor (2001), with permission.

It is not clear whether the synovial folds of the lateral atlanto-axial joints possess extracapsular communications similar to those observed in the lumbar spine. The few observations that have been made to date are contradictory. Contrast medium has been observed to pass from the lateral atlanto-axial joint cavity to the median atlanto-axial, contralateral lateral atlanto-axial and homolateral atlanto-occipital joints in patients and cadavers during arthrography (Dirheimer et al., 1977; Mellstrom et al., 1980; Chevrot et al., 1995; Aprill et al., 2002). In contrast, studies of postmortem whiplash victims suggest that, if undamaged, the lateral atlanto-axial fibrous capsule forms an uninterrupted boundary around each joint since extracapsular haematoma without bruising of the synovial folds has been observed, and vice versa (Schonstrom et al., 1993). Ibatullin et al. (1987) did not describe holes in the fibrous capsule of the lateral atlanto-axial joints but observed synovial folds of the lateral atlanto-axial joints that extended into the median atlanto-axial joints. Further studies documenting the existence and frequency of extracapsular communications at the lateral atlanto-axial joints are required since their presence, or absence, may affect the behaviour of the synovial folds during normal physiological loading and trauma.

2.4 Function of the synovial folds

A variety of functions have been attributed to the intra-articular synovial folds based upon extrapolations made from their gross morphology, disposition and histological composition. The synovial folds are believed to adapt themselves intimately to the contour of the joint space in all positions of the joint and act as 'passive space-fillers' that fill peripheral non-congruent parts of the joint in its neutral position but displace when the joint moves (Lewin et al., 1962; Tondury, 1972; Giles and Taylor, 1982; Bogduk and Engel, 1984; Giles, 1986; Taylor and McCormick, 1991; Mercer and Bogduk, 1993). It is not clear how the 'passive space-filling' role of the synovial folds affects physiological loading and motion of the spinal articulations (Chang et al., 1992) but it has been suggested that the synovial folds may protect and lubricate the articular surfaces, enhance joint congruity and stability or assist weight-bearing (Lewin et al., 1962; Engel and Bogduk, 1982; Bogduk and Engel, 1984; Chang et al., 1992; Mercer and Bogduk, 1993).

In synovial articulations throughout the body, adipose tissue is thought to play an important role in forming flexible and deformable cushions that fill spaces and irregularities within the joint and accommodate changes in joint shape and volume during movement (Standring et al., 2005). Schonstrom et al. (1993) noted that adipose synovial folds of the lateral atlanto-axial joints in unfixed cadavers were soft and changed shape readily on joint movement whilst fibro-fatty synovial folds appeared to be stiffer. In fresh unfixed cadaveric lumbar spines, the synovial folds have been observed to change shape and position during movements of the spine (McFadden and Taylor, 1990). The change in shape and position appears to be related to the movement of adipose tissue between the intracapsular synovial fold and extracapsular articular recess through the hole in the fibrous capsule (Figure 1.6) (McFadden and Taylor, 1990). The observation of McFadden and Taylor (1990) has been frequently cited but has not been subjected to further rigorous investigation. The specimens used in the study by McFadden and Taylor (1990) had been frozen, which may have affected their mechanical properties, and the observations did not take into account the behaviour of fibrous synovial folds. Furthermore, the behaviour of adipose tissue *in vivo* is likely to be different to that observed in cadavers, even cadavers that are not fixed/embalmed. It is not clear whether the synovial folds of the lateral atlanto-axial joints possess extracapsular communications similar to those reported in the lumbar spine. The presence of an extracapsular communication may affect the behaviour of the synovial

folds during normal spinal motion and during abnormal spinal motion that causes injury. Further studies are required to determine whether the synovial folds of the lateral atlanto-axial joints possess extracapsular communications or not.

The synovial folds may be involved in the facilitation of movement between the articular surfaces (Lewin et al., 1962). When the spinal articulations are in the neutral position, the synovial folds lie between the articular surfaces (Bogduk and Jull, 1985; Yu et al., 1987; Schonstrom et al., 1993). As the joint moves and the joint surfaces become displaced from each other, the synovial folds appear to cover the articular surfaces which otherwise would become exposed as the joint moves (Engel and Bogduk, 1982; Mercer and Bogduk, 1993). By covering the exposed articular surfaces, the synovial folds are thought to ensure that a film of synovial fluid remains applied to the surface of the cartilage, in preparation for the return motion to the neutral position (Engel and Bogduk, 1982; Mercer and Bogduk, 1993; 2001). Like the fibrocartilaginous menisci of the knee joint, the synovial folds may obviate the need for large collections of synovial fluid by filling non-congruent spaces within joints whilst preserving a film of synovial fluid over the articular surfaces at all times (Mercer and Bogduk, 1993; Standring et al., 2005).

By enhancing joint congruity it has been suggested that the synovial folds may contribute to the stability of a joint (Lewin et al., 1962; Yu et al., 1987; Chang et al., 1992). The synovial folds may also promote the dissipation of stress and/or assist in weight-bearing (Tondury, 1940; Dorr, 1958). The fat pads of the foot possess the same adipose and fibrous tissue composition as the synovial folds and form a pressure tolerant structure that functions to absorb shock and protect against excessive local stress (Miller-Young, Duncan and Baroud, 2002; Benjamin et al., 2004).

The presence of nerve endings within the synovial folds suggests that the synovial folds may also have a mechanosensory role. As described in Section 2.3.2, the synovial folds of the vertebral column have been found to contain proprioceptive and nociceptive nerve fibres ranging from 0.2 to 12.0µm in diameter that are immunoreactive to Substance P and CGRP, plus mechanoreceptors have been observed at the interface between the synovial fold and the fibrous capsule (Giles and Harvey, 1987; Giles and Taylor, 1987a; Giles and Taylor, 1987b; Giles, 1988; McLain, 1994; McLain and Pickar, 1998; Erwin et al., 2000; Inami et al., 2001). It has been suggested that

innervated adipose tissue may be important in giving proprioceptive feedback for sensorimotor control (Benjamin et al., 2004) which would be especially important in the upper cervical spine which has direct neurophysiological connections via cervical proprioceptors to the vestibular and visual systems (Dutia, 1991). Disturbances in balance and vision have been reported to accompany upper cervical pain and dysfunction and are areas of increasing interest particularly in relation to whiplash (Treleaven et al., 2003; Sterling et al., 2004; Montfoort et al., 2006; Treleaven et al., 2006). Therefore, in addition to being a potential pain source, the synovial folds may have a proprioceptive function that has not yet been recognised.

Another potential role that has not been considered to date is that the synovial and adipose tissues forming the synovial folds may have a paracrine role (Mohamed-ali et al., 1998). The synovium and articular adipose tissues have been found to release growth factors and pro-inflammatory cytokines ('adipokines' or 'adipocytokines') into the joint (Ushiyama et al., 2003). Thus products of the synovial folds may contribute to inflammatory and degenerative processes that underlie joint diseases such as osteoarthritis and rheumatoid arthritis (Toussirot et al., 2007).

In conclusion, gross anatomical and histological descriptions of the synovial folds from cadavers currently provide the only basis for hypothesising the potential functional significance of the synovial folds in the vertebral column. Due to differences in tissue properties between cadavers and living tissue, there is a need to study the synovial folds *in vivo*. To date no studies have objectively described the normal structure and function of the cervical synovial folds either *in vitro* or *in vivo* nor investigated their behaviour during normal or abnormal physiological loading.

2.5   Synovial folds and neck pain

Correlation of synovial fold injury to clinical presentations of low back pain and neck pain, whose pathological basis remains elusive to date and where radiological investigations have proven to be insufficiently sensitive to elucidate the source of pain and disability, has been attempted by many authors (Table 2.4). The hypotheses that have been proposed to explain these clinical presentations include synovial fold **EN**trapment, synovial fold **EX**trapment, intra-articular adhesions, synovial fold rupture and synovial fold impingement following whiplash injury (Table 2.4). The majority of these theories depend upon the existence of sensory nerve elements within the synovial

folds that may become irritated by deformation and/or inflammation. The major limitation of these theories is that they are solely based on the anatomy of the synovial folds reported at postmortem as the normal structure and function of the synovial folds *in vivo* is not known. Furthermore, it is currently not possible to investigate or verify these theories due to the inability to image the synovial folds *in vivo*.

Table 2.4. Clinical presentations of spinal pain and disability linked to theories of synovial fold (SF) injury.

Clinical presentation	Definition	Theory of SF injury	References
"Acute locked back "	A disorder of the lumbar spine characterised by the sudden onset of pain and movement restriction during lumbar flexion. Pain develops on attempting to return to the neutral position and the patient is unable to straighten (Bogduk and Jull, 1985). Acute locked back is reported to respond well to spinal manipulation (Bogduk and Jull, 1985).	Entrapment Extrapment Rupture	Kraft and Levinthal., 1951; Engel and Bogduk, 1982; Bogduk and Engel, 1984; Bogduk and Jull, 1985
Torticollis (acute wry neck)	Cervical spinal pain that is associated with sustained rotatory "deformity" of the neck (Merskey and Bogduk, 1994).	Entrapment Extrapment	Kawabe et al., 1989; Mercer and Bogduk, 1993; Inami et al., 2000; Tang et al., 2007
Articular hypomobility (joint fixation)	A spinal joint fixation is defined as a restriction in articular mobility that produces a loss of segmental motion (Byfield et al., 2002).	Entrapment Intra-articular adhesions	Lewit, 1985; Jones et al., 1989; Mercer and Bogduk, 1993
Neck pain and headache caused by trauma (whiplash)	"Whiplash is an acceleration-deceleration mechanism of energy transfer to the neck. It may result from rear-end, frontal or side-impact motor vehicle collisions, but can also occur during diving or other mishaps. The impact may result in bony or soft tissue injuries (whiplash injuries), which in turn may lead to a variety of clinical manifestations (whiplash-associated disorders)", Quebec Task Force, (Spitzer et al., 1995). Neck pain and headache are the most common symptoms following whiplash (Teasell and Shapiro, 2002).	Impingement Rupture	Schonstrom et al., 1993; Taylor and Taylor, 1996; Kaneoka et al., 1999; Inami et al., 2000

The theories regarding synovial fold involvement in disorders of the spine are closely related to theories concerning the mechanism of spinal manipulative therapy in resolving some types of spinal pain and disability. Spinal manipulative therapy is a generic term given to describe manually applied therapeutic interventions, including 'manipulation' and 'mobilisation', that are typically applied with the intention of inducing motion at the spinal articulations by directing forces to the vertebrae (Herzog et al., 2001; Harvey et al., 2003). There is evidence for the clinical efficacy of spinal manipulative therapy for both low back pain and neck pain (Koes et al., 1996; van Tulder et al., 1997; Gross et al., 2004; NLH Neck Pain Guidelines, 2005; Airaksinen et al., 2006; Vernon et al., 2007), however, the physiological mechanisms behind these

clinical effects are not yet known. Four main theories have been proposed to explain the clinical effects of spinal manipulation for the treatment of spinal pain and disability, three of which are related to the synovial folds (Shekelle, 1994; Evans, 2002; Hearn and Rivett, 2002):

1. the release of trapped intra-articular material such as the synovial folds

2. the disruption of articular or periarticular adhesions

3. 'mechanoreceptor-pain gate' or 'reflexogenic' theory, i.e. the relaxation of 'hypertonic' muscle by sudden stretching

4. 'unbuckling' spinal motion segments that have undergone 'disproportionate displacements'

Using magnetic resonance imaging, spinal manipulation and mobilisation have been shown to increase separation (gapping) of the zygapophysial joints (Cramer et al., 2002; Lee et al., 2005) which is in agreement with many of the proposed models of synovial fold injury and its treatment using spinal manipulative therapy. The effects of these manual therapy techniques upon the synovial folds have not yet been demonstrated as there are currently no techniques available to image the synovial folds *in vivo*. The development of new methods for studying the synovial folds, especially the development of *in vivo* imaging techniques, is required in order to enable future research into the mechanical effects of spinal manipulation and mobilisation, and the potential role of the synovial folds, to be investigated.

2.5.1 Synovial fold ENtrapment

Synovial fold ENtrapment, referred to as the "imprisonment theory", was proposed by Zukschwerdt et al. (1955) and elaborated upon by Kos and Wolf (1972a; 1972b; 1976) in an attempt to explain some types of low back pain. Kos and Wolf (1972a; 1972b; 1976) hypothesised that an abnormal joint movement may cause a synovial fold to move from its normal position at the articular margins to become imprisoned between the articular cartilage surfaces (Figure 2.7). They suggested that a synovial fold with a firm fibrous apex might indent the articular cartilages and produce a small depression in which the synovial fold apex becomes imprisoned (Kos and Wolf, 1972b; Kos and Wolf, 1972a; Kos and Wolf, 1976). Pain and articular hypomobility could result from the entrapment of the synovial fold itself and/or from tension on the innervated fibrous capsule. Both outcomes could lead to an accompanying reflex muscle spasm (Kos and Wolf, 1972b; Kos and Wolf, 1972a; Kos and Wolf, 1976). This theory has been used to

explain the pathophysiology of torticollis and acute locked back (Bogduk and Engel, 1984; Saboe, 1988; Kawabe et al., 1989) and has been extrapolated further to explain the relief of pain and disability from these conditions following spinal manipulation (Bogduk and Jull, 1985; Evans, 2002).
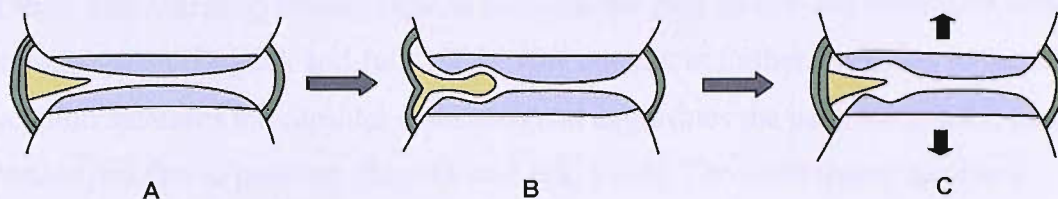
Figure 2.7. Schematic illustration of the synovial fold **EN**trapment theory. A – a fibro-adipose synovial fold projects between the articular surfaces. B – the fibrous apex of the synovial fold indents the hyaline articular cartilage forming a depression in which the apex becomes entrapped. The synovial fold undergoes traction which in turn creates tension in the fibrous capsule. C – it is hypothesised that manipulation separates the articular cartilages and releases the trapped synovial fold. Based on Kos and Wolf (1972a).

To determine whether synovial folds have the potential to indent the articular cartilage, Kos and Wolf (1972a; 1972b; 1976) pressed a variety of different objects (e.g. pig tendon, human hair, steel ball) onto the surface of fresh articular cartilage and were able to create temporary indentations. Bogduk and Jull (1985) support the suggestion by Kos and Wolf (1972a; 1972b; 1976) that a fibrous synovial fold apex may be capable of indenting the cartilage but disagree that a synovial fold base composed of adipose tissue would be capable of generating tension in the fibrous capsule. Instead Bogduk and Jull (1985) have proposed that the traction forces generated in a fibro-adipose synovial fold with a trapped apex would cause rupture or tearing of the synovial fold from the fibrous capsule. A tear of the synovial fold would probably result in intra-articular haemarthrosis and possibly the formation of a loose body (Bogduk and Jull, 1985). Bogduk and Jull (1985) did not consider the possibility of a fibrous synovial fold with a fibrous base becoming trapped between the articular surfaces in this way.

2.5.2 Synovial fold **EX**trapment

In the **EX**trapment theory the synovial fold is trapped outside of the joint cavity. This is different to the **EN**trapment theory in which the synovial fold is trapped inside the joint cavity. Bogduk and Jull (1985) proposed the synovial fold extrapment theory as a possible alternative to the synovial fold entrapment theory to explain the pathophysiology of acute locked back and its reported resolution following spinal manipulation. The extrapment theory proposes that the lumbar articular processes move apart upon full flexion of the lumbar spine and the exposed articular surfaces become

covered by the synovial folds (Figure 2.8) (Bogduk and Jull, 1985). The synovial folds then fail to re-enter the joint cavity upon return to the neutral position from full flexion. Instead of re-entering the joint cavity, the tip of the synovial fold engages with the margin of the inferior articular process and is deflected toward the fibrous capsule resulting in buckling of the synovial fold and capsular distension (Bogduk and Jull, 1985). The distended fibrous capsule becomes the pain source and stimulates reflex muscle spasm (Bogduk and Jull, 1985). Any attempt at further extension to the neutral position increases the capsular distension and aggravates the pain, forcing the patient to remain in a flexed position (Bogduk and Jull, 1985). The same theory has been proposed to explain the clinical features of acute torticollis in the cervical spine precipitated by excessive axial rotation (Mercer and Bogduk, 1993; Merskey and Bogduk, 1994).
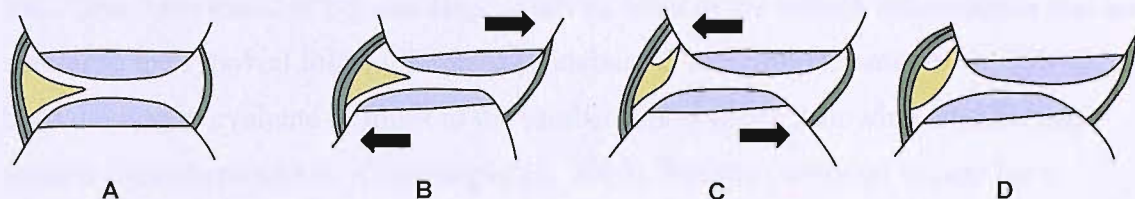
Figure 2.8. Schematic illustration of the synovial fold **EX**trapment theory. A – a synovial fold projects between the articular surfaces. B – as the joint moves, the synovial fold accompanies the caudal articular process and covers its exposed hyaline articular cartilage surface. C – on return to the neutral position, the apex of the synovial fold fails to re-enter the synovial cavity and contacts the articular margin of the cranial vertebra. D – the synovial fold buckles and distends the fibrous capsule causing pain. Based on Bogduk and Jull (1985).

The extrapment theory is consistent with the clinical features of acute locked back in the lumbar spine and torticollis affecting the cervical spine. Whilst extrapment is probably not dependent on the tensile strength of the synovial fold it is likely to depend on how pliable and mobile the synovial fold is, whether the synovial fold is of sufficient size to distend the fibrous capsule and the presence/absence of extracapsular communications. The larger and more flexible synovial folds of children are thought to be more likely to become extrapped causing children to be more susceptible to torticollis compared to adults (Tang et al., 2007). This may explain why torticollis caused by atlanto-axial rotatory deformity is more frequently seen in children than adults (Ono et al., 1985; Herman, 2006; Tang et al., 2007). It is thought that the small fibrous synovial folds that are typically found in adults are less likely to become extrapped.

2.5.3 Intra-articular adhesions

Synovial fold **EX**trapment proposed by Bogduk and Jull (1985) has been refuted by Lewit (1987) who believed that the model failed to explain articular hypomobility characterised by reduced intersegmental spinal motion, with or without pain, on manual examination of the spine (Jull, 1986; Jull et al., 1997; Lewit, 1985; Mercer and Bogduk, 1993). It has been speculated that the intra-articular synovial folds may act as a nidus for the proliferation of fibrous tissue that results in the formation of adhesions in joints that are habitually immobilised or under-used (Jones et al., 1989; Mercer and Bogduk, 1993) and that spinal manipulation may separate the joint surfaces breaking up the adhesions allowing for increased mobility (Evans, 2002; Cramer et al., 2004). This pathological process of adhesion formation has been observed in immobilised knee joints of both animals and humans (Enneking and Horowitz, 1972; Akeson et al., 1980) and in lumbar zygapophysial joints (Baker Wde et al., 1969). More recently, a rat model (rats have been found to possess large synovial folds in the lumbar articulations that are similar to the synovial folds of humans (Ginsburg et al., 2000; Cramer et al., 2004)) has been devised to evaluate changes to the lumbar articulations following fixation that renders joints hypomobile (Ginsburg et al., 2000). Results published to date have demonstrated that joint fixation results in the formation of connective tissue adhesions that extend across the joint cavity that are directly dependent upon the duration of fixation (Cramer et al., 2004).

2.5.4 Synovial fold rupture

It has been hypothesised that if the apex of the synovial fold becomes trapped between the articular surfaces it may be torn from its base producing intra-articular haemorrhage or alternatively the detached apex may form a loose body (Engel and Bogduk, 1982; Bogduk and Jull, 1985). No published studies to date have documented the presence of ruptured or torn synovial folds in the spinal articulations of cadavers that have died for reasons other than trauma (Yu et al., 1987; Chang et al., 1992; Mercer and Bogduk, 1993; Kos et al., 2002). In a postmortem study of victims of motor vehicle trauma, Jonsson et al. (1991) reported the presence of torn synovial folds. In contrast Taylor and colleagues (Schonstrom et al., 1993; Taylor and Taylor, 1996), in their extensive studies of articular damage following motor vehicle trauma at post-mortem, described intra-articular haemorrhage but not the presence of torn or ruptured synovial folds. This difference in results may be due to the absence of a control group (i.e. individuals that had died for reasons other than trauma) in the study of Jonsson et al. (1991). Traumatic

rupture of the synovial plicae of the knee resulting in haemarthrosis is reported to be rare (Garcia-Valtuille et al., 2002).

2.5.5 Synovial fold impingement and whiplash

The majority of evidence regarding the possible role of synovial folds in the generation of neck pain relates to their potential to become impinged (pinched) between the articular surfaces as a result of abnormal spinal motion (Giles and Taylor, 1982; Giles and Harvey, 1987), for example during whiplash associated with motor vehicle trauma. Impingement may cause irritation of the pain-sensitive nerve fibres reported to exist within the synovial folds and inflammation. There is evidence to support impingement of the synovial folds from postmortem studies following whiplash trauma. Bruising of the synovial folds of the lateral atlanto-axial joints (Figure 2.10) is one of the most common soft tissue injuries of the cervical spine reported at autopsy following fatal motor vehicle trauma (Schonstrom et al., 1993; Taylor and Taylor, 1996; Taylor and Twomey, 1993; Taylor and Finch, 1993).

Whiplash-related injuries (often referred to as 'whiplash-associated disorders' [WAD]), although not associated with a high fatality rate, are among the most commonly reported injuries associated with low impact motor vehicle trauma and represent a significant cost to society (Barnsley, Lord and Bogduk, 1994; Yoganandan, Pintar and Kleinberger, 1999; Richter, Otte, Pohlemann, Krettek and Blauth, 2000). In the United Kingdom the estimated incidence of whiplash injury is approximately 250,000 new cases annually (Galasko et al., 1996 in Yoganandan et al., 2002) whilst in the United States the annual incidence is about 1 million (Evans, 1992). Between 6% and 50% of people who sustain whiplash injuries are reported to develop chronic WAD that may be disabling and persist for years (Norris and Watt, 1983; Gargan and Bannister, 1990; Hildingsson and Toolanen, 1990; Evans, 1992; Parmar and Raymakers, 1993; Radanov et al., 1994; Mayou and Bryant, 1996). The estimated annual cost associated with chronic and acute whiplash-related disorders in the United States is $4.5 billion (Yoganandan et al., 1999). Given that these seemingly minor neck injuries are both costly and debilitating, an improved understanding of the pathoanatomy of whiplash injury is needed to provide a rationale for injury mitigation and to serve as a guide for improvements in clinical management.

A variety of different symptoms may result from motor vehicle trauma including neck pain, headache, cognitive difficulties, visual disturbances and dizziness, the most common being neck pain and headache (Sturzenegger et al., 1994; Karlsborg et al., 1997; Cassidy et al., 2000). The persistence of these symptoms beyond a 3-month interval constitutes chronic whiplash syndrome (Lord et al., 1996; Verhagen et al., 2007). The majority of whiplash injuries are considered to be 'soft-tissue injuries' affecting the joints, ligaments and muscles of the cervical spine, including minor fractures that do not compromise the stability of the cervical spine (e.g. fractures of the articular process) (Lovell and Galasko, 2002; Bogduk and Yoganandan, 2003). Major fractures and dislocations that threaten the stability of the cervical spine and the integrity of its neural contents are not common following motor vehicle trauma but must be excluded (Lovell and Galasko, 2002; Bogduk, 2003; Bogduk and Yoganandan, 2001). The symptoms of whiplash are not usually associated with objective radiological abnormalities or clinical examination findings. Whilst plain film radiographs can be used to exclude major fracture or dislocation and CT scans may help to identify occult fractures, neither are able to demonstrate soft tissue injuries (Binet, Moro, Marangola and Hodge, 1977; Woodring and Goldstein, 1982; Jonsson et al., 1991). MRI does have the capacity to resolve certain soft tissue structures but no correlations have yet been established between neck pain and any feature evident of soft tissue injury on MRI (Borchgrevink et al., 1995, Ronnen et al., 1996).

Until the 1990s, it was believed that the injuries resulting from whiplash resulted from a non-physiological hyperextension-hyperflexion movement of the head (Macnab, 1971). Modern studies of the biomechanics of whiplash have utilised photographic studies of cadavers and human volunteers and cineradiographic studies of human volunteers to provide a detailed picture of what occurs to the head, neck and body during whiplash caused by a rear-end impact (Figure 2.9) (Kaneoka et al., 1999; Bogduk and Yoganandan, 2001). At 44ms following impact, the cervical spine straightens and is thrust upwards by the rising trunk resulting in compression of the cervical spine. By 110ms the cervical spine undergoes a non-physiological sigmoid (S-shaped) deformation in which the lower cervical spine is extended and the upper cervical spine is flexed. At this point the posterior elements of the lower cervical spine are compressed and the anterior elements are distracted. The upper cervical spine then moves into extension forming a C-shape.

Current biomechanics data indicates that during the S-shaped phase, the lower cervical zygapophysial joints undergo shear and distraction in the ventral region of the joint and shear plus compression in the dorsal region of the joint (Cusick et al., 2001; Stemper et al., 2004; Stemper et al., 2005). The entire joint has been shown to undergo stretch but the greatest magnitudes of stretch are evident at the ventral region of the joint (Winkelstein et al., 2000; Stemper et al., 2004; Stemper et al., 2005). Therefore a possible whiplash injury mechanism at the ventral aspect of the joint is tensile failure of the fibrous capsule (possibly involving the synovial membrane and folds) resulting in nociceptive firing (Avramov et al., 1992; Pickar and McLain, 1995; Winkelstein et al., 2000; Stemper et al., 2004; Stemper et al., 2005). Injury to the dorsal region of the joint is thought to stem from impingement of the fibrous capsule or synovial folds causing pain as a result of nociceptive activation and/or inflammation (Cusick et al., 2001; Stemper et al., 2004). Because articular cartilage does not cover the entire surface of the osseous articular facets, it has also been suggested that compression at the dorsal region of the joint may result in contact between the articular facets producing pain and possibly fracture (Cusick et al., 2001; Yoganandan et al., 2003; Stemper et al., 2004). The articular lesions identified in postmortem studies of the victims of motor vehicle trauma match those predicted by the biomechanical model of whiplash and include partial and complete ruptures of the fibrous capsule; contusions, rupture and displacement of the synovial folds; damage to the articular cartilage; fractures of the articular processes; and intra-articular haemarthrosis (Jonsson et al., 1991; Taylor and Finch, 1993; Taylor and Taylor, 1996; Yoganandan et al., 2001).
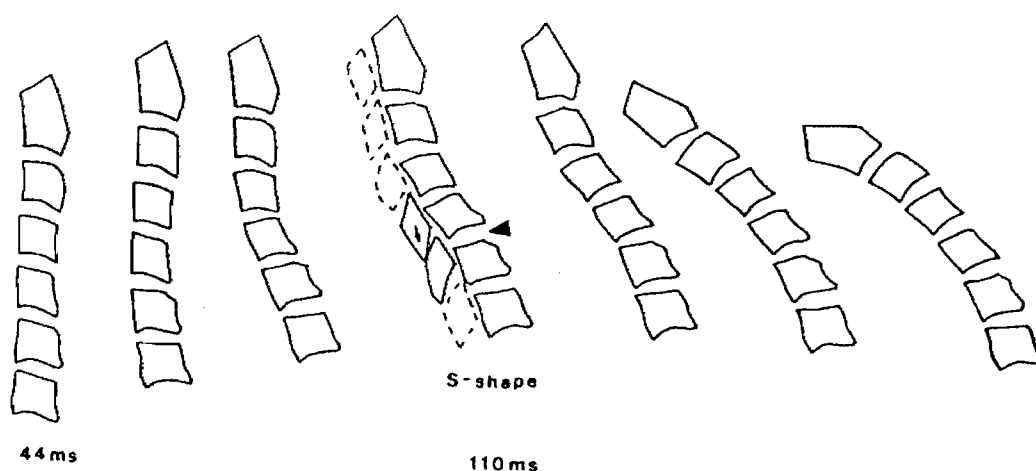
Figure 2.9. Illustration of sequential radiographs of the cervical spine during rear-end impact at 4kph with no head rest. Initially after impact (44ms) the cervical spine straightens. It then assumes an S-curve (110ms) with the upper spinal levels in flexion and the lower spinal levels in extension. At this point the posterior elements are impacted and the anterior elements distracted. The S-curve is followed by extension of the upper cervical segments and the cervical spine finally assumes a C-curve. From Bogduk and Yoganandan (2001), with permission.

31

Whilst the lower cervical spine is in extension during the S-shaped phase, the upper cervical spine is in flexion. This has led to the hypothesis that upper cervical dorsal capsular structures are at risk of distraction injury, including stretch and increased tensile forces, in association with the elongation of neural structures such as the dorsal roots and dorsal root ganglia (Luan, Yang, Deng, Begeman, Tashman and King, 2000; Cusick, Pintar and Yoganandan , 2001; Yoganandan, Pintar and Cusick, 2002; Stemper et al., 2004). There is evidence, however, that extension of the upper cervical spine (during the C-shaped phase following impact) rather than flexion (during the S-shaped phase) exceeds functional limits, especially at higher impact accelerations (Grauer et al., 1997; Ordway et al., 1999; Panjabi et al., 2004). Hypothetically this would suggest that the resultant injuries would be the same as those reported for lower cervical spine extension during the S-shaped phase such as ventral capsular stretch, dorsal synovial fold bruising and articular fractures and intra-articular haemarthrosis. At post-mortem the most common injuries affecting the upper cervical spine include bruising of the lateral atlanto-axial synovial folds and haematoma around the second cervical spine nerve and its dorsal root ganglion (Figure 2.10) (Schonstrom et al., 1993; Taylor and Finch, 1993; Taylor and Twomey, 1993; Taylor and Taylor, 1996).
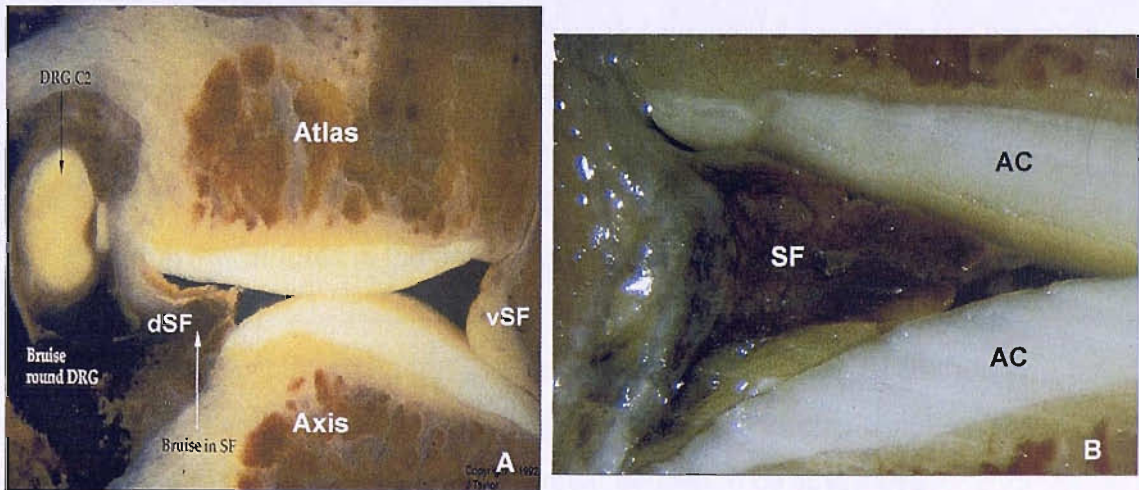
Figure 2.10.A. Sagittal section of the lateral atlanto-axial joint: bruising of the dorsal synovial fold (dSF), associated with perineural hematoma around the C2 spinal nerve and dorsal root ganglion (DRG), following fatal motor vehicle trauma (66 year old male) The ventral SF (vSF) is normal. Adapted from Taylor (2001), with permission. **B.** Sagittal section of the lateral atlanto-axial joint (close-up): bruising of the dorsal synovial fold (SF), following fatal motor vehicle trauma (29 year old male). AC - articular cartilage. Adapted from Taylor (2001), with permission.

Bruising of the synovial folds has been found most frequently to affect the dorsal compared to the ventral synovial folds (Schonstrom et al., 1993) which would support an extension rather than a flexion mechanism of injury. Additional injuries observed at post-mortem include tears of the fibrous capsule (whether these affect the dorsal or

ventral capsule has not been reported), intra-articular haemarthrosis and fractures affecting the articular surfaces (Jonsson et al., 1991; Schonstrom et al., 1993). Thus whilst there is general agreement regarding the articular tissues of the upper cervical spine most likely to be injured following whiplash trauma, the mechanism of injury is contentious. This is possibly because the majority of biomechanical studies investigating localised cervical facet joint kinematics have to date focussed on the mechanisms of injury affecting the lower rather than upper cervical spine.

Confirmation of injuries affecting the cervical articulations following whiplash trauma comes from clinical studies of patients with neck pain which have suggested that the cervical zygapophysial joints are the single most common source of chronic neck pain following whiplash trauma (Barnsley, Lord, Wallis and Bogduk, 1995; Lord, Barnsley and Bogduk, 1995; Lord, Barnsley, Wallis and Bogduk, 1996). The mechanisms underlying chronic neck pain following whiplash injury are unclear. At the lateral atlanto-axial joints, marked brown discolouration of the dorsal synovial folds, extracapsular haematoma around the second cervical spinal nerve and rupture of the ventral capsule have been observed 1 to 2 months after the initial injury, in post-mortem studies of the survivors of motor vehicle trauma who died later from other causes (Schonstrom et al., 1993). Therefore injury to the synovial folds following whiplash may be a potential source of acute and chronic neck pain.

Thus there is substantial biomechanical, clinical and post-mortem evidence to suggest a role for the synovial folds in the production of neck pain and disability that results from trauma such as whiplash. To date there is no means of objectively identifying the lesions caused by whiplash injury. The ability to image the synovial folds *in vivo* may change that and provide a method for diagnosing this debilitating condition that would enable appropriate treatment and management options to be developed.

2.6   Conclusion

The synovial fold studies conducted to date have documented the gross anatomy, histology and innervation of the synovial folds. This has resulted in the generation of a number of hypotheses to explain their potential function and potential role in the generation of neck pain. To validate or replace these theoretical models, new methods of studying the synovial folds need to be developed to determine the normal structure and function of the synovial folds *in vitro* and *in vivo* to provide a basis for investigating

changes in the synovial folds related to neck pain and disability. Potential areas for the development of new methods include:

1. Imaging. Cadaveric synovial folds have been successfully visualised using MRI (Yu et al., 1987) and arthrography (Okada, 1981). MRI is regarded as the best imaging tool for the differentiation of soft tissue structures and so is more likely to detect synovial fold pathology than plain film xrays or CT. Ultrasound is another imaging tool that should be considered for identifying the synovial folds. At present, an optimal method for imaging the synovial folds *in vivo* does not exist and the normal structure and function of the synovial folds *in vivo* is not known or understood.

2. Biomechanical models. Accurate and validated biomechanical models provide a versatile tool for examining the biomechanical properties of structures of the cervical spine. To date the geometrical and mechanical properties of the synovial folds have not been determined for inclusion in the most current biomechanical models of the cervical spine. Quantification of the normal structure and dimensions of the synovial folds would enable the determination of synovial fold behaviour during both normal functional and traumatic loading conditions.

3. Animal models. Synovial folds have been documented in the spinal articulations of rats (Ginsburg et al., 2000) and an animal model has been developed to investigate the role of the synovial folds in the development of intra-articular adhesions (Cramer et al., 2004). Whilst animal models are regarded as being biologically accurate, differences in size and anatomy cannot be adjusted for in any simple way (Bogduk and Yoganandan, 2001). Nevertheless, animal models serve a useful purpose, particularly in the demonstration of normal and abnormal function, and provide an indication of what can be expected in the human.

4. Human cadaveric models. Cadaveric experiments are the most applicable to the living human. Human cadaver studies have been used and continue to be used to provide information on the descriptive and quantitative morphology of the cervical spine and provide an experimental model for the determination of how the cervical spine behaves biomechanically. The location of the synovial folds limits biomechanical investigations as access to the synovial folds involves disruption of the fibrous capsule and differences in the material properties of the synovial folds (e.g. adipose tissue) limits extrapolations to the *in vivo* situation.

Chapter 3

The use and interpretation of statistical methods in the determination of measurement precision

3.1   Introduction

New methods of quantifying spinal morphology using anatomical and imaging methods are continuously being developed to inform patient treatment and management. For example, quantification of the dimensions of the pedicles from cadaver spines to determine the potential for safe transpedicular screw fixation (McLain et al., 2002) and the measurement of cervical muscle cross-sectional area using magnetic resonance imaging for the diagnosis of headache (Fernandez-de-Las-Penas et al., 2007b).

In order to objectively judge the acceptability of a new method of measurement for clinical and research use it is necessary to determine its precision. The error associated with a measurement should be small enough to detect actual changes in what is being measured (Rankin and Stokes, 1998). This is especially important for clinical methods. Failure to do so may reduce or delay an accurate diagnosis and detrimentally affect patient treatment and management.

Numerous different statistical tests are used in the literature for the study of precision. A review of recent editions of journals associated with the study of the vertebral column highlighted the variation in statistical approaches. Statistical tests used in journals such as *Spine*, *European Spine Journal*, *The Spine Journal* and *Manual Therapy* included correlation coefficients (Ohara et al., 2006; Vialle et al., 2006; De Carvalho et al., 2007; Gupta et al., 2007), intra-class correlation coefficients (Fehlings et al., 2006; Vialle et al., 2006; De Carvalho et al., 2007; Gille et al., 2007; Gupta et al., 2007; Ropponen et al., 2007), regression (Lee et al., 2007), *t*-tests/ANOVA (Fehlings et al., 2006; Ohara et

al., 2006; Vialle et al., 2006; De Carvalho et al., 2007; Gille et al., 2007) and limits of agreement (Vialle et al., 2006; Lee et al., 2007); or the determination of precision was ignored (Lien et al., 2006; Çatan et al., 2007; Christensen et al., 2007; Hirasawa et al., 2007). Some of these statistical methods are not appropriate for the determination of measurement precision. An understanding of which statistical tests are appropriate and which are not is important because the improper use or faulty interpretation of statistical parameters may result in invalid judgements on the acceptability of new methods of measurement and ultimately may affect patient diagnosis, treatment and management. Furthermore, the use of different statistical tests prevents the comparison of results between studies.

The aim of this review was critically to analyse and evaluate the statistical methods most commonly used in the literature for the assessment of precision and includes:

> 1. an introduction to the terminology associated with the determination of measurement error in studies of precision
>
> 2. a critical evaluation of the most commonly used statistical methods that includes models produced using data collected from the present study to illustrate the strengths and weaknesses associated with each statistical test
>
> 3. recommendations on which statistical parameters are most sensitive for the detection of measurement error in precision studies

3.2   Definition of terms

Any observed measurement value (O) may be regarded as a function of two components, the true value (T) and an error component (E), i.e. $O = T \pm E$, where the difference between the true value and the observed value is the amount of measurement error (Bruton et al., 2000). The two main components of measurement error include 'systematic bias' and 'random error' (Atkinson and Nevill, 1998).

Systematic bias refers to predictable errors that are constant and occur in a particular direction (Atkinson and Nevill, 1998; Bruton et al., 2000). There are two potential sources of systematic bias, 'fixed bias' and 'proportional bias' (Westgard and Hunt, 1973; Ludbrook, 1997). Fixed bias refers to measurements that are consistently higher or lower by a constant amount across the whole range of measurements. Proportional bias denotes measurements that are higher or lower by an amount that is proportional to the level of the measured variable (Westgard and Hunt, 1973; Ludbrook, 1997).

Random errors are unpredictable errors due to chance that may originate, for example, from the inherent biological variation of subjects, random imperfections in the equipment or the fallibility of examiners using the equipment (Westgard and Hunt 1973; Ludbrook, 1997; Atkinson and Nevill, 1998). Random error that increases as the magnitude of the measured variable increases is referred to as 'heteroscedasticity'(also known as 'proportional error') (Ludbrook, 1997; Atkinson and Nevill, 1998). Heteroscedasticity appears to be common in studies involving biological data and although its origins have not been closely studied it has been suggested that it may be a biological phenomenon in which biological responses become more erratic as the strength of the stimulus increases (Ludbrook, 1997; Bland, 2005). However, it is more likely to occur because measurement error typically increases in proportion to the level of the measured variable (Ludbrook, 1997).

Studies of measurement error are typically designed to assess the extent of measurement error contributed by one or more of the following variables (Altman and Bland, 1983; Bruton et al., 2000):

1. Measurement method, device, equipment or instrument
2. Researcher/observer/examiner administering the measurement method
3. Response, i.e. the stability of the variable being measured.

A variety of different terms have been used in the literature to describe such studies (Table 3.1) (Atkinson and Nevill, 1998; Bruton et al., 2000). Often these terms do not accurately reflect the design of the study and are applied inconsistently and inappropriately making translation between studies difficult and contributing to the use of erroneous statistical methods.

Table 3.1. Descriptive terms used in the literature to describe the extent of potential measurement error contributed by the measurement method, researcher and response.

Variable	Measurement method	Researcher	Response
Descriptive terms used in the literature	Validity Criterion validity Method agreement Instrument reliability†	**A. Same Observer** Intra-observer reliability† Test-retest reliability† Intra-session test-retest reliability† Intra-tester reliability†	Inter-session reliability† Test-retest reliability† Response reliability† Intra-observer reliability†
		B. Different Observer Inter-tester reliability† Inter-examiner reliability† Inter-observer reliability†	

† The terms repeatability, reproducibility, variability, consistency, concordance, stability, response often appear in the literature instead of 'reliability'

The BS ISO 5725 (1994) terminology, 'precision' and 'accuracy', has been adopted in the present study. Accuracy is defined as the closeness of agreement between the average value of a large number of test results and the true or accepted reference value (i.e. it is the ability of a measurement method to determine exactly the true value). Precision is defined as the closeness of agreement between test results (i.e. it is the ability of a measurement method to replicate a given result) (BS ISO 5725, 1994). Two conditions of precision, 'repeatability' and 'reproducibility', have been described and represent the two extremes of precision (BS ISO 5725, 1994). Between these two extreme conditions of precision are the intermediate conditions of precision (BS ISO 5725, 1994) that occur when one or more factors are allowed to vary (Figure 3.1).
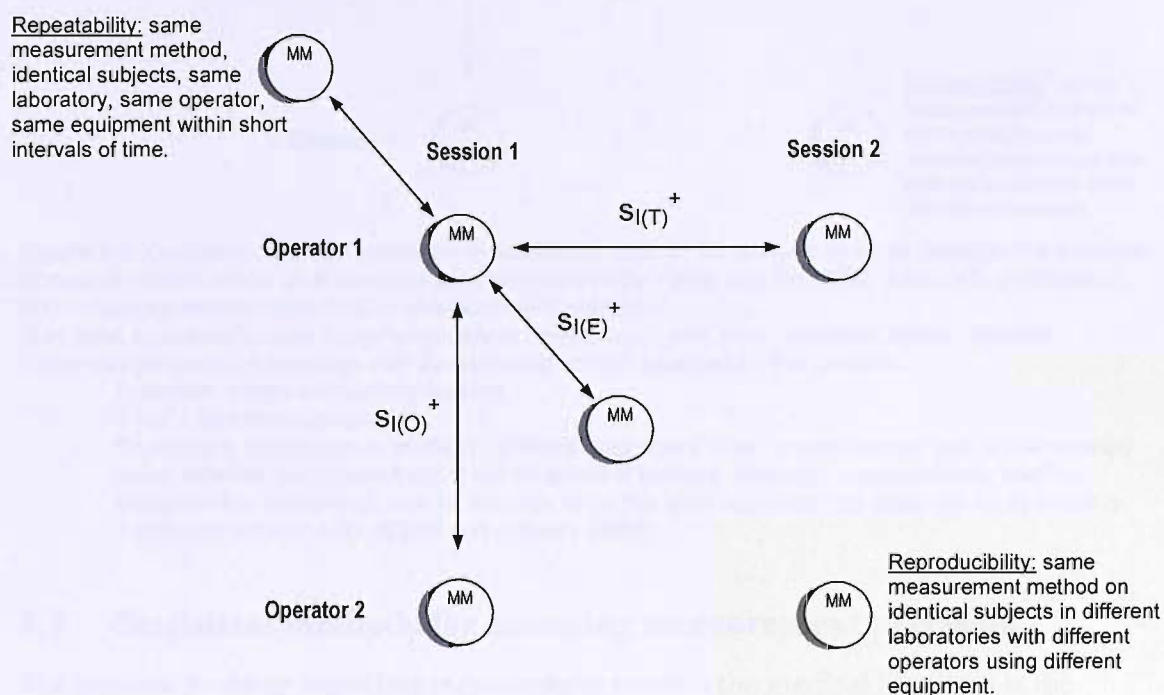
Figure 3.1. Diagrammatic representation of BS ISO 5725 (1994) definitions for the precision of measurements made on a continuous scale (devised by Webb and Rix, 2005, used with permission). MM – measurement method; [+]Intermediate conditions of precision are specified as "precision conditions with M factor(s) different" (BS ISO 5725, 1994), where M is the number of factors not maintained under constant conditions. The BS ISO 5725 (1994) guidelines recommend the use of suffixes to specify which factors are not kept constant under intermediate precision conditions:

Operator	$s_{I(O)}$ = operator-different intermediate precision standard deviation	
Time	$s_{I(T)}$ = time-different intermediate precision standard deviation	
Equipment	$s_{I(E)}$ = equipment-different intermediate precision standard deviation	

If more than one factor is not maintained under constant conditions, it is specified as follows:

Example:	$s_{I(TO)}$ = [time + operator]-different intermediate precision standard deviation

The BS ISO 5725 (1994) terminology used for describing intermediate conditions of precision is not widely recognised nor commonly used in the medical literature. Therefore for the purposes of this study, familiar terms have been matched as accurately

as possible to the BS ISO 5725 (1994) definitions for the intermediate levels of precision (Figure 3.2) and are used throughout this thesis.

Repeatability[*]: same measurement method, identical subjects, same laboratory, same examiner, same equipment within short intervals of time.

Session 1   Session 2

Test-retest precision[+x]

Examiner 1   M1   M1

Method agreement[+x]

Inter-examiner[*] precision[+x]

M2

Reproducibility[*]: same measurement method on identical subjects in different laboratories with different operators using different equipment.

Examiner 2   M1   M1

Figure 3.2. Diagrammatic representation of definitions used in the present study to describe the precision of measurements made on a continuous scale (devised by Webb and Rix, 2005, used with permission). M1 – measurement method 1; M2 – measurement method 2
*The term examiner is used interchangeably in the literature with rater, observer, tester, operator.
[+]Intermediate levels of precision with the following factors selected as the variable:
   Examiner – inter-examiner precision
   Time – test-retest precision
   Equipment, instrument or method - method agreement Note: encompasses both same method using different equipment/instrument or different method. Although an established method, equipment or instrument may be referred to as the 'gold standard' this does not imply that it is measured without error (Bland and Altman, 1999).

3.3   Statistical methods for assessing measurement precision

The greatest problem regarding measurement error in the medical literature is the erroneous use of statistical methods. A diversity of statistical approaches have been inconsistently adopted in the study of precision which has made it difficult to evaluate correctly and interpret study results and to make comparisons between studies (Haas, 1991; Rankin and Stokes, 1998; Ludbrook, 2002). Furthermore it presents the researcher with the problem of deciding which statistical test is most appropriate to use (Haas, 1991; Rankin and Stokes, 1998). The problem is perpetuated by researchers imitating statistical methods used in published papers to arrive at their own results regardless of whether those methods are correct. This has led to a vicious cycle that is hard to break (Bland and Altman, 1995). A number of authors have attempted to outline some of the problems associated with commonly used statistical approaches yet despite this inappropriate and incorrect methods of analysis continue to be used (Bruton et al., 2000; Ludbrook, 2002; Bland and Altman 2003; White, 2004).

Unlike hypothesis testing, the statistical analysis of measurement error should not provide yes or no answers regarding the acceptability of a method but should provide a specific estimate of the types and magnitudes of measurement errors (Westgard and Hunt, 1973; Bruton et al., 2000). All types of measurement error (systematic bias and random error) should be meaningfully quantified in order to relate the described error to judgements regarding 'analytical goals', i.e. the requirements of the measurement for effective practical use, rather than the statistical significance of any reliability indicators (Atkinson and Nevill, 1998). This information is essential in deciding whether a measurement method is acceptable for its intended use, especially when this will affect clinical judgement and patient management (Westgard and Hunt, 1973; Bruton et al., 2000).

Commonly used statistical methods employed for the determination of precision, for data measured on a continuous scale, include correlation coefficients, paired t-test, linear regression and Bland and Altman limits of agreement. To illustrate why these methods should or should not be used for the determination of measurement precision, each statistical method was used to analyse the following data from Chapter 4: the method agreement between two different measurement methods ('auto-CAT' and 'manual-CAT') for the determination of synovial fold cross-sectional area (n=143) (Table A2.1, Appendix 2). Known quantities of fixed bias, proportional bias and random error were added to the auto-CAT and manual-CAT data sets to highlight the potential limitations of these statistical methods in the determination of measurement error (Table A2.1). Because the auto-CAT and manual-CAT variables are experimentally derived it is important to be aware that they already contain unknown quantities of systematic bias and/or random error. The results of these analyses have been used to highlight how an 'acceptable' level of measurement error may be falsely accepted and forms the basis of a discussion of why some statistical methods should not be used in the determination of measurement precision. Recommended approaches to the analysis of measurement precision are presented and discussed.

If two measurements agree perfectly and there is no systematic bias or random error present, all values on a scatter diagram of one measurement plotted against the other will fall exactly along a line marking a 45° angle and intersecting the axes at the origin (Westgard and Hunt, 1973; Bland, 2005). This line is known as the line of equality (line of identity) and has a slope of 1 and an intercept of 0 ($Y = 0.0 + 1.0X$). Data clustered

around the line of equality is an indicator of good agreement between measurements and hence good precision (Figure 3.3). Data that is not clustered around the line of equality may be affected by a systematic bias or random error. The appearance of data affected by a systematic bias or random error is illustrated in Figures 3.4 and 3.5.
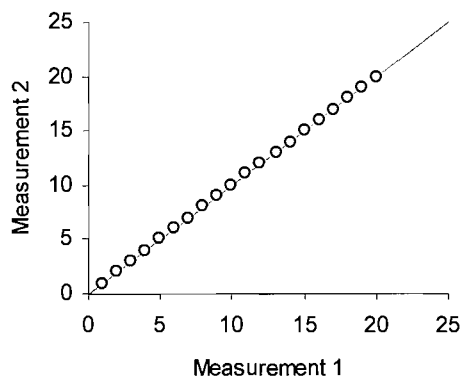
Figure 3.3. Data clustered around the line of equality ($Y = 0.0 + 1.0X$) indicates good agreement.
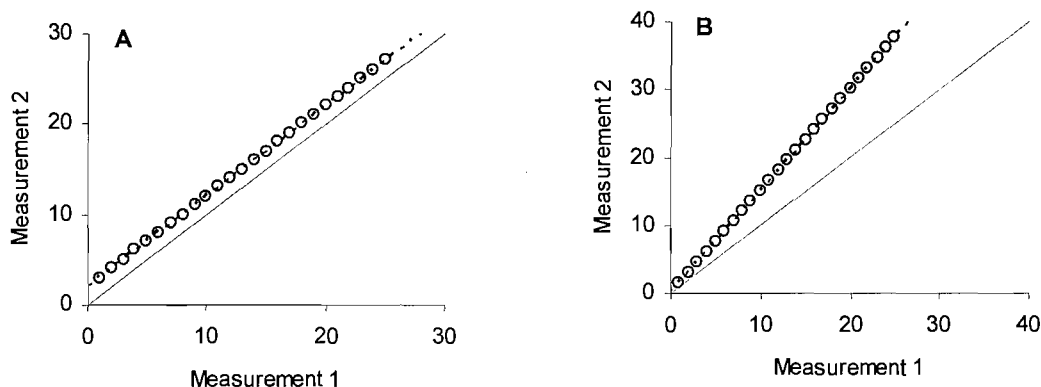
Figure 3.4.A. Fixed bias is the result of an additive constant represented by a (i.e. $Y = a + bX$) and leads to a change in the intercept of a regression line (line of best fit) fitted to the data. **B.** Proportional bias is caused by a multiplicative constant represented by b (i.e. $Y = a + bX$) and changes the slope of a regression line fitted to the data. Line of equality (——). Regression line (- - -).
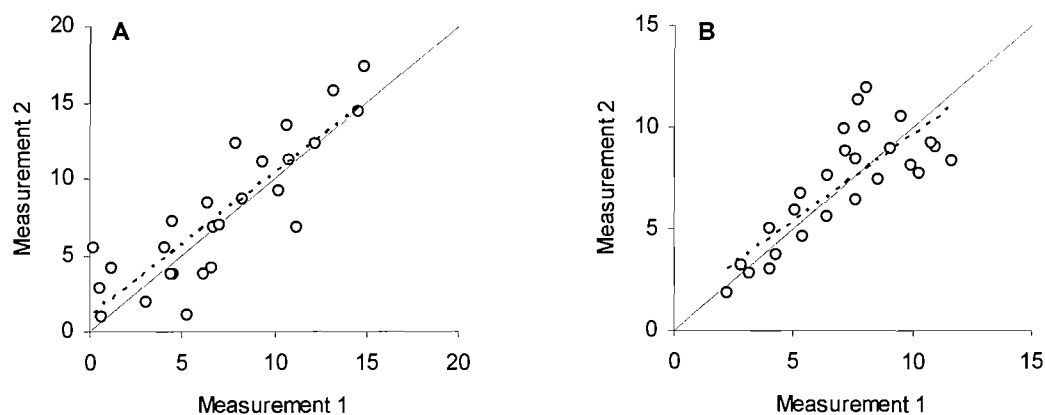
Figure 3.5.A. Random error is evident on a scatter diagram as increased scatter of the variables around the regression line. **B.** Heteroscedasticity (proportional error) is random error that increases in proportion to the magnitude of measurement and is distinguished by data points that progressively diverge or 'fan out' from a regression line fitted to the data. Line of equality (——). Regression line (- - -).

41

3.3.1 Correlation coefficients

Despite attracting widespread criticism, Pearson's (product moment) correlation coefficient (r) is frequently used in the medical literature to evaluate the precision of a measurement method (Atkinson and Nevill, 2000; Bruton et al., 2000; Ludbrook, 2002; Bland and Altman, 2003). Pearson's correlation coefficient measures the degree of linearity between two variables and describes how well a measurement Y (the second measurement in the context of a precision study) can be equated to another measurement X (the first measurement in the context of a precision study) by a transformation of the kind $Y = a + bX$ (Ludbrook, 1997; Schuck, 2004). Perfect linearity and hence perfect correlation is achieved if the variables lie on a straight line and is indicated by $r = +1$. If there is no linear relationship and the variables are randomly scattered and do not lie on a straight line, the value of r is close to zero. A P-value is typically quoted and tests the null hypothesis that $r = 0$, i.e. that there is no linear relationship (Bland and Altman, 1986; 1995).

In precision studies, an r-value that is close to $+1$ and significantly different from zero is interpreted as good agreement (Atkinson and Nevill, 2000). However, as stated earlier, for perfect agreement the variables must lie along the line of equality (Figure 3.3). In contrast, for perfect correlation the variables may lie along any straight line (Bland and Altman, 1986; 1995). Thus the problem with Pearson's r is that it is a measure of the degree of relationship/association and not the agreement between two variables and because of this it is unable to detect systematic bias (Kramer, 1981; Ludbrook, 1997; Bland, 2003; White, 2004). This means that a high correlation coefficient and significant P-value can be obtained when there is poor agreement between measurements (Bland and Altman, 1986; Ludbrook 2002; Bland, 2003; White, 2004).

To illustrate this, the correlation between the auto-CAT and manual-CAT (Table 3.2) was calculated ($r = .99$, P$=.000$). The high r value and significant P-value suggested good agreement and this was supported by a scatter diagram of the manual-CAT against the auto-CAT which demonstrated that the linear relationship between the two variables was clustered around the line of equality (Figure 3.6.A). A fixed bias of $2mm^2$ (represented by a, i.e. $Y = 2mm^2 + bX$) added to the manual-CAT values did not change the correlation between the auto-CAT and the manual-CAT ($r = .99$, P$=.00$) (Table 3.2) and continued to suggest good agreement. However, a scatter diagram of manual-CAT$+2mm^2$ against the auto-CAT clearly demonstrated that the measurements deviate

from the line of equality indicating poor agreement (Figure 3.7.A). Figure 3.7.B further illustrated that manual-CAT+2mm^2 was consistently different from the auto-CAT. The r-value did not change with the introduction of 2mm^2 fixed bias because the linear relationship between the two variables did not change. Thus although there was a strong relationship between the two measurements there was poor agreement, which illustrates that systematic bias does not affect correlation but does affect agreement.

Table 3.2. Correlation coefficients for the assessment of method agreement between the auto-CAT (AC) and manual-CAT (MC) for the measurement of synovial fold cross-sectional area (mm^2).

					Intraclass Correlation Coefficients (ICC's) r_1				
		Pearson's r			Absolute			Consistency	
Data sets	n	r	P-Value	R^2	(1,1)	(2,1)	(3,1)	(2,1)	(3,1)
ACMC	143	0.99	.000	0.99	0.99	0.99	0.99	0.99	0.99
ACMC+2 (additive)	143	0.99	.000	0.99	0.88	0.88	0.88	0.99	0.99
ACMCx2 (multiplicative)	143	0.99	.000	0.99	0.58	0.62	0.62	0.79	0.79
ACMCx2+2 (add & mult)	143	0.99	.000	0.99	0.23	0.41	0.41	0.79	0.79
ACMC (heteroscedasticity)	143	0.88	.000	0.78	0.88	0.88	0.88	0.88	0.88
ACMC (increased random error)	143	0.84	.000	0.71	0.84	0.84	0.84	0.84	0.84
ACMC (range 2 to 8.5mm^2)†	54	0.20	.15	0.04	0.18	0.18	0.18	0.18	0.18
ACMC (range 0 to 22mm^2)†	54	0.93	.000	0.86	0.93	0.93	0.93	0.93	0.93

† equal sample sizes with different ranges of values selected from the increased random error data set (Table A2.2, Appendix 2)

Similarly, when a proportional bias of 2mm^2 was multiplied to the manual-CAT values (i.e. $Y = a + 2mm^2 X$), the r-value remained the same (Table 3.2) because the linear association between the two variables had not changed but the variables deviated from the line of equality indicating poor agreement (Figure 3.8.A and 3.8.B). The effect of both fixed and proportional bias combined is demonstrated in Table 3.2 and Figures 3.9.A and 3.9.B.

Therefore Pearson's r merely indicates the scatter of variables around a regression line (line of best fit), regardless of whether the intercept or slope of that line differs from the line of equality (Ludbrook, 1997). It does no more than indicate the strength of linear association between the X and Y variables in a population and is of no value in detecting systematic bias between two measurements (Westgard and Hunt, 1973; Ludbrook, 1997; Bland and Altman 2003).
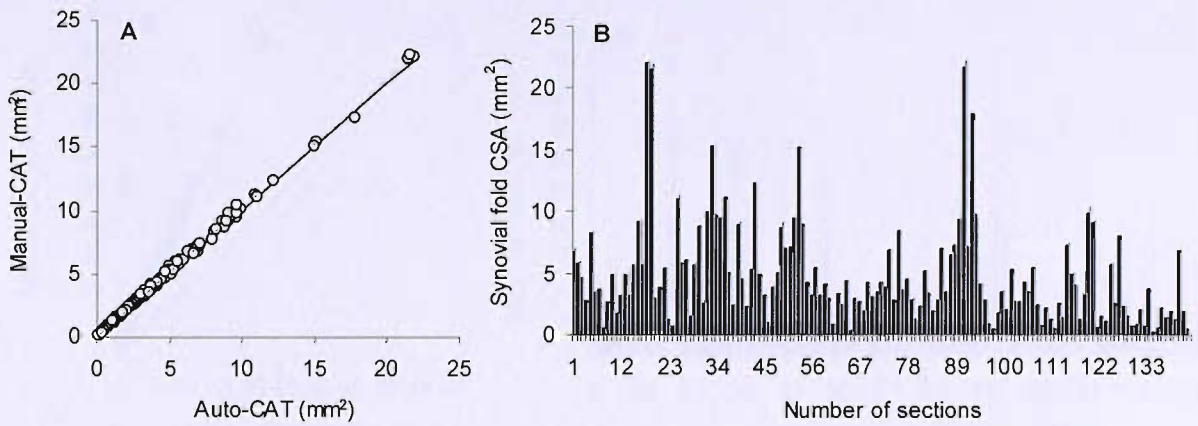
Figure 3.6.A. Auto-CAT and manual-CAT measurements of synovial fold cross-sectional area (CSA) (mm^2) with the regression line ($- - -$) Y = 1.01X + 0.03 and line of equality ($—$) Y = 1.0X + 0.0. **B.** Synovial fold CSA (mm^2) measurements by the auto-CAT (■) and manual-CAT (■).
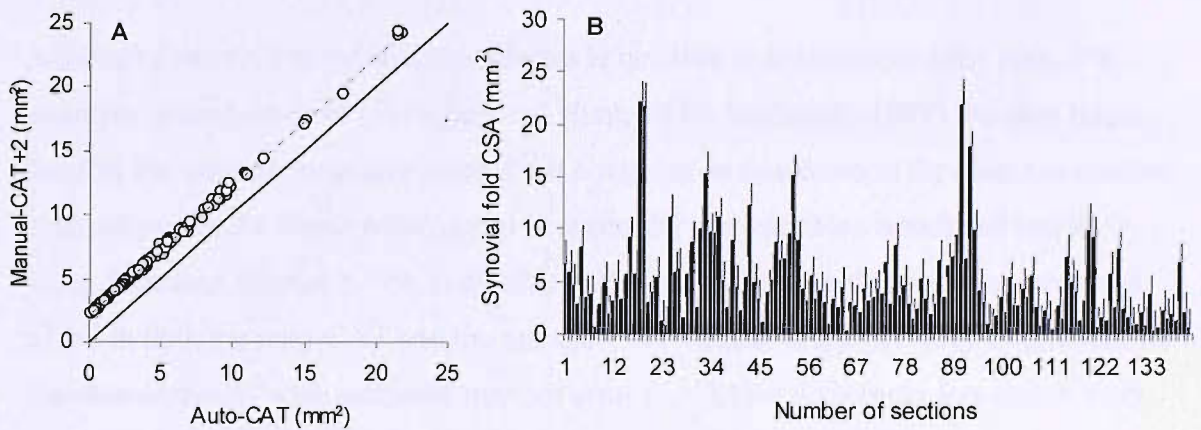
Figure 3.7. Fixed bias. **A.** Auto-CAT and manual-CAT+2mm^2 synovial fold cross-sectional area (CSA) measurements with the regression line ($- - -$) Y = 1.01X + 2.03 and line of equality ($—$) Y = 1.0X + 0.0. Fixed bias changes the intercept of the regression line. **B.** Synovial fold CSA measurements by the auto-CAT (■) and manual-CAT+2mm^2 (■).
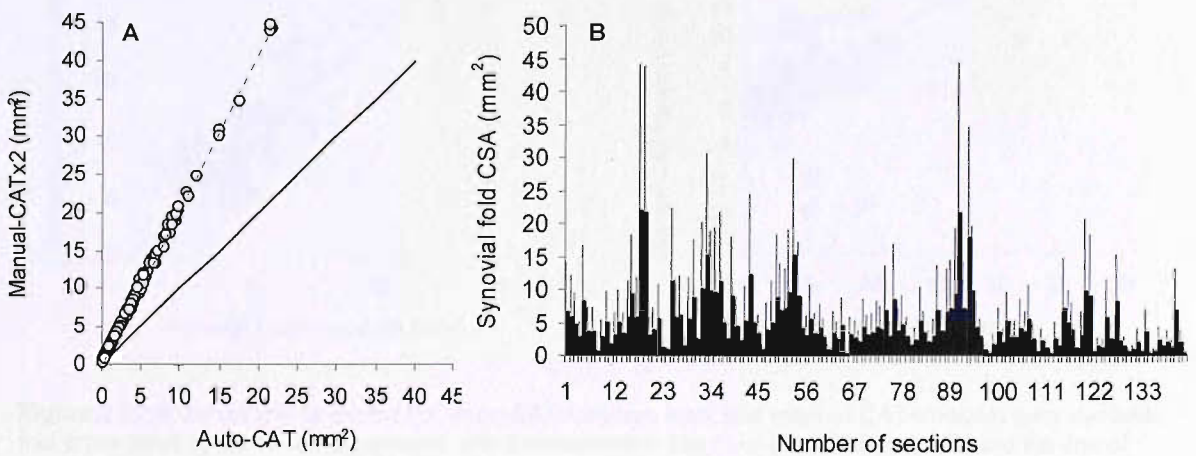
Figure 3.8. Proportional bias. **A.** Auto-CAT and manual-CATx2mm^2 synovial fold cross-sectional area (CSA) measurements with the regression line ($- - -$) Y = 2.03X + 0.06 and the line of equality ($—$) Y = 1.0X + 0.0. Proportional bias changes the slope of the regression line. **B.** Synovial fold CSA measurements by the auto-CAT (■) and manual-CATx2mm^2 (■).
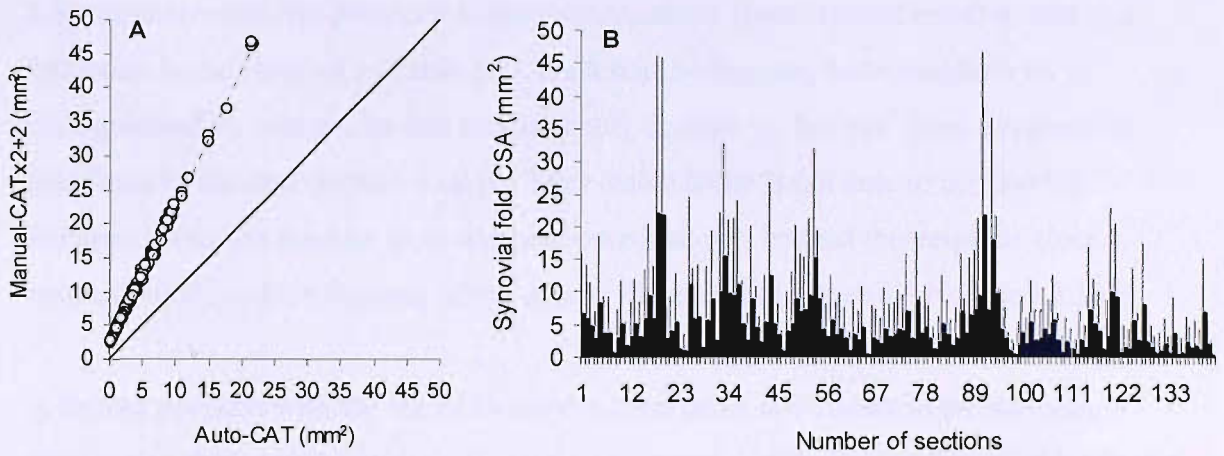
Figure 3.9. Fixed and proportional bias. **A.** Auto-CAT and manual-CATx2+2mm^2 synovial fold cross-sectional area (CSA) measurements with the regression line (- - -) Y = 2.03X + 4.06 and the line of equality (——) Y = 1.0X + 0.0. Fixed and proportional bias changes the intercept and the slope of the regression line. **B.** Synovial fold CSA measurements by the auto-CAT (■) and manual-CATx2+2mm^2 (■).

Although Pearson's correlation coefficient is not able to detect systematic bias, it is sensitive to random error (Westgard and Hunt, 1973; Ludbrook, 1997). As data points become increasingly scattered away from a regression line fitted to the data, i.e. random error increases, the linear relationship between the two variables is reduced and the *r*-value decreases (Figure 3.10A and Table 3.2). To demonstrate this, random error was added to both the auto-CAT and the manual-CAT values. The correlation coefficient for the measurements with increased random error (*r* = .84) is noticeably less than *r* = .99 calculated for the original data (Table 3.2).
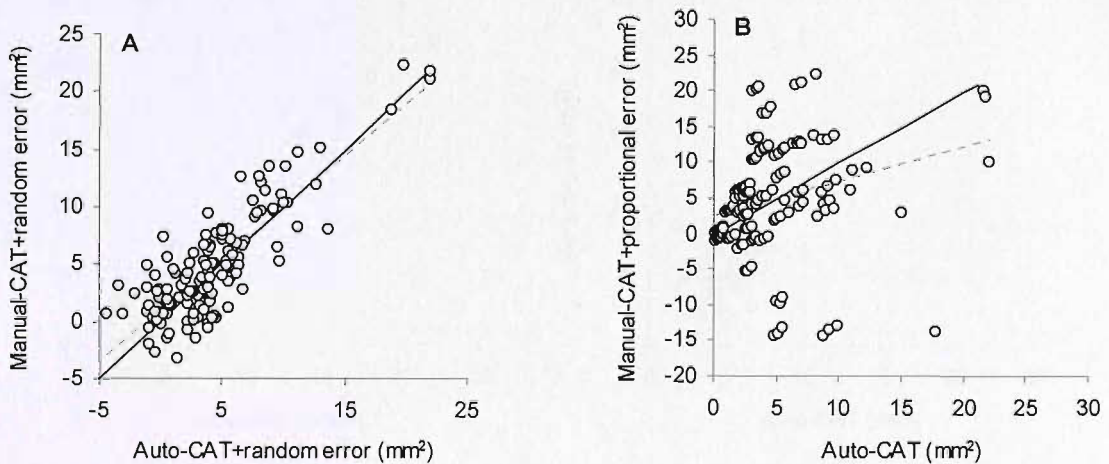
Figure 3.10.A. Increased random error. Auto-CAT+random error and manual-CAT+random error synovial fold cross sectional area measurements with the regression line (- - -) Y = 0.90X + 0.97 and the line of equality (——) Y = 1.0X + 0.0. **B.** Heteroscedasticity (proportional error). Auto-CAT and manual-CAT+proportional error synovial fold cross sectional area measurements with the regression line (- - -) Y = 0.48X + 2.61 and the line of equality (——) Y = 1.0X + 0.0.

45

Like random error, the presence of heteroscedasticity (proportional error) results in a reduction in the value of r (Table 3.2). On a scatter diagram, heteroscedasticity is distinguished by data points that progressively diverge or 'fan out' from a regression line fitted to the data (Figure 3.10.B). The r-value alone is not able to distinguish between increased random error and heteroscedasticity. Instead this requires close inspection of a scatter diagram of the data as illustrated in Figures 3.10.A and 3.10.B.

A further problem with the use of Pearson's correlation coefficient in the analysis of precision is that correlation depends on the range and distribution of the variables in the sample and hence on the way in which the sample of subjects was chosen (Bland and Altman, 1986; Bland and Altman, 2003; White, 2004). To illustrate this, the auto-CAT and manual-CAT data sets with increased random error were split into two ranges (2 to 8.5mm^2 and 0 to 22mm^2) of equal sample size (n=54). The scatter diagrams of these restricted ranges are shown in Figure 3.11.A and Figure 3.11.B. The correlation between the auto-CAT and the manual-CAT for data in the range 0 to 22mm^2 was $r = .93$, P=.000 compared to $r = .20$, P=.15 for data in the range 2 to 8.5mm^2 (Table 3.2). This example demonstrates that Pearson's correlation coefficient has the potential to be affected by the range and distribution of the sample under investigation. The greater the range of values in the sample, the higher the r-value; the narrower the range of values in the sample, the lower the value of r (Bland and Altman, 2003).
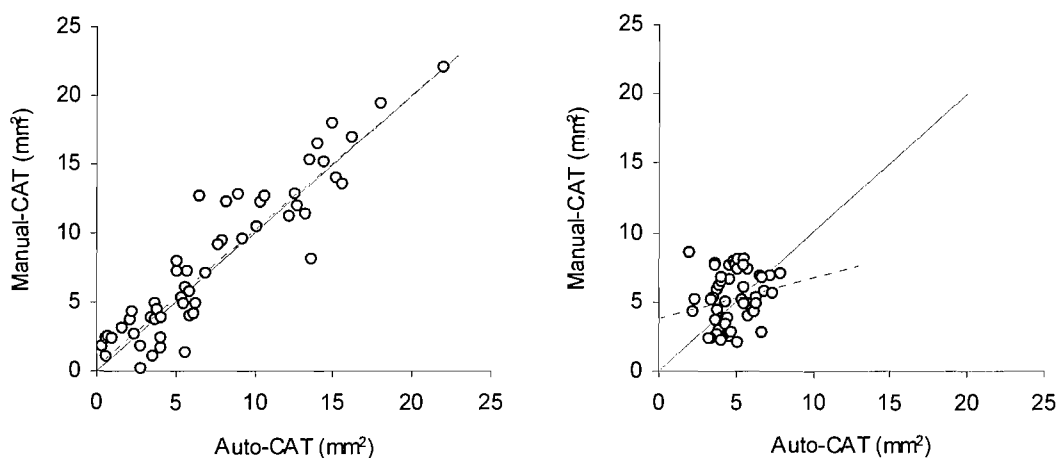
Figure 3.11.A. Auto-CAT and manual-CAT synovial fold cross-sectional area measurements within the range 0 to 22mm^2, with the regression line (- - -) Y = 0.99X + 0.43 and the line of equality (——) Y = 1.0X + 0.0. **B.** Auto-CAT and manual-CAT synovial fold cross-sectional area measurements within the range 2 to 8.5mm^2, with the regression line (- - -) Y = 0.29X + 3.81 and the line of equality (——) Y = 1.0X + 0.0.

In the study of precision, it is typically desirable to explore differences between measurements over a range of measurements rather than a representative sample with a

defined range of values. The dependence of the *r*-value on range may cause different investigators to calculate diverse *r*-values simply because their range of measurements was different thus limiting comparisons between studies (Westgard and Hunt, 1973). Since the *r*-value depends greatly on the range of values in a sample it is not appropriate for the study of precision unless the study population consists of a representative sample (Bland and Altman, 1986; Atkinson and Nevill, 1998; Bland and Altman, 2003).

Finally, Pearson's *r* is a single unit-free value that may range from -1 to +1. The *r*-value does not indicate the magnitude of disagreement between measurements and is not in the same units of scale as the original measurements thus it cannot be interpreted and applied clinically.

Therefore Pearson's correlation coefficient is widely regarded as an inappropriate indicator of measurement precision that should no longer be used for this purpose (Atkinson and Nevill, 1998; Bruton, 2000; Ludbrook, 2002). Pearson's *r* does no more than indicate the strength of linear association between the *X* and *Y* variables making it of no value in detecting systematic bias (Ludbrook, 1997; Atkinson and Nevill 1998; Bruton et al., 2000). The calculation of *r* alone, without exploration of the data using a scatter plot and line of equality, can lead to highly misleading inferences on the level of agreement and researchers should be cautious in extrapolating the results of measurement precision studies that have demonstrated good agreement using Pearson's correlation coefficient only (Atkinson and Nevill, 1998). Because Pearson's correlation coefficient is sensitive to random error, it has been suggested that it may be used when it has been demonstrated that there is no systematic bias present in the sample of interest. However, even in the absence of systematic bias, the correlation coefficient does not help to interpret the measurement of a given subject because the *r*-value does not quantify the size of measurement error in the scale of measurement used and because the value of *r* depends greatly on the range of variables in the study sample (Westgard and Hunt, 1973; Bland and Altman, 2003).

Conventionally used for the analysis of inter-examiner precision, the intra-class correlation coefficient (ICC) (r_I) is increasingly being used as a replacement to Pearson's correlation coefficient for the analysis of all types of measurement precision (Bruton et al., 2000). Like Pearson's *r*-value, an r_I-value that is close to +1 and significantly different from zero is interpreted as good agreement. The similarities and

differences between Pearson's correlation coefficient and the intra-class correlation coefficient are summarised in Table 3.3.

Table 3.3. Comparison between Pearson's correlation coefficient and the intra-class correlation coefficients (ICCs).

Pearson's correlation coefficient (r)	Intra-class correlation coefficients (r_i)
Inter-class bivariate correlation coefficient i.e. variables not required to share a common population variance nor possess the same metric (McGraw and Wong, 1996) (Schuck, 2004)	Intra-class univariate correlation coefficient i.e. variables assumed to share both a common population variance and possess a common metric (McGraw and Wong 1996; Schuck, 2004).
Calculates the degree of linearity (Y=a+bX). Perfect association can be computed even if the measurement pairs differ by an additive constant (a) and a multiplier constant (b) (McGraw and Wong, 1996; Schuck 2004)	Absolute ICCs Calculates the degree of identity (Y=X). Any departure from identity is regarded as error. Consistency ICCs Calculates the degree of additivity (Y=a+X). Perfect association can be computed even if the measurement pairs differ by an additive constant. (McGraw and Wong, 1996; Schuck, 2004)
Single unit-free value that ranges from +1 to -1	Single unit-free value that ranges from +1 to -1
Used for two groups only	Can be used for two or more groups
Depends on the range of measurements therefore population specific (Bland and Altman, 1990; Muller and Buttner, 1994).	Depends on the range of measurements therefore population specific (Bland and Altman 1990; Muller and Buttner, 1994).
Does not relate to the actual scale of measurement or the size of error which might be clinically allowable (Bland and Altman, 1990).	Does not relate to the actual scale of measurement or the size of error which might be clinically allowable (Bland and Altman, 1990).

ICCs are calculated from repeated measures analysis of variance (ANOVAs) and are defined according to study design and formula for calculating r_i (Figure 3.12): Case 1 (subject factor random), Case 2 (subject factor random; measurement factor random) and Case 3 (subject factor random; measurement factor fixed). Each Case can be further defined depending on whether measures are single (indicated as follows: Case 1 (1,1), Case 2 (2,1), Case 3 (3,1)) or an average of k repeated measures (indicated as follows: Case 1 (1,k), Case 2 (2,k), Case 3 (3,k)) and whether the Case has an absolute agreement definition of concordance (Cases 1, 2 and 3) or consistency definition of concordance (Cases 2 and 3). Thus there are at least 10 different ICC models derived from different sampling theories that are appropriate for different situations (Bruton et al., 2000; Schuck, 2004).

Different equations are used to calculate r_i for each model producing different numerical results and/or different interpretations of the results when applied to the same data (McGraw and Wong, 1996; Bruton 2000). This is illustrated in Table 3.2 where each of the data sets have been analysed using 5 different ICC models producing different r_i- values. In some cases, two different ICC equations applied to the same data set may produce the same r_i-value, however, the interpretation of the results is different.

For example, Case (2,1) and Case (3,1) produce the same results but Case (2,1) is for different examiners randomly selected from the population but Case (3,1) is for different examiners chosen from a defined/specified population. Unfortunately many researchers are not aware of the differences between the various ICC models and equations and fail to report which model they have used and the reasons for their choice (Shrout and Fleiss, 1979; Muller and Buttner, 1994; Rankin and Stokes, 1998). In order for other researchers to judge and interpret the results of ICC analysis, it is important for authors to clearly define the ICC model and equation used in their analysis (Rankin and Stokes, 1998).
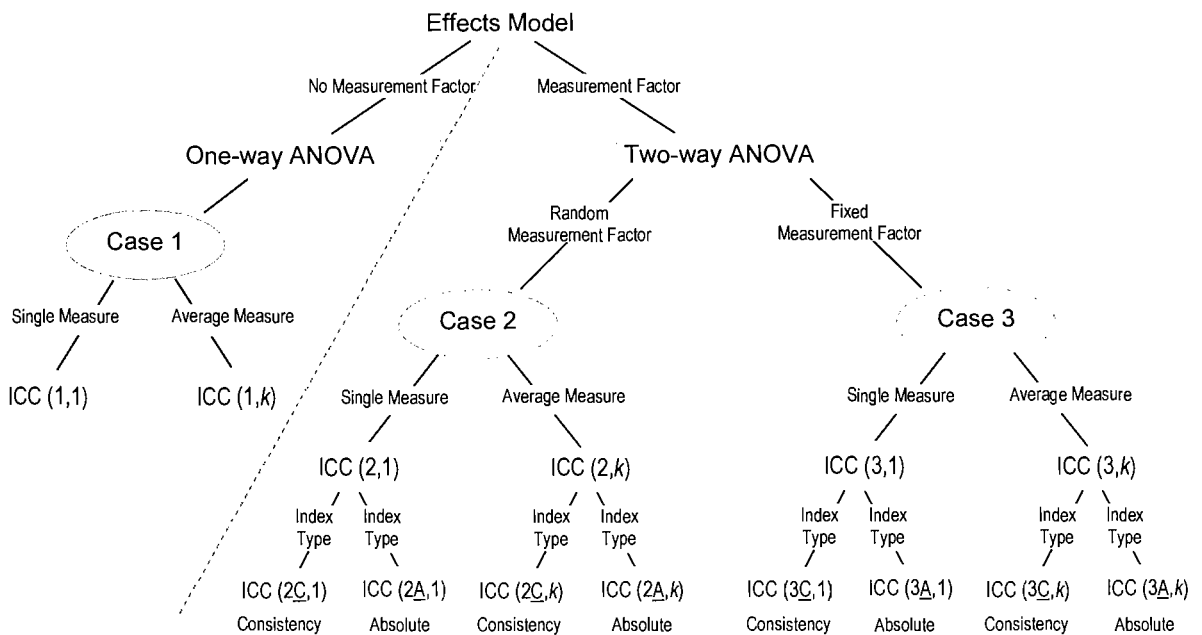
Figure 3.12. Flow chart for selecting an appropriate intra-class correlation coefficient model [note: the measurement factor may be observers, repeat tests, measurement methods etc.]. For more information on selecting an appropriate ICC model see McGraw and Wong (1996), Muller and Buttner (1994) and Schuck (2004). Devised by Rix (2005), used with permission.

The advantage of ICCs over Pearson's correlation coefficient is that ICCs avoid the problem of a linear relationship, i.e. the degree to which one variable Y can be equated to another variable X by a linear transformation ($Y = a + bX$), being mistaken for agreement (Figure 3.13) (Bland and Altman, 1990; McGraw and Wong 1996; Schuck, 2004). ICCs with absolute agreement definition of concordance capture the degree of identity, i.e. the degree to which one variable Y can be exactly equated to another variable X ($Y = X$) and so are sensitive to both fixed and proportional bias (i.e. systematic bias) (Schuck, 2004). Thus for all absolute ICC models the r_I-value decreases as a result of the addition and/or multiplication of 2mm^2 to the manual-CAT values whilst Pearson's r-value remains unchanged (Table 3.2).

ICCs with a consistency definition of concordance measure the degree of additivity, i.e. the degree to which one variable Y can be equated to another variable X by adding a constant ($Y = a + X$), and are sensitive to proportional bias but not fixed bias (Table 3.2) (McGraw and Wong, 1996; Schuck 2004). Therefore for ICC models with a consistency definition, r_l decreases with the multiplication of $2mm^2$ to the manual-CAT values whilst r remains unchanged but when $2mm^2$ is added to the manual-CAT values both r_l and r remain unchanged (Table 3.2). The r_l-values of both absolute and consistency ICCs decrease in response to the presence of random error in the same way that Pearson's r-value does and like Pearson's correlation coefficient a scatter diagram is required in order to distinguish heteroscedasticity from increased random error.
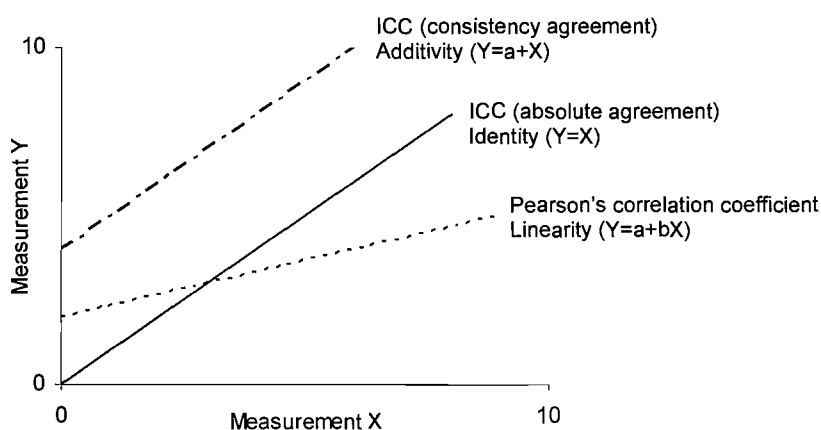
Figure 3.13. Agreement definitions for the correlation coefficients. Based on Schuck (2004).

Although ICCs avoid the problem of a linear relationship being mistaken for agreement, they are prone to some of the same constraints as Pearson's correlation coefficient in the context of precision studies (Atkinson and Nevill, 1998; Bland and Altman, 1990). Like Pearson's correlation coefficient, ICCs are dependent on the range of measurements (Atkinson and Nevill, 1998; Muller and Buttner, 1994). This is illustrated in Table 3.2 by comparing the ICC values of data with different ranges. The r_l-values are lower for measurements with the range 2 to $8.5mm^2$ compared to measurements ranging from 0 to $22mm^2$ (Table 3.2). Thus if there is little variability between subjects r_l will be low suggesting poor agreement (even if agreement is good) whilst if there is great variability between subjects correlation will be high implying good agreement (though agreement may be poor) (Bland and Altman 1995; Atkinson and Nevill 2000). The reason for this is that both ICCs and Pearson's correlation coefficient are ratios of the between-subjects variance (i.e. differences between measurements for different subjects) to the total

50

variance (i.e. between-subjects variance plus error) (Bland and Altman, 1990; Keating and Matyas, 1998; Rankin and Stokes, 1998). When r_I and r are high, most of the observed total variance is accounted for by the between-subjects variance and hence proportionately little variability is due to the error associated with the repeated measurements (Keating and Matyas, 1998). Therefore as the range of measurements obtained by individual subjects (i.e. the variance of subjects' measurements) increases the within-subject variance will represent proportionately less of the total variance and the coefficient will increase (Keating and Matyas, 1998; Rankin and Stokes, 1998). Because the ICC equation is affected by sample heterogeneity it is not possible to compare ICC values for samples or populations with different between-subject variance making ICCs inappropriate for the study of precision (Bland and Altman, 1990; Muller and Buttner, 1994; Rankin and Stokes, 1998).

Like Pearson's r, an ICC can vary between –1 and +1 with scores closer to +1 interpreted as reflecting increasing agreement in studies of precision (Atkinson and Nevill, 1998). Some ICCs may appear as negative values and it is not clear how these should be viewed or interpreted (Muller and Buttner, 1994). As with other correlation coefficients, there is no standard universally agreed cut-off point for acceptability (Bruton et al., 2000). Shrout and Fleiss (1979) recommend a minimum ICC value of +0.75 whilst Chinn (1991), Greenfield et al. (1990) and Wennerberg (1991) advocate ICC values of at least +0.6, >+0.8 and ≥+0.95, respectively. Vincent (1994) (in Atkinson and Nevill, 1998) recommends categories of agreement based on the ICC ranging from 'questionable' (+0.7 to +0.8) to 'high' (>+0.9). Because ICCs vary with the range of between-subject variance, a fixed cut-off point is incongruous (Bruton et al., 2000). Rather than specify a cut-off point it is more informative to state the 95% confidence intervals for a given ICC, however, confidence intervals also have limitations because they are affected by sample size (Bland and Altman, 1990; Atkinson and Nevill, 1998). A large sample size will result in narrower confidence intervals whilst a small sample size leads to wider confidence intervals (Bland and Altman 1990).

Both r and r_I are single, dimensionless values that are not related to the actual scale of measurement and do not quantify the size of the measurement error (Bland and Altman 1990; Muller and Buttner, 1994). Although it may appear convenient to have a single measure of agreement, a single r_I-value is not practical when cited on its own as it is an indicator of 'total error' and combines both systematic bias and random error into a

single coefficient (Atkinson and Nevill, 1998). Because r_I is unit-free and not related to the actual scale of measurement it gives no indication of the size of measurement error which might be clinically allowable (Bland and Altman, 1990).

Therefore, ICCs do not overcome all of the flaws of Pearson's correlation coefficient in the study of measurement error and should not be considered to be a suitable replacement. The only advantage of using an ICC in the study of precision is that it is the only form of analysis available for the determination of agreement between more than two measures (Muller and Buttner, 1994; Atkinson and Nevill, 1998).

3.3.2 Simple Linear Regression

Simple (ordinary or standard) linear regression is frequently used as a natural extension to Pearson's correlation coefficient in the determination of measurement precision. If a linear relationship between two measurements has been demonstrated by r then it seems logical to plot the observed X and Y values as a scatter diagram and calculate a regression line and equation to describe the nature of the relationship between the two measurements. Unlike Pearson's correlation coefficient, regression analysis is able to detect both systematic bias and random error and the output parameters from regression analysis can be used to quantify the magnitude of the systematic bias and random error in the same units of scale as the original measurements. However, some types of regression analysis are unsuitable for the determination of measurement agreement (Ludbrook 1997; Bland and Altman, 2003).

Like Pearson's r, regression analysis was not originally conceived as a measure of agreement between two data sets (Atkinson and Nevill, 1998). The intention of regression analysis is to make predictions for variables that demonstrate a linear relationship (Atkinson and Nevill, 1998). A predictive model is fitted to the data and the model is used to predict or estimate values of an outcome (dependent) variable Y from a known variable referred to as the predictor (independent) variable X (Field, 2005). When used for agreement studies, a model with good predictive power is equated with good agreement. The linear regression model is based on fitting a straight 'line of best fit' (known as the regression line) to a sample of X and Y variables to describe the predictive relationship between the two variables. The linear relationship can be summarised by the following equation (Bland, 2005):

$$Y = a + bX + E \qquad\qquad (3.1)$$

where Y is the outcome variable and X is the predictor variable. a and b are constants known as the regression coefficients that describe the intercept of the regression line fitted to the X and Y variables and the slope of that line, respectively. E is a random variable called the error and represents the difference between the observed measurement and the measurement value predicted by the regression line. It is used to calculate and fit a straight regression line that best describes the data with minimum error and is not reported when the regression equation is quoted, i.e. $Y = a + bX$.

The nature of the relationship and the predictive power of the model can be assessed using the following output parameters related to the regression line and its equation: the regression coefficients a and b, accompanied by confidence intervals and a test of significance, the coefficient of determination (R^2) and the 95% prediction intervals (Figure 3.14).
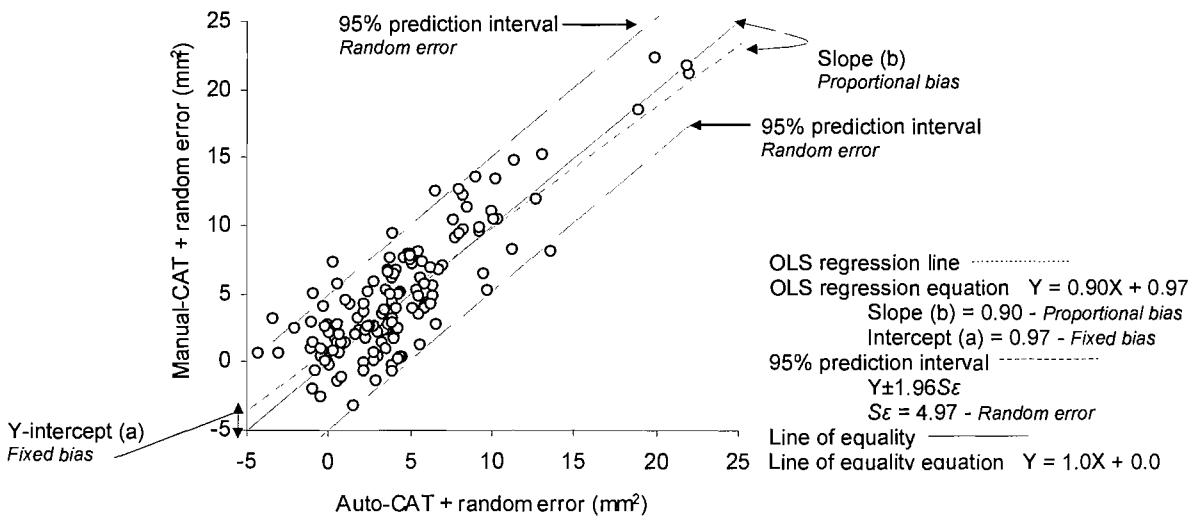
Figure 3.14. The output parameters related to the regression line and its equation as indicators of systematic bias and random error demonstrated by ordinary least squares regression of the manual-CAT+random error on the auto-CAT+random error for the measurement of synovial fold cross-sectional area (n=143). Random error causes no change in the slope and intercept of the regression line but $S\varepsilon$ reflects the magnitude of the random error. The slope of the regression line and the $S\varepsilon$ are not sensitive to fixed bias but the intercept reflects it exactly. Proportional bias does not affect the intercept and the $S\varepsilon$ but changes the steepness of the regression line and the exact magnitude of the proportional bias is quantified by the changes in its slope. Devised by Rix and Webb (2005), used with permission.

The slope of the regression line, b, represents the change in value of the outcome variable that results from a unit change in the predictor variable (Field, 2005). A slope that is significantly different from zero denotes a statistically significant relationship between the variables and indicates that the predictor variable contributes significantly to the estimation of values of the outcome variable (Field, 2005). In the assessment of

53

precision using regression analysis, proportional bias is indicated if the slope differs significantly from one or equivalently if the 95%CI of the slope does not include one, i.e. the slope of the regression line differs from the slope of the line of equality $Y = 0.0 + 1.0X$ (Ludbrook, 1997). This is illustrated in Table 3.4 where the addition of proportional bias does not affect the intercept, standard error of the estimate or R^2 but changes the slope of the regression line. The magnitude of the proportional bias is quantified by the change in the slope (b) (Table 3.4).

Table 3.4. Output parameters of ordinary least squares regression analysis for the assessment of method agreement between the auto-CAT (AC) and manual-CAT (MC) for the measurement of synovial fold cross-sectional area (mm^2).

| Data sets | n | Slope | | | Y-Intercept | | | R^2 | $S\varepsilon$ |
		b	95%CI	P-Value	a	95%CI	P-Value		
ACMC	143	1.01	1.01→1.02	< .01	0.03	-0.01→0.07	.16	0.99	0.16
ACMC+2 (additive)	143	1.01	1.01→1.02	< .01	2.03	1.99→2.07	< .01	0.99	0.16
ACMCx2 (multiplicative)	143	2.03	2.01→2.04	< .01	0.06	-0.02→0.14	.16	0.99	0.32
ACMCx2+2 (add & mult)	143	2.03	2.01→2.04	< .01	4.06	1.98→2.14	< .01	0.99	0.32
ACMC (increased random error)	143	0.90	0.80→0.99	< .01	0.97	0.38→1.55	< .01	0.71	2.54
ACMC (heteroscedasticity)	143	0.48	0.17→0.80	< .01	2.61	0.68→4.54	< .01	0.06	7.68
ACMC (range 2 to 8.5mm²)†	54	0.29	-0.11→0.69	.15	3.81	1.81→5.81	< .01	0.04	1.91
ACMC (range 0 to 22mm²)†	54	0.99	0.88→1.09	<0.01	0.43	-0.58→1.43	.40	0.86	2.06

† equal sample sizes with different ranges of values selected from the increased random error data set (Table A2.2, Appendix 2)

The regression coefficient a, is the intercept of the outcome variable when the predictor variable equals zero. The intercept is used as a measure of fixed bias in measurement precision studies. If the intercept differs significantly from zero or if the 95%CI of the intercept does not cross zero, i.e. the intercept of the regression line differs from the intercept of the line of equality $Y = 0.0 + 1.0X$, then this indicates the presence of fixed bias (Table 3.4) (Ludbrook, 1997). Thus it can be seen from the data presented in Table 3.4 that the slope, standard error of the estimate and R^2 are not sensitive to fixed bias but the intercept reflects it exactly.

The dimensionless coefficient of determination (R^2) measures the relative strength of the regression model. When expressed as a percentage it represents the amount of variance of the outcome variable that can be accounted for by its linear relationship with the predictor variable. R^2 is the square of the correlation coefficient r and like r is sensitive to random error but not systematic bias (Table 3.4). Thus the use of R^2 alone as an indicator of measurement precision is not appropriate.

Finally, the 95% prediction intervals represent the area in which you would expect 95% of the data points to fall and are a better measure of random error than R^2 as the prediction intervals quantify the random error in the same units of scale as the original measurements. The 95% prediction intervals represent the predicted value of:

$$Y \pm 1.96S\varepsilon \; ([Y = bX + a] \pm 1.96S\varepsilon) \tag{3.2}$$

where $S\varepsilon$ (or Sy) is the standard error of the estimate (or standard deviation of the predicted values) and represents the spread of scores about the regression line in the same way that the standard deviation is a spread of scores about the mean. Thus $S\varepsilon$ directly quantifies the random error (Table 3.4). The 95% prediction intervals are considered analogous to the Bland and Altman 95% limits of agreement (Bland and Altman, 2003).

There are two different types of simple linear regression analysis typically used in the assessment of measurement precision, ordinary least squares regression and ordinary least products regression. Both models are based on similar assumptions and share the same output parameters (described above), however, one is appropriate for the determination of precision and the other is not.

Ordinary least squares regression analysis is a type of Model I regression in which the sum of the squares of the vertical deviations of the observed Y values from the regression line (Y residuals, represented by ΔY in Figure 3.15.A) are minimised (Figure 3.15.A) (Ludbrook, 1997). Thus one of the assumptions of ordinary least squares regression is that the values of Y (outcome variable) are attended by random error but the values of X (predictor variable) are fixed in advance and without random error, i.e. E in Equation 3.1 reflects only the vertical deviations (ΔY in Figure 3.15.A) of the X,Y data points from the regression line. This assumption is rarely fulfilled in studies of precision because both the Y and X values (i.e. both measurements) are likely to be attended by random error (Altman and Bland, 1983). For an ordinary least squares regression line fitted to data with random error in both Y and X, the random error in X will reduce the slope of the regression line below one and so raise the lower end of the line and lower the upper end of the line causing the intercept to increase above zero (Altman and Bland, 1983; Ludbrook, 1997; Bland and Altman, 2003). This may falsely suggest the presence of proportional and/or fixed bias and is particularly a problem when the random error is large and when measurements are made over a narrow range

of values located some distance from zero. This is illustrated in Table 3.4 where the addition of random error causes the slope to decrease from 1.01 to 0.90 and the intercept to increase from 0.03 to 0.97; and the slope decreases from 0.99 to 0.29 and the intercept increases from 0.43 to 3.81 when the range of data is reduced from 0 to 22 mm^2 to 2 to $8.5mm^2$ (Ludbrook, 1997).

A second limitation to ordinary least squares regression is that two different regression lines and equations can be computed depending on which measurement is selected as the predictor variable and which measurement is designated as the outcome variable (Figure 3.15.B) (Ludbrook, 2002). For one regression line, the sum of the squared Y residuals is minimised and for the other regression line the sum of the squared X residuals is minimised (Figure 3.15.B). Neither line is appropriate for the determination of measurement precision because both measurements are attended by random error and neither measurement is likely to provide the 'true' value (Ludbrook, 2002). It is worth noting that in some studies of method agreement, one measurement method is treated as the 'gold standard' and assumed to measure the 'true' value. However, it is unlikely that any medical measurements are made without any error whatsoever (Bland and Altman, 1995).
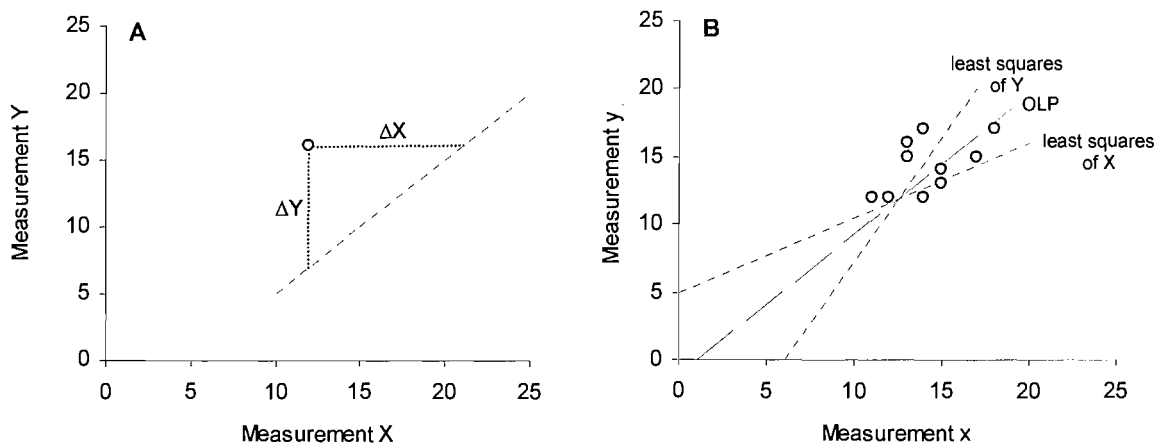
Figure 3.15.A. Techniques of regression analysis. ΔX is the horizontal distance of the XY point from the regression line. ΔY is the vertical distance of the XY point from the regression line. The functions that can be minimised include ordinary least squares regression $\sum(\Delta Y)^2$, ordinary least squares regression $\sum(\Delta X)^2$ and ordinary least product regression $\sum(\Delta Y)(\Delta X)$. Based on Ludbrook (1997). **B.** Model I and model II regression lines using hypothetical data. Model I regression by ordinary least squares of Y (- - -) and ordinary least squares of X (- - -). Model II regression by ordinary least products (OLP) (— — —). Based on Ludbrook (1997).

Ordinary least products regression analysis (also known as reduced major axis regression, standardised principal component regression, geometric mean regression) is a type of Model II regression analysis that is designed for situations in which both the Y and X variables are attended by random error and it is impossible to decide which

56

variable should be designated as the outcome variable. In ordinary least products regression, the sum of the products of the vertical (ΔY in Figure 3.15.A) and horizontal (ΔX in Figure 3.15.A) deviations of the X,Y values (i.e. the X and Y residuals) from the regression line are minimised, i.e. $\sum(\Delta Y)(\Delta X)$ (Fig 3.15.A). Thus in Model I there are two regression lines that could describe the XY relationship whilst in Model II there is only one regression line which is sometimes referred to as 'the line of symmetry' (Figure 3.15.B). Therefore it does not matter which measurement is designated as the predictor variable or outcome variable as the two measurements can be interchanged (Ludbrook, 2002). Consequently, when both measurements are attended by random error, ordinary least products regression is more a suitable approach for the determination of precision than ordinary least square regression. However, there are some limitations to the ordinary least products regression approach.

Like the correlation coefficients, ordinary least products (and ordinary least squares) regression is affected by sample heterogeneity. Comparing the regression output parameters for the data sets with different ranges (0 to 22 mm^2 compared to 2 to 8.5mm^2) it is apparent that the slope (b), Y-intercept (a) and R^2 are affected by the range of measurements but the standard error of the estimate ($S\varepsilon$) is not (Table 3.4). The output parameters suggest good agreement with greater sample heterogeneity and poor agreement with greater sample homogeneity. Thus sample heterogeneity may result in inaccurate conclusions regarding the systematic bias of a measurement and create problems for the extrapolation of the results of regression analysis.

One assumption that underlies ordinary least products (and ordinary least squares) regression analysis is that the scatter of values around the regression line is constant over the whole range of measurements (homoscedasticity) (Ludbrook, 2002). However, in biological studies it is common to observe increasing scatter (random error) as the values of X and Y increase (i.e. heteroscedasticity or proportional error) (Figure 3.10.B). Heteroscedasticity reduces the value of R^2 (Table 3.4) and widens the 95% prediction intervals (indicated by an increase in $S\varepsilon$ in Table 3.4). A violation of the assumption of homoscedasticity can be overcome by log transformation of the data or weighted least products regression analysis (Ludbrook, 1997; 2002).

Finally, whilst ordinary least squares regression analysis is widely available on a range of different statistical software packages and is relatively simple to perform, ordinary

least products regression is difficult to find within statistical software packages and is an uncommon method of precision analysis in the literature. The ordinary least products regression coefficients can be calculated by hand, however, calculating the 95% confidence intervals for the coefficients can be difficult (Ludbrook, 1997). For the calculation of ordinary least products regression the reader is referred to Ludbrook (1997).

Thus in studies of measurement precision where both measurements are likely to be attenuated by random error, ordinary least products regression rather than ordinary least products regression is regarded as the most suitable method of analysis. The regression parameters slope, Y-intercept and standard error of the estimate provide specific estimates of proportional bias, fixed bias and random error, respectively, in the same units of scale as the original measurement. Homoscedasticity can be checked by graphical presentation of the data and alternative methods of analysis are available when the assumption of homoscedasticity is violated. The major limitation of regression analysis is that the regression parameters that provide estimations of systematic bias are affected by the range of measures.

3.3.3 Paired t-test

The paired t-test is another widely but inappropriately used method of analysing precision. In measurement error studies the paired t-test tests the null hypothesis that the mean difference between the measurements is zero (Bland and Altman, 1995). The t-test is usually interpreted by comparing the calculated value with the "critical" value found in a statistics table. When the calculated t-value is larger than the critical value (i.e. significant difference) it is generally concluded that the difference between the two measurements is large and that the agreement between the two measurements is poor (Westgard and Hunt, 1973). Conversely, when the calculated t-value is smaller than the critical value (i.e. no significant difference) it is typically deduced that the measurements agree well (Westgard and Hunt, 1973; Bland, 2005). The validity of such judgments may be erroneous when based on the t-value alone because t is the ratio of the fixed bias to the random error and is calculated as follows (Westgard and Hunt, 1973; Field, 2005):

$$t = \frac{\text{mean difference } (d) - \text{expected difference between population means } (\mu_d)}{\text{standard error of the differences } (s_d/\sqrt{n})} \qquad (3.3)$$

where the mean difference (*d*) is an estimate of the fixed bias and the standard deviation of the differences (s_d) is an estimate of the random error. Thus the *t*-value alone only provides information on the relative magnitude of the fixed bias and random error terms. What is most important for judging the agreement between two measurements is the individual assessment of the fixed bias and random error terms represented by the *t*-test parameters, *d* and s_d, respectively (Westgard and Hunt, 1973).

From Table 3.5 it is evident that s_d is not sensitive to fixed bias but reflects the magnitude of random error whilst *d* does not change with the addition of random error but reflects exactly the amount of fixed bias. Therefore a more appropriate means of using the *t*-test in the study of measurement error is to present all of the *t*-test parameters and not just the *t*-value alone. However, *d* and s_d only provide estimates of fixed bias and random error, respectively, when proportional bias is absent as the presence of proportional bias causes both *d* and s_d to increase (Table 3.5) (Westgard and Hunt, 1973). The *t*-test parameters therefore are not useful in estimating proportional bias and furthermore should not be used when proportional bias is present because they do not provide specific estimates of fixed bias and random error in this situation (Westgard and Hunt, 1973). Unlike the correlation coefficients and regression parameters, *d* and s_d are not affected by the range of the data. This is demonstrated in Table 3.5 by comparing the *d* and s_d values for data in the range 2 to 8.5mm^2 and 0 to 22mm^2.

Table 3.5. *t*-test parameters for the assessment of method agreement between the auto-CAT (AC) and manual-CAT (MC) for the measurement of synovial fold cross-sectional area (mm^2).

Data sets	n	d	s_d	SE	95%CI	t	P-Value
ACMC	143	-0.88	0.17	0.14	-0.12→ -0.06	-6.31	< .01
ACMC+2 (additive)	143	-2.88	0.17	0.14	-2.12→ -2.06	-149.7	< .01
ACMCx2 (multiplicative)	143	-4.86	4.21	0.35	-5.55→ -4.16	-13.81	< .01
ACMCx2+2 (add & mult)	143	-6.86	4.21	0.35	-7.55→ -6.16	-19.50	< .01
ACMC (increased random error)	143	-0.52	2.57	0.22	-0.95→ -0.96	-2.42	< .05
ACMC (heteroscedasticity)	143	-0.20	7.94	0.66	-1.51→ 1.11	-0.30	.76
ACMC (range 2 to 8.5mm²)†	54	-0.36	2.11	0.29	-0.94→ 0.22	-1.26	.21
ACMC (range 0 to 22mm²)†	54	-0.31	2.05	0.28	-0.87→ 0.25	-1.12	.27

† equal sample sizes with different ranges of values selected from the increased random error data set (Table A2.2, Appendix 2)

There are at least four situations in which erroneous judgments may be made by considering the *t*-value alone (Westgard and Hunt, 1973; Atkinson and Nevill, 1998; White, 2004):

(Note: Examples 1 & 2 are based on artificial data; Examples 3 & 4 are based on data from Table A2.1 in Appendix 2).

1. The *t*-value may be small when the fixed bias is small and the random error is large (Figure 3.16.A). The means of the two measurements are approximately equal (i.e. small mean difference/fixed bias) and there is no significant difference between the measurements (i.e. small *t*-value) which implies good agreement. However, the standard deviation of the difference (random error) between the measurements is large indicating poor agreement (Figure 3.16.A).

2. The *t*-value may be small when both the fixed bias and the random error are large (Figure 3.16.B). There is no significant difference between the measurements (i.e. small *t*-value) which would suggest good agreement. However, the means of the two measurements are not equal (i.e. large mean difference/fixed bias) and the standard deviation of the difference (random error) between the repeated measurements is large indicating poor agreement (Figure 3.16.B).
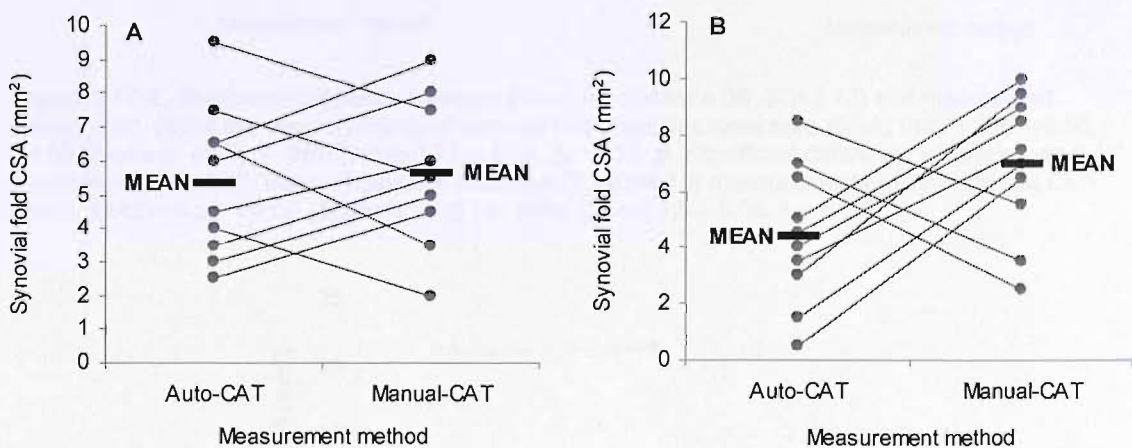
Figure 3.16.A. No significant difference between auto-CAT (mean=5.35, SD=2.22) and manual-CAT (mean=5.65, SD=2.11) artificial measurements of synovial fold cross-sectional area (CSA) (mm²). t(9)=-0.43, P=.68 (2-tailed), d=-0.30, 95%CI(d)=-1.89→1.29, s_d =2.23. **B.** No significant difference between auto-CAT (mean=4.40, SD=2.47) and manual-CAT artificial measurements of synovial fold CSA (mm²) (mean=6.95, SD=2.51). t(9)=-1.90, P=.09 (2-tailed), d=-2.55, 95%CI(d)=-5.59→0.49, s_d = 4.25.

3. The *t*-value may be large when both the fixed bias and the random error are small (Figure 3.17.A). There is a significant difference between the measurements (i.e. large *t*-value) which would suggest poor agreement. However, the means of the two

60

measurements are approximately equal (i.e. small mean difference/fixed bias) and the standard deviation of the difference (random error) between the repeated measurements is small indicating good agreement (Figure 3.17.A).

4. The *t*-value may give different values for given error levels if the sample size varies. An increase in the sample size (n) causes an increase in the *t*-value and reflects the decrease in the standard error of the differences in the *t*-test formula. The consequences of this may be the acceptability of measurement agreement being related to sample size the inference of which is acceptable agreement with low sample sizes (Figure 3.18) and unacceptable agreement with large sample sizes (Figure 3.17.B).
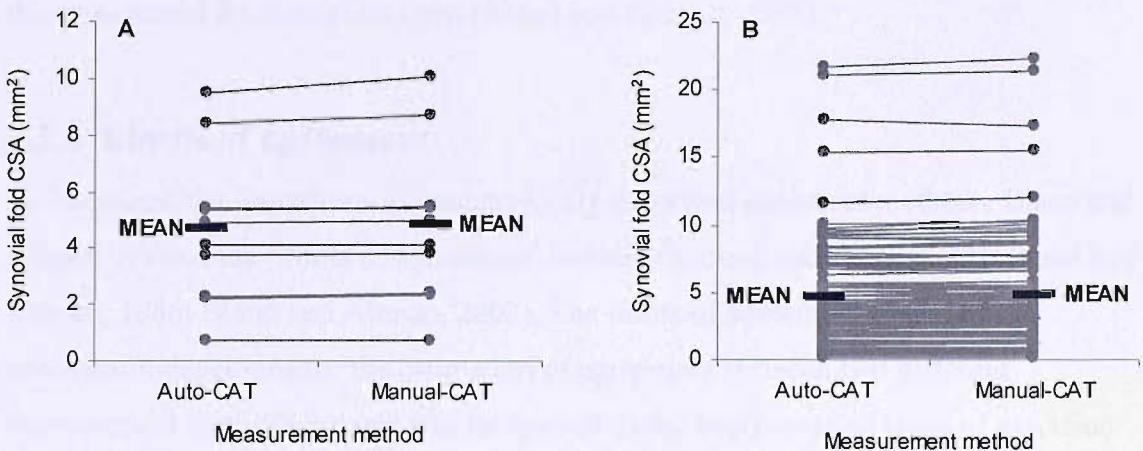
Figure 3.17.A. Significant difference between auto-CAT (mean=4.66, SD=2.72) and manual-CAT (mean=4.80, SD=2.86) measurements of synovial fold cross-sectional area (CSA) (mm^2). t(9) =-2.60, P=.03 (2-tailed), d=-0.15, 95%CI(d)=-0.27→-0.02, s_d =0.18. **B.** Significant difference between auto-CAT (mean=4.68, SD=4.10) and manual-CAT (mean=4.77, SD=4.15) measurements of synovial fold CSA (mm^2). t(142)=-6.31, P=.00 (2-tailed), d=-0.09, 95%CI(d)=-0.12→-0.06, s_d= 0.17.
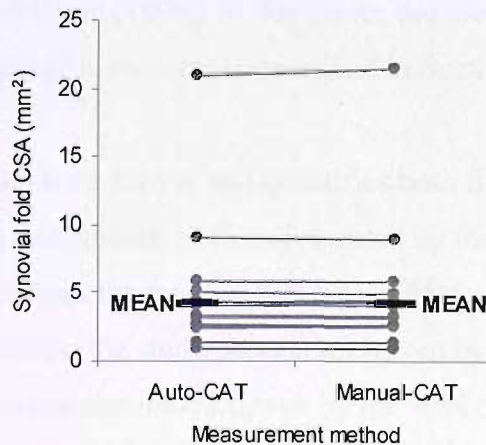
Figure 3.18 No significant difference between auto-CAT (mean=4.20, SD=4.25) and manual-CAT (mean=4.24, SD=4.32) measurements of synovial fold cross-sectional area (CSA) (mm^2). t(20)=-1.51, P=.15 (2-tailed), d=-0.04, 95%CI(d)=-0.09→0.15, s_d = 0.12.

61

Thus, the paired t-test using the t-value alone is not appropriate for the determination of precision because it may lead to the wrong conclusions regarding whether agreement is good or poor (Bland and Altman 1995; Bruton et al., 2000). The t-test can be used to provide specific estimates of fixed bias and random error but only when proportional bias is absent. Consequently, in practice when the t-test is applied, regression analysis should also be performed to determine whether proportional bias is present and whether the t-test parameters do represent specific estimates of errors (Westgard and Hunt, 1973). However, this seems to be a rather long-winded approach when other more comprehensive forms of analysis are available. The terms in the formula for the t-value can be used in a different approach for assessing measurement precision, the Bland and Altman limits of agreement method, described later. Analysis of variance (ANOVA) with repeated measures is not suitable for the study of precision for the same reasons as those presented for the paired t-test (Bland and Altman, 1995).

3.3.4 Limits of agreement

To overcome the limitations of the previously described statistical methods, Bland and Altman devised the 'limits of agreement' method (Altman and Bland, 1983; Bland and Altman, 1986; Bland and Altman, 2003). The limits of agreement method was specifically developed for the estimation of agreement between two different measurement methods but can also be applied to the analysis of all types of precision (Bland and Altman, 2003). The Bland and Altman method of analysis has evolved since first being published in 1983 (Altman and Bland, 1983) with some extensions and additions to the original method in later publications (Bland and Altman, 1999). The most current and comprehensive description of the Bland and Altman method can be found in Bland and Altman (1999). In this thesis, the method of analysis for determining the limits of agreement is described in Section 4.2.3iii.

Bland and Altman analysis detects and quantifies both fixed bias (represented by the mean difference, d) and random error (represented by the standard deviation of the difference, s_d) and defines the range within which 95% of the differences between measurements will lie for the study population (given by the 95% limits of agreement, $d \pm 1.96 s_d$) and the whole population (given by the 95% confidence intervals of the limits of agreement). Provided that the differences within the observed limits of agreement are not deemed to be clinically important then the measurement is regarded as having adequate precision (Bland and Altman, 1999). This approach is superior to the

use of a single dimensionless correlation coefficient because the magnitude of measurement error is quantified in the same units of scale as the original measurements and systematic bias and random error are identified and quantified separately (Bland and Altman, 1990; Atkinson and Nevill, 1998; Keating and Matyas, 1998).

A scatter diagram of the difference (between the two measurements) against the mean (of the two measurements) is plotted to expose possible relationships between the difference and the mean (including proportional bias and heteroscedasticity) and to demonstrate any extreme or outlying measurements (Rankin and Stokes, 1998; Bland and Altman, 1999). In precision studies the true value of the quantity being measured is typically not known so the mean of the measurements is used as the best estimate of the true value (Bland and Altman, 1995; 1999). A scatter diagram of the difference versus the mean is more likely to expose possible relationships and trends in the data compared to a scatter diagram of one measurement against the other because the scale of the y-axis (difference) has a small unit size compared to the scale of the x-axis (mean). This is evident on comparison of Figures 3.19.A and 3.19.B where the scatter diagram of the auto-CAT versus the manual-CAT (Figure 3.19.A) does not indicate the presence of heteroscedasticity but the scatter diagram of difference versus mean does (Figure 3.19.B).

A one sample t-test, testing the hypothesis that the mean difference equals zero, is used to test for the presence of fixed bias (referred to as 'relative' bias by Altman and Bland, 1983). The presence of fixed bias is indicated by a mean difference (d) significantly different to 0 or a 95% confidence interval for the mean difference for the population that does not include zero. Fixed bias is directly quantified by the value of d. This is illustrated in Table 3.6 and Figure 3.20 with the addition of $2mm^2$ to the manual-CAT values.

To examine for potential proportional bias, Bland and Altman (1999) recommend calculating Pearson's correlation coefficient (between the differences and the mean) and testing the null hypothesis that $r = 0$ (or alternatively testing that the slope of the regression line of differences on means equals 0) in conjunction with an examination of the difference versus mean scatter diagram (Altman and Bland, 1983). The presence of proportional bias is indicated by $r \neq 0$, P<.05 (or a regression slope that differs significantly from 0) and an increasing between-measurement difference as the

magnitude of the measurement increases on the scatter diagram (Figure 3.21.B) (Bland and Altman 1995; 2003). The presence of proportional bias causes both d and s_d to increase thus affecting the quantification of fixed bias and random error, respectively (Table 3.6). If proportional bias is ignored the analysis will still give limits of agreement that include the majority of differences but the limits of agreement will be crude estimates that widen in direct relation to the degree of proportional bias (Bland and Altman, 1999). A proportional bias will almost inevitably cause d to deviate from zero. For example, manual-CAT multiplied by 2mm^2 causes d to increase from -0.09 to -4.86mm^2 (Table 3.6). Thus with proportional bias present there is the risk that fixed bias will be over-diagnosed (Ludbrook, 1997; 2002). If there is proportional bias in one direction and fixed bias is in the opposite direction then d may be close to zero and fixed bias will be under-diagnosed (Ludbrook, 1997; 2002).

The influence of proportional bias on fixed bias and random error is one of the major criticisms that Ludbrook (2002) has directed at the Bland and Altman method, however, Bland and Altman (1999) do emphasise the importance of checking the assumptions of the limits of agreement method and stipulate that if a proportional bias is present then this should be corrected for by either logarithmic transformation of the raw data or a modified regression approach (Table 3.7). These corrections will remove the influence of a proportional bias on the fixed bias and random error and the modified regression approach will quantify the proportional bias in the same units of scale as the original measurements.

Table 3.6. Limits of agreement parameters for the assessment of method agreement between the auto-CAT (AC) and manual-CAT (MC) for the measurement of synovial fold cross-sectional area (mm^2).

Data sets	n	d	95%CI	1.96s$_d$	LoA	95%CI LoA
ACMC	143	-0.09	-0.11→-0.06	0.33	-0.41→0.24	-0.46→-0.37; 0.19→0.29
ACMC+2 (additive)	143	-2.09	-2.12→-2.06	0.33	-2.41→-1.76	-2.46→-2.37; -1.71→-1.81
ACMCx2 (multiplicative)	143	-4.86	-5.55→-4.17	8.23	-13.10→3.39	-14.28→-11.92; 2.20→4.56
ACMCx2+2 (add & mult)	143	-6.86	-7.55→-6.17	8.27	-15.14→1.41	-16.32→-13.96; 0.22→2.59
ACMC (increased random error)	143	-0.52	-0.94→-0.10	5.04	-3.09→2.05	-3.81→-2.37; 1.33→2.77
ACMC (heteroscedasticity)	143	-0.12	-0.44→0.21	3.90	-2.10→ 1.11	-1.55→-2.66; 1.31→2.43
ACMC (range 2 to 8.5mm^2)†	54	-0.36	-0.94→0.21	4.14	-2.48→1.75	-3.44→-1.51; 0.79→2.72
ACMC (range 0 to 22mm^2)†	54	-0.31	-0.87→0.25	4.02	-2.36→1.74	-3.30→-1.43; 0.80→2.68

† equal sample sizes with different ranges of values selected from the increased random error data set (Table A2.2, Appendix 2)
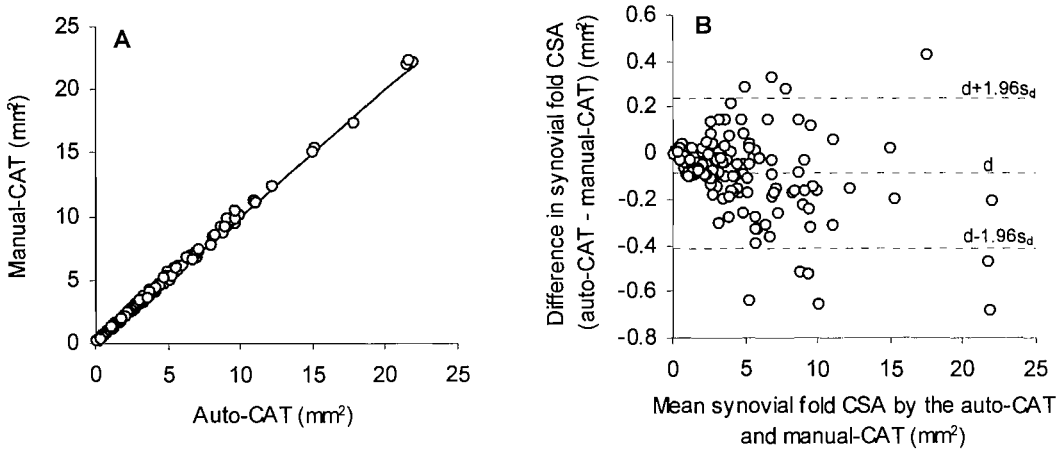
Figure 3.19.A. Scatter diagram of the manual-CAT against the auto-CAT measurements of synovial fold cross-sectional area (CSA) (mm^2) with the line of equality (——). **B.** Scatter diagram of the difference between the auto-CAT and manual-CAT against the mean of the auto-CAT and manual-CAT measurements of synovial fold CSA (mm^2) with lines representing the mean difference (d) and limits of agreement (d±1.96s_d).
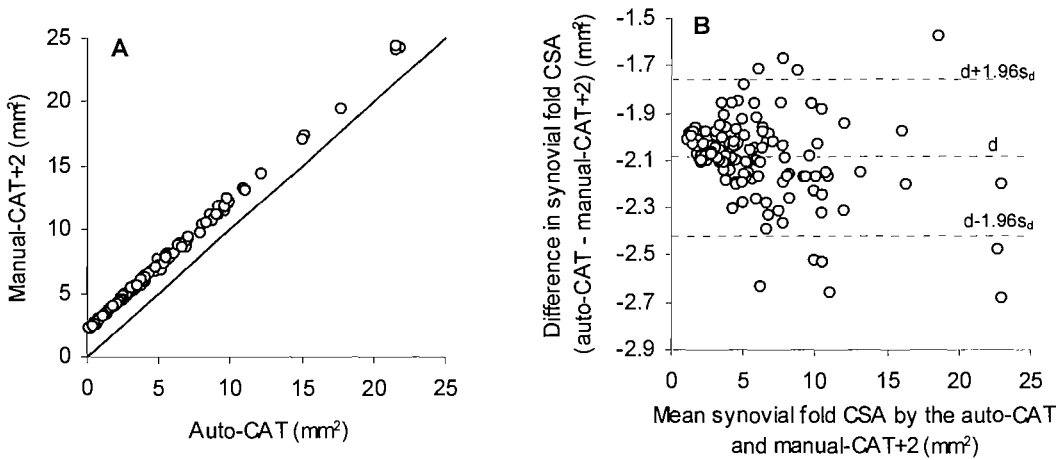
Figure 3.20. Fixed bias. **A.** Scatter diagram of the manual-CAT+2mm^2 against the auto-CAT measurements of synovial fold cross-sectional area (CSA) (mm^2) with the line of equality (——). **B.** Scatter diagram of the difference between the auto-CAT and manual-CAT+2mm^2 against the mean of the auto-CAT and manual-CAT+2mm^2 measurements of synovial fold CSA (mm^2) with lines representing the mean difference (d) and limits of agreement (d±1.96s_d).
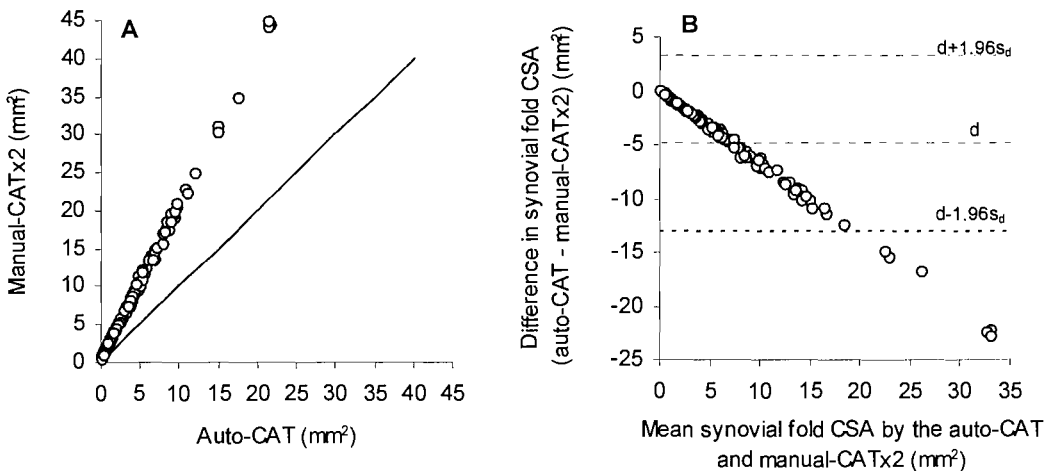
Figure 3.21. Proportional bias. **A.** Scatter diagram of the manual-CATx2mm^2 against the auto-CAT measurements of synovial fold cross-sectional area (CSA) (mm^2) with the line of equality (——). **B.** Scatter diagram of difference between the auto-CAT and manual-CATx2mm^2 against the mean of the auto-CAT and manual-CATx2mm^2 measurements of synovial fold CSA (mm^2) with lines representing the mean difference (d) and limits of agreement (d±1.96s_d).

Bland and Altman analysis is sensitive to random error and heteroscedasticity and this is reflected in the value of $1.96s_d$. The presence of increased random error causes the value of $1.96s_d$ to increase and will result in wide limits of agreement (Table 3.6 and Figure 3.22.B). Heteroscedasticity is indicated by an increase in the value of $1.96s_d$ (Table 3.6) and on the scatter diagram a divergence of the between-measurement differences as the magnitude of the measurements increases (Figure 3.23.B) (Bland and Altman, 2003). If heteroscedasticity is ignored, the analysis will still give limits of agreement which will include the majority of differences but the limits of agreement will be wider apart than necessary for measurements of small magnitude and narrower than they should be for measurements of large magnitude (Bland and Altman, 1999).
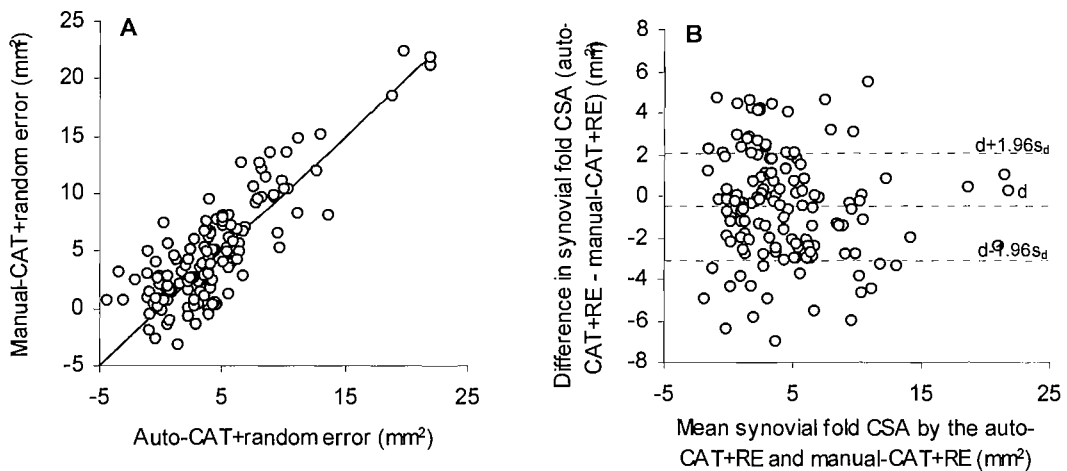
Figure 3.22. Increased random error (RE). **A.** Scatter diagram of the manual-CAT+RE against the auto-CAT+RE measurements of synovial fold cross-sectional area (CSA) (mm²) with the line of equality (——). **B.** Scatter diagram of difference between the auto-CAT+RE and manual-CAT+RE against the mean of the auto-CAT+RE and manual-CAT+RE measurements of synovial fold CSA (mm²) with lines representing the mean difference (d) and limits of agreement (d±1.96s_d).
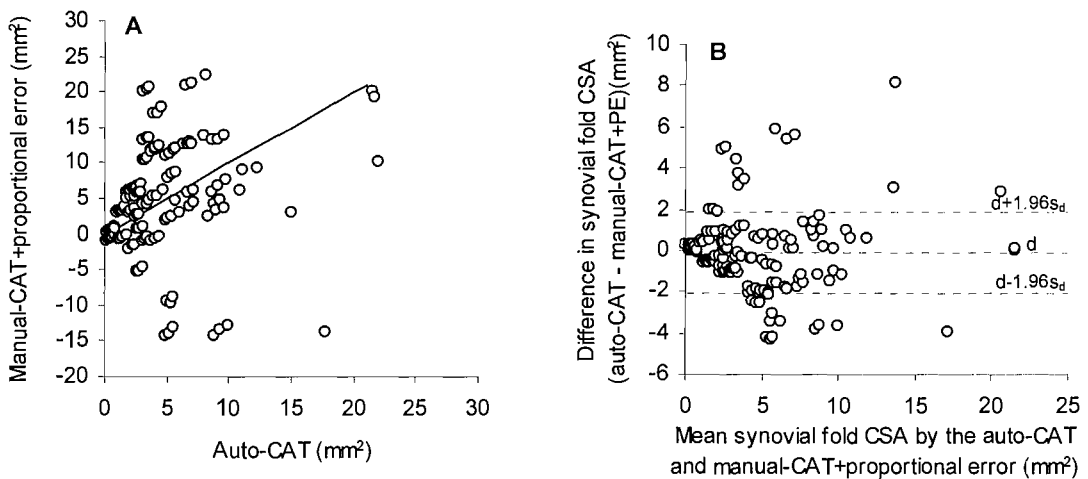
Figure 3.23. Heteroscedasticity/proportional error (PE). **A.** Scatter diagram of the manual-CAT+PE against the auto-CAT measurements of synovial fold cross-sectional area (CSA) (mm²) with the line of equality (——). **B.** Scatter diagram of difference between the auto-CAT and manual-CAT+PE against the mean of the auto-CAT and manual-CAT+PE measurements of synovial fold CSA (mm²) with lines representing the mean difference (d) and limits of agreement (d±1.96s_d).

As with simple linear regression analysis, there are two ways of coping with heteroscedastic data (Table 3.7). Log-transformation of the raw data is one suggested option and although this reduces the fan-shaped scatter of the differences it results in output parameters in the form of ratios which are difficult to interpret although 95% confidence intervals can be calculated (Bland and Altman, 1986; Ludbrook, 1997; Bland and Altman, 1999). An alternative approach in which the output parameters remain in the original units of scale is the modified regression approach.

A major advantage of limits of agreement analysis is that, unlike correlation coefficients and regression analysis, the limits of agreement are independent of the range and variance of the sample (Atkinson and Nevill, 1998; Bland and Altman, 1990). This is illustrated in Table 3.6 where the values of d and $1.96s_d$ do not change when data in the ranges of 2 to 8.5mm^2 (Figure 3.25) and 0 to 22mm^2 (Figure 3.24) are compared. This is, however, provided that the assumptions of the limits of agreement have been met and there is no relationship between the difference and the mean. If the difference is related to the mean then the limits of agreement will be related to the range of measurements indicating the need to perform a logarithmic transformation of the raw data or the modified regression approach in order to correct for this (Table 3.7).
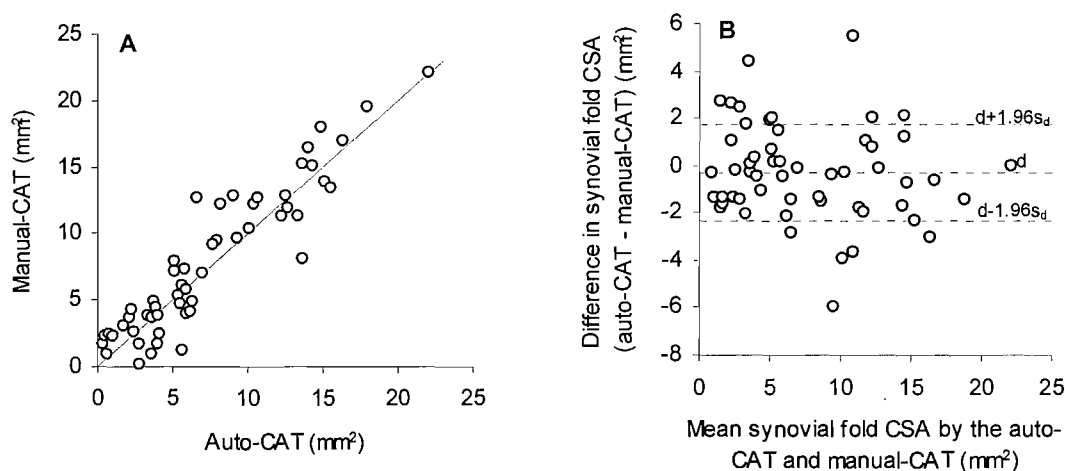
Figure 3.24. Range 0 to 22mm^2. **A.** Scatter diagram of the manual-CAT against the auto-CAT of synovial fold cross-sectional area (CSA) (mm^2) with the line of equality (——). **B.** Scatter diagram of difference between the auto-CAT and manual-CAT against the mean of the auto-CAT and manual-CAT measurements of synovial fold CSA (mm^2) with lines representing the mean difference (d) and limits of agreement (d±1.96s$_d$).
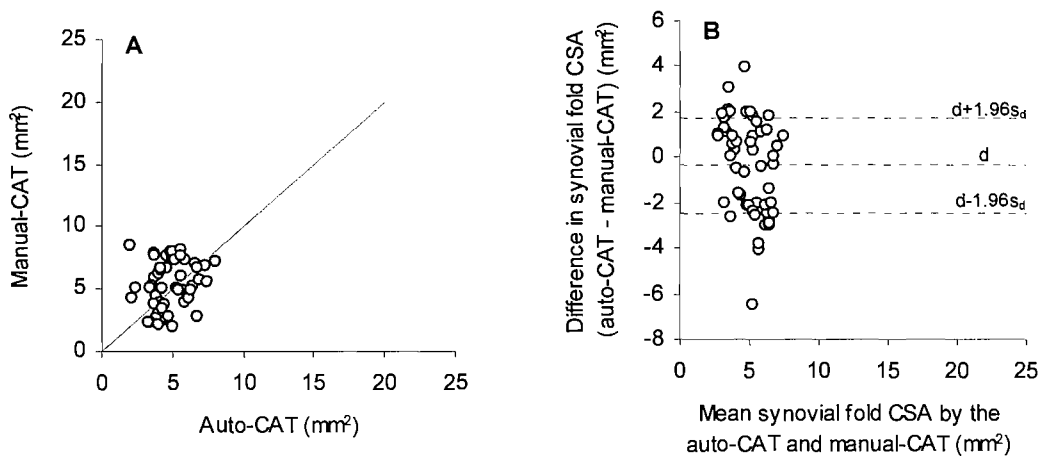
Figure 3.25. Range 2 to 8.5mm^2. **A.** Scatter diagram of the manual-CAT against the auto-CAT measurements of synovial fold cross-sectional area (CSA) (mm^2) with the line of equality (——). **B.** Scatter diagram of difference between the auto-CAT and manual-CAT against the mean of the auto-CAT and manual-CAT measurements of synovial fold CSA (mm^2) with lines representing the mean difference (d) and limits of agreement (d±1.96s$_d$).

Unlike the paired t-test, the calculation of the limits of agreement does not depend on sample size but the 95% confidence intervals (CI) for the limits of agreement are calculated from terms in the formula for the t-value and are thus affected by sample size (Atkinson and Nevill, 1998; Rankin and Stokes, 1998; Bland, 2005). This is an important factor to consider when comparing studies. A sample size of 100 gives a 95% CI of approximately ± $0.34s_d$, a sample size of 200 gives a 95% CI of ± $0.24s_d$ and a sample size of 12 gives a 95% CI of approximately ± s_d (Bland, 2005; Rankin and Stokes, 1998).

Most commonly in the literature the limits of agreement are expressed as a measure of 'total error' (e.g. -0.41 to 0.24mm^2). If the assumptions of the limits of agreement method have been thoroughly checked and there is no relationship between the differences and the mean (i.e. no proportional bias or heteroscedasticity) then this total measurement error constitutes only fixed bias and random error. If the limits of agreement are symmetrical and there is no significant fixed bias then there is a rationale for presenting the data in this format, however, if the limits of agreement are asymmetrical and/or there is significant fixed bias then it is not appropriate as the limits may imply that there is no fixed bias in the data. A limitation of using the t-test, in the limits of agreement method, to detect fixed bias is that it may not detect clinically significant fixed bias if the random error is large. Therefore the results of the limits of agreement analysis are more informative if the fixed bias and random error components are cited separately, i.e. $d±1.96s_d$ (e.g. -0.09±0.33mm^2) rather than expressing them as a

68

measure of 'total error' (e.g. 0.41 to 0.24mm^2) as it more transparent about where the biases and errors lie and facilitates comparison between studies.

The limits of agreement approach uses simple graphical techniques and basic statistical calculations. The analysis is simple for non-statisticians to understand and perform, requires readily-accessible basic statistical software and produces estimates which are easy to interpret and in the same units as the original observations (Bland and Altman, 1999; 2003). It has been suggested that although ordinary least products regression is more difficult to compute than the limits of agreement method, the outcome variables may be easier for medical investigators to understand as generally they are more accustomed to viewing scatter diagrams of one measurement plotted against the other measurement with regression lines of best fit superimposed than they are with scatter diagrams of the difference versus the mean with lines for the limits of agreement and mean difference superimposed (Ludbrook, 1997). However, the ordinary least products regression method is difficult to locate within statistical software packages and to date has been rarely used in the literature to analyse measurement precision (Bland, 2005; Ludbrook 1997). Like regression analysis, Bland and Altman analysis can be adapted when the data does not meet the assumptions of the test (Table 3.7). The limits of agreement method can also be adapted and extended to more complex situations such as when there are replicate measurements (Table 3.7). However, it cannot be used for measurements with different units (Chinn, 1991).

Table 3.7. Variations on the Bland and Altman limits of agreement method.

Assumptions not met	Analysis
The difference is related to the magnitude of the measurements:	Modified regression approach (See Section 4.2.3iii)
1. Heteroscedasticity 2. Proportional bias	Logarithmic transformation (see Bland and Altman, 1999)
The differences follow a non-normal distribution	Non-parametric approach (see Bland and Altman, 1999)
	Logarithmic transformation (see Bland and Atlman, 1999)
Replicate measurements	**Analysis**
Equal numbers of replicates	(see Section 4.2.3.iii)
Unequal numbers of replicates	(see Bland and Altman, 1999)
Replicated data collected in pairs	(see Bland and Altman, 1999)

Thus the Bland and Altman limits of agreement produce specific estimates of fixed bias and random error in the same units of scale as the original measurements. A critical part of the analysis is a graphical check of the assumption that the difference is not related to

the magnitude of the variable, i.e. there is no proportional bias or heteroscedasticity. If this assumption is not met an alternative method of limits of agreement analysis (logarithmic transformation or modified regression approach) must be undertaken otherwise the estimates of fixed bias and random error may be unduly affected.

3.4 Summary and recommendations

In order to judge the acceptability of any method of measurement, the precision of the method needs to be assessed and characterised in a manner that is useful to others who use the method in clinical or research settings (Westgard and Hunt, 1973). If the measurements are to be used to monitor changes or differences in individual subjects or patients then it is essential to identify and quantify all potential biases and errors (Keating and Matyas 1998). Table 3.8 summarises the sensitivities of the statistical parameters reviewed, analysed and evaluated in this Chapter. The table has been devised in collaboration with a colleague (G. Rix) and is based upon the statistical tests computed and modelled in this Chapter.

Table 3.8. Sensitivity of statistical parameters to systematic bias and random error. Devised by Webb and Rix (2005), used with permission.

| Type of measurement error | Correlation | | | Regression | | | t-test | | LoA | |
| | r | r_1 | | Slope | Y-intercept | $S\varepsilon$ | d | s_d | d | $1.96s_d$ |
		Abs	Con							
Systematic bias										
Fixed bias	No	Yes	No	No	Yes	No	Yes	No	Yes	No
Proportional bias	No	Yes	Yes	Yes	No	No	Yes	Yes	Yes†	Yes†
Random error										
Increased random error	Yes	Yes	Yes	No	No	Yes	No	Yes	No	Yes
Heteroscedasticity	Yes	Yes	Yes	No	No	Yes*	No	Yes	No	Yes†

Abbreviations: r – Pearson's correlation coefficient; r_1 – ICC; Abs – absolute; Con – consistency; $S\varepsilon$ – standard error of the estimate; d – mean difference between measures; s_d – standard deviation of d; LoA – limits of agreement

* $S\varepsilon$ will also be sensitive to heteroscedasticity unless a modified approach (i.e. logarithmic transformation or weighted regression analysis) is used.

† If a proportional bias is present, using a modified regression approach provides a quantification of this bias type. If a proportional bias or heteroscedasticity are present and a modified regression approach or logarithmic transformation are not adopted, d will be sensitive to proportional bias and $1.96s_d$ will be sensitive to proportional bias and heteroscedasticity.

Note: when there is a combination of biases and/or errors present in a data set, the sensitivities of individual statistical parameters are the same as when single biases and/or errors are present (Westgard and Hunt, 1973).

The clinical and research utility of any measurement will depend upon both the amount of bias and error typical of those measurements and the intended application of the

measurements (Westgard and Hunt, 1973; Bland and Altman, 1999; Keating and Matyas 1998). If the researcher/clinician wants to be able to detect small differences between the measurements of interest, the typical variability associated with the measurements must be even smaller but if larger differences are expected then more measurement error can be tolerated (Keating and Matyas, 1998). For example consider an instrument measuring cervical range of motion that has a measurement error of $6°$. If following surgery we expect cervical range of motion to improve $30°$, $6°$ of measurement error would be clinically acceptable. However, if we are hoping to detect a $3°$ improvement in cervical range of motion post-surgery the instrument would not be regarded as an acceptable clinical measure and we would have to decide whether to abandon its use, consider ways to reduce its error or accept that a higher post-surgical measurement was not a guarantee of patient improvement. Thus precision should not necessarily be conceived as a property that a particular measurement method, instrument or researcher does or does not possess since any measurement will have a certain degree of precision when applied to certain populations under certain conditions. The issue to be addressed is what degree of measurement error is considered to be clinically acceptable.

Consideration of what degree of measurement error is acceptable is most clearly conducted when the measurement errors and the effects of interest are both quantified in the same units of scale (Keating and Matyas, 1998). Quantifying the magnitude of the biases and errors in the same units of scale as the original measurements also facilitates data transferability making it easier to extrapolate the results to new individuals and to compare precision between different measurement methods and studies (Atkinson and Nevill, 1998). It is clear that these considerations cannot be undertaken when only unit-free proportions such as r and r_l are employed thus despite their common use these statistical parameters have no practical value in characterising measurement error and should not be used as indicators of precision.

Analysis by t-test is more useful than correlation but will not provide specific estimates of random error and fixed bias when proportional bias is present (Table 3.8). Thus when used it is imperative to check for the presence of proportional bias by graphing the measurement values and determining the slope of the regression line. The interpretation must consider the individual t-test parameters rather than the t-value itself.

The limits of agreement and regression analysis are the most valuable methods for identifying and estimating error and bias although it is important to be conscious of their limitations (Table 3.8). In order to detect errant points, heteroscedasticity and, in the case of the limits of agreement method proportional bias, the data must be presented graphically using a scatter diagram and a modified approach employed if the data does not meet the test assumptions. Unfortunately this essential part of the analysis is often overlooked or not done properly in the literature (Bland and Altman, 2001).

There are three main advantages of using the limits of agreement method rather than regression analysis in the assessment of precision. The first advantage is that d and $1.96s_d$ are unaffected by the range and variance of the sample whilst all but one of the regression coefficients are affected. Secondly, it is clear that ordinary least squares regression will produce biased results because it does not account for the error attached to both measurements hence Ludbrook (1997; 2002) has suggested ordinary least products regression as a solution to this problem. Unfortunately, ordinary least products regression is not available within standard statistical software packages, is complex to perform and has not been widely picked up and used in the literature for precision analysis. In contrast the limits of agreement method is becoming an increasingly well known and frequently cited method that has been pivotal in encouraging a move away from inappropriate methods such as Pearson's correlation coefficient, it is relatively simple to execute using widely available statistics packages and is easy to perform and interpret by non-statisticians (Altman and Bland, 1983; Bland and Altman, 1995; Bruton et al., 2000). Finally, the limits of agreement method can be modified or extended to a variety of complex situations (Table 3.7) (Bland and Altman, 2003). Thus it is recommended that the limits of agreement method be adopted and used for the analysis of precision.

The continued use of inappropriate statistics is of great concern. The widespread use of correlation coefficients, ordinary least squares regression and t-tests implies that many measurement methods and devices used routinely in medical research may have been erroneously concluded as being sufficiently precise. It would be prudent to reappraise the results of such studies using absolute indicators of measurement error such as the limits of agreement and ordinary least products regression methods since good methods of measurement may have been rejected and poor ones may have been adopted which ultimately affects patient care and management (Atkinson and Nevill, 1998; Bland,

2005). Even researchers who do use limits of agreement analysis often fail to undertake an adequate investigation of the underlying assumptions thus potentially missing relationships between the mean and the difference that will ultimately affect the estimations of systematic bias and random error (Bland, 2005). It is important that researchers understand that the statistical philosophy for analysing measurement error is very different to that surrounding the testing of research hypotheses as the concept entails the researcher relating measurement error to analytical goals and clinical application rather than the significance of hypothesis tests (Westgard and Hunt, 1973; Bland and Altman, 1990; Atkinson and Nevill, 1998). Researchers should have an appreciation of the underlying theory behind the different measurement error statistics so that they can understand the potential limitations of their results (Atkinson and Nevill, 1998).

Chapter 4

The development of a measurement technique to determine the geometrical properties of the intra-articular synovial folds of the lateral atlanto-axial joints: a cadaveric study

4.1 Introduction

Due to their location within the fibrous joint capsule of the lateral atlanto-axial joints, it is very difficult to gain access to the intra-articular synovial folds without disrupting surrounding structures. A variety of different techniques have been developed to expose the synovial folds of the cervical spine (Table 4.1).

The different techniques used can be categorised into two main types: dissection of the joint to expose the joint cavity, which includes the incision and reflection of the fibrous joint capsule (Chang et al., 1992; Kos et al., 2002; Tang et al., 2007) or drilling through the articular processes (Mercer and Bogduk, 1993; Inami et al., 2000), and sectioning of the joint (Yu et al., 1987; Bland, 1990; Schonstrom et al., 1993). Both the dissection and sectioning techniques have been successfully used to describe the gross appearance of the synovial folds but to date none have been applied to the determination of the geometrical properties of the synovial folds. Thus in order to quantify the dimensions of the synovial folds, a suitable technique needs to be developed and evaluated.

Table 4.1. Macroscopic techniques for determining the morphology of the intra-articular synovial folds of the lateral atlanto-axial articulations.

Study	Anatomical techniques
Bland & Boushey, 1990	Dissected cervical spines sectioned with a bandsaw in the sagittal, coronal and transverse planes at 10mm intervals.
Chang et al., 1992	Specimens cleaned of extraneous soft tissue. Fibrous capsules dissected longitudinally at the middle of the joint, incised and reflected to reveal the joint cavity and synovial folds.
Ibattulin et al., 1987	A. Frozen Pirogov's* saw-cuts and histo-topographical kristellerov sections in the sagittal, coronal and transverse planes. B. Dissection of the articulations (technique not described).
Kawabe et al., 1989	Not described.
Kos et al., 2002	Dissection of fibrous capsule from the inferior articular process of the superior vertebra.
Mercer & Bogduk, 1993	The articular process of each joint was drilled away with a dental burr leaving the articular cartilage *in situ* and intact. The cartilage was gently dissected free of the joint capsule to produce a superior view of the joint cavity and its contents.
Schonstrom et al., 1993	A. Posterior muscles removed, laminectomy performed and the spinal cord removed. Specimens hemisected, immersed in 5% gelatin and frozen at -70°C. Frozen specimens sectioned in the sagittal plane in 2mm slices using a bandsaw. B. Dissection of the lateral atlanto-axial joints (technique not described).
Tang et al., 2007	Specimens stripped of soft tissues. Fibrous joint capsules incised to reveal the joint cavity and synovial folds.
Yu et al., 1987	A. Specimen frozen at -70°C and sectioned in the sagittal plane at 40μm intervals on a cryomicrotome. B. Specimens stripped of muscles. Fibrous capsule incised and adjacent vertebrae separated to view the synovial folds.

*The Russian anatomist and surgeon N.I. Pirogov (1810-1881) developed a freezing technique for producing thin sections of the human body. However, he was not the innovator of this technique, that tribute goes to P. DeRiemer (Enersen, 2003)

The purpose of this study was to devise and evaluate a method for quantifying the dimensions of the intra-articular synovial folds of the lateral atlanto-axial joints. The aims of the study were to:

1. develop a method and measurement technique to quantify the geometry of the intra-articular synovial folds of the lateral atlanto-axial articulations

2. evaluate the precision and accuracy of the measurement technique.

3. determine the prevalence of the lateral atlanto-axial synovial folds, establish their anatomical relationships and investigate the potential existence of extracapsular communications between the synovial folds and surrounding structures

4. quantify the dimensions of the synovial folds of the lateral atlanto-axial joints

5. determine whether there is a difference in the volume of the synovial folds due to symmetry (ventral-dorsal and left-right) and gender

4.2   Methods

4.2.1 Subjects

Whole cervical spines were carefully removed from embalmed cadavers. Each specimen was examined using plain film radiography. An anteroposterior view and a lateral view were taken of each specimen. All radiographs were reviewed and reported upon by a Radiologist who was independent to the study and blinded to the results of the anatomical study.

Six cervical and lumbar spine specimens were utilised in the process of developing the sectioning technique used in the measurement process. The specimens were used in trials to determine the optimal slice thickness, an appropriate embedding material and a consistent method of specimen orientation. No geometric data was collected from these specimens and they are not included in the results of this study.

4.2.2 Sectioning procedure

The sectioning technique developed in this study was based upon the method originally developed by Taylor and Twomey (1986) and since used by Schonstrom et al. (1993). The cervical spine was removed *enbloc* between the occiput, at the level of the external occipital protuberance, and the 1st thoracic vertebra (T1) using a bandsaw (Startrite Engineering Co. Ltd., Pat. No. 1024527). Posteriorly, the superficial neck muscles, including the trapezius, levator scapulae and splenius muscles, were dissected away leaving the semispinalis cervicis and capitis muscles intact. Anteriorly, the viscera and blood vessels of the neck, and the sternocleidomastoid and scalene muscles were removed leaving the longus colli and capitis muscles and their covering fascia intact. The specimens were trimmed laterally to the tips of the C1 transverse processes and, if necessary, the specimens were trimmed superiorly to the inferior nuchal line.

Each specimen was positioned within a 2 Litre white polypropylene sterilising tray (210x122x91mm, VWR International, Cat. No. 272/0078/02). The specimen was positioned so that the left and right transverse processes and anterior and posterior tubercles of the atlas were aligned in the coronal and sagittal planes, respectively. The specimen was immersed in warm 5% gelatin (Gelatine Powder Product 440454B, BDH Lab Supplies, Poole, England) for 24 hours and then frozen at $-28^{\circ}C$ (LabCold,

England) for a minimum of 24 hours. The frozen, gelatin embedded specimen (Figure 4.1) was removed from its tray and sectioned in the sagittal, coronal or transverse plane at 3mm intervals using the bandsaw, fitted with a fine-toothed blade (6 teeth/cm), and an adjustable precision guide (Figure 4.2).
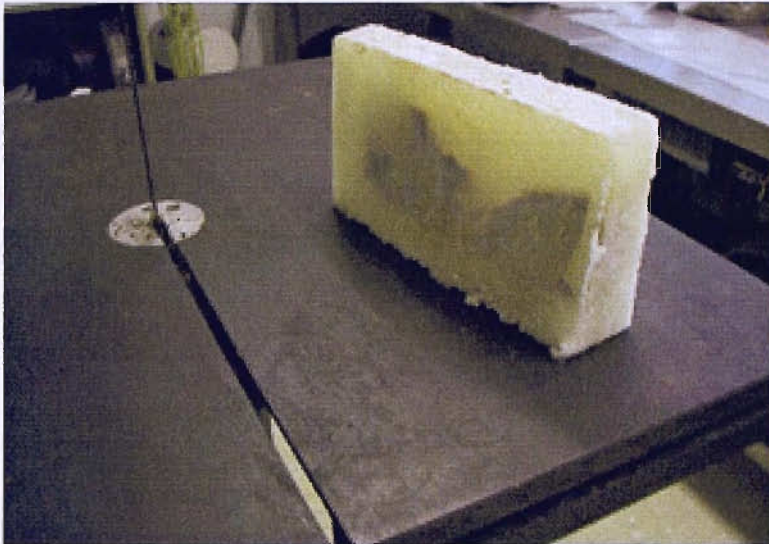
Figure 4.1 A frozen gelatin-embedded cervical spine specimen following sectioning.
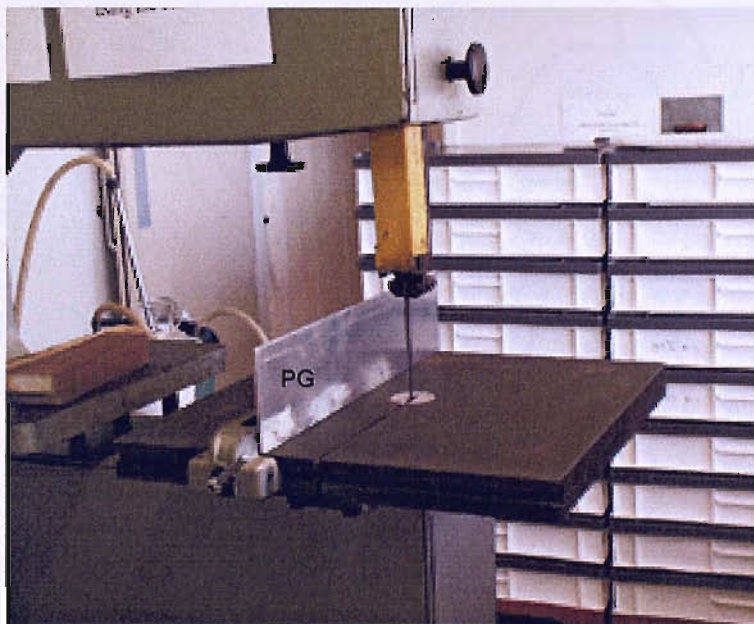
Figure 4.2 The bandsaw (Startrite Engineering Co. Ltd., Pat. No. 1024527) and adjustable precision guide (PG) used for sectioning specimens.

The section thickness was measured using a digital micrometer (Mitutoyo Digimatic, RS 193-253, accurate to 0.01mm) to confirm that 3mm slices had been taken. The specimens were sectioned and numbered as follows:

A. <u>Sagittal sections</u> (Figure 4.3): the cervical spine was positioned either right or left side down in the tray. If positioned right side down, the cervical spine was sectioned

from right to left with the first section made at the right transverse process of C1. If positioned left side down, the cervical spine was sectioned from left to right with the first section made at the left transverse process of C1. The slices were numbered sequentially in the same order the sections were made in with the first slice labelled section 1.

B. <u>Coronal sections</u> (Figure 4.4): the cervical spine was positioned anterior side down in the tray. The whole cervical spine was sectioned from anterior to posterior with the first section made at the anterior tubercle of C1. The sections were numbered sequentially in the same order the sections were taken in with the first slice labelled section 1.

C. <u>Transverse sections</u>: the cervical spine was positioned superior side down in the tray. The cervical spine was sectioned from superior to inferior with the first section made through the occiput. The sections were numbered sequentially in the same order that the sections were made in with the first slice labelled section 1.
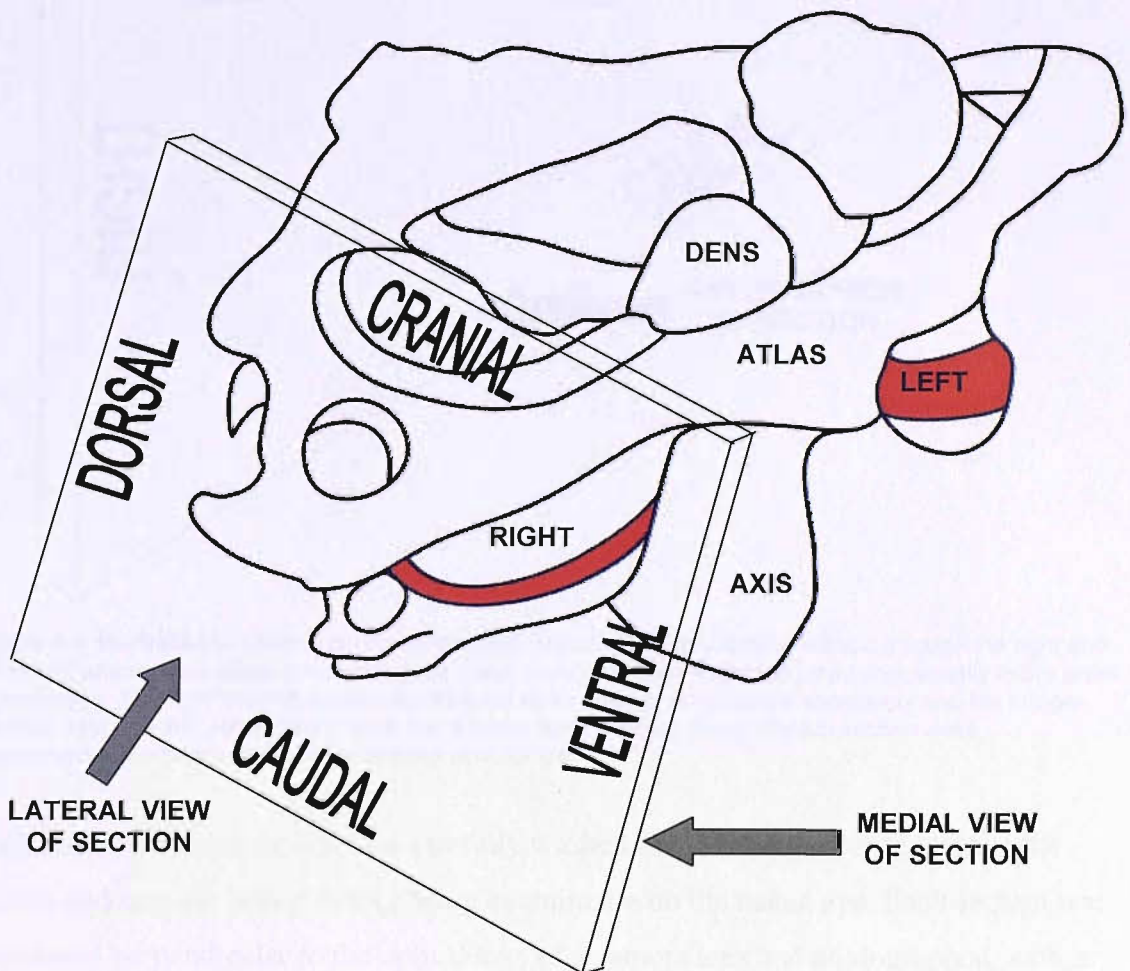
Figure 4.3. Illustration of sagittal section orientation showing a 3mm sagittal slice through the right lateral atlanto-axial joint (shaded in red). Each sagittal section was numbered sequentially in the order of sectioning. Each section was photographed and the images labelled right or left (based on whether the section passed through the right or left side of the cervical spine). Both the medial and lateral views of each section were photographed and the images were labelled accordingly.
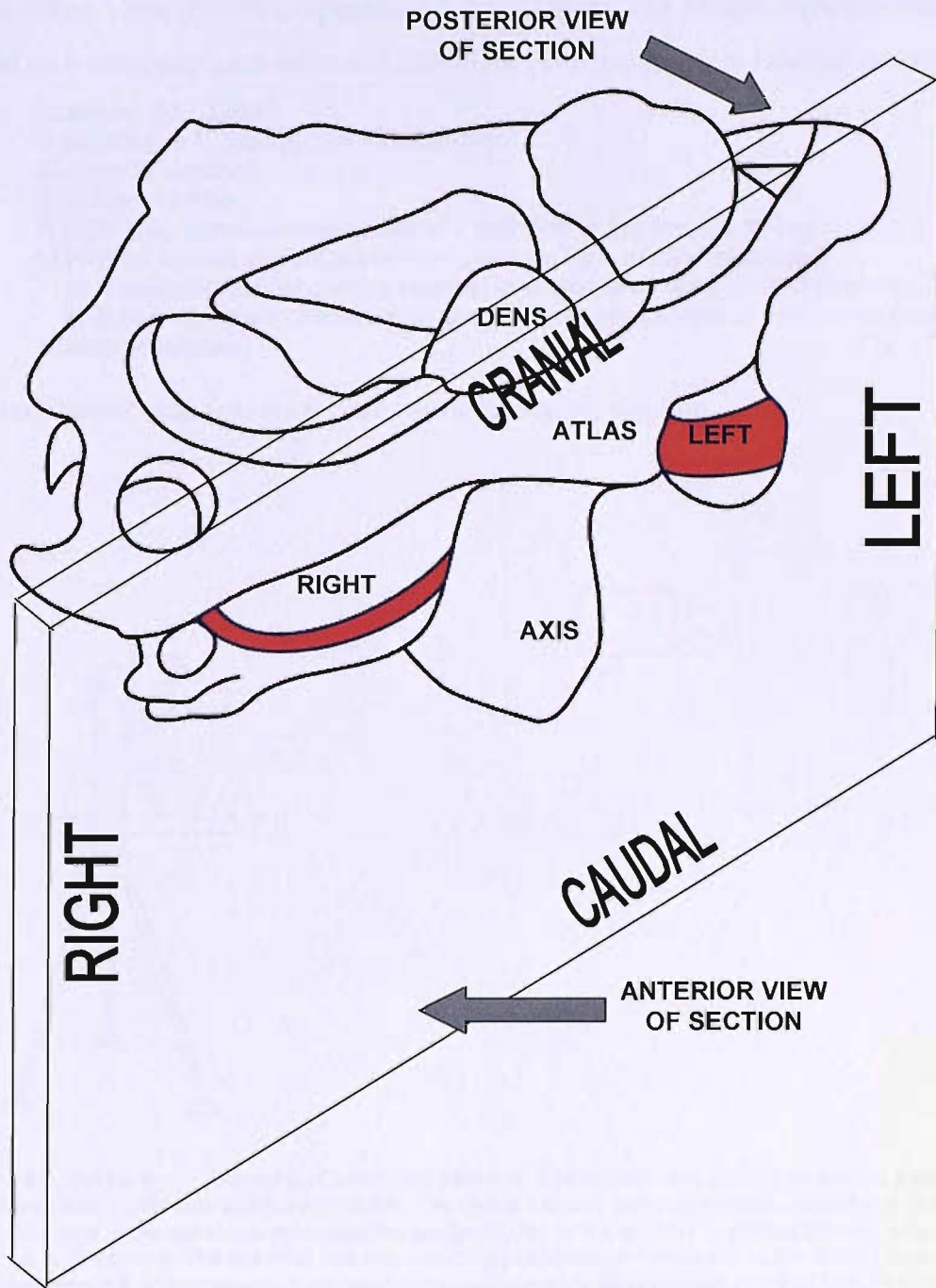
Figure 4.4. Illustration of coronal section orientation showing a 3mm coronal section through the right and left lateral atlanto-axial joints (shaded in red). Each coronal section was numbered sequentially in the order of sectioning. The right and left lateral atlanto-axial joints were photographed separately and the images labelled right and left, respectively. Both the anterior and posterior views of each section were photographed and the images were labelled accordingly.

Each unstained 3mm section was carefully washed under warm water to remove the gelatin and saw-cut debris before being examined with the naked eye. Each section was positioned perpendicular to the optical axis of a camera lens and photographed, with a millimetre scale, using a digital camera (Nikon Coolpix 5000/5400, Nikon Corporation, Tokyo, Japan) fixed to a tripod (GX-86, OSAWA, Japan) (Figure 4.5). Both sides of each section were photographed. The digital images were then uploaded to a computer

79

using Nikon View (Nikon Corporation, Tokyo, Japan). The images were labelled and stored on a computer hard-drive and CD-ROM. The images were labelled as follows:

Example: S03.2.RM5
S (sagittal) or C (coronal) or T (transverse)
03 (year of section)
2 (subject number)
R (right side of the cervical spine) or L (left side of the cervical spine)
M (medial view of sagittal section) or L (lateral view of sagittal section)
    or A (anterior view of coronal section) or P (posterior view of coronal section)
    or S (superior view of transverse section) or I (inferior view of transverse section)
5 (section number)

The sections of each specimen were stored in wetting solution.
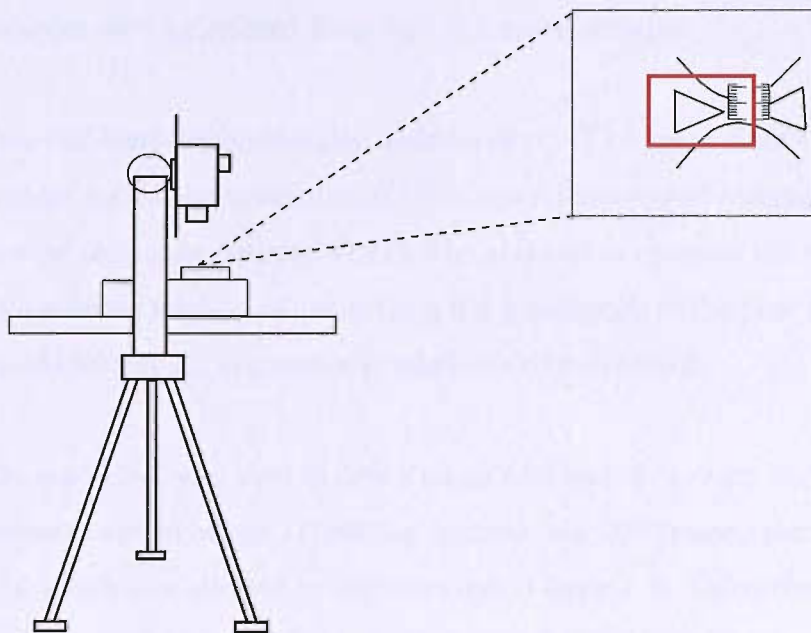
Figure 4.5. Set-up for photography of specimen sections. The section was placed on a white background on a level table, confirmed using a spirit level. The digital camera was attached to a tripod and tilted so that the optical lens of the camera was positioned perpendicular to the section. A spirit-level was used to ensure a level camera. The synovial fold was carefully positioned in the centre of the field of view (red rectangle) and the measurement scale positioned as close as possible to the synovial fold. The camera was focussed and the photograph was taken using the timer setting.

4.2.3 Data collection and analysis

4.2.3i Prevalence and gross morphology

The sagittal, coronal and transverse sections of the cervical spine were carefully studied and the morphology of the synovial folds and related structures described. The prevalence of the intra-articular synovial folds at the lateral atlanto-axial joints was determined.

4.2.3ii Dimensions of the synovial folds

The digitised images of the sagittal sections were used for the quantification of the dimensions of the synovial folds. Each section was carefully studied so that all sections that contained the synovial folds were included. The fibrous capsule was used as a reference to determine the medial and lateral boundaries of the synovial folds. Measurements were made from one side of the section, either the medial or lateral view.

IMAQ™ Vision Builder Version 6.1 (National Instruments, Austin, Texas, USA) was used to measure synovial fold cross-sectional area (CSA) and depth of projection (DOP) from the digitised images of all sagittal sections. Sectional and whole synovial fold volumes were calculated from the CSA measurements.

Two different computer-aided techniques (CAT) were available in IMAQ™ Vision Builder for the determination of CSA, a semi-automated technique (auto-CAT) and a manual technique (manual-CAT). The aim was to compare the two CATs and determine the preferred method of quantifying the dimensions of the synovial folds. This method should be precise, accurate and relatively time efficient.

The auto-CAT was used to detect edges (defined as 'a sharp transition in the pixel intensities in an image') (National Instruments, 2002) along the border of each synovial fold which was selected by the examiner (Figure 4.6). Using the caliper tool, all of the edges around the entire border of the synovial fold were connected and the CSA measured in pixels. The manual-CAT was used to trace around the border of each synovial fold using a cursor to quantify the CSA in pixels. A millimetre scale photographed with each section was used to convert the synovial fold CSA measurements from pixels to millimetres. 1mm was measured in pixels by taking a line parallel to the edge of the measurement scale using the auto-CAT (Figure 4.4) and this value was entered into the Simple Calibration tool of IMAQ™ Vision Builder. The sectional volume of each synovial fold was determined by multiplying the CSA with the thickness of each sagittal section (3mm). Whole synovial fold volume was given by the sum of the synovial fold sectional volumes. All sagittal sections were thoroughly examined to ensure that the entire synovial fold was included in the calculation of synovial fold volume.

Synovial fold depth of projection (DOP), the distance from the midpoint of the synovial fold base to the apex, was measured using the auto-CAT (Figure 4.6). The midpoint of the synovial base was determined from the outline of synovial fold CSA. A line perpendicular to the base was drawn from the midpoint of the base to the apex and measured in pixels. The millimetre scale was used to convert the DOP measurement from pixels to millimetres using the method described for CSA above.
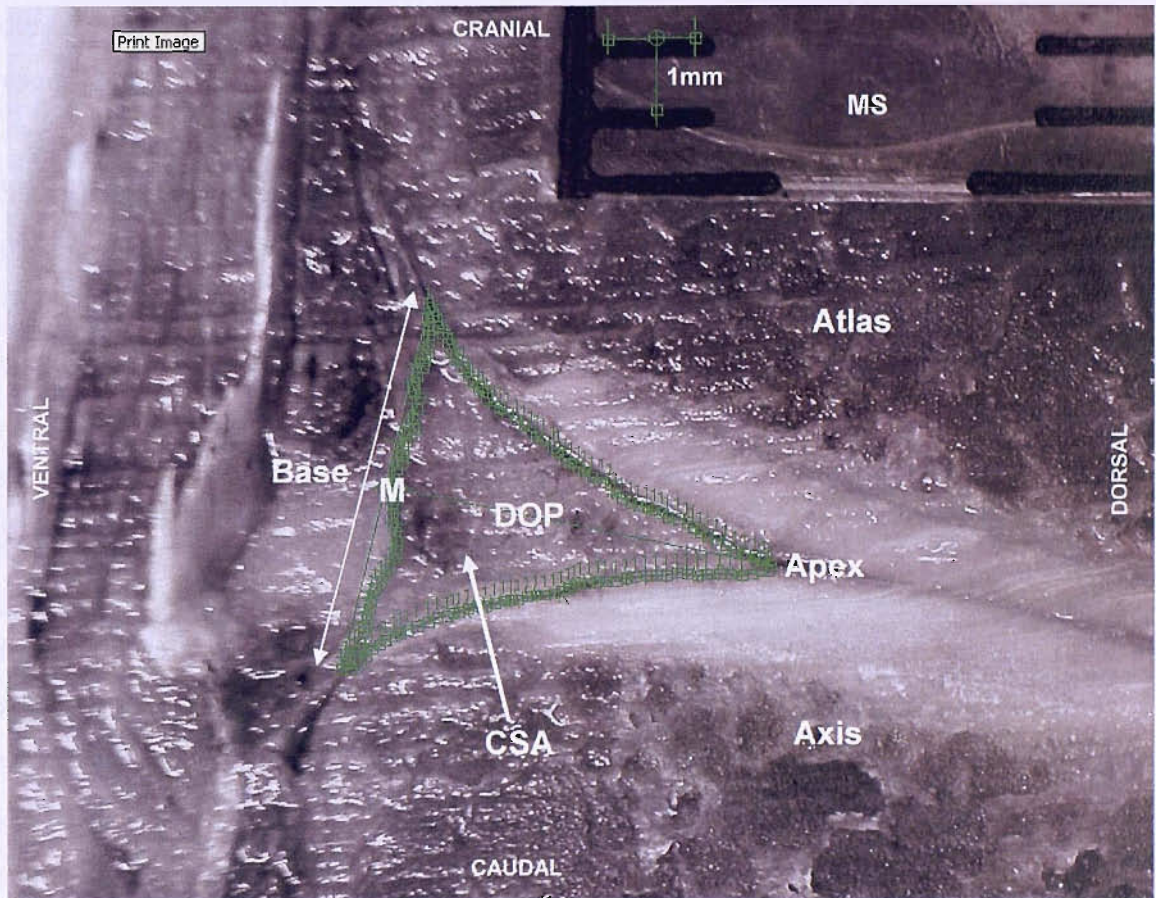
Figure 4.6. The National Instruments IMAQ™ Vision Builder screen showing a gray-scale digitised image of a sagittal section of the ventral synovial fold of the right lateral atlanto-axial joint (medial view) of Subject 3. The cross-sectional area (CSA) of the synovial fold has been outlined on the image using the auto-CAT. Synovial fold depth of projection (DOP) is represented by the line perpendicular to the base extending between the midpoint of the base (M) and the apex. The length in pixels between two graduations demarcating 1mm on the measurement scale (MS) was measured using a line parallel to the vertical edge of the measurement scale. This value was entered into the Simple Calibration tool of IMAQ™ Vision Builder to convert the CSA and DOP measurements from pixels to millimetres.

The dimensions of the synovial folds were presented as means, standard deviations, medians and ranges. Boxplots were used to display the medians and ranges of synovial fold volume for the ventral and dorsal synovial folds of the right and left lateral atlanto-axial joints of all subjects and males compared to females. The data was explored and examined for normality using histograms with Normal curves, quantile-quantile plots and the Kolmogorov-Smirnov (KS) test. Homogeneity of variance was examined using Levene's test.

82

The sample sizes were small and not all data demonstrated a Normal distribution thus the data was analysed using non-parametric statistics. Friedman's ANOVA was used to determine whether there was a difference in volume between the right ventral, right dorsal, left ventral and left dorsal synovial folds. If there was a significant difference, Wilcoxon's signed-rank test was used for *post hoc* analysis with *Bonferroni correction*. Wilcoxon's signed-rank test with *Bonferroni correction* was used to determine whether there was a difference in volume between the right and left ventral and right and left dorsal synovial folds; and between the ventral and dorsal synovial folds of the left and ventral and dorsal synovial folds of the right lateral atlanto-axial joints.

Statistical analysis was performed using SPSS version 14.0 for Windows (SPSS Inc., Chicago, Illinois, USA) and Microsoft Excel 2000 (Microsoft Corporation, Redmond, WA, USA). A probability level of $P=.05$ was set as the minimum criterion of statistical significance for all tests.

4.2.3iii Measurement precision

Figure 4.7 summarises the precision data collected. Synovial fold cross-sectional area was measured by both the auto-CAT and manual-CAT methods by the same examiner for all sagittal sections for the determination of method agreement. Repeat measurements using both methods were performed immediately after the original measurements (repeatability) and at least 3 months after the original measurements (test-retest precision) by the same examiner. A second inexperienced examiner was trained to measure synovial fold cross-sectional area using both the auto-CAT and manual-CAT measurement methods for the determination of inter-examiner precision.

The precision of the synovial fold cross-sectional area measurements and synovial fold (whole) volumes calculated from the cross-sectional area measurements (method agreement, repeatability, test-retest precision, inter-examiner precision) were determined using the Bland and Altman limits of agreement method, with single measures. In addition the method agreement data was combined with the repeatability and test-retest precision data to calculate the method agreement with repeated measures between the auto-CAT and manual-CAT, for synovial fold cross-sectional area and volume, using the Bland and Altman limits of agreement method, with repeated measures (see Appendix 3).
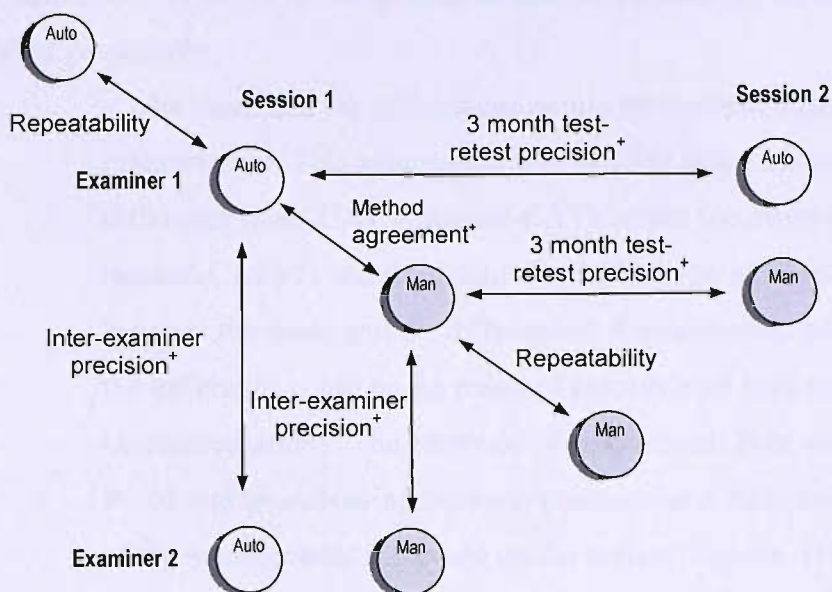
Figure 4.7. Diagrammatic representation of precision data collected and analysed in the present study. Auto – auto-CAT; Man – manual-CAT
[+]Intermediate conditions of precision with the following factors selected as the variable:
    Examiner – inter-examiner precision
    Time – 3 month test-retest precision
    Measurement method/equipment - method agreement

Limits of agreement with single measures

The Bland and Altman limits of agreement method was used to estimate method agreement, repeatability, test-retest precision and inter-examiner precision for the measurement of synovial fold cross-sectional area and volume (Bland and Altman, 1986; Bland and Altman, 1999; Bland and Altman, 2003). The method of the limits of agreement analysis is described in this section by referring to method agreement between the auto-CAT and the manual-CAT as an illustrative example.

The difference between the two measurements (i.e. auto-CAT – manual-CAT) was calculated for each section (synovial fold cross-sectional area) and for each articulation (synovial fold volume). The mean difference (d) and the standard deviation of the differences (s_d) were then determined. The mean difference represents the fixed bias and the standard deviation of the differences represents the random error (or variability) about the mean difference. The mean of the two measurements was also calculated for each section (synovial fold cross-sectional area) and for each articulation (synovial fold volume). The 95% limits of agreement were calculated from the mean difference ± 1.96 standard deviations ($d \pm 1.96s_d$). The limits of agreement define the range within which 95% of the differences between the two measurements will lie.

The calculation of the 95% limits of agreement was based on two assumptions that were verified graphically:

a. The mean and the differences should be uniform throughout the range of measurement. This assumption was verified using a scatter diagram of the difference (auto-CAT – manual-CAT) versus the mean ([auto-CAT + manual-CAT]/2) and the calculation of Pearson's correlation coefficient (r) between the mean and the differences. A relationship between the mean and the difference could be the result of proportional bias and/or heteroscedasticity. The presence of proportional bias was indicated by $r{\neq}0$, P<.05 and an increasing between-measurement difference as the magnitude of the measurement increased on the scatter diagram. Heteroscedasticity was indicated by a divergence of the between-measurement differences as the magnitude of the measurements increased on the scatter diagram. Lines representing the 95% limits of agreement and the mean difference were added to the scatter diagram. If the differences are normally distributed then 95% of the differences would be expected to lie between the limits of agreement.

If there was a relationship between the difference and the mean, caused by proportional bias and/or heteroscedasticity, a modified regression approach was used (see 'modified regression approach' below).

b. The differences (auto-CAT – manual-CAT) should come from an approximately Normal distribution. This was checked using a histogram of the differences and the Kolmogorov-Smirnov (KS) test for normality.

The standard error and confidence interval for the mean difference (d) and the 95% limits of agreement ($d \pm 1.96s_d$) were calculated as follows:

The standard error of the mean difference, SE(d):

$$s_d/\sqrt{n} \tag{4.1}$$

where n represents the size of the sample.

The 95% confidence interval for the mean difference:

$$d \pm t^{*}\text{SE}(d) \tag{4.2}$$

where the value for t was determined by finding the appropriate point of the t distribution with n-1 degrees of freedom.

The standard error for the 95% limits of agreement (SE($d \pm 1.96s_d$)):

$$1.71\text{SE}(d) \tag{4.3}$$

The 95% confidence interval for the upper and lower limits of agreement was given by:

95% confidence interval for the upper limits of agreement

$$d + 1.96s_d \pm t\text{SE}(d \pm 1.96s_d) \tag{4.4}$$

95% confidence interval for the lower limits of agreement

$$d - 1.96s_d \pm t\text{SE}(d \pm 1.96s_d) \tag{4.5}$$

where the value for t was determined by finding the appropriate point of the t distribution with n-1 degrees of freedom.

Modified regression approach

The relationship between the mean difference and the magnitude of the measurement was modelled by regressing the difference between the measurements (D) on the mean of the measurements (A) giving:

$$D = b_o + b_1 A \tag{4.6}$$

If b_1 was significantly different from zero, the estimated difference between the measurements was determined from the equation above. If b_1 was not significant then $D = d$, the mean difference.

The relationship between the standard deviation of the differences and the magnitude of the measurement was modelled by taking the residuals around the regression line (i.e. differences between the observed difference and the difference predicted by Equation 4.6) and then regressing the absolute values of the residuals (R) on A giving:

$$R = c_o + c_1 A \tag{4.7}$$

The standard deviation of the residuals was obtained by multiplying c_o and c_1 by $\sqrt{\pi/2}$. If c_1 was significantly different from zero, the estimated standard deviation of the differences was predicted from Equation 4.7 and the 95% limits of agreement were calculated by combining the two regression equations:

$$D \pm 1.96\sqrt{\pi/2} \, R = D \pm 2.46R \text{ (or } b_o + b_1 A \pm 2.46 \{c_o + c_1 A\}) \tag{4.8}$$

If there was no significant relationship between R and A, the estimated standard deviation of the differences was calculated as the standard deviation of the adjusted

differences (i.e. the residuals of Equation 4.6) and the 95% limits of agreement were calculated as follows:

$$D \pm 1.96 \text{ standard deviation}(R) \text{ (or } b_o + b_l A \pm \text{ standard deviation} \{R\}) \qquad (4.9)$$

Lines representing the mean difference and the 95% limits of agreement, calculated using regression, were plotted onto the difference versus mean scatter diagram.

Statistic analyses for the limits of agreement were performed using Microsoft Excel 2000 (Microsoft Corporation, Redmond, WA, USA) and SPSS version 14.0 for Windows (SPSS Inc, Chicago, Illinois, USA).

4.2.3iv Acquisition error

The same set-up (Figure 4.5) was carefully replicated for photographing all sections. To investigate the measurement error that may have arisen as a result of the image acquisition and the use of the millimetre scale to convert pixels to millimetres, the image distortion and millimetre scale accuracy and precision, respectively, were determined

Image distortion

Distortion refers to variations of the accurate representation in scale and perspective of various elements of an object and its plane of context, and is described as the deviation of the distorted image point from its geometrically correct position, expressed in percent (Ray, 1988 in Masters et al., 2005). Generally, distortion increases more or less evenly from the centre of the image to the periphery of the image. To determine the extent of possible distortion when photographing the sections, the aspect ratio between two perpendicular lines (x and y) was determined from the millimetre scale photographed with each section. The length of x and y were first measured in millimetres using digital calipers (Mitutoyo Digimatic, RS 193-253, accurate to 0.01mm) and the ratio x:y calculated. The length of x and y were then measured in pixels from the digital images using IMAQ^{TM} Vision Builder Version 6.1 (National Instruments, Austin, Texas, USA) and the ratio x:y determined. The percentage difference between the two ratios was then calculated.

Millimetre scale accuracy

To determine the accuracy of the millimetre scale an object of known dimensions was

photographed with the millimetre scale. The length of the object was measured in pixels from the digital image using IMAQ™ Vision Builder Version 6.1 and the millimetre scale was used to convert the length of the object from pixels to millimetres (as described in Section 4.2.3ii and Figure 4.6). The length of the object measured from the digital image was compared to the known length of the object.

Millimetre scale precision

The repeatability, test-retest precision and inter-examiner precision (Figure 4.7) of measuring 1mm in pixels from the millimetre scale to convert synovial fold cross-sectional area measurements from pixels to millimetres was determined using the limits of agreement method (see section 4.2.3iii limits of agreement with single measures).

4.2.3v Measurement accuracy

Water displacement frequently serves as the gold standard for quantifying the volume of anatomical structures (Peterfy et al., 1995; Partik et al., 2002). To assess the accuracy of the computer-aided technique of measuring and calculating synovial fold volume from sagittal sections developed in the present study, a 'water displacement method' was devised to measure the volume of the synovial folds (Figure 4.8). In addition, a plastic cylinder of known dimensions was used to examine the accuracy of the water displacement method devised for this study. A 25ml glass burette (Volac, Poulten and Graf, Germany; accurate to 0.05ml) attached to a burette stand was positioned in front of a digital camera (Nikon Coolpix 5400, Nikon Corporation, Tokyo, Japan) fixed to a tripod (GX-86, OSAWA, Japan) (Figure 4.8).

The burette was filled with approximately 20ml of water and carefully checked to ensure that no air bubbles were present. The interior of the burette above the meniscus was thoroughly dried. A spirit level was used to ensure that both the burette and camera were aligned and level. The meniscus was photographed using the timer setting. A plastic cylinder of known volume (diameter 4.00mm and height 5.00mm) was dropped into the burette and once it had reached the bottom of the burette, the meniscus was photographed a second time. Prior to dropping the plastic cylinder into the burette the dimensions of the cylinder were measured using the digital calipers and the volume calculated (volume=$\Pi r^2 h$). The portion of the ventral synovial fold from a cervical spine sagittal section was carefully resected from the adjacent fibrous capsule and released into the burette. The meniscus was photographed once the synovial fold had fallen to

the bottom of the burette. The dorsal synovial fold portion was then removed from the section, dropped into the burette and the meniscus photographed a final time. The burette was emptied and the ventral and dorsal synovial folds stored in labelled microtubes containing wetting fluid. The whole process was repeated for each sagittal section of three lateral atlanto-axial joints.
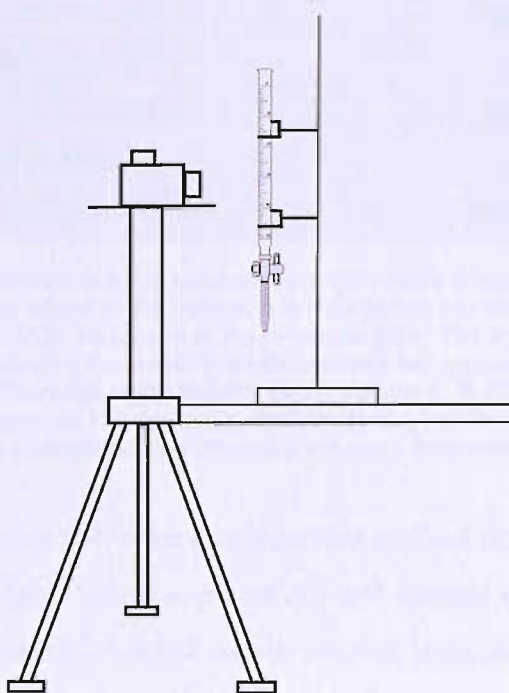
Figure 4.8. Set-up for water displacement method. The burette was fastened to the burette stand and the digital camera was fixed to the tripod. A spirit level was used to ensure a level burette and camera position. The burette was filled with approximately 20ml water and the meniscus positioned in the centre of the field of view. The camera was focussed and the photograph was taken using the timer setting.

The digital images were uploaded to a computer using Nikon View (Nikon Corporation, Tokyo, Japan), labelled and stored on a computer hard-drive and CD-ROM. IMAQ^{TM} Vision Builder Version 6.1 (National Instruments, Austin, Texas, USA) was used to quantify the amount of water displacement and hence volume of the cylinder and synovial folds. From the same graduation line on each digital image, a line parallel to the vertical edge of the burette was drawn to the bottom of the meniscus (Figure 4.9). The length of the line was converted from pixels to cubic millimetres by measuring the length in pixels between two graduations demarcating 0.01mm^3, using a line parallel to the vertical edge of the burette, and entering these values into the Simple Calibration tool of IMAQ^{TM} Vision Builder (Figure 4.9). The volume of the cylinder and synovial fold portions was calculated by subtracting the volume of water measured from the same graduation line between photographs, e.g. volume plus cylinder minus volume

without cylinder (Figure 4.9). For the synovial folds this gave the 'sectional volume' which was summed to give the 'total volume' of a whole synovial fold.
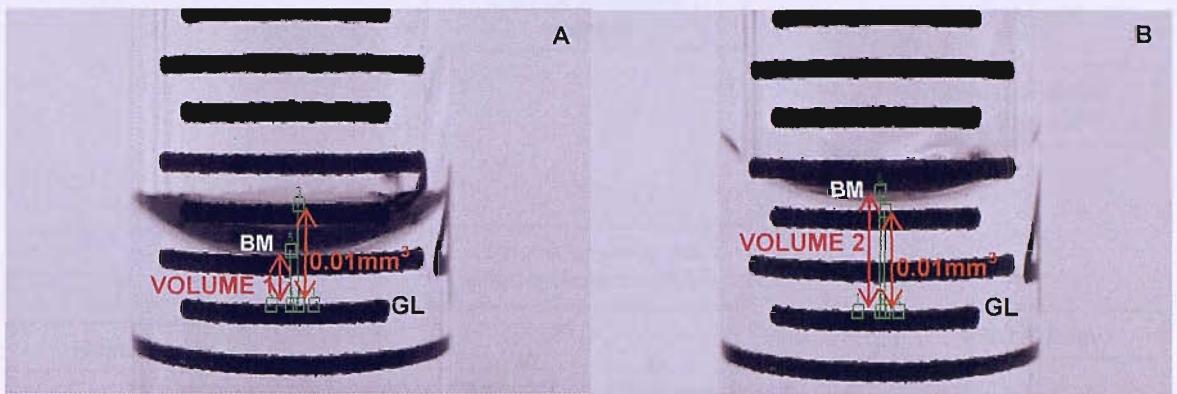
Figure 4.9. The measurement of water displacement from digital images. **A.** Before the cylinder (or synovial fold portion) was added to the burette, a line parallel to the vertical edge of the burette was drawn from a graduation line (GL) to the bottom of the meniscus (BM). The line was converted from pixels to cubic millimetres by measuring the length in pixels between two graduations demarcating $0.01mm^3$, using a line parallel to the vertical edge of the burette, giving Volume 1. **B.** This process was repeated after adding the cylinder (or synovial fold portion) to the burette to give Volume 2. The volume of the cylinder (or synovial fold portion) was calculated by subtracting Volume 1 from Volume 2.

The agreement between the water displacement method and the CAT measurement methods devised in this study (i.e. auto-CAT and manual-CAT), for the measurement of synovial fold sectional volume and whole volume, were calculated using the limits of agreement method (see section 4.2.3iii limits of agreement with single measures). The accuracy of the water displacement method of measurement was determined by assessing the agreement between the known volume of the cylinder and the cylinder volume determined from water displacement using the limits of agreement method of analysis (see section see section 4.2.3iii limits of agreement with single measures).

4.2.3vi Summary of measurement precision and accuracy for the determination of synovial fold volume

Figure 4.10 summarises the data collected for the determination of measurement precision of the computer-aided techniques developed in the present study. The accuracy of the computer-aided techniques was determined by assessing the method agreement between the computer-aided techniques and the water displacement method.
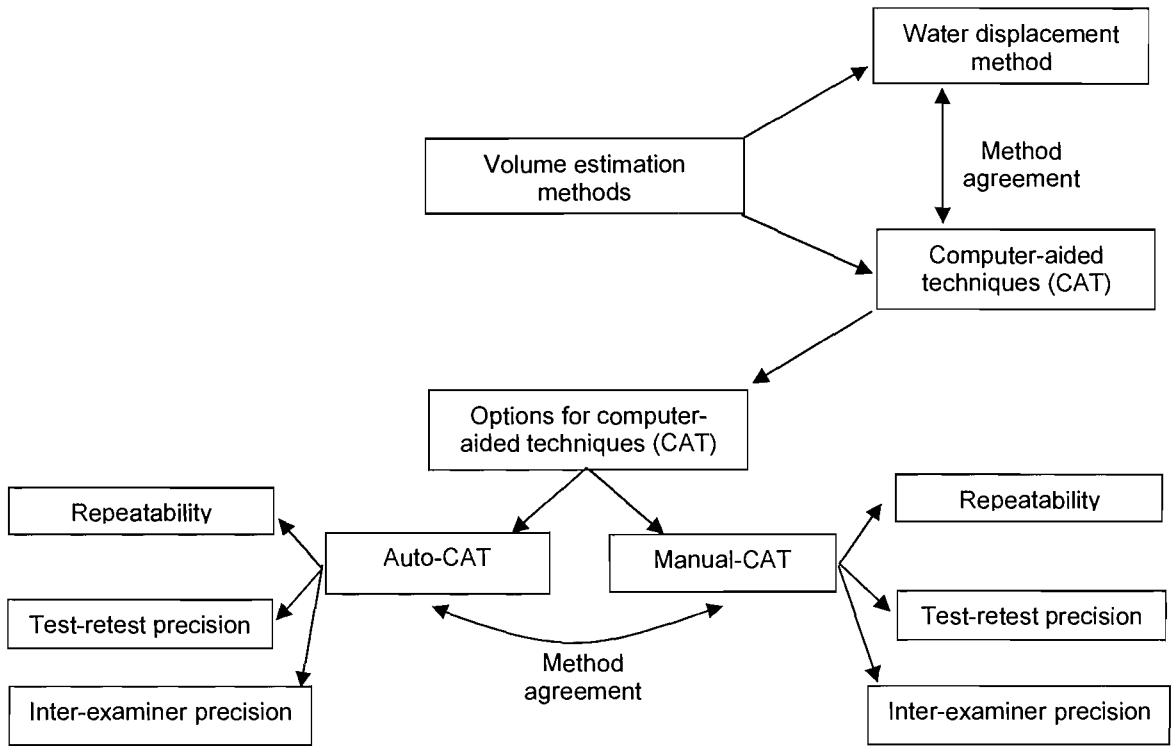
Figure 4.10. Summary of data collected for the determination of precision and accuracy for the measurement of synovial fold volume using the computer-aided techniques (CAT).

4.3 Results

The cervical spines of 10 female (mean 86.6 years, SD 7.88 years) and 4 male (mean 83 years, SD 7.62 years) embalmed cadavers, aged from 75-102 years (mean 85.57 years, SD 7.69 years), were used in this study. A total of 27 lateral atlanto-axial joints (13 left and 14 right) were available for study, as one cervical spine had previously been hemisected. Gender, age at death and cause of death were recorded for all specimens (Table 4.2). The radiological report for each specimen is given in Table 4.2. 10.5 cervical spines were sectioned in the sagittal plane, 2 cervical spines in the coronal plane and 1 cervical spine in the transverse plane.

4.3.1 Prevalence and gross morphology

Good quality sections were obtained in all planes and the synovial folds and their anatomical relationships were clearly demonstrated. Synovial folds were present in 100% of the lateral atlanto-axial joints studied, and were located at both the ventral and dorsal poles of the right and left joints in all specimens. In the present study, ventral and dorsal synovial folds of the right lateral atlanto-axial joints are referred to as the right ventral and right dorsal synovial folds, respectively; and the ventral and dorsal synovial folds are referred to as the left ventral and left dorsal synovial folds, respectively.

Table 4.2. Specimen characteristics

Subject number	Age (years)	Gender	Cause of death	Anatomical sections	Plain film radiography
1	90	Female	Bronchopneumonia	Sagittal[a]	-
2	102	Female	Old age Pneumonia	Sagittal	Lateral atlanto-axial joint space decreased bilaterally. Decreased ADI with associated sclerosis. Reduced intervertebral disc space at C4/C5. Hypertrophy and sclerosis of C2/C3 to C5/C6 articular pillars bilaterally.
3	92	Female	Bronchial carcinoma	Sagittal	Right lateral atlanto-axial joint space slightly decreased laterally with mild osteophytosis of the C1 lateral mass. Sclerosis at median atlanto-axial joint. Reduced intervertebral disc height C4/C5, C5/C6 & possibly C6/C7, with anterior osteophytes. Facet hypertrophy & sclerosis from right C3/C4 to C6/C7, worse at right C4/C5 level. Bilateral uncinate process hypertrophy & sclerosis C5, C6, C7.
4	84	Male	Old age Rheumatoid arthritis	Sagittal	Apparent reduction of left lateral atlanto-axial joint space, however, this could be a positional loss of joint space. List to left. Slight anterior translation of C1. Increased atlanto-dental interspace. Kyphosis at C2/C3. Total loss of intervertebral disc space C3/C4 & C4/C5 with anterior osteophytes and end-plate sclerosis. Mild C4/C5 facet hypertrophy bilaterally. Bilateral C4/C5 uncinate process hypertrophy, worse on the right.
5	80	Male	Myocardial infarction	Sagittal	Reduced intervertebral disc height C4/C5 & C5/C6 with anterior osteophytes and possibly posterior osteophytes at the C5/C6 level. Hypertrophy of the C5 & C6 uncinate processes (especially C6) & C5/C6 facet hypertrophy.
6	93	Male	Bronchopneumonia	Sagittal	Possible left lateral atlanto-axial joint sclerosis so possibly some reduction in joint space (difficult to see due to xray beam divergence). Reduced intervertebral disc height, anterior osteophytes & end-plate sclerosis between C3/C4 & C6/C7. Posterior osteophytes at C5/C6. Bilateral uncinate process hypertrophy between C4 & C7, appears worse on the left. Mild facet hypertrophy bilaterally between C4/C5 & C6/C7.
7	75	Female	Acute myocardial infarction	Sagittal	Reduced atlanto-dental interspace associated with an irregular & reduced joint space & sclerosis. Difficult to view lateral atlanto-axial joint spaces, but right lateral atlanto-axial joint space appears to be reduced. Decreased C5/C6 intervertebral disc space with small anterior osteophytes. Facet hypertrophy bilaterally at C4/C5 & C5/C6.
8	75	Male	Myocardial infarction	Sagittal	Minor osteophyte and mild narrowing of the joint space at the left lateral atlanto-axial joint.
9	81	Female	Stroke	Sagittal	Reduced ADI and sclerosis of the median atlanto-axial joint.

Subject number	Age (years)	Gender	Cause of death	Anatomical sections	Plain film radiography
10	83	Female	Myocardial infarction	Sagittal	Spinous processes rotated to the right. Median atlanto-axial joint narrowed with sclerosis. Right lateral atlanto-axial joint narrowed. Reduced intervertebral disc height and bilateral zygapophysial joint hypertrophy and sclerosis at C3/C4, C4/C5 and C5/C6.
11	79	Female	Bronchopneumonia	Sagittal	Asymmetry of the right and left lateral atlanto-axial joints. Slight narrowing of the right lateral atlanto-axial joint with marginal sclerosis indicative of early degeneration. Bilateral hypertrophy of the C2/C3, C3/C4 and C4/C5 zygapophysial joints with sclerosis especially evident at C3/C4 and C4/C5. C2 spinous process rotated to the right which may account for the reduced joint space at the right lateral atlanto-axial joint space.
12	85	Female	Bronchopneumonia	Coronal	Reduced joint space left lateral atlanto-axial joint with lateral osteophytosis & sclerosis. Pronounced C2/C3 facet hypertrophy & sclerosis. Mild facet hypertrophy at all other levels bilaterally. Reduced intervertebral disc space, end-plate sclerosis & anterior osteophytes C3/C4, C4/C5 & C5/C6.
13	86	Female	Myocardial infarction	Coronal	Reduced atlanto-dental interspace with sclerosis. Mild decrease in C4/C5 & C5/C6 intervertebral disc spaces. Facet hypertrophy and sclerosis at C3/C4, C4/C5 & C5/C6, worse on the right compared to the left. Difficult to view lateral atlanto-axial joint spaces.
14	93	Female	Bronchopneumonia Heart disease	Transverse	Reduced joint space left lateral atlanto-axial joint. Decreased atlanto-dental interspace & sclerosis. Decreased intervertebral disc height, anterior osteophytes & end-plate sclerosis at C5/6 & C6/7. Bilateral facet hypertrophy C3/4, C4/C5, C5/C6 & C6/C7 that is greatest at C3/C4.

[a]Left hemisection of the cervical spine. ADI – atlanto-dental interspace

Sagittal sections

In sagittal section, the articular surfaces were convex and covered by hyaline articular cartilage that was thick centrally and thinner peripherally at the ventral and dorsal joint margins (Figure 4.11). The incongruency of the convex hyaline articular cartilage surfaces created large ventral and dorsal articular recesses that were filled by the triangular-shaped intra-articular synovial folds (Figure 4.11).
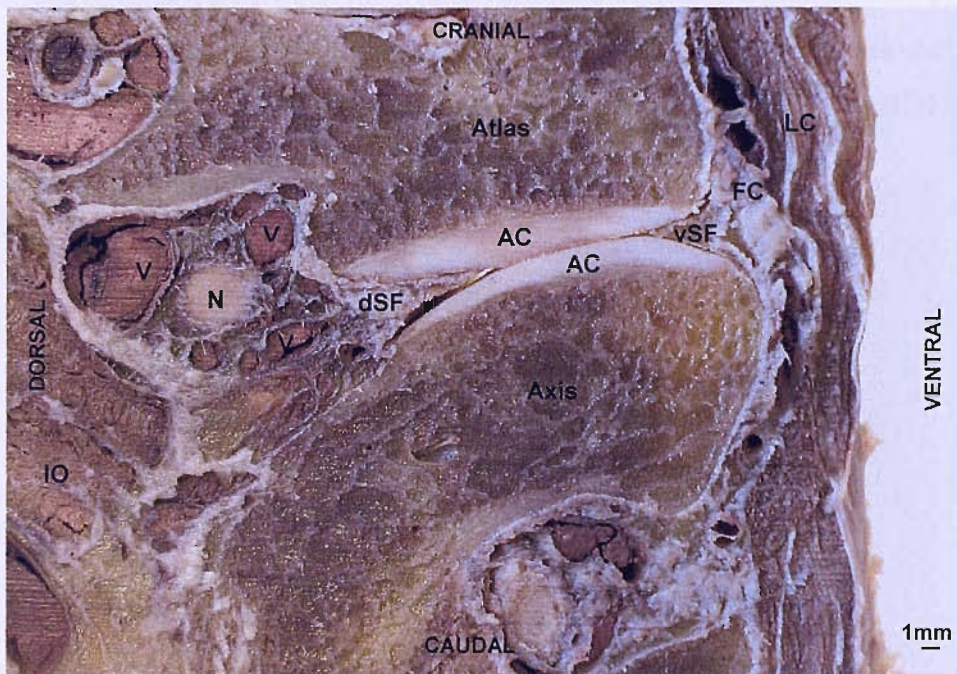
Figure 4.11. Sagittal section of the right lateral atlanto-axial joint (lateral view) of Subject 5. The convex hyaline articular cartilages (AC) are in contact at the centre of the joint but diverge ventrally and dorsally to form the articular recesses containing the ventral (vSF) and dorsal (dSF) synovial folds. Posterior to the articulation lies the C2 spinal nerve (N), surrounded by veins (V), and the inferior oblique suboccipital muscle (IO). Anterior to the fibrous capsule (FC) lie the longus colli and capitis muscles (LC).

The articular fibrous capsule was attached to the periosteum of the atlas and axis two to three millimetres distant from the edges of the hyaline articular cartilage. 'Bare-areas' (see Figure 2.1, Chapter 2) filled the intervening two to three millimetre space between the fibrous capsule attachment and the hyaline articular cartilage. The ventral fibrous capsule was thicker and better defined than the dorsal fibrous capsule and was reinforced by the longus colli and longus capitis muscles (Figure 4.11). A plexus of veins surrounded the C2 spinal nerve as it passed transversely close to the external surface of the dorsal fibrous capsule. The inferior oblique suboccipital muscle was posterior to the C2 spinal nerve (Figure 4.11). On sagittal section, the ventral and dorsal synovial folds appeared to be completely enclosed by the fibrous capsule and there was no evidence of openings in the capsule that could enable the synovial folds to form extracapsular communications.

The shape and size of the synovial folds appeared to be quite variable between specimens. In all specimens the wide, thick base of the synovial fold was continuous with the internal aspect of the fibrous capsule and tapered to form a thin free border (apex) which projected varying distances between the articular surfaces. On sagittal section, the synovial folds typically appeared triangular in shape and frequently reciprocated the shape of the hyaline articular cartilage surfaces. All the synovial folds in this study projected between the hyaline articular cartilage surfaces. 38% of synovial folds were observed to have a tufted or ragged apex, the majority of these were dorsal synovial folds. Blood vessels were occasionally apparent within the synovial folds.
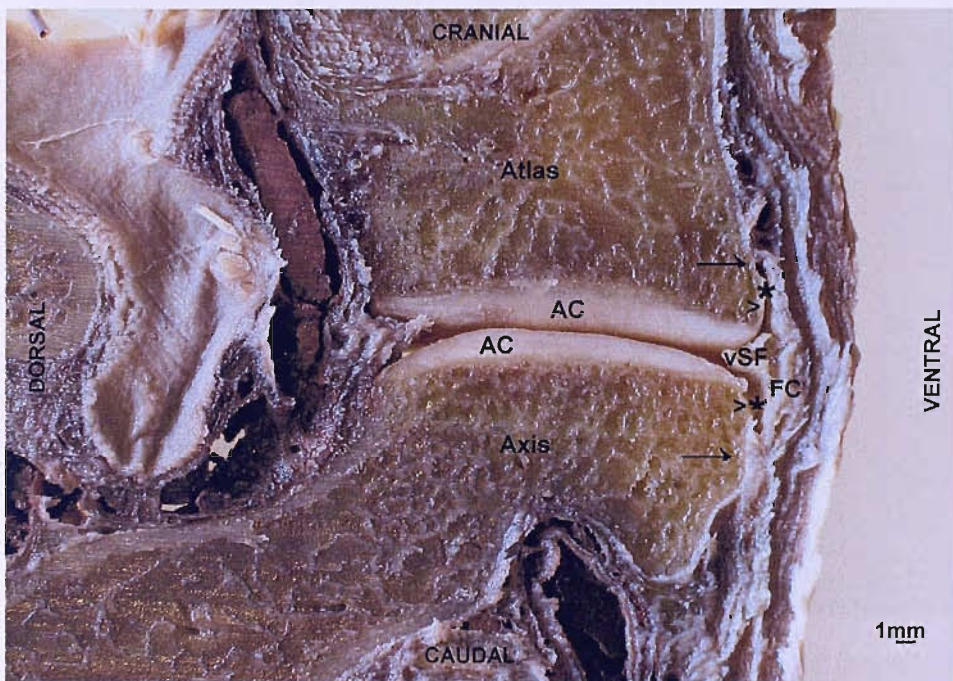
Figure 4.12. Sagittal section of the left lateral atlanto-axial joint (medial view) of Subject 5. The ventral fibrous capsule (FC) attaches (→) to the lateral masses a few millimetres distant to the hyaline articular cartilage (AC) creating superior and inferior extensions (*) of the articular recess which are bordered ventrally by the fibrous capsule and dorsally by the bare area (>) and contain the ventral synovial fold (vSF).

In all specimens, the articular recess extended superiorly and inferiorly over the edges of the C1 and C2 lateral masses and appeared to be more extensive at the ventral aspect of the joint (Figure 4.12). The superior and inferior extensions of the articular recesses were formed by the fibrous capsule attaching distant to the hyaline articular cartilage and did not typically contain the synovial folds. The superior and inferior extensions of the ventral articular recesses were bordered ventrally by the fibrous capsule and dorsally by the adjacent bare area. The superior extension was bordered by the synovial fold inferiorly and the fibrous capsule attachment site superiorly and vice versa for the inferior extension.

The hyaline articular cartilage covering the inferior articular facet of the atlas at the dorsal aspect of the left lateral atlanto-axial joint of Subject 6 was indented. The adjacent dorsal synovial fold occupied the indentation and the shape of the synovial fold reciprocated that of the cartilage indentation (Figure 4.13). The dorsal synovial fold of the left lateral atlanto-axial joint of Subject 7 and the ventral synovial fold of the right lateral atlanto-axial joint of Subject 9 occupied similar indentations in the adjacent hyaline articular cartilage covering the articular facets of the axis and atlas, respectively.
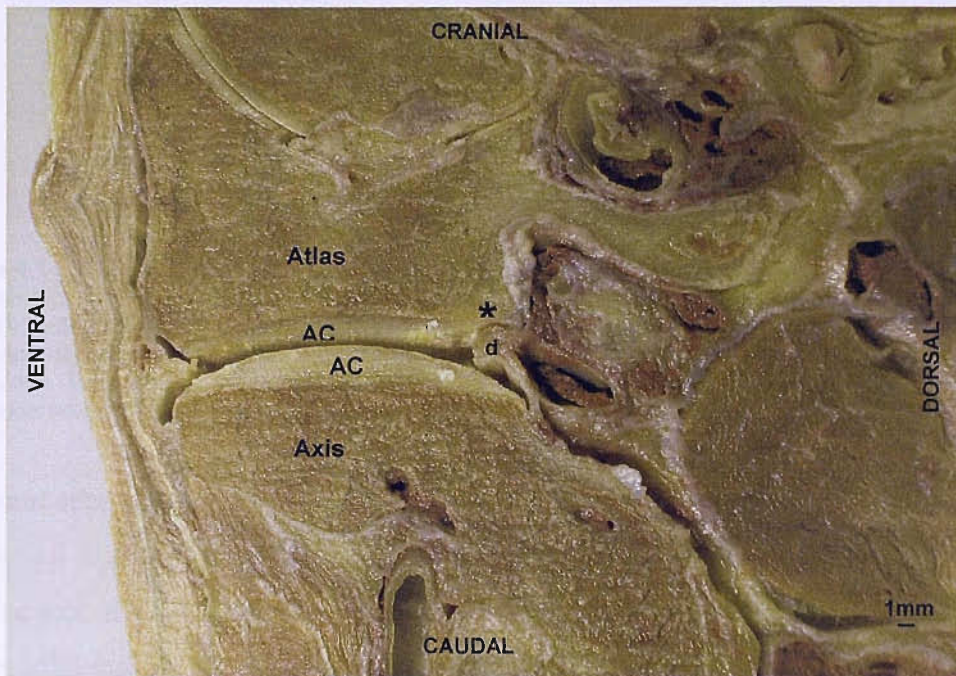
Figure 4.13. Sagittal section of the right lateral atlanto-axial joint (medial view) of Subject 6. The dorsal intra-articular synovial fold (d) is rounded in shape and lies in a reciprocally shaped recess (*) within the hyaline articular cartilage covering the inferior articular facet of the atlas.

The right ventral, right dorsal and left dorsal synovial folds of Subject 4 were very large. The base of these synovial folds extended into and filled the superior and inferior extensions of the articular recesses (Figure 4.14). These enlarged synovial folds appeared to consist of layers of tissue in parts and the right ventral synovial fold contained a cyst-like structure (Figure 4.14). The elaborate apices were tortuous and bulbous and extended into the joint cavity, nearly covering the entire articular surface which was virtually devoid of hyaline articular cartilage (Figure 4.14). Erosions of the joint margins were also observed. From the medical history, it was noted that this subject had suffered from rheumatoid arthritis (Table 4.2).
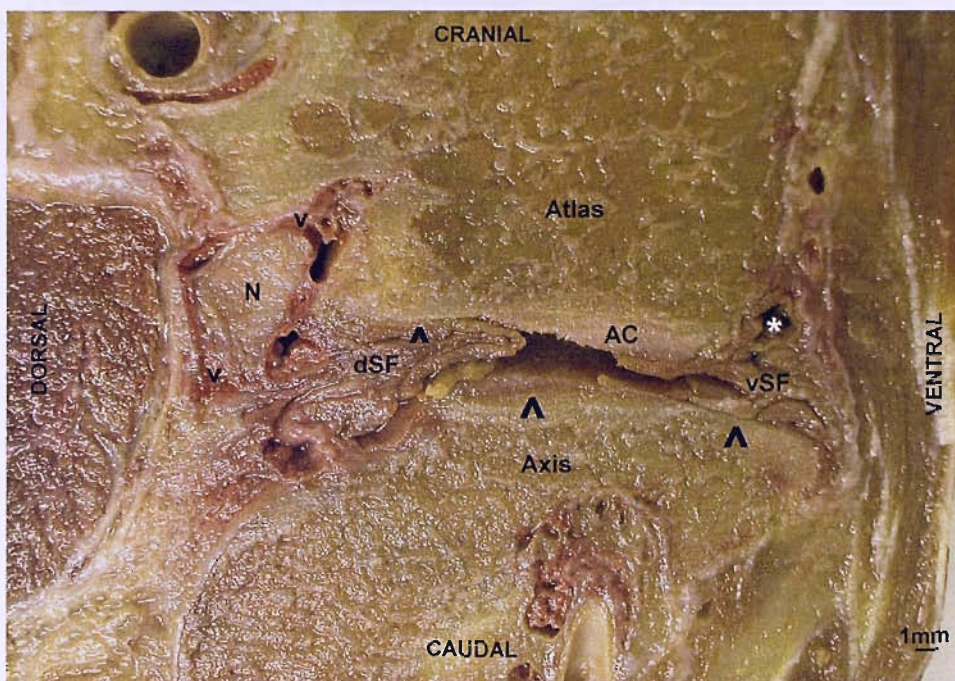
Figure 4.14. Sagittal section of the right lateral atlanto-axial joint (lateral view) of Subject 4 (medical history of rheumatoid arthritis). The hyaline articular cartilage (AC) is virtually absent over the C2 superior articular facet (^) and absent at the dorsal aspect of the C1 inferior articular facet (^). Large convoluted ventral (vSF) and dorsal (dSF) intra-articular synovial folds fill the articular recesses and their superior and inferior extensions. The veins (v) surrounding the C2 spinal nerve (N) are not clearly evident. A 'cyst-like' structure (*) can be seen in the ventral synovial fold.

Coronal sections

In coronal section, the articular surfaces of the atlas and axis were virtually flat. The hyaline articular cartilage was thick centrally and thinner peripherally at the medial and lateral joint margins. Parts of the synovial folds were observed protruding into the medial and lateral aspects of the joint cavity and were continuous with the internal aspects of the medial and lateral fibrous capsule, respectively (Figure 4.15 and Figure 4.16). No holes were visible in the fibrous capsule and the synovial folds were not observed to extend through the fibrous capsule. There appeared to be some continuity between the fibrous capsule of the lateral atlanto-axial joints and the articular connective tissues of the median atlanto-axial and atlanto-occipital joints (Figure 4.16).

Transverse sections

The attachments of the fibrous capsule to the ventral and dorsal articular margins of the atlas and axis were evident on transverse section and the base of the synovial folds could be seen attached to the inner aspect of the fibrous capsule. No extracapsular communications were visible in this plane of section.

97
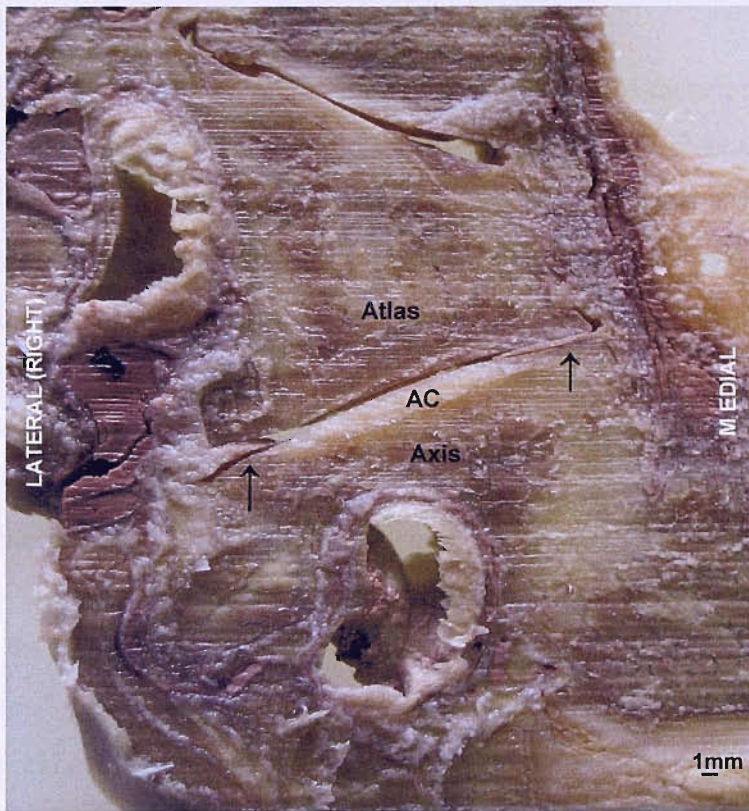
Figure 4.15. Coronal section through the dorsal aspect of the right lateral atlanto-axial joint (anterior view) of Subject 12. The hyaline articular cartilage (AC) covering the superior articular facet of the axis appears flat and a thin layer of cartilage can be seen covering the inferior articular facet of the atlas. The medial and lateral aspects of the dorsal synovial fold (↑) are visible.
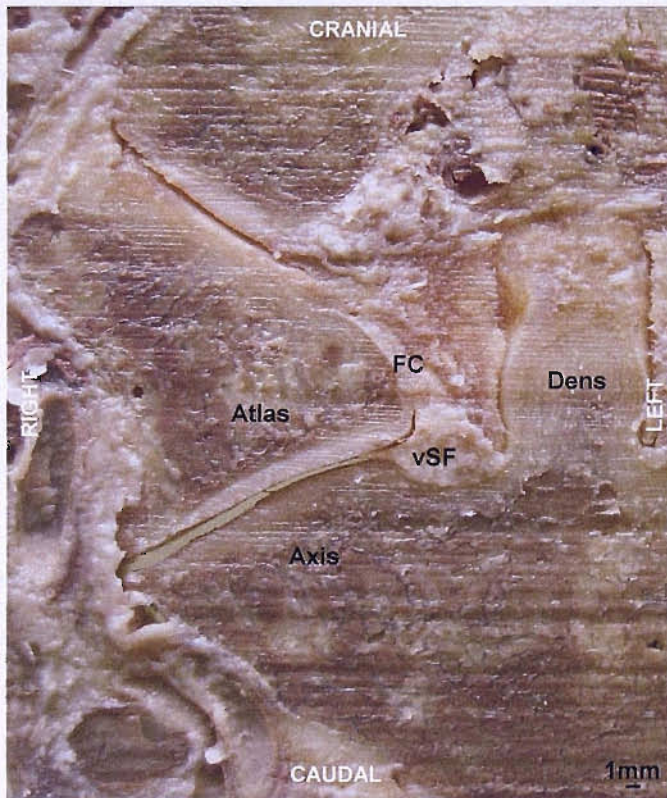
Figure 4.16. Coronal section through the ventral aspect of the right lateral atlanto-axial joint (anterior view) of Subject 12. The medial aspect of the ventral synovial fold (vSF) can be seen projecting between the articular surfaces of the atlas and the axis. The synovial fold appears to be enclosed by the medial fibrous capsule (FC).

4.3.2 Dimensions of the synovial folds

10 paired (10 left, 10 right) lateral atlanto-axial joints, and therefore 40 synovial folds, were available for study from 4 male (mean 83 years, SD 7.62 years) and 6 female (mean 87.5 years, SD 11.96 years) subjects aged 75 to 102 years (mean 85 years, SD 9 years). Subject 4 was excluded from this part of the study as this subject had a medical history of rheumatoid arthritis (Tables 4.2 and 4.4). Rheumatoid arthritis is known to cause hypertrophy of the synovial membrane. With Subject 4 excluded, 9 paired lateral atlanto-axial joints (9 left, 9 right), and therefore 36 synovial folds, were available from 3 male (mean 82.67 years, SD 9.29 years) and 6 female (mean 87.5 years, SD 11.96 years) subjects aged 75 to 102 years (mean 85.43 years, SD 10.34 years).

Synovial folds were present in 3 to 4 sagittal sections per joint. The depth of projection (DOP), cross-sectional area (CSA) and sectional volume of the synovial folds were measured and calculated from 137 sagittal sections of the cervical spine (Table 4.3).

Table 4.3. The depth of projection (DOP) (mm), cross-sectional area (CSA) (mm^2) and sectional volume (mm^3) of the synovial folds of the lateral atlanto-axial joints.

	Dimensions of the synovial folds from sagittal sections			Dimensions of the synovial folds (Subject 4 excluded) from sagittal sections		
	n	Median (range)	Mean (SD)	n	Median (range)	Mean (SD)
DOP (mm)	137	2.96 (0.61 to 9.37)	3.35 (1.84)	123	2.86 (0.61 to 6.81)	3.13 (1.54)
CSA (mm^2)	137	3.59 (0.17 to 22.13)	4.79 (4.19)	123	3.44 (0.17 to 15.31)	4.28 (3.16)
Sectional volume (mm^3)	137	10.78 (0.51 to 66.14)	14.39 (12.56)	123	10.33 (0.51 to 45.94)	12.83 (9.47)

Whole synovial fold volume was calculated from the CSA and subsequent sectional volume measurements. The volume of the ventral and dorsal synovial folds of the right and left lateral atlanto-axial joints are presented in Table 4.4 and Figure 4.17. There was a significant difference in volume between the synovial folds ($\chi^2(3)=8.73$, P=.03) (n=9). Wilcoxon's signed-rank test was used to follow up this finding. A *Bonferroni correction* was applied so all effects are reported at a .0125 level of significance. Right ventral was greater than right dorsal synovial fold volume (Z=-1.96, P=.06) and left ventral was greater than left dorsal synovial fold volume (Z=-2.19, P=.03) but the differences were not significant. Right ventral and left ventral synovial fold volume was the same and not significantly different (Z=-0.30, P=.82). Left dorsal was larger than right dorsal synovial fold volume but the difference was not significant (Z=-1.60, P=.13).

Table 4.4. The volume (mm³) of the synovial folds at the lateral atlanto-axial joints of 9 subjects and 1 subject with a medical history of rheumatoid arthritis.

	Age	Gender	Synovial fold volume (mm³)			
			Right ventral synovial fold	Right dorsal synovial fold	Left ventral synovial fold	Left dorsal synovial fold
Female subjects						
Subject 2	102	Female	68.88	8.62	47.86	31.69
Subject 3	92	Female	83.46	28.59	105.17	35.34
Subject 7	75	Female	47.33	10.87	34.55	33.45
Subject 9	81	Female	26.61	30.23	54.52	67.30
Subject 10	83	Female	35.73	20.77	31.45	26.87
Subject 11	79	Female	32.49	12.25	30.42	11.29
Mean (SD)	87.5 (11.96)		48.68 (22.28)	18.24 (9.05)	54.11 (27.41)	33.94 (17.72)
Male subjects						
Subject 5	80	Male	59.78	64.87	47.94	36.59
Subject 6	93	Male	33.63	34.48	61.88	51.46
Subject 8	75	Male	114.91	26.41	63.83	41.92
Mean (SD)	82.67 (9.29)		68.87 (41.85)	41.51 (20.32)	57.53 (9.33)	42.93 (7.38)
All subjects						
Mean (SD)	**84.44 (9.22)**		**55.41 (29.16)**	**26.00 (17.02)**	**55.25 (22.23)**	**36.94 (15.17)**
Subject with rheumatoid arthritis						
Subject 4	84	Male	140.19	115.45	32.71	102.65
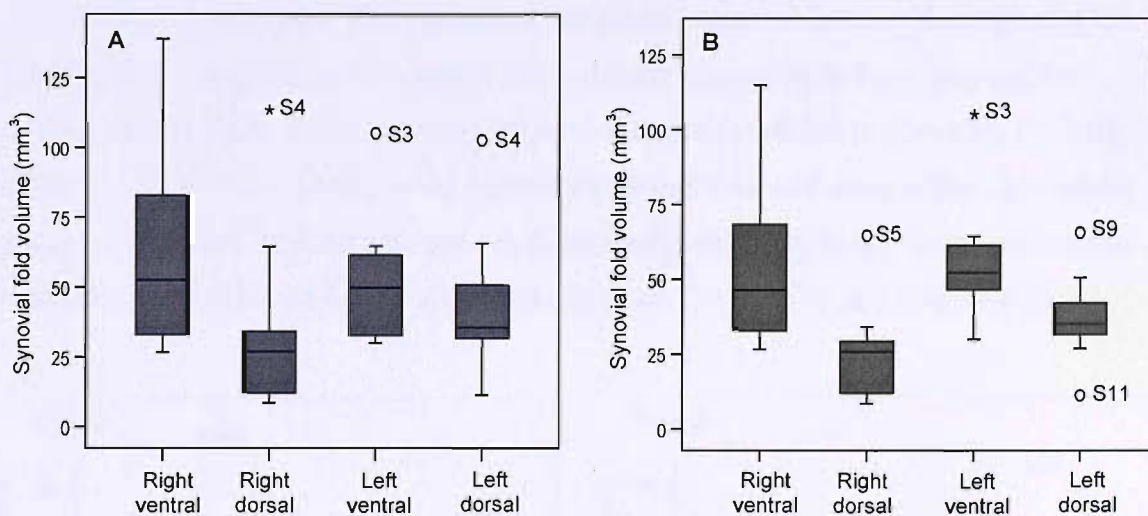
Figure 4.17. Boxplot of ventral and dorsal synovial fold volume (mm³) at the right and left lateral atlanto-axial joints of **A.** all subjects (n=10) and **B.** all subjects with Subject 4 excluded (n=9) showing the range of values and the median (——). o=outlier; *=extreme outlier; S=subject number

The volume of the ventral and dorsal synovial folds of the right and left lateral atlanto-axial joints of male and female subjects are compared in Table 4.4 and Figure 4.18. Both male and female subjects demonstrated the same general trend of larger right ventral compared to right dorsal synovial folds and larger left ventral compared to left dorsal synovial folds. The synovial fold volume of the male subjects was greater than that of the female subjects.
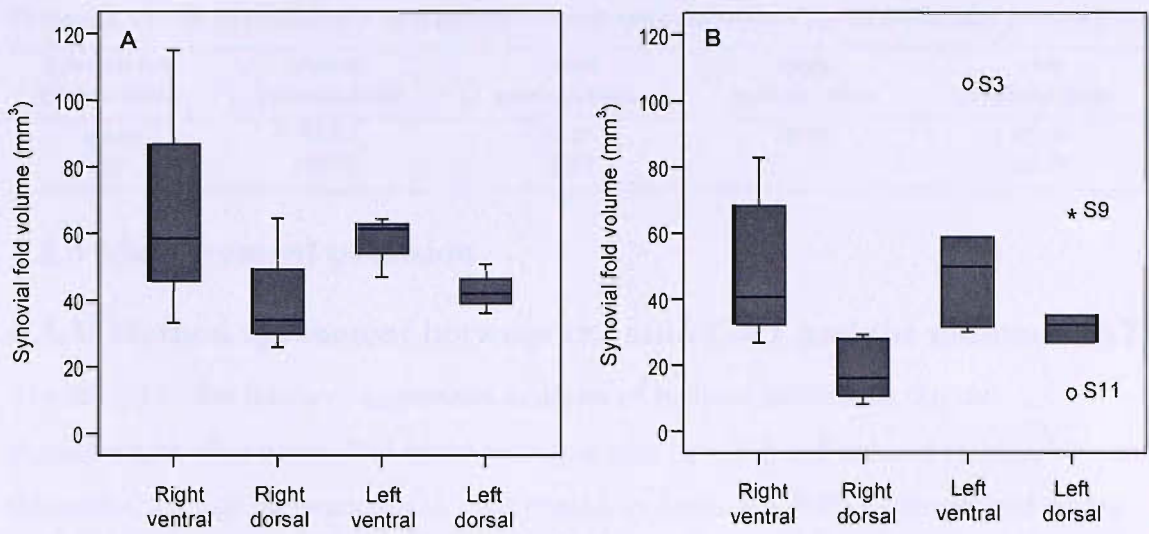
Figure 4.18. Boxplot of ventral and dorsal synovial fold volume (mm³) at the right and left lateral atlanto-axial joints of **A.** male (n=3) and **B.** female (n=6) subjects. Median (——); o=outlier; *=extreme outlier; S=subject number

Further analysis was undertaken to compare the volume of the ventral and dorsal synovial folds and the left and right synovial folds (Table 4.5). The Wilcoxon signed-rank test was used and a *Bonferroni correction* applied, so all effects are reported at a .025 level of significance. The volume of the ventral synovial folds of the right and left lateral atlanto-axial joints were significantly greater compared to the volume of the dorsal synovial folds of the right and left lateral atlanto-axial joints (Z=-3.11, P=.001) (Figure 4.19.A). The volume of the ventral and dorsal synovial folds of the right lateral atlanto-axial joints were similar and not significantly different to the ventral and dorsal synovial folds of the left lateral atlanto-axial joints (Z=-1.29, P=.21) (Figure 4.19.B).
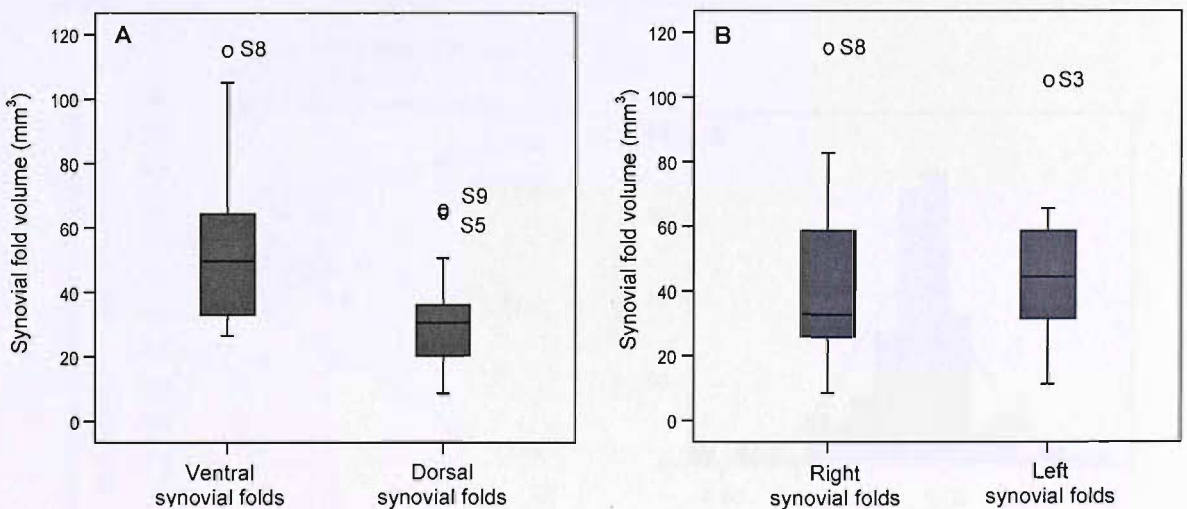
Figure 4.19. Boxplot showing the range of values and the median (——) for the volume (mm³) of the **A.** ventral synovial folds of the right and left lateral atlanto-axial joints and dorsal synovial folds of the right and left lateral atlanto-axial joints (n=18) **B.** ventral and dorsal synovial folds of the right lateral atlanto-axial joints and ventral and dorsal synovial folds of the left lateral atlanto-axial joints (n=18). o=outlier; S=subject number

101

Table 4.5. Ventral and dorsal and right and left synovial fold volume (mm^3) at 18 lateral atlanto-axial joints.

Synovial fold volume (mm^3)	Ventral synovial folds	Dorsal synovial folds	Right synovial folds	Left synovial folds
Mean	55.33	31.47	40.70	46.09
SD	25.15	16.62	27.67	20.73

4.3.3 Measurement precision

4.3.3i Method agreement between the auto-CAT and the manual-CAT

The results of the limits of agreement analysis of method agreement, for the measurement of synovial fold cross-sectional area (n=137) and volume (n=40), between the auto-CAT and the manual-CAT are shown in Table 4.6. 93% of the plotted points were within the limits of agreement (Figures 4.20.A and 4.21.A). The differences diverged as the magnitude increased and Pearson's correlation coefficient showed that the difference was negatively related to the mean indicating the presence of both heteroscedasticity and proportional bias, respectively. To adjust for this the modified regression approach was performed (Figures 4.20.A and 4.21.A).

Table 4.6. Method agreement between the auto-CAT and the manual-CAT for the measurement of synovial fold cross-sectional area (CSA) (mm^2) (n=137) and volume (mm^3) (n=40).

					Comparison of two measurement methods: auto-CAT and manual-CAT			
	d	1.96s$_d$	SE(d)	95%CI(d)	95%LoA	SE(LoA)	95% CI lower LoA	95% CI upper LoA
CSA (mm^2)	-0.09	0.33	0.01	-0.12→ 0.19	-0.41→ 0.24	0.02	-0.46→ -0.37	0.19→ 0.29
Volume (mm^3)	-0.89	2.25	0.03	-0.95→ -0.82	-3.14→ 1.36	0.05	-3.25→ -3.03	1.25→ 1.47
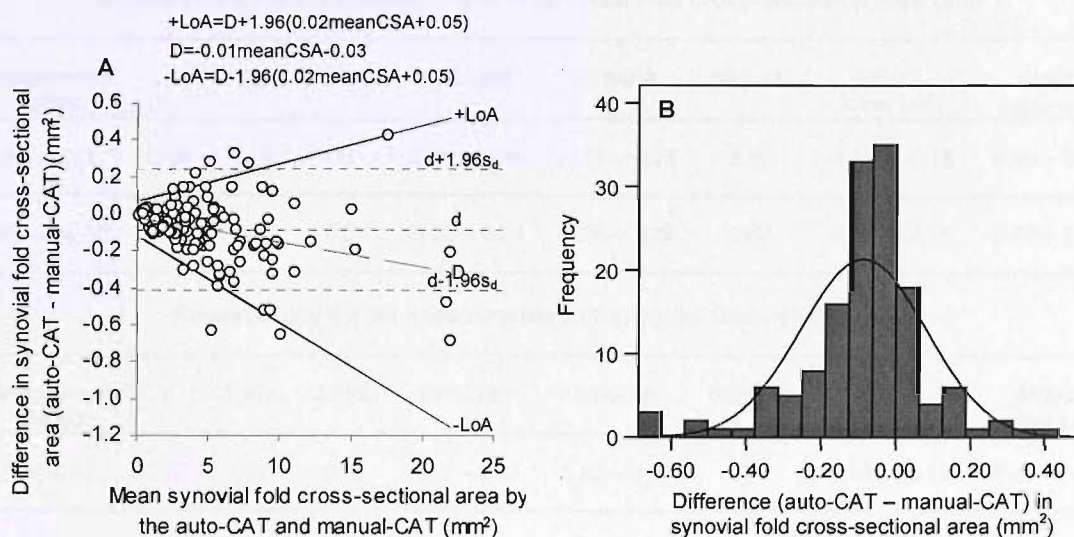
Figure 4.20.A. Difference against mean for synovial fold cross-sectional area (CSA) (mm^2) measured by the auto-CAT and manual-CAT (r=-.33, P=.000. **B.** Histogram of differences for synovial fold CSA (mm^2) measured by the auto-CAT and the manual-CAT (KS test P=.000).
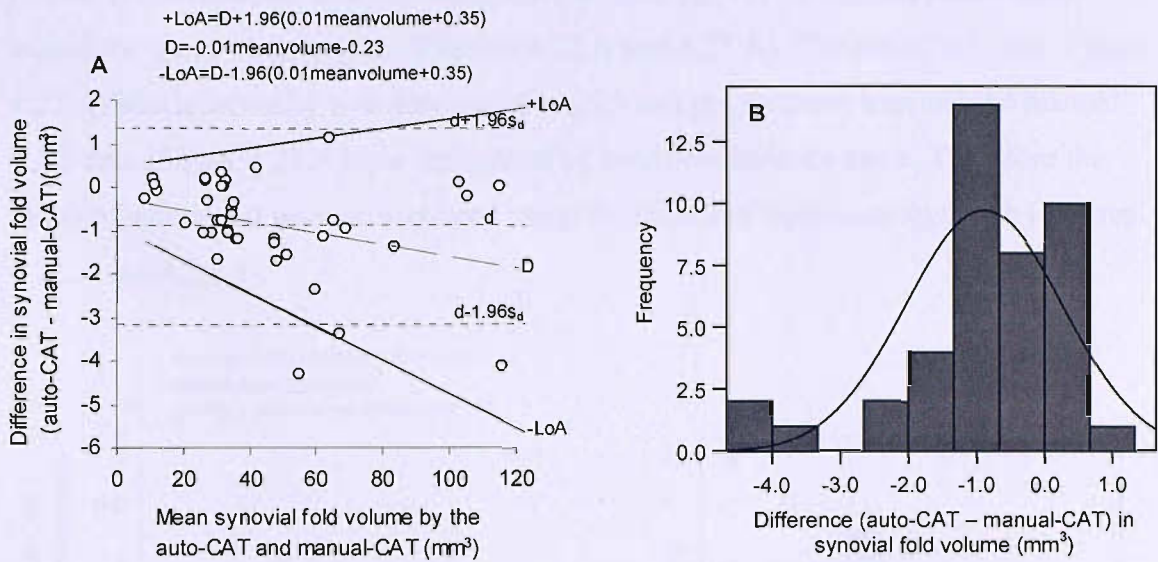
Figure 4.21.A. Difference against mean for synovial fold volume (mm^3) measured by the auto-CAT and the manual-CAT (r =-.37, P=.02). **B.** Histogram of differences for synovial fold volume measured by the auto-CAT and the manual-CAT (KS test P=.02).

4.3.3ii Repeatability of the auto-CAT and the manual-CAT

The results of the limits of agreement analysis of repeatability, for the measurement of synovial fold cross-sectional area and volume, for the auto-CAT and the manual-CAT are shown in Table 4.7. 66 repeat measurements of synovial fold cross-sectional area and 14 repeat measurements of synovial fold volume were made for both the auto-CAT and the manual-CAT.

Table 4.7. Repeatability of the auto-CAT and the manual-CAT for the measurement of synovial fold cross-sectional area (mm^2) (n=66) and volume (mm^3) (n=14).

Repeatability for the measurement of synovial fold cross-sectional area (mm^2)

Measurement method	d	1.96s$_d$	SE(d)	95%CI(d)	95%LoA	SE(LoA)	95%CI lower LoA	95%CI upper LoA
Auto-CAT	0.04	0.22	0.01	0.01→ 0.06	-0.17→ 0.25	0.02	-0.21→ -0.13	0.20→ 0.29
Manual-CAT	0.01	0.25	0.01	-0.02→ 0.04	-0.24→ 0.26	0.03	-0.30→ -0.19	0.20→ 0.31

Repeatability for the measurement of synovial fold volume (mm^3)

Measurement method	d	1.96s$_d$	SE(d)	95%CI(d)	95%LoA	SE(LoA)	95%CI lower LoA	95%CI upper LoA
Auto-CAT	0.37	0.90	0.12	0.10→ 0.63	-0.53→ 1.27	0.21	-0.94→ -0.12	0.86→ 1.68
Manual-CAT	0.12	0.71	0.10	-0.09→ 0.32	-0.58→ 0.81	0.16	-0.90→ -0.26	0.49→ 1.13

For the cross-sectional area measurements, at least 93% of the plotted points were within the limits of agreement (Figures 4.22.A and 4.23.A). The auto-CAT data (Figure 4.22.A) was affected by both heteroscedasticity and proportional bias and the manual-CAT data (Figure 4.23.A) was influenced by heteroscedasticity alone. Therefore the limits of agreement were recalculated using the modified regression approach (Figures 4.22.A and 4.23.A).
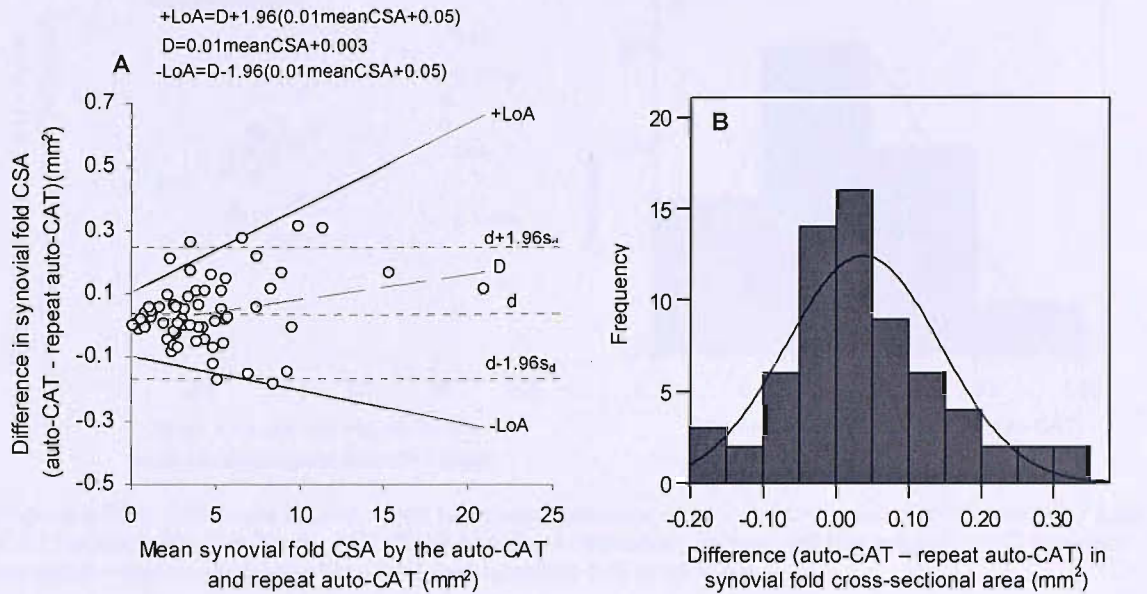
Figure 4.22.A. Difference against mean for repeat measures of synovial fold cross-sectional area (CSA) (mm^2) using the auto-CAT (repeatability) (r =.27, P=.03). **B.** Histogram of differences for synovial fold cross-sectional area (mm^2) between repeated measures using the auto-CAT (repeatability) (KS test P=.01).
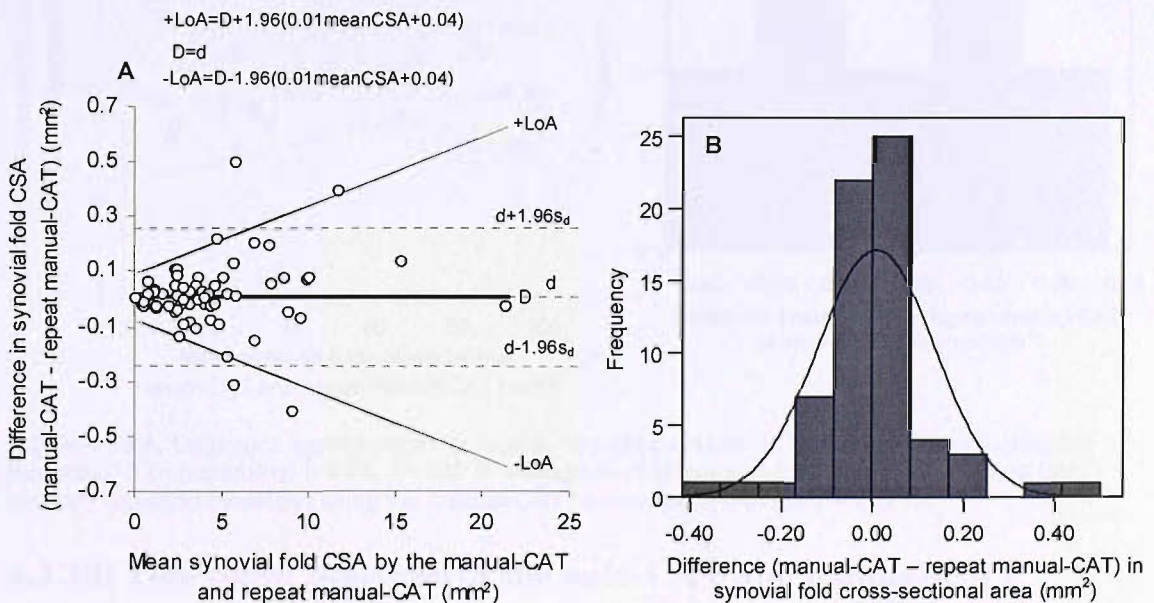
Figure 4.23.A. Difference against mean for repeat measures of synovial fold cross-sectional area (CSA) (mm^2) using the manual-CAT (repeatability) (r =.12, P=.33). **B.** Histogram of differences for synovial fold cross-sectional area (mm^2) between repeated measures using the manual-CAT (repeatability) (KS test P=.001).

For the synovial fold volume measurements, at least 93% of the plotted points were within the limits of agreement (Figures 4.24.A and 4.25.A). The scatter diagrams and Pearson's correlation coefficient indicated the presence of proportional bias thus the modified regression approach was performed (Figures 4.24.A and 4.25.A).
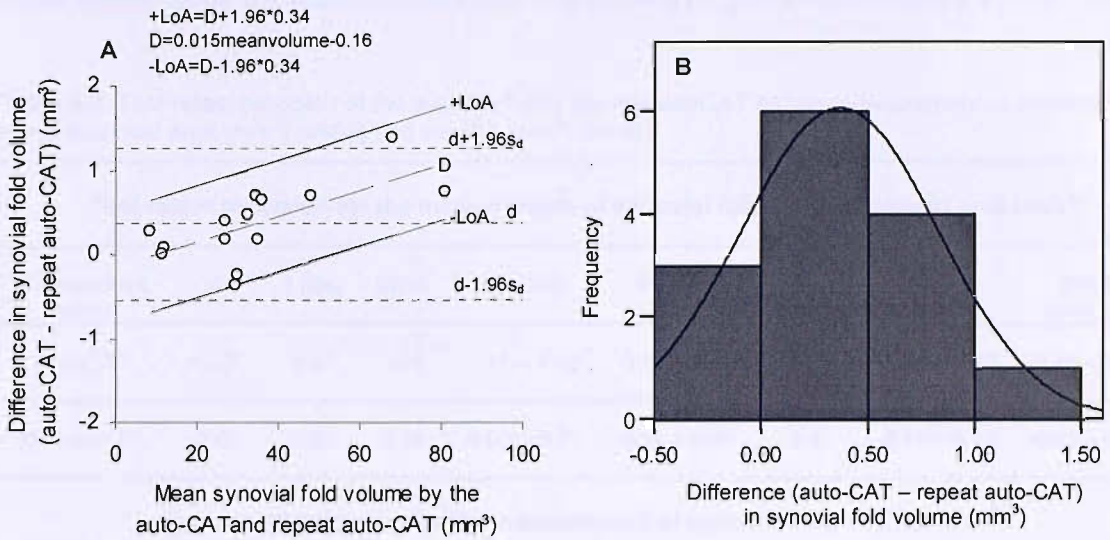
Figure 4.24.A. Difference against mean for repeat measures of synovial fold volume (mm^3) using the auto-CAT (repeatability) (r =.67, P=.008). **B.** Histogram of differences for synovial fold volume (mm^3) between repeated measures using the auto-CAT (repeatability) (KS test P=.20).
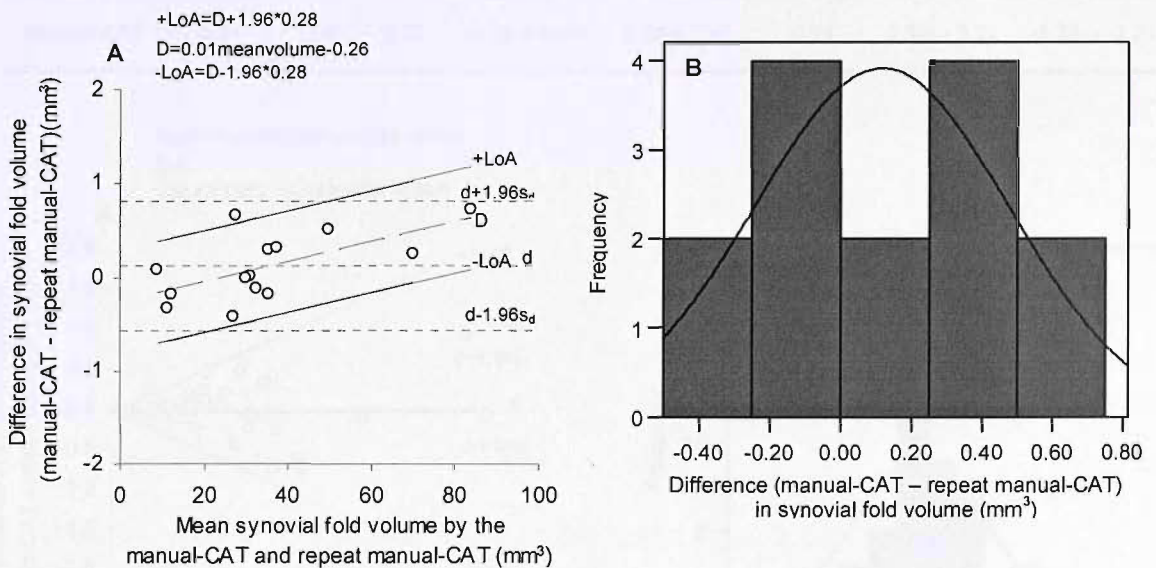
Figure 4.25.A. Difference against mean for repeat measures of synovial fold volume (mm^3) using the manual-CAT (repeatability) (r =.63, P=.02). **B.** Histogram of differences for synovial fold volume (mm^3) between repeated measures using the manual-CAT (repeatability) (KS test P=.20).

4.3.3iii Test-retest precision of the auto-CAT and manual-CAT

The results of the limits of agreement analysis of test-retest precision, for the measurement of synovial fold cross-sectional area (n=53) and volume (n=10), for the auto-CAT and the manual-CAT are shown in Table 4.8.

93% of the plotted points were within the limits of agreement for both the auto-CAT and the manual-CAT cross-sectional area measurements (Figures 4.26.A and 4.27.A). From the scatter diagrams for both the auto-CAT (Figure 4.26.A) and the manual-CAT (Figure 4.27.A), it was evident that the differences diverged as the magnitude increased indicating the presence of heteroscedasticity. Therefore the limits of agreement were recalculated using the modified regression approach (Figures 4.26.A and 4.27.A).

Table 4.8. Test-retest precision of the auto-CAT and the manual-CAT for the measurement of synovial fold cross-sectional area (mm^2) (n=53) and volume (mm^3) (n=10).

Test-retest precision for the measurement of synovial fold cross-sectional area (mm^2)

Measurement method	d	$1.96s_d$	SE(d)	95%CI(d)	95%LoA	SE(LoA)	95%CI upper LoA	95%CI lower LoA
Auto-CAT	-0.03	0.57	0.04	-0.11→ 0.05	-0.59→ 0.53	0.07	0.66→ 0.40	-0.46→ -0.72
Manual-CAT	-0.01	0.59	0.04	-0.09→ 0.07	-0.59→ 0.57	0.07	0.71→ 0.43	-0.45→ -0.73

Test-retest precision for the measurement of synovial fold volume (mm^3)

Measurement method	d	$1.96s_d$	SE(d)	95%CI(d)	95%LoA	SE(LoA)	95%CI upper LoA	95%CI lower LoA
Auto-CAT	-0.40	2.06	0.33	-1.14→ 0.34	-2.46→ 1.65	0.57	0.54→ 2.77	-3.57→ -1.35
Manual-CAT	-0.31	1.96	0.32	-1.02→ 0.40	-2.27→ 1.65	0.54	0.59→ 2.71	-3.33→ -1.21

+LoA=D+1.96(0.05meanCSA -0.004)
D=d
-LoA=D-1.96(0.05meanCSA -0.004)
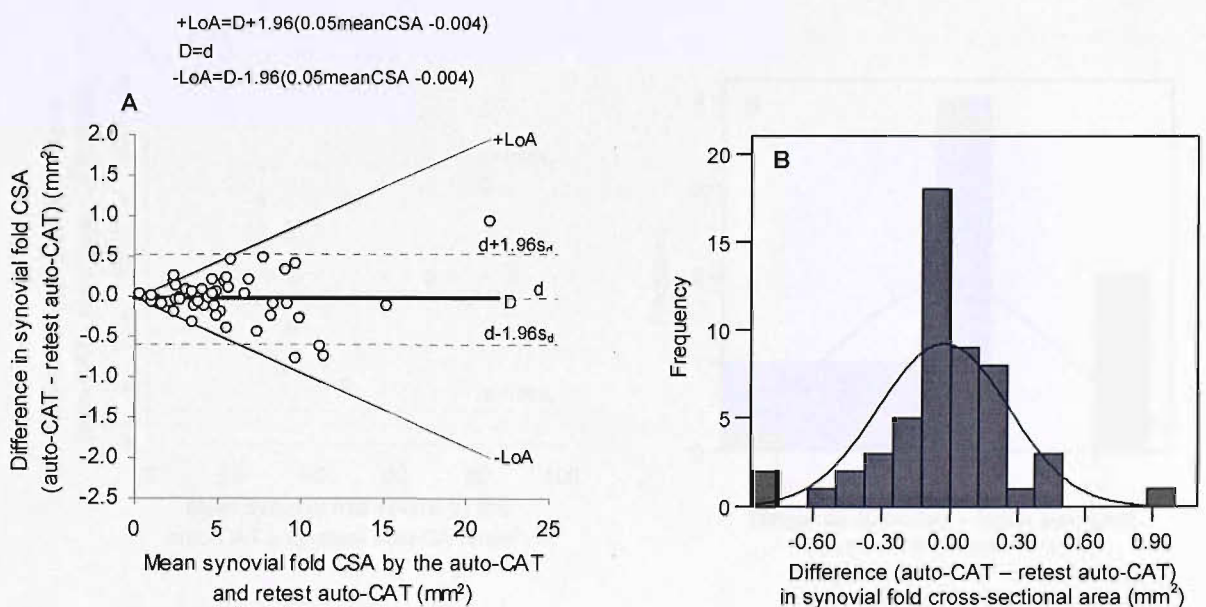
Figure 4.26.A. Difference against mean for repeat measures of synovial fold cross-sectional area (CSA) (mm^2) using the auto-CAT (test-retest precision) (r =.07; P=.60). **B.** Histogram of differences for synovial fold cross-sectional area (mm^2) between test-retest measurements using the auto-CAT (test-retest precision) (KS test P=.01).

106
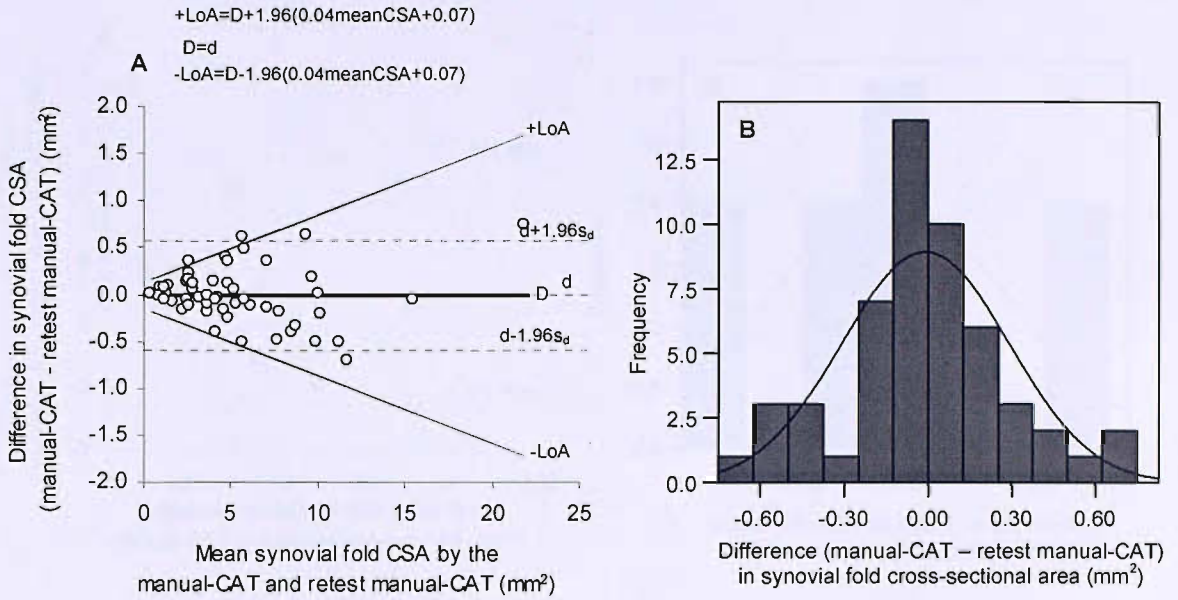
Figure 4.27.A. Difference against mean for repeat measures of synovial fold cross-sectional area (CSA) (mm^2) using the manual-CAT (test-retest precision) ($r=-.02$, P=.91). **B.** Histogram of differences for synovial fold cross-sectional area (mm^2) between test-retest measurements using the manual-CAT (test-retest precision) (KS test P=.20).

For the measurement of synovial fold volume, 100% of the plotted points were within the limits of agreement and there was no evidence of a relationship between the difference and the magnitude of measurement from the scatter diagrams and Pearson's correlation coefficient (Figures 4.28.A and 4.29.A).
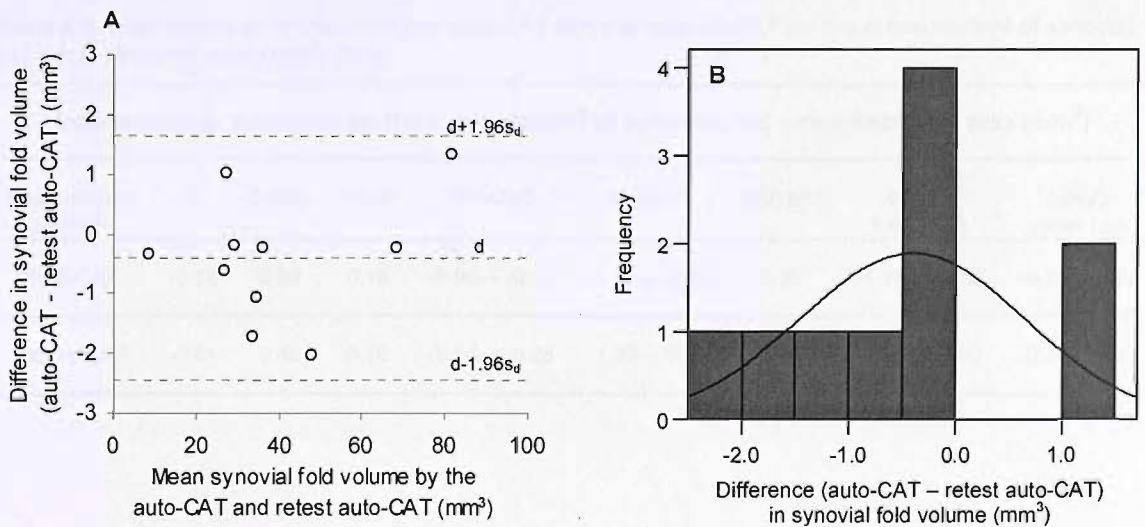
Figure 4.28.A. Difference against mean for repeat measures of synovial fold volume (mm^3) using the auto-CAT (test-retest precision) ($r=.27$, P=.45). **B.** Histogram of differences for synovial fold volume (mm^3) between test-retest measurements using the auto-CAT (test-retest precision) (KS test P=.20).

107
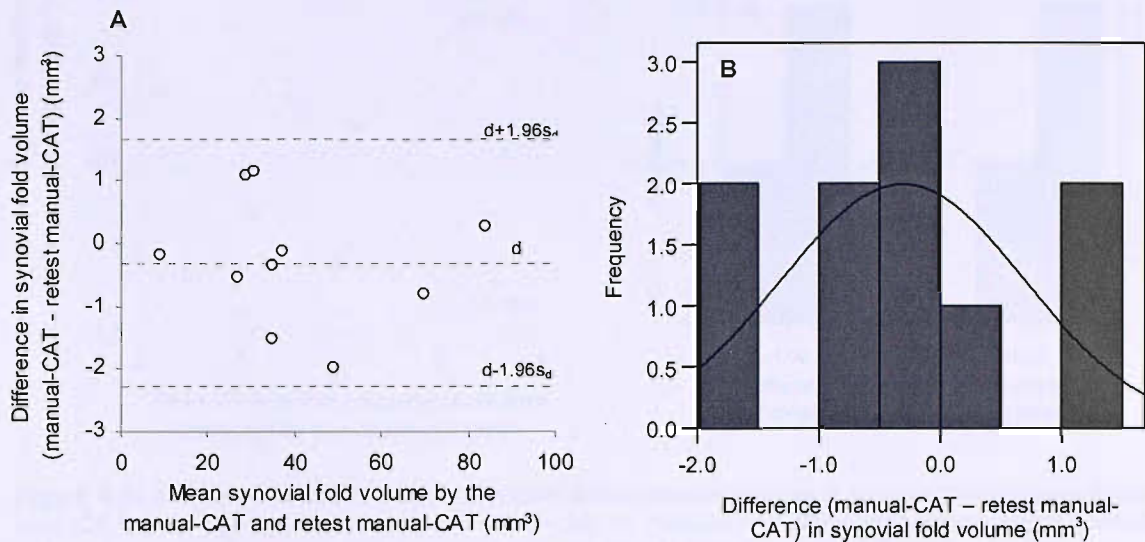
Figure 4.29.A. Difference against mean for repeat measures of synovial fold volume (mm^3) using the manual-CAT (test-retest precision) (r =-.15, P=.68). **B.** Histogram of differences for synovial fold volume (mm^3) between test-retest measurements using the manual-CAT (test-retest precision) (KS test P=.20).

4.3.3iv Inter-examiner precision of the auto-CAT and the manual-CAT

The results of the limits of agreement analysis of inter-examiner precision, for the measurement of synovial fold cross-sectional area (n=6) using the auto-CAT and the manual-CAT, is shown in Table 4.9. 100% of the plotted points were within the limits of agreement and there was no relationship between the difference and the magnitude of measurement (Figures 4.30.A and 4.31.A).

Table 4.9. Inter-examiner precision of the auto-CAT and the manual-CAT for the measurement of synovial fold cross-sectional area (mm^2) (n=6).

Inter-examiner precision for the measurement of synovial fold cross-sectional area (mm^2)								
Measurement method	d	1.96s$_d$	SE(d)	95%CI(d)	95%LoA	SE(LoA)	95%CI lower LoA	95%CI upper LoA
Auto-CAT	-0.55	0.84	0.18	-0.90→ -0.19	-1.39→ 0.30	0.30	-1.98→ -0.80	-0.29→ 0.89
Manual-CAT	-0.61	0.40	0.16	-0.94→ -0.28	-1.39→ 0.18	0.28	-1.94→ -0.85	-0.37→ 0.72

108
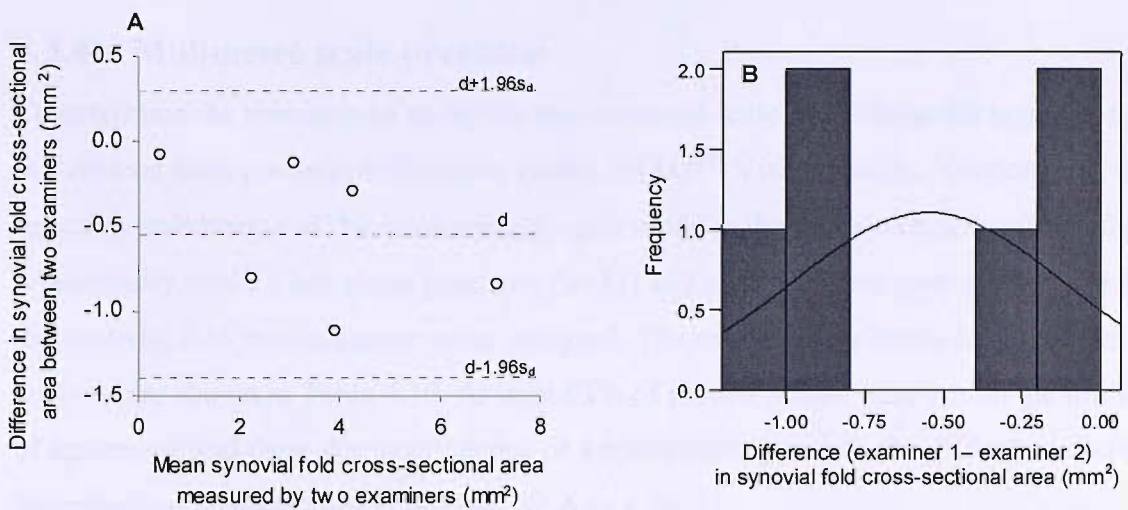
Figure 4.30.A. Difference against mean for inter-examiner measurements of synovial fold cross-sectional area (CSA) (mm^2) using the auto-CAT (r =-.50, P=.32). **B.** Histogram of differences for synovial fold cross-sectional area (mm^2) between inter-examiner measurements using the auto-CAT (KS test P=.20).
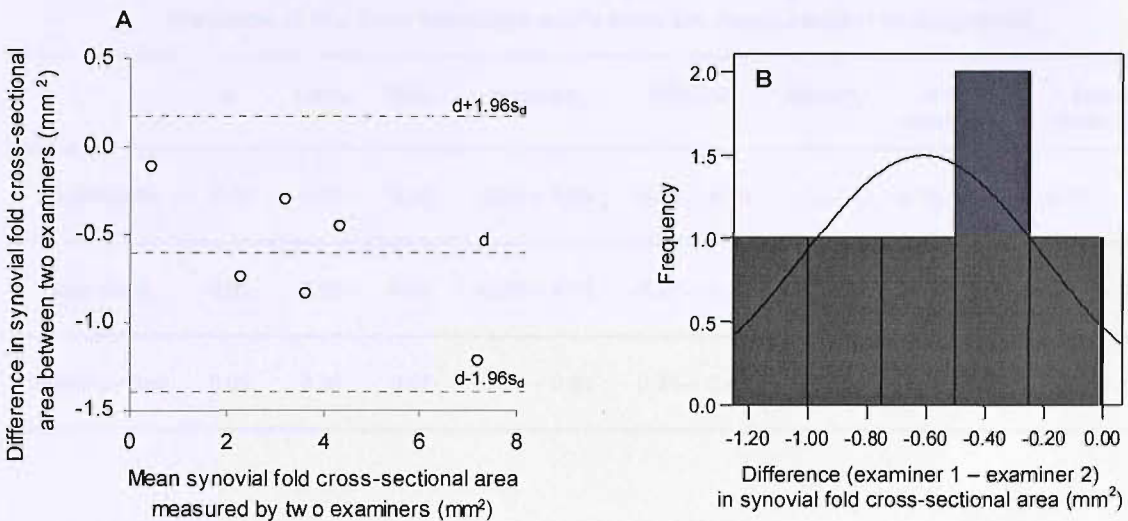
Figure 4.31.A. Difference against mean for inter-examiner measurements of synovial fold cross-sectional area (CSA) (mm^2) using the manual-CAT (r =-.80, P=.06). **B.** Histogram of differences for synovial fold cross-sectional area (mm^2) between inter-observer measurements using the manual-CAT (KS test P=.20).

4.3.4 Acquisition error

4.3.4i Image distortion

The x:y ratio measured from the measurement scale using digital calipers (1:0.45) differed from the x:y ratio measured from the measurement scale on the digital image using IMAQ Vision Builder (1:0.46) by 2.22%.

4.3.4ii Millimetre scale accuracy

The known length of the object was 5.00mm. The length of the object measured from a digital image using IMAQ^{TM} Vision Builder Version 6.1 and the millimetre scale for calibration was 5.04mm. Therefore millimetre scale error was 0.008mm per 1mm.

4.3.4iii Millimetre scale precision

To determine the precision of using the measurement scale to calibrate the synovial fold dimensions from pixels to millimetres (using IMAQ^{TM} Vision Builder Version 6.1), the repeat measurements of the measurement scale made in the process of determining the repeatability (n=66), test-retest precision (n=53) and inter-observer precision (n=6) of the synovial fold measurements were analysed. The results of the limits of agreement analysis are shown in Table 4.10. At least 93% of plotted points were within the limits of agreement and there was no evidence of a relationship between the difference and the magnitude of measurement (Figures 4.32.A to 4.34.A).

Table 4.10. Precision of the 1mm measures made from the measurement scale (pixels) to convert the dimensions of the synovial folds from pixels to millimetres.

	Precision of the 1mm measures made from the measurement scale (pixels)							
	d	1.96s$_d$	SE(d)	95%CI(d)	95%LoA	SE(LoA)	95%CI upper LoA	95%CI lower LoA
Repeatability	-0.04	0.30	0.03	-0.08→ 0.00	-0.33→ 0.25	0.07	0.19→ 0.31	-0.27→ -0.39
Test-retest	0.02	0.29	0.02	-0.02→ 0.06	-0.27→ 0.32	0.03	0.38→ 0.25	-0.20→ -0.34
Inter-examiner	0.09	0.34	0.07	-0.05→ 0.23	-0.24→ 0.43	0.12	0.19→ 0.66	-0.48→ -0.01
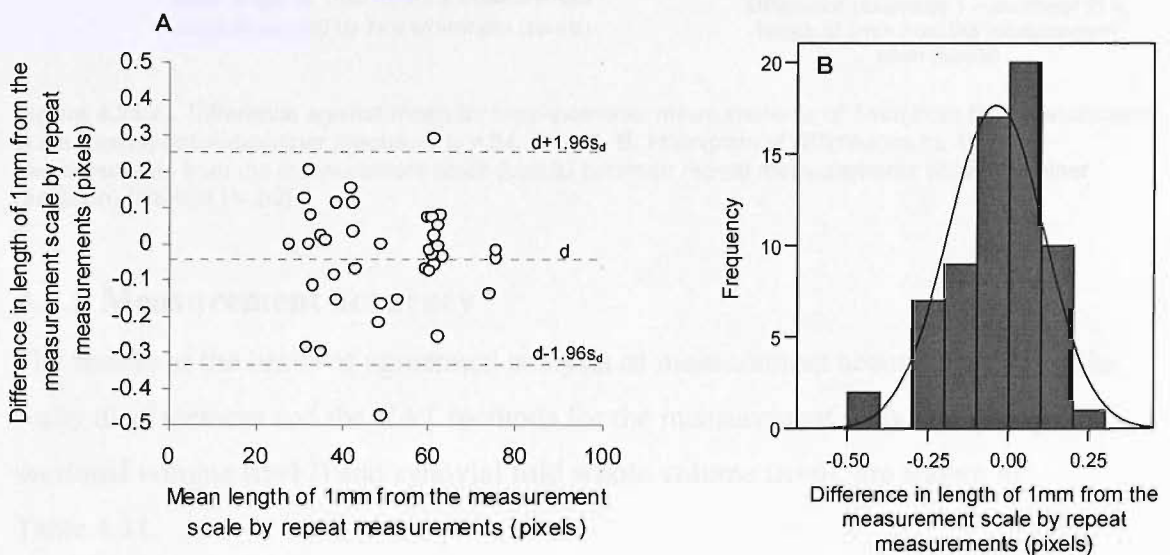
Figure 4.32.A. Difference against mean for repeat measures of 1mm from the measurement scale (pixels) (repeatability) (r =-.04, P=.75). **B.** Histogram of differences for 1mm measurements from the measurement scale (pixels) between repeat measurements (repeatability) (KS test P=.02).
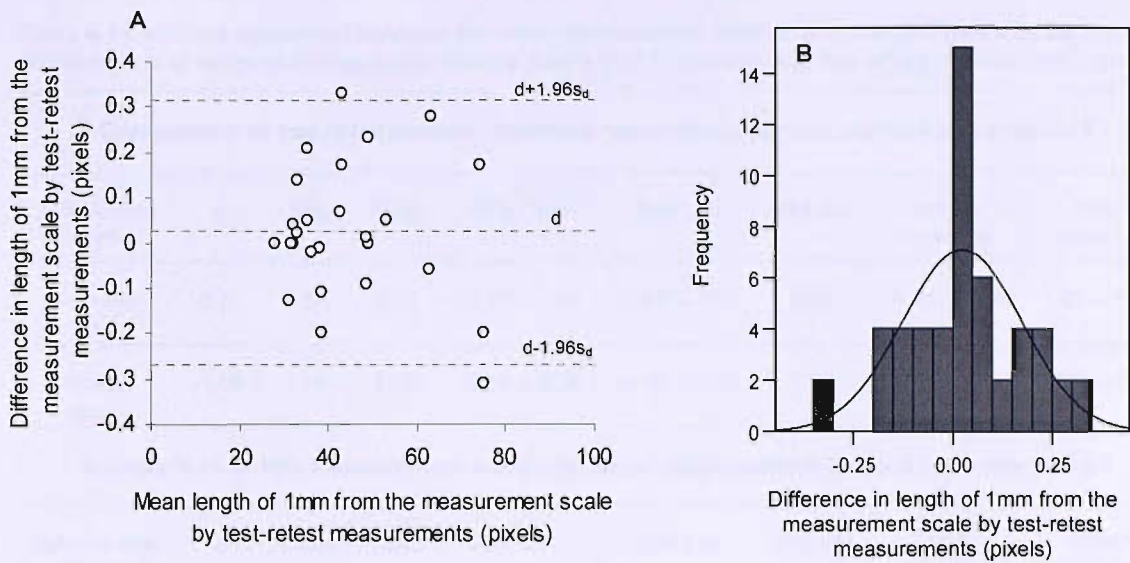
Figure 4.33.A. Difference against mean for repeat measures of 1mm from the measurement scale (pixels) (test-retest precision) (r =-.14, P=.32). **B.** Histogram of differences for 1mm measurements from the measurement scale (pixels) between repeat measurements (test-retest precision) (KS test P=.03).
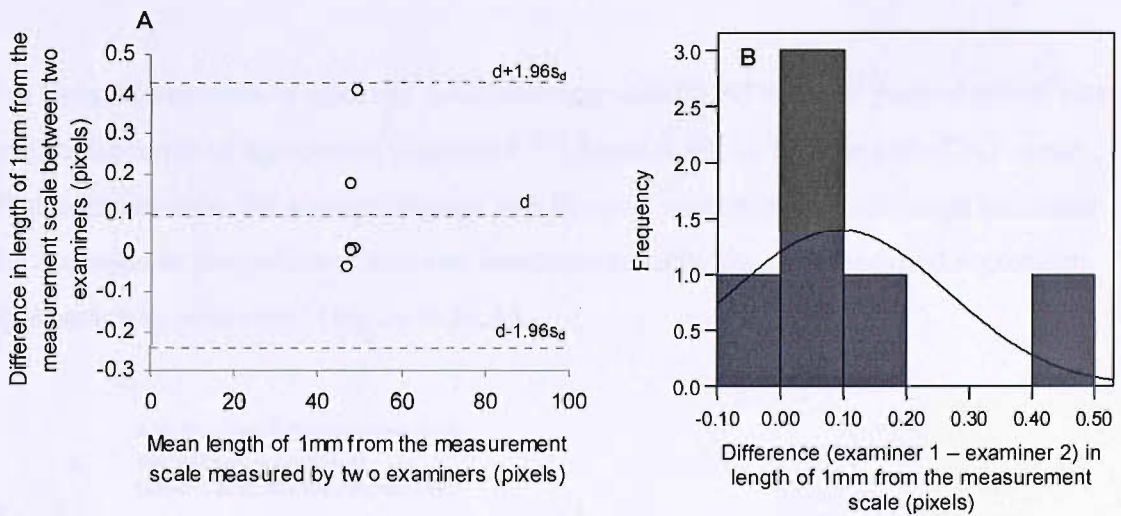
Figure 4.34.A. Difference against mean for inter-examiner measurements of 1mm from the measurement scale (pixels) (inter-examiner precision) (r =.64, P=.17). **B.** Histogram of differences for 1mm measurements from the measurement scale (pixels) between repeat measurements (inter-examiner precision) (KS test P=.02).

4.3.5 Measurement accuracy

The results of the limits of agreement analysis of measurement accuracy between the water displacement and the CAT methods for the measurement of synovial fold sectional volume (n=17) and synovial fold whole volume (n=6), are shown in Table 4.11.

Table 4.11. Method agreement between the water displacement method and the CAT methods for the measurement of synovial fold sectional volume (mm^3) (n=17) and synovial fold whole volume (mm^3) (n=6).

Comparison of two measurement methods: water displacement method and auto-CAT

Synovial fold volume	d	1.96s$_d$	SE(d)	95% CI(d)	95% LoA	SE(LoA)	95%CI lower LoA	95%CI upper LoA
Sectional (mm^3)	-0.37	1.55	0.19	-0.77→ 0.04	-1.91→ 1.17	0.33	-1.27→ -2.55	1.81→ 0.53
Whole (mm^3)	-1.04	3.35	0.70	-2.84→ 0.76	-4.40→ 2.32	1.20	-2.06→ -6.74	-0.03→ 4.66

Comparison of two measurement methods: water displacement method and manual-CAT

Synovial fold volume	d	1.96s$_d$	SE(d)	95% CI(d)	95% LoA	SE(LoA)	95%CI lower LoA	95%CI upper LoA
Sectional (mm^3)	-0.26	1.55	0.19	-0.67→ 0.14	-1.82→ 1.29	0.33	-1.17→ -2.46	0.64→ 1.93
Whole (mm^3)	-0.75	2.90	0.60	-2.30→ 0.80	-3.65→ 2.15	1.03	-5.67→ -1.63	0.12→ 4.17

For the measurement of synovial fold sectional volume, 95% of the plotted points were within the limits of agreement (Figures 4.35.A and 4.36.A). For the auto-CAT-water displacement data, the scatter diagram and Pearson's correlation coefficient indicated the presence of proportional bias and heteroscedasticity thus the modified regression approach was performed (Figure 4.35.A).
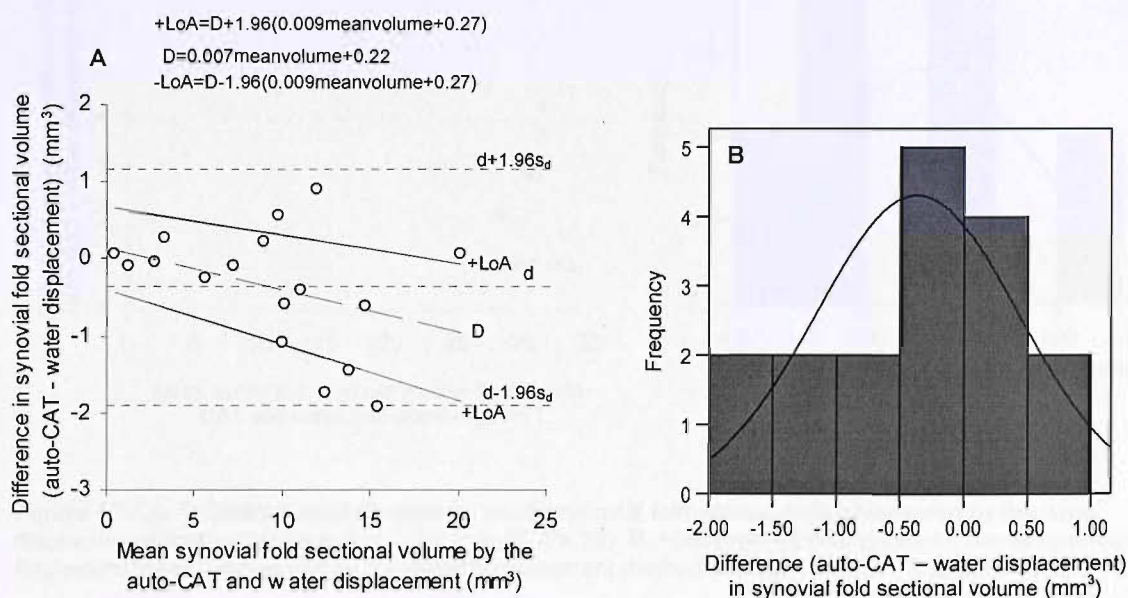
Figure 4.35.A. Difference against mean for synovial fold sectional volume (mm^3) measured by the auto-CAT and the water displacement method (r=.99, P=.000). **B.** Histogram of differences for synovial fold sectional volume (mm^3) measured by the auto-CAT and the water displacement method (KS test P=.20).
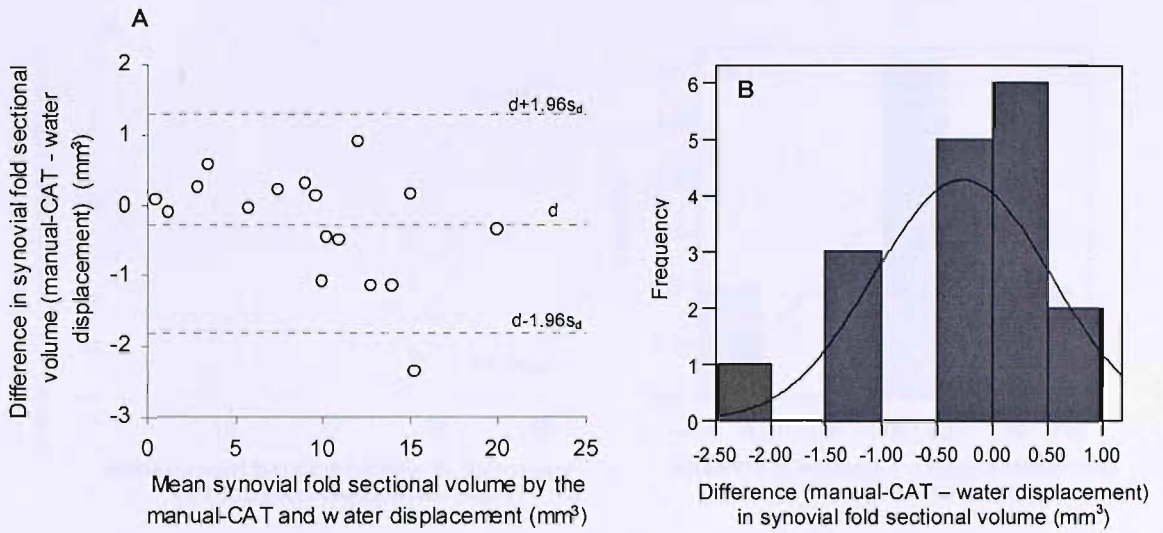
Figure 4.36.A. Difference against mean for synovial fold sectional volume (mm^3) measured by the manual-CAT and the water displacement method (r =-.45, P=.07). **B.** Histogram of differences for synovial fold sectional volume (mm^3) measured by the manual-CAT and the water displacement method (KS test P=.20).

For the measurement of whole synovial fold volume, 100% of the plotted points were within the limits of agreement and there was no evidence of a relationship between the difference and the magnitude of measurement from the scatter diagrams and Pearson's correlation coefficient (Figures 4.37.A and 4.38.A).
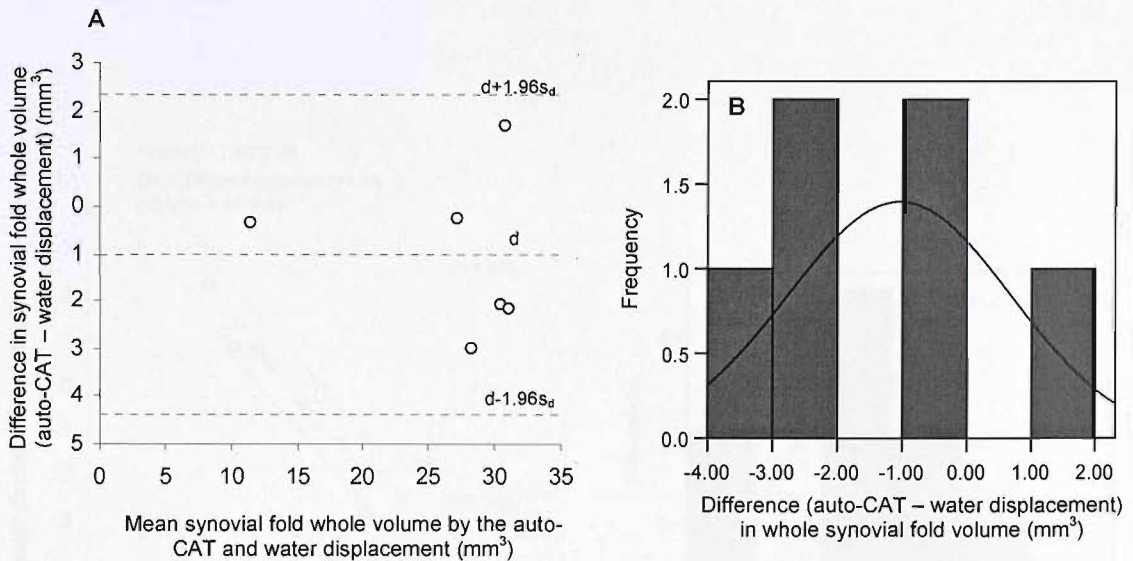
Figure 4.37.A. Difference against mean for whole synovial fold volume (mm^3) measured by the water displacement method and the auto-CAT (r =-.17, P=.75). **B.** Histogram of differences for whole synovial fold volume (mm^3) measured by the water displacement method and the auto-CAT (KS test P=.20).
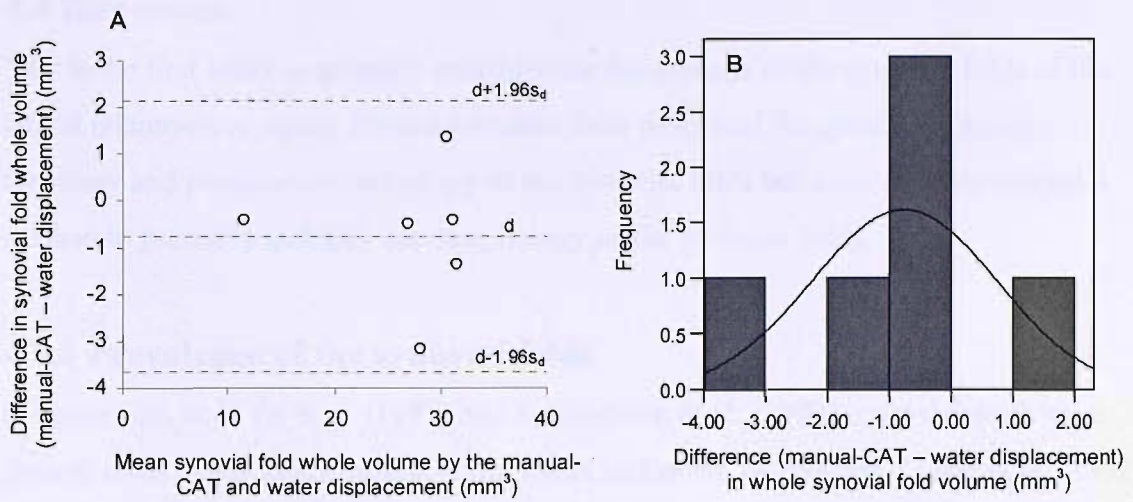
Figure 4.38.A. Difference against mean for whole synovial fold volume (mm³) measured by the manual-CAT and the water displacement method (r=-.03, P=.96). **B.** Histogram of differences for synovial fold total volume measured by the manual-CAT and the water displacement method (KS test P=.20).

20 measurements of the volume of the cylinder were made using the water displacement method. 100% of the plotted points were within the limits of agreement and there was evidence of a proportional bias from the scatter diagram and Pearson's correlation coefficient thus the limits of agreement were recalculated using the modified regression approach (Figure 4.39.A). The regressed limits of agreement for mean cylinder volume were 0.02±0.76mm³.
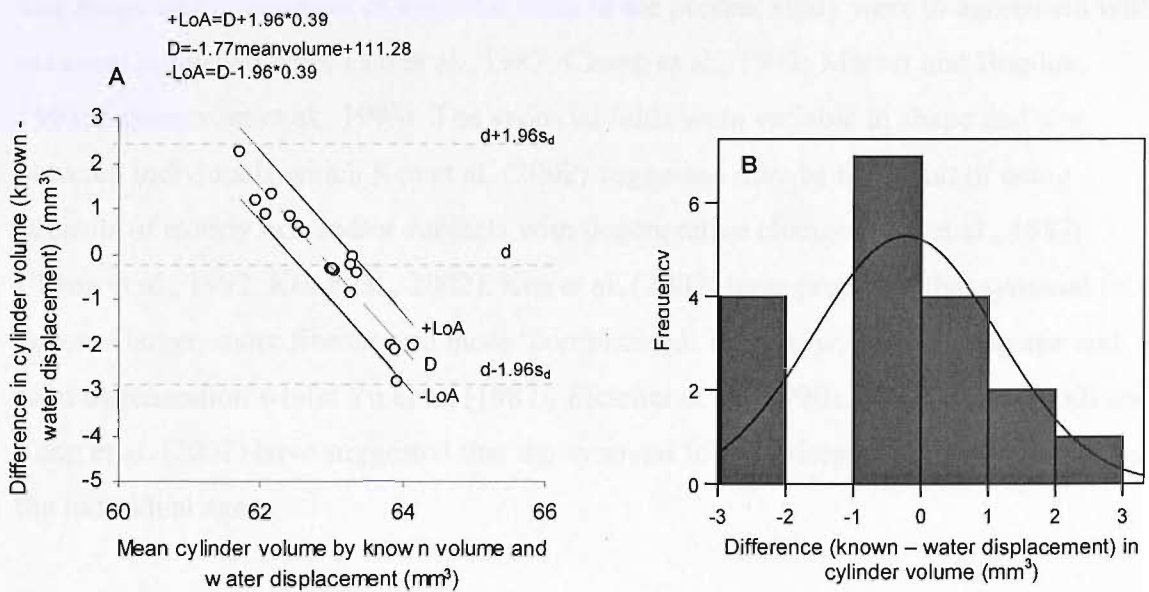
Figure 4.39.A. Difference against mean for cylinder volume (mm³) of known volume measured by the water displacement method (r = -.96, P=.000). **B.** Histogram of differences for cylinder volume (mm³) of known volume measured by the water displacement method (KS test P=.20).

114

4.4 Discussion

This is the first study to quantify critically the dimensions of the synovial folds of the lateral atlanto-axial joints. Previous studies have described the gross morphology, histology and postmortem pathology of the synovial folds but none have developed a method to precisely quantify the morphology of the synovial folds.

4.4.1 Prevalence of the synovial folds

In agreement with Yu et al. (1987) and Schonstrom et al. (1993), synovial folds were present in all of the lateral atlanto-axial joints sectioned. In contrast, Chang et al. (1992), Mercer and Bogduk (1993) and Kawabe et al. (1980), reported a prevalence of 72%, 97% and 0%, respectively. These discrepancies may be explained by the use of different methodologies. Small synovial folds visualised upon sectioning of the joints in the present study and the studies of Yu et al. (1987) and Schonstrom et al. (1993) may have been overlooked in the dissection studies of Chang et al. (1992) and Mercer and Bogduk (1993) where the synovial folds may not have been visible within the interior of the fibrous capsule to which they firmly adhere. Kawabe et al. (1980) is the only published study which reported no synovial folds at the lateral atlanto-axial joints but did not describe the methodology employed in their study.

4.4.2 Gross morphology of the synovial folds

The shape and disposition of synovial folds in the present study were in agreement with previous published work (Yu et al., 1987; Chang et al., 1992; Mercer and Bogduk, 1993; Schonstrom et al., 1993). The synovial folds were variable in shape and size between individuals which Kos et al. (2002) suggested may be the result of using subjects of elderly age and/or subjects with degenerative changes (Yu et al., 1987; Chang et al., 1992; Kos et al., 2002). Kos et al. (2002) have proposed that synovial folds become larger, more fibrous and more 'complicated' in form with increasing age and joint degeneration whilst Yu et al. (1987), Fletcher et al. (1990), Inami et al. (2000) and Tang et al. (2007) have suggested that the synovial folds undergo regressive changes as the individual ages.

In the present study three synovial folds were observed to occupy reciprocally-shaped indentations in the hyaline articular cartilage. Such cartilage indentations related to the synovial folds have not previously been described in the literature. The synovial fold entrapment theory developed by Kos and Wolf (1972) and endorsed by Lewit (1978)

was based on the assumption that the hyaline articular cartilage may be deformed by the synovial folds creating a depression in the cartilage in which the synovial fold may become entrapped. The cartilage indentations observed in the present study did not appear to be temporary deformations. It was not possible to determine whether the synovial folds had deformed the cartilage or the synovial folds had filled existing deficiencies in the cartilage and conformed to the shape of those deficiencies. The ability to image the synovial folds *in vivo* would enable this observation to be investigated further.

4.4.2i Extracapsular communications of the synovial folds

The extracapsular communications described in the lumbar zygapophysial joints (Lewin et al., 1962; Engel and Bogduk, 1982; Giles et al., 1989; Taylor, 1991) and proposed to exist at the lateral atlanto-axial joints (Ibatullin et al., 1987; Chevrot et al., 1995; Aprill et al., 2002) were not observed in the present study. This is in agreement with Schonstrom et al. (1993). The presence of (intracapsular) extensions of the ventral and dorsal articular recesses, previously described by Schonstrom et al. (1993), were confirmed in this study. Like the articular recesses observed at the cervical zygapophysial joints (Dory, 1983), in the present study the ventral articular recesses of the lateral atlanto-axial joints appeared to be larger than the dorsal recesses.

The atlanto-axial joints account for approximately 50% of the total range of cervical rotation. It has been hypothesised that as the atlas rotates on the axis, the synovial folds move out of the articular recesses and the articular facets move into the articular recesses (Mercer and Bogduk, 2001). It is not known where the synovial folds move to when the articular facets move into the articular recesses. The synovial folds may move into the superior and inferior extensions of the articular recesses identified in the present study. This would prevent the synovial folds from either becoming trapped between the articular surfaces or causing distension of the innervated fibrous capsule during normal cervical motion. Therefore the extensions of the articular recesses reported in the present study may accommodate movements of the synovial folds during cervical spine motion without the need for the extracapsular communications observed in the lumbar spine. Articular recess extensions appear to be unique to the lateral atlanto-axial joints and may possibly be a reflection of the great range of motion present at these articulations.

In the present study, it was observed that the extensions of the articular recess appeared to be larger at the ventral aspect of the lateral atlanto-axial joint compared to the dorsal aspect. This may be to accommodate the larger ventral synovial folds, which in the present study were found to have a greater volume than the dorsal synovial folds. The larger extensions of the ventral articular recesses may also afford greater mobility to the ventral synovial folds and enable the ventral synovial folds to escape impingement injury more readily than the dorsal synovial folds. This may account for injuries to the dorsal synovial folds being twice as common as injuries to the ventral synovial folds following whiplash injury (Schonstrom et al., 1993). However, the higher incidence of dorsal synovial fold injury could also be due to rear-end motor vehicle collisions being more common than frontal and side-impact collisions (Radanov et al., 1995; Spitzer et al., 1995; Ronnen et al., 1996).

4.4.2ii Rheumatoid arthritis and the synovial folds

The present study is the first to describe changes in the morphology of the synovial folds as a result of rheumatoid arthritis. Rheumatoid arthritis is a chronic systemic inflammatory disease of unknown cause and affects 1% of the population (Markenson, 1991) with women affected more frequently. The reported prevalence of cervical spine involvement in patients with rheumatoid arthritis varies between 17% and 88% and most commonly affects the atlanto-axial articulations (Nguyen et al., 2004; Shen et al., 2004; Vesela et al., 2005). The most frequently reported craniocervical abnormality is atlanto-axial subluxation and the literature is replete with studies investigating this lesion and its sequelae (Puttlitz et al., 2000).

The pathogenesis of rheumatoid arthritis begins with inflammation leading to synovial hyperplasia, hyperaemia and oedema. As the disease progresses the hyperplasia of the synovial membrane forms villous projections which can protrude into the synovial cavity. Healing processes are initiated and fibrovascular granulation tissue develops in the synovium and extends onto the cartilage and bare area. This is termed pannus. As the inflammatory response and healing processes become established as chronic inflammation, the pannus will involve all articular structures over time leading to weakening of the fibrous capsule, the ligaments and entheses. In the present study, three out of four synovial folds of Subject 4, who had a medical history of rheumatoid arthritis, were observed to be hypertrophied and villous. The enlarged synovial folds extended into and filled the articular recesses and their extensions (Figure 4.14). With

117

the exception of the left ventral synovial fold, the volume of the rheumatoid synovial folds were at least two times greater compared to the mean synovial fold volume of the subjects without rheumatoid arthritis (Table 4.4). The present study is the first to demonstrate morphological changes affecting the synovial folds as a result of rheumatoid arthritis.

The erosions of the joint margins evident on the sagittal sections in the present study were not visible on plain film xray and it was not possible to make a definitive diagnosis of rheumatoid arthritis from the radiographs alone. Although plain film xrays are regarded as the gold standard imaging modality they have limited sensitivity to bone damage, especially in early rheumatoid disease, and are not suitable for the assessment of synovial inflammation (McGonagle et al., 2001). Recognition of these limitations has led to increasing interest in the use of MRI due to its ability to visualise soft tissue structures and neural elements in multiple planes (Jacobsen and Riise, 2000; Oostveen and van de Laar, 2000; Narvaez et al., 2002).

Zoli et al. (2000) compared plain-film xray, CT and MRI for identifying craniocervical junction involvement in rheumatoid patients. Plain film xray detected 41.3% of patients with craniocervical involvement but only in the advanced stages of the disease whilst MR images detected 61% of patients including those in the early stages of craniocervical disease (Zoli et al., 2000). Thus MRI is more sensitive than plain film xray in detecting bone erosions and is able to depict inflammatory lesions (McGonagle et al., 2001; Hermann and Bollow, 2004; Østergaard et al., 2005). Furthermore, quantitative MRI assessment of synovial volume has shown good correlation with arthroscopic and histological inflammation scores (Tamai et al., 1994; Gaffney et al., 1995; Østergaard et al., 1997) and may be a useful prognostic marker and outcome measure in rheumatoid arthritis. Enlargement of the synovial folds, as observed in the present study, may be a useful indicator of craniocervical involvement in rheumatoid disease.

The effects of rheumatoid change affecting the lateral atlanto-axial joints and their synovial folds is an area for future study that could be explored using the techniques developed in this study. Correlation with MRI detection of synovial fold changes affecting rheumatoid patients may provide early imaging of this disease that could be used for diagnosis, prognosis, treatment or management.

118

4.4.3 Dimensions of the synovial folds

Four previous studies reported the depth of projection (DOP) of the synovial folds (referred to as synovial fold length or width in previous studies). Comparisons are limited because the measurement techniques used were not clearly described. Chang et al. (1992), Mercer and Bogduk (1993) and Tang et al. (2007) reported synovial fold DOP to range between 1-5mm, 2-5mm and <3mm to >5mm, respectively. Yu et al. (1987) described synovial folds that covered between 10 to 50% of the articular surface on sagittal section. With the exception of three synovial folds that had a DOP greater than 6mm, the DOP of synovial folds in the present study was in agreement with the results of previous studies (Chang et al., 1992; Mercer and Bogduk, 1993; Tang et al., 2007). Synovial fold cross-sectional area and volume measurements were not available for comparison because previous studies have not investigated these parameters.

In the present study, the ventral synovial folds were typically larger than the dorsal synovial folds in both male and female subjects. It has been suggested that the synovial folds are nipped during vertebral motion causing them to become more fibrous and ragged (Inami et al., 2000). Inami et al. (2000) observed smaller synovial folds at the dorsal aspect of the cervical zygapophysial joints in cadavers aged 42 to 94 years of age. The dorsal synovial folds were typically thin, ragged and fibrous whilst the ventral synovial folds were larger and composed predominantly of adipose tissue. The findings in the current study, performed on the lateral atlanto-axial joints, are in agreement with those of Inami et al. (2000). The variations between ventral and dorsal articular morphology may be related to the distribution of mechanical stress within the joint. For example, with advancing age there is an associated increase in forward head posture and hence an increase in upper cervical extension that would increase biomechanical stress in the dorsal region of the joint (Dalton, 1994). The original shape and size of the synovial fold is also likely to play a role.

Ventral-dorsal asymmetry affecting the hyaline articular cartilage of the lateral atlanto-axial and cervical zygapophysial joints has previously been reported in a similar cadaveric study of cervical spine sagittal sections (Yoganandan et al., 2003). Yoganandan et al. (2003) noted less hyaline articular cartilage at the dorsal compared to the ventral region of the lateral atlanto-axial joint. The effect of synovial fold and cartilage asymmetry on the biomechanical responses of the cervical spine to normal and abnormal (e.g. whiplash) cervical motion is not currently known. The incorporation of

the synovial fold morpohometry quantified in the present study into current biomechanical models of the cervical spine should improve predictions of the biomechanical behaviour of the cervical spine during both normal and traumatic conditions.

Previous studies of cervical spine dimensions have documented differences between left and right articulations (Van Roy et al., 1997; Pfirrmann et al., 2001). In the present study there was no obvious pattern of left-right asymmetry affecting synovial fold volume.

Both age and gender have an effect upon the likelihood of sustaining cervical spine injury (Pintar et al., 1998). Thus it is important to understand age and gender variations for the determination of injury mechanisms and the assessment and treatment of patients. In the present study, the synovial folds of male subjects tended to be larger than the synovial folds of female subjects. Both males and females demonstrated the same trend of larger right and left ventral synovial folds compared to right and left dorsal synovial folds, respectively.

Yoganandan et al. (2003) found less cartilage at the dorsal aspect of female compared to male cervical articular facets which they hypothesised may predispose females to fracture when the joint undergoes dorsal compression following a rear-end whiplash injury (Figure 2.9). Furthermore, Yoganandan et al. (2003) suggested that these gender differences may account for the strong epidemiological evidence that females are more vulnerable to whiplash-associated disorders such as chronic neck pain despite being involved in fewer motor vehicle collisions than males (Cassidy et al., 2000; Temming and Zobel; 2000; Sapir and Gorup, 2001). In the lumbar spine, Tanno et al. (2004) found the fibrous capsule was thinner in females compared to males and Masharawi et al. (2005) reported that the size of the articular facets are greater in males compared to females.

Like the majority of previous studies, the present study of the synovial folds was conducted using embalmed cadavers. The average age of specimens in this study (86.33 ± 8.05 years) was greater than in previous studies (Table A1.1, Appendix 1): 48.3 years (Yu et al., 1987), 77 years (Chang et al., 1992) and 36 years (Schonstrom et al., 1993). Mercer and Bogduk (1993) and Kos et al. (2002) did not record average specimen age

but the age range of specimens was ≥65 years and 20 to 80 years, respectively. Despite differences in specimen age between the current study and the literature, the descriptive results obtained were very similar. The effect of embalming upon the absolute dimensions of the synovial folds in this study is not known. Cadaveric skeletal muscle tissue that has been fixed *in situ* has been found to not shrink significantly during fixation (Cutts, 1988).

4.4.4 Measurement method

Although several reports describing the synovial folds of the lateral atlanto-axial joints have been published, the present study is the first to quantify the morphology of the synovial folds. Previous anatomic studies have investigated the cervical synovial folds using dissection techniques (Chang et al., 1992; Mercer and Bogduk, 1993; Schonstrom et al., 1993; Kos et al., 2002; Tang et al., 2007) or sectioning techniques (Yu et al., 1987; Schonstrom et al., 1993; Taylor and Taylor, 1996). In the present study a sectioning technique was adopted because it enabled the soft tissue structures to be clearly visualised intact and preserved the anatomic interrelationships between the hard and soft tissues of the cervical spine *in situ*.

The sectioning technique used in the present study was simple, rapid and inexpensive and has been successfully used in a number of studies to produce good quality serial sections of the vertebral column that clearly demonstrate the lateral atlanto-axial synovial folds in normal and pathological specimens (Taylor, 1986; Schonstrom et al., 1993; Taylor, 1993). Sagittal, coronal and transverse sections were taken in the present study in order to determine the optimal plane for visualisation of the synovial folds using imaging techniques. Sagittal sections provided optimal visualisation of the synovial folds and were used for the measurement and calculation of the dimensions of the synovial folds

Schonstrom et al. (1993) and Taylor and Taylor (1996) sectioned the cervical spine sagittally at 2 to 2.5mm intervals whilst Yu et al. (1987) used sections of 40μm thickness. In the developmental phase of the present study, the optimal slice thickness for visualisation of the synovial folds and the production of slices of consistent thickness was found to be 3mm sections. Sectioning the cervical spine at 3mm intervals also enabled the synovial folds to be excised from surrounding structures and their volume quantified using the water displacement method.

Some tissue loss would have occurred during the process of sectioning the cervical spine. Based on the thickness of the bandsaw blade (0.5mm), it was estimated that for each sagittal section there was, on average, approximately 5% of synovial fold tissue loss. This equates to an average of 15% to 20% of synovial fold volume.

In the present study a computer aided technique (CAT) was used to measure the dimensions of the synovial folds directly from digitised images to reduce the potential for error. Comparable studies have quantified the dimensions of articular cartilage and ligaments from cervical spine sagittal sections by projecting photographs of the sections onto paper affixed to the laboratory wall and tracing the outline of the ligaments and cartilage before digitising the tracings and taking measurements from them (Yoganandan et al., 2000; Yoganandan et al., 2003). The advantages of the measurement method used in the present study were that the image analysis software had a function for calibrating directly from the measurement scale photographed with the anatomical section, the software provided the option of semi-automated (auto-CAT) or manual (manual-CAT) measurement methods that measured with subpixel accuracy and images could be magnified during the measurement process to improve operator performance in the placement of the cursor (National Instruments, 2004).

Yoganandan et al., (2000; 2003) did not investigate the precision or accuracy of the sagittal sectioning techniques they developed to quantify cervical spine ligament and cartilage morphology. As discussed in Chapter 3, new methods of measurement must be assessed to determine their precision in order objectively to judge their acceptability for research and/or clinical use.

4.4.4i Measurement precision

In the present study, the majority of measurement precision data was affected by heteroscedasticity and/or proportional bias (i.e. relationship between the difference and the mean as indicated by the scatter diagrams and/or Pearson's correlation coefficient, see Section 4.2.3iii). The modified regression approach was chosen to correct for heteroscedasticity and proportional bias as the limits of agreement remain in the original units of measurement making them easier to interpret than the ratios that result from correction using logarithmic transformation. Furthermore, the modified regression approach provides a specific estimate of proportional bias, in addition to fixed bias and

random error. However, it is not possible using the modified regression approach to calculate confidence intervals for the mean difference or the limits of agreement. Both the limits of agreement and the regressed limits of agreement were presented to facilitate comparison between each aspect of precision in the present study. The presence of heteroscedasticity and proportional bias could have been ignored. Without correction the limits of agreement will include most differences and the limits will be too far apart rather than too close if proportional bias is present or wider apart than necessary for small synovial fold dimensions and narrower than they should be for large synovial fold dimensions if heteroscedasticity is present. Thus limits of agreement that are not corrected will be crude and will not fit the data well but should not lead to the acceptance of poor methods of measurement. Nevertheless it is better to try to remove such relationships by regression or transformation (Bland and Altman 1986; 1999). In the present study, the limits of agreement and regressed limits of agreement were similar with the regressed limits of agreement typically narrower.

Bland and Altman (1999) state that if the differences are normally distributed then it is expected that 95% of the differences would lie between the 95% limits of agreement. In this study at least 93% of differences were within the limits of agreement and regressed limits of agreement for all measurements. Bland and Altman (1999; 2003) only recommend a graphical check (using a histogram) of the assumption that the differences come from an approximately Normal distribution. In the present study a formal examination of normality using the Kolmogorov-Smirnov (KS) test was included in the analysis in addition to the histogram.

It was noted in the present study that the histogram and KS test often contradicted each other. For example the data presented in Figure 4.20.B (n=137) demonstrated a Normal distribution on the histogram but the KS test was significant indicating a non-Normal distribution whilst in Figure 4.35.B, the histogram was negatively skewed yet the K-S test indicated that the data was not significantly different from Normal. These contradictions may be explained by the recognised limitations of both the histogram and the KS test in the assessment of normality caused by sample size. Small samples taken from a population in which the distribution is Normal will not necessarily look Normal themselves when plotted as a histogram (Bland and Altman, 1995) and the KS test has little power to detect whether or not a small sample of data comes from a Normal distribution (Field, 2005). With large sample sizes it is very easy to get statistically

significant results for small deviations from normality using the KS test (Field, 2005). Thus for the assessment of normality in the present study, both histograms and the KS test were considered in order to make an informed decision about the extent of non-normality. Although normality of the data was extensively explored in this study, Bland and Altman (1999) advise that in the analysis of precision using the limits of agreement method, the assumption of a Normal distribution is less important than the assumption of independence between the difference and the magnitude (i.e. no heteroscedasticity or proportional bias). Furthermore it has been suggested that a non-Normal distribution may be more likely when the difference and the mean are related, in which case corrective action can be taken (i.e. logarithmic transformation or modified regression approach) (Bland and Altman, 1995; 1999).

A non-Normal distribution of differences may not be as serious in the assessment of precision as it is in other statistical contexts since non-Normal distributions are still likely to have about 95% of observations within about two standard deviations of the mean, although most of the values outside the limits may be differences in the same direction (Bland and Altman, 1999). The assumption that the differences follow a distribution which is approximately Normal is most important for the calculation of standard errors and confidence intervals for the limits of agreement (Bland and Altman, 1999). In this study, where the differences were frequently related to the mean and thus the modified regression approach was applied, deviations from normality were not of great importance since standard errors and confidence intervals for the limits of agreement cannot be calculated for the modified regression approach.

4.4.4ii Method agreement between the auto-CAT and the manual-CAT

There was a small proportional bias between the auto-CAT and manual-CAT with the manual-CAT over-estimating the auto-CAT (or the auto-CAT under-estimating the manual-CAT) in the measurement of synovial fold cross-sectional area and volume. In addition a small fixed bias was evident for the measurement of synovial fold volume, with the manual-CAT over-estimating the auto-CAT. Both the cross-sectional area and volume measurements were affected by a small amount of random error. Synovial fold volume was calculated from synovial fold cross-sectional area measurements. Therefore the systematic bias and random error values were larger for volume compared to cross-sectional area method agreement.

The auto-CAT whilst very time-consuming to execute enabled the examiner to progressively identify and define the cross-sectional area of the synovial fold and continuously re-examine and amend the demarcated area. In contrast it was not possible to revisit and adjust measurements made by the manual-CAT which may explain the small amount of systematic bias present between the two measurement methods. Although the degree of fixed and proportional bias was small and very close to zero, it may be possible to remove these systematic differences by using a manual method that is more flexible and that can be continuously reviewed and altered.

4.4.4iii Repeatability and test-retest precision of the auto-CAT and the manual-CAT

In the assessment of repeatability there should be no systematic bias between replicate measurements (Bland and Altman, 1999). This was true for the repeatability and test-retest measurements of synovial fold cross-sectional area, where the fixed and proportional bias were either zero or very close to zero. The limits of agreement, and hence random error, were greater for test-retest precision compared to repeatability measurements for both the auto-CAT and the manual-CAT reflecting the 3-month time interval between test-retest measurements. The stability of the subjects did not change in the 3-month test-retest period as the subjects used were cadavers. Therefore the most likely source of the increased random error was the examiner. Generally, the limits of agreement for the auto-CAT and the manual-CAT were similar and thus the two methods were equally precise for both repeatability and test-retest precision.

For the measurement of synovial fold volume, the limits of agreement for the repeatability measurements were narrower than for the test-retest precision measurements for both the auto-CAT and the manual-CAT. This was primarily the result of greater s_d (i.e. random error) in the test-retest precision measurements the source of which is most likely to be the examiner and the 3-month time lapse between test-retest measurements. For test-retest precision, the small amounts of fixed bias and random error present were similar between the auto-CAT and manual-CAT measurements and there was no proportional bias. For repeatability the fixed bias and random error of the auto-CAT were greater than the fixed bias and random error of the manual-CAT but conversely a smaller proportional bias was present for the manual-CAT compared to the auto-CAT. Overall the limits of agreement were wider for the repeatability of the auto-CAT compared to the manual-CAT.

4.4.4iv Inter-examiner precision of the auto-CAT and manual-CAT

For inter-examiner precision the limits of agreement were similar for both the auto-CAT and the manual-CAT. The inter-examiner precision was affected by fixed bias but no proportional bias. The fixed bias indicated that the second inexperienced examiner systematically over-estimated the measurements made by the first experienced examiner. The random error for inter-examiner precision was similar to that for test-rest precision but greater than that for repeatability. Overall the inter-examiner limits of agreement were wider than the limits of agreement for repeatability but similar to the test-retest limits of agreement.

The results for inter-examiner precision suggest that experience in recognising and delineating the synovial folds is imperative in achieving adequate precision for the auto-CAT and manual-CAT methods.

4.4.5 Acquisition error

4.4.5i Image distortion

Each synovial fold was positioned in the centre of the camera field of view. The measurement scale, used to quantify the extent of potential distortion associated with the acquisition of each digital image, was located just off the centre of the field of view as close as possible to the synovial fold being photographed. The measurement scale in each digital image was found to be affected by 2.2% distortion. Because distortion increases from the centre to the periphery of the image each synovial fold was affected by <2.2% distortion. A distortion of 2% or less is regarded as imperceptible. Thus a negligible amount of distortion affected the acquisition of each synovial fold digital image and the subsequent quantification of the synovial fold dimensions.

4.4.5ii Millimetre scale accuracy and precision

The millimetre scale provided an accurate means of converting pixels to millimetres with an error of 0.008mm per 1mm. Therefore the conversion of pixels to millimetres using the measurement scale contributed very little to the measurement error associated with the measurement of synovial fold cross-sectional area and volume using the auto-CAT and the manual-CAT.

The repeatability and test-retest precision of measuring 1mm from the measurement scale was adequate for the purposes of this study. There was no proportional bias and virtually no fixed bias. The majority of the error was due to random error, the source of which was most likely from the examiner subjectively selecting the points on the measurement scale from which to take the measure of 1mm.

The inter-examiner precision for the measurement of 1mm from the measurement scale was similar to the repeatability and test-retest precision.

4.4.6 Measurement accuracy

In the process of validating a new method of measurement, it is often difficult or impossible to compare the results with any known true standard value. Thus the usual approach is to collect observations by the new method and a standard method on the same sample of subjects and compare the values obtained by the two different methods (Bland and Altman, 1995). Currently there is no accepted standard method for measuring the dimensions of the synovial folds. Water displacement is widely regarded as the 'gold standard' method for determining the volume of anatomical structures (Peterfy et al., 1995; Partik et al., 2002; Graichen, et al., 2003) and therefore was used to assess the accuracy of the new measurement method devised in the present study.

Although the water displacement method is regarded as the gold standard for the determination of volume of anatomical structures this does not mean it does not measure without error. Therefore the limits of agreement method was used to determine the accuracy of the CAT methods developed in the present study by assessing the method agreement between the CAT (auto-CAT and manual-CAT) methods and the water displacement method.

The measurement of the volume of a cylinder of known volume using the water displacement method demonstrated that the water displacement method was affected by both systematic bias and random error. The limits of agreement indicated that the water displacement method may over-estimate volume by $0.74mm^3$ and under-estimate volume by $0.78mm^3$. This represents approximately 1% of cylinder volume and 2% of average synovial fold volume. Potential sources of error that may have affected the water displacement method include: calibration of the digital images using a measurement scale to convert pixels to millimetres, inaccurate cursor placement when

taking measurements from the digital images using Vision Builder and tissue loss when resecting the synovial folds from the fibrous capsule.

There was better agreement between the manual-CAT and the water displacement method compared to the auto-CAT and the water displacement method. The results indicated that the auto-CAT may under-estimate synovial fold volume by up to $4.40mm^3$ and over-estimate synovial fold volume by up to $2.32mm^3$. In comparison the manual-CAT may under-estimate synovial fold volume by up to $3.65mm^3$ and over-estimate by $2.15mm^3$.

4.4.7 Summary of measurement precision and accuracy

The precision and accuracy of the auto-CAT and manual-CAT methods for the determination of synovial fold volume are summarised in Figure 4.40.
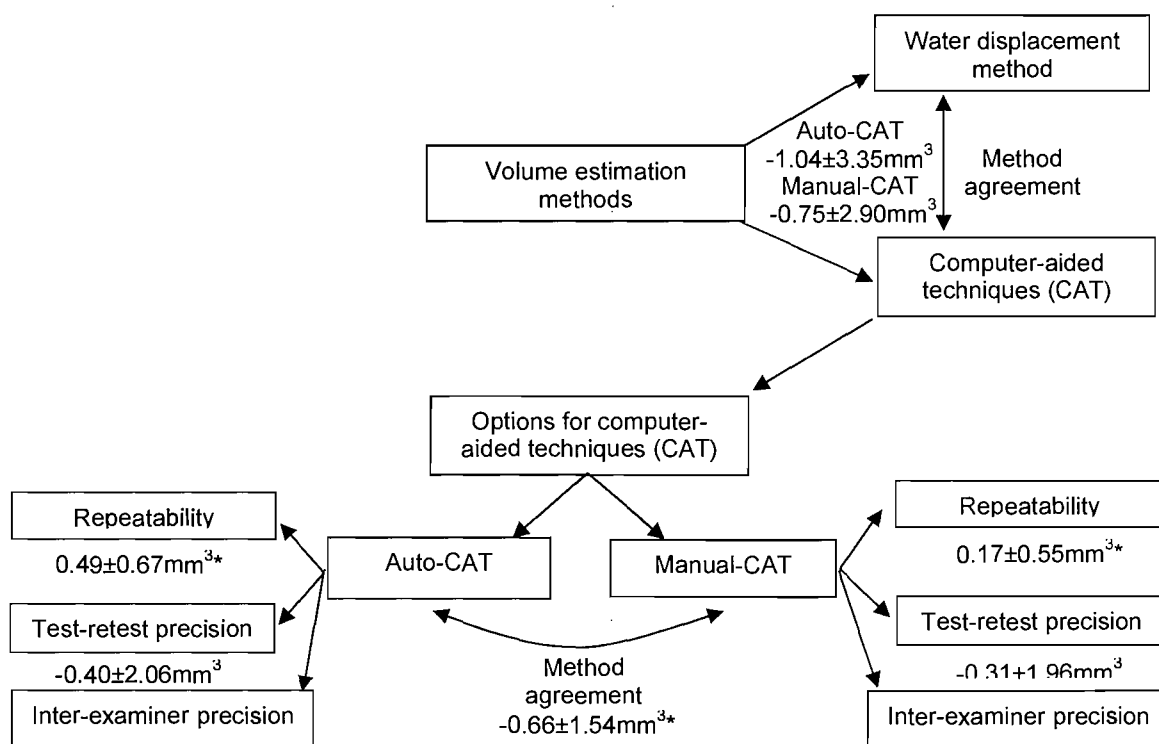
Figure 4.40. Summary of the limits of agreement ($d\pm1.96s_d$) for the precision and accuracy of the CAT methods for the determination of synovial fold volume (mm^3). * - regressed limits of agreement based on mean synovial fold volume.

It is evident from this extensive study of the precision and accuracy of the auto-CAT and manual-CAT that they share a similar degree of precision and accuracy and thus can be used interchangeably in the measurement of synovial fold volume. The type and magnitude of measurement errors (i.e. performance of the measurement methods) were similar for both the auto-CAT and manual-CAT, with the manual-CAT marginally more precise and accurate than the auto-CAT. With regard to applicability, the auto-CAT and manual-CAT used the same equipment and had equal expense. The auto-CAT was more flexible and adaptable to use compared to the manual-CAT but more time consuming to operate. Therefore it is recommended that the manual-CAT be used in future studies that require quantification of the dimensions of the synovial folds.

As discussed in Chapter 3, whether the precision of the auto-CAT and manual-CAT is acceptable for the measurement of synovial fold dimensions will be dependent upon their intended use in either a clinical or research setting (Westgard and Hunt, 1973; Bland and Altman, 1999; Keating and Matyas 1998). In the present study, the precision of the measurement method (method agreement, repeatability, test-retest and inter-examiner) was sufficient for the detection of differences in synovial fold volume between the right ventral, left ventral, right dorsal and left dorsal synovial folds. The precision of both the auto-CAT and the manual-CAT methods was also sufficient for the detection of synovial fold enlargement in joints affected by rheumatoid arthritis. Therefore it is suggested that the CAT techniques developed in the present study are suitable for use in future studies investigating the pathoanatomy of the synovial folds and their potential role in neck pain and disability.

4.5 Conclusion

A precise and accurate method for quantifying the dimensions of the synovial folds of the lateral atlanto-axial joints has been developed. Both the auto-CAT and manual-CAT are acceptable methods for the measurement of synovial fold dimensions with the manual-CAT being slightly superior with regard to performance and applicability.

The normal morphology of the synovial folds of the lateral atlanto-axial joints varies with respect to the location of the synovial folds. The volume of the right ventral and left ventral synovial folds was greater than the volume of the right dorsal and left dorsal synovial folds, respectively. This trend is evident in both male and female subjects. The

volume of the synovial folds does not appear to be affected by right-left asymmetry. Males tend to have a greater synovial fold volume compared to females. Enlargement of the synovial folds appears to be associated with rheumatoid arthritis affecting the lateral atlanto-axial joints.

Chapter 5

The development of a method to image the intra-articular synovial folds of the lateral atlanto-axial joints *in vivo* and determine their geometrical properties: a MRI study

5.1 Introduction

A number of imaging techniques have been used to visualise the intra-articular synovial folds of the spine. These include arthrography, computed tomography (CT), ultrasound and magnetic resonance imaging (MRI). In arthrography contrast media is injected into the joint space which can then be seen using fluoroscopy and/or X-ray; in CT successive X-ray scans are taken through a joint to create cross-sectional images that can be assimilated by computer to produce a three dimensional image. In ultrasonography high frequency sound waves are used to create images of sections through the body and these can also be correlated to produce three dimensional images. In MRI radiofrequency pulses are used to generate images of sectional planes through the body which again can be correlated to produce three dimensional images.

The synovial folds of the zygapophysial joints have been visualised in cadavers using arthrography (Okada, 1981) but *in vivo* images have not been obtained consistently with this technique (Dory, 1981; Dory, 1983). Synovial folds of the lumbar spine have occasionally been identified from *in vivo* CT scans, appearing as radiolucent areas within the zygapophysial joints (Taylor and McCormick, 1991). Overall neither technique produces images of articular soft tissue components at the level of discrimination achieved by MRI (Xu et al., 1990). The unnecessary exposure to ionising radiation in asymptomatic subjects required to obtain the images also make

arthrography and CT less than ideal techniques for assessing the morphology of the synovial folds *in vivo*.

Ultrasound has been used increasingly for imaging the vertebral column as it is a quick, non-invasive and cost-effective technique (Hides et al., 1995; Kristjansson, 2004; Rankin et al., 2005). The zygapophysial joint space has been depicted under ultrasound guidance (Galiano et al., 2005; 2006), making it a prospective tool for imaging the synovial folds *in vivo*.

MRI is frequently cited as the imaging technique that may one day reveal the physiological and pathological significance of the synovial folds (Mercer and Bogduk, 1993; Schonstrom et al., 1993; Inami et al., 2000). It has been successfully used to identify changes in size and signal intensity of the synovial folds (plicae) and fat pads of patients with knee pain (Jee et al., 1998; Garcia-Valtuille et al., 2002; Roth et al., 2004); and changes in the size and signal intensity of the spinal muscles (Ranson et al., 2006; Elliott et al., 2006; 2007b; Fernandez-de-Las-Penas et al., 2007), ligaments (Kaale et al., 2005; Krakenes and Kaale, 2006) and articulations (Pettersson et al, 1997; Vaccaro et al., 2001, Johansson, 2006) in patients with neck pain, headache and previous whiplash injury.

Yu et al. (1987) were the first to evaluate the use of MRI for the identification of synovial folds of the spine. They correlated anatomical sections and MR images of ten cadaver cervical spines. The synovial folds of the lateral atlanto-axial joints appeared on the MR images as regions of fibrous tissue of low signal intensity with adipose tissue having higher signal intensity. The images were positively correlated with corresponding sagittal anatomical sections of the cervical spine and cervical articulations dissected to display the synovial folds *in situ* (Yu et al., 1987). However, the spatial resolution of the images was not considered very good and the scanning acquisition time to obtain them was far longer than could be used in patients. Friedrich et al. (2007) similarly imaged the cervical synovial folds of one cadaver successfully and positively correlated sagittal scan images with histological sections. Again, the scan acquisition time was long and the method was not tested *in vivo*. Neither Yu et al. (1987) or Friedrich et al. (2007) documented the prevalence of the synovial folds that were visible on MR images.

The purpose of the present study was to investigate the use of MRI as a potential tool for imaging the intra-articular synovial folds of the lateral atlanto-axial joints *in vivo* and to establish a reliable measure of synovial fold volume and signal intensity. The use of ultrasound was initially considered and a preliminary trial of this imaging modality was undertaken. It enabled the articular cavity of the cervical and lumbar zygapophysial joints to be identified, however, the synovial folds could not be differentiated. MRI was thus chosen as the imaging technique for this study because of its non-invasive nature, use of non-ionising radiation and the excellence of the derived images. Although MR images are not acquired as rapidly as ultrasound images and MR is more expensive to perform, the ability of MRI to visualise soft tissue structures and differentiate spinal tissues is far superior to that of ultrasound

On MR images, each tissue has a different signal intensity (i.e. different level of 'brightness') that enables the boundaries between anatomical structures to be delineated. The basic appearance of different body tissues imaged using common MR sequences is summarised in Table 5.1.

Table 5.1. The typical appearance of different body tissues when imaged using common MRI sequences.

Signal intensity ('brightness') of body tissues on MR images			
Image sequences	Fluids e.g. synovial fluid, CSF, oedema	Water-based tissues e.g. muscle, cartilage, brain	Fat-based tissues e.g. fat, bone marrow
T1-weighted (short TE, short TR)	Low (very dark)	Medium (mid-grey)	High (very bright)
T2-weighted (long TE, long TR)	High	Medium	Medium
Proton density (long TR, short TE)	Medium	Medium	Medium

Signal (or pixel) intensity values are numbers that represent the MR signal intensity from a small three dimensional volume of tissue within the body being scanned known as a voxel (volume element). The brightness of the pixel intensity value on the image represents the MR signal intensity from the voxel with a higher MR signal being represented by a higher pixel number and a brighter image. The actual signal intensity depends on many factors, including the sequence timings and the intrinsic T1, T2 and proton density properties of the tissue of interest.

Based on the different signal intensity values of tissues on an MR image, segmentation (tissue classification) techniques can be developed to quantify the morphometry of

anatomical structures *in vivo*. Such techniques need to be able to obtain measurements of sufficient sensitivity and precision for use in patient diagnosis, treatment and management. Tissue segmentation also forms the basis of the reconstruction of 3D images from sets of 2D MRI scans.

The aims of the present study were to:

1. establish an imaging protocol in order to characterise the normal morphology of the intra-articular synovial folds of the lateral atlanto-axial joints
2. develop a measurement technique to quantify the volume and signal intensity of the synovial folds of the lateral atlanto-axial joints from MR images
3. evaluate the precision of the measurement techniques used to quantify the volume and signal intensity of the synovial folds from MRI scans
4. determine the prevalence of lateral atlanto-axial intra-articular synovial folds in a sample of normal healthy volunteers aged between 20 and 50 years from MRI images of the cervical spine
5. determine whether there is a difference in the volume and signal intensity of the synovial folds due to symmetry (ventral-dorsal and left-right) and gender
6. determine whether there is a relationship between the volume and signal intensity of the synovial folds and age.

5.2 Methods

A series of T1-weighted sagittal MRI scans of the cervical spine and lumbar spine were reviewed at the outset of this study. The synovial folds could be clearly and consistently visualised at the lateral atlanto-axial joints but not at the cervical and lumbar zygapophysial joints. Thus imaging of the synovial folds of the lateral atlanto-axial joints was planned.

5.2.1 Subjects

Ten volunteer subjects aged 20 to 50 years were recruited. Volunteers were not permitted onto the study if they were pregnant or claustrophobic or did not meet the inclusion/exclusion criteria to have an MRI scan. Approval for the study was obtained from the Local Research Ethics Committee. All subjects provided written informed consent prior to inclusion in the study.

5.2.2 Image acquisition

'Image acquisition' refers to the process of MR scanning to produce an MR image. MRI of the cervical spine was performed with a 1.5-Tesla scanner (Siemens MAGNETOM Symphony, Siemens AG Medical Solutions, Erlangen Germany) (Figure 5.1.A). Each volunteer was positioned supine on the scanner table and their external auditory meatus used to align their head and neck with respect to the table. The subject's head and neck were placed in a comfortable neutral position. Circularly polarised head and neck array coils (Siemens AG Medical Solutions, Erlangen, Germany) were fitted to each subject to obtain optimal image resolution of the upper cervical spine (Figure 5.1.B). With the aid of a T1-weighted sagittal locator image, the cervical spine was imaged using a variety of different sequences (Table 5.2). Two dimensional (2D) and three dimensional (3D) sequences of between 11 and 72 slices were taken with 1.25 to 4.0mm slice thickness. As determined through the cadaveric study (Chapter 4), the sagittal plane was the optimal plane for identifying and visualising the synovial folds and was thus selected as the acquisition plane for all image sequences.
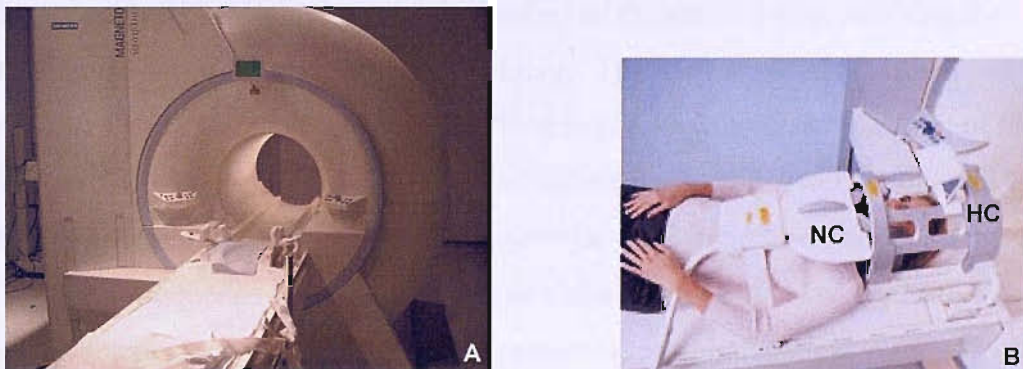
Figure 5.1.A. 1.5-Tesla MRI scanner (Siemens MAGNETOM Symphony, Siemens AG Medical Solutions, Erlangen, Germany). **B.** Each volunteer was positioned supine with the head in neutral and the head (HC) and neck (NC) array coils affixed. Adapted from www.medical.siemens.com, with permission.

Table 5.2. MRI acquisition sequences.

	MRI acquisition sequence	Abbreviation
Sequence 1	T1-weighted spin echo (SE) sequence in the sagittal plane	t1_se_sag
Sequence 2	T1-weighted SE sequence in the sagittal plane (512x192 matrix)	t1_se_sag_512
Sequence 3	T1-weighted multiplanar reformatting (MPR) non-selective	t1_mpr_ns_sag
Sequence 4	T1-weighted fast low angle shot (FLASH) 3D-acquisition sequence in the sagittal plane	t1_fl3d_sag
Sequence 5	T2-weighted 3D-acquisition double-echo steady-state (DESS) water-excitation sequence in the sagittal plane	t2_de3d_we_sag
Sequence 6	Proton-density sequence in the sagittal plane	pd_sag
Sequence 7	Proton-density sequence with fat saturation (FS)	pd_fs_tra
Sequence 8	Proton-density sequence without fat saturation (FS)	pd_no fs_tra
Sequence 9	T1-weighted fast low angle shot (FLASH) 2D-acquisition sequence in the sagittal plane	t1_fl2d_sag

135

The imaging parameters for each sequence are summarised in Table 5.3. All MRI scans were anonymised and stored as Digital Imaging and Communications in Medicine (DICOM) format files on computer and CD-ROM.

Table 5.3. Imaging parameters for MRI sequences.

	TE/TR (msec)	FOV (cm)	Acq. matrix (pixels)	Pixel size (mm)	Flip angle (°)	Acq type	Slice thickness (mm)	Interslice gap (mm)	No. slices	Acq time[†] (min)
Sequence 1	14/600	28	512x223	0.9x0.5	90	2D	3.00	0.30	11	4:34
Sequence 2	14/411	28	512x192	1.1x0.5	70	2D	3.00	0.30	13	6:02
Sequence 3	3.93/1900	25	256x179	1.4x1.1	15	3D	1.25	0.00	72	5:42
Sequence 4	10/25	15	256x192	0.8x0.6	50	3D	1.50	0.00	64	4:36
Sequence 5	6.63/23.68	15	256x192	0.8x0.6	25	3D	1.50	0.00	64	6:32
Sequence 6	13/2500	18	256x250	0.7x0.7	160	2D	4.00	0.20	15	4:58
Sequence 7	15/3000	18	512x256	0.7x0.4	150	2D	3.00	0.60	19	5.38
Sequence 8	15/3000	18	512x256	0.7x0.4	150	2D	3.00	0.60	19	5.38
Sequence 9	21/637	28	256x224	1.1x1.1	30	2D	3.5	0.85	15	6.08

Abbreviations: TE - echo time; TR - repetition time; FOV - field of view; Acq – acquisition; No. – number; 2D – two-dimensional; 3D – three-dimensional; † - total acquisition (scanning) time.

5.2.3 Image analysis

'Image analysis' or 'image processing' refers to the method of quantifying the dimensions of a structure from the MR image. The MRI scans of all volunteers were visualised and examined using OSIRIS (Version 4.18, University Hospital of Geneva, Geneva, Switzerland). The MR images of different sequences were compared to determine which sequence enabled the synovial folds to be visualised with the greatest clarity. The sequence that enabled optimal visualisation of the synovial folds was used for the determination of synovial fold prevalence, morphology and volume. For the determination of synovial fold signal intensity, the T1-weighted and the T2-weighted sequences that produced optimal resolution of the synovial folds were selected.

5.2.3i Prevalence and morphology

Sequence 5 images of each volunteer were carefully studied and the prevalence of the intra-articular synovial folds at the lateral atlanto-axial joints determined and their morphology described.

5.2.3ii Synovial fold volume

Synovial fold volume was quantified from Sequence 5 images using Materialise's Interactive Medical Image Control System (Mimics) version 8.11 (Materialise NV,

Leuven, Belgium). Mimics is an interactive tool for the visualisation, segmentation and 3D reconstruction of anatomical structures from MR images. A user-defined region of interest (ROI) was manually created for each synovial fold using a segmentation mask (Figure 5.2). The ROI demarcated the cross-sectional area of each synovial fold on all contiguous sagittal slices on which the synovial folds were visible. Once the ROI was segmented, a 3D model of each synovial fold was reconstructed and its volume measured using Mimics.
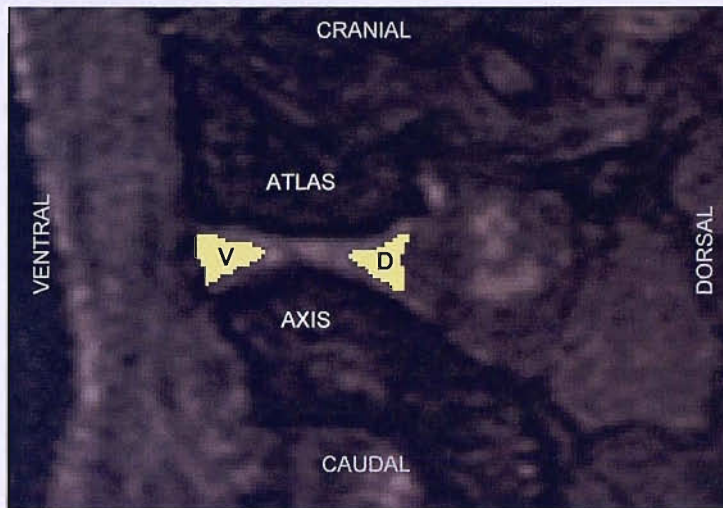
Figure 5.2. Region of interest (ROI) of ventral (V) and dorsal (D) synovial folds of the left lateral atlanto-axial joint (lateral view) of Volunteer 8 created using a segmentation mask on a sagittal T2-weighted 3D-acquisition DESS water-excitation (Sequence 5) image.

A 3D model of the axis vertebra and synovial folds of Volunteer 7 were reconstructed from Sequence 5 images. The lateral atlanto-axial joints of one cadaver were dissected, using the method described by Mercer and Bogduk (1993) (Table 4.1, Chapter 4), to show the 3D morphology of the synovial folds and their relationship to the axis vertebra. The synovial folds of the cadaver were photographed *in situ* and following resection from the fibrous joint capsule. The 3D reconstructed MRI models and images of the cadaver synovial folds were compared to confirm that the MRI models produced an accurate representation of the synovial folds.

5.2.3iii Synovial fold signal intensity

Sequence 5 (T2-weighted) and Sequence 2 (T1-weighted) were selected for the determination of synovial fold signal intensity (pixel value). The signal intensity of each synovial fold was measured and standardised by calculating the ratio of synovial fold signal intensity to synovial fluid signal intensity (FOLD/FLUID) from Sequence 5 and the ratio of synovial fold signal intensity to subcutaneous fat signal intensity (FOLD/FAT) from Sequence 2, as follows:

137

FOLD/FLUID ratio

Using Mimics the average signal intensity of the synovial folds was measured by manually selecting the cross-sectional area of the synovial fold (size ranged from 7.26 to 31.33mm^2) at the midsagittal slice of the lateral atlanto-axial joint (Figure 5.3). The average signal intensity of the synovial fluid was measured from a triangular-shaped region of interest composed of 10 pixels at the apex of the dorsal synovial fold at the midsagittal slice of the lateral atlanto-axial joint (Figure 5.3). The FOLD/FLUID signal intensity ratio was calculated as follows:

FOLD/FLUID = average signal intensity synovial fold/average signal intensity of synovial fluid. Using this formula, the ratio is <1.0 when the synovial fold has a lower signal intensity than the synovial fluid and vice versa.
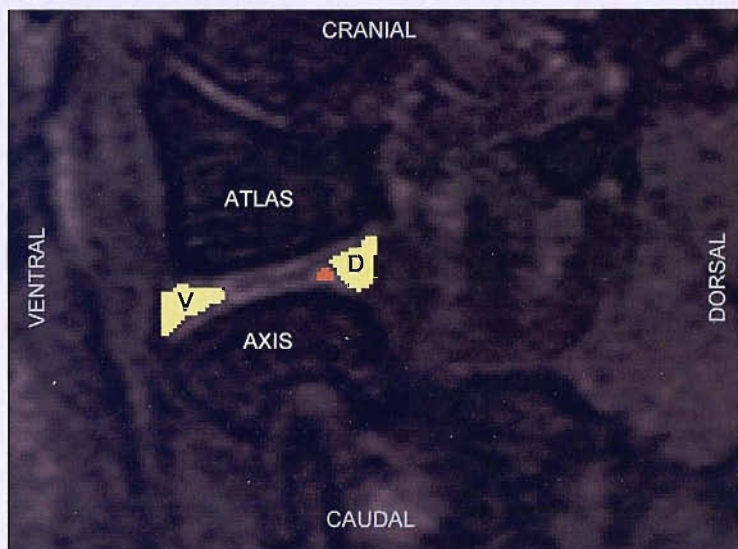
Figure 5.3. Region of interest (ROI) of ventral (V) and dorsal (D) synovial folds (yellow masks) and synovial fluid (orange mask) of the left lateral atlanto-axial joint (lateral view) of Volunteer 7 for the determination of the FOLD/FLUID signal intensity ratio from Sequence 5 images.

FOLD/FAT ratio

The average signal intensity of the synovial folds was measured by manually selecting the cross-sectional area of the synovial fold (size ranged from 19.60 to 24.19mm^2) at the midsagittal slice of the lateral atlanto-axial joint (Figure 5.4). The average signal intensity of the subcutaneous fat (of the posterior neck) was measured from a rectangular-shaped region of interest composed of 35 pixels located at the level of the apex of the dorsal synovial fold at the midsagittal slice of the lateral atlanto-axial joint (Figure 5.4). The FOLD/FAT signal intensity ratio was calculated as follows:

FOLD/FAT = average signal intensity synovial fold/average signal intensity of subcutaneous fat. Using this formula, the ratio is <1.0 when the synovial fold has a lower signal intensity than the subcutaneous fat and vice versa.
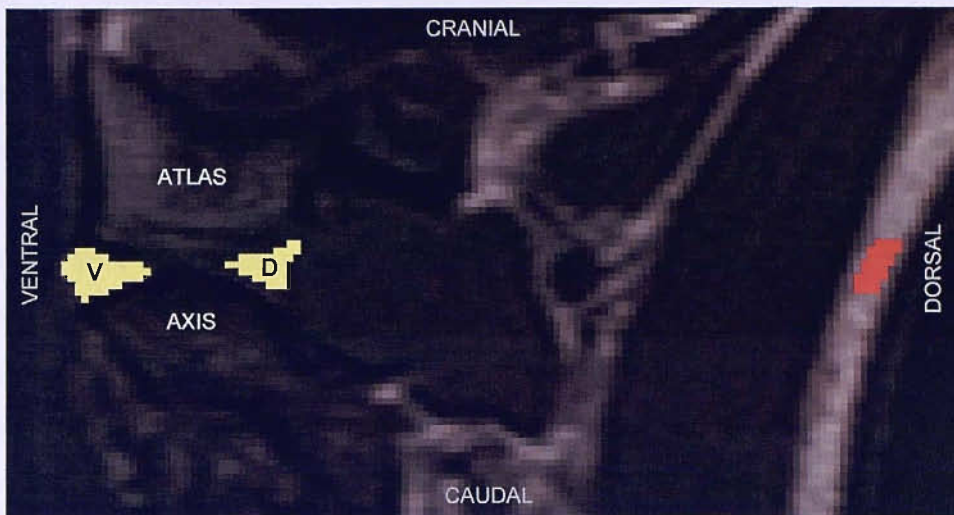
Figure 5.4. Region of interest (ROI) of ventral (V) and dorsal (D) synovial folds (yellow masks) of the right lateral atlanto-axial joint (medial view) and subcutaneous fat (red mask) of Volunteer 8 for the determination of the FOLD/FAT signal intensity ratio from Sequence 2 images.

5.2.3iv Statistical analysis

Synovial fold volume and signal intensity data were presented as means and standard deviations and boxplots were used to display the medians and ranges. The data was explored and examined for normality using histograms with Normal curves, quantile-quantile plots and the Kolmogorov-Smirnov (KS) test. Homogeneity of variance was examined using Levene's test.

The sample sizes were small and not all data demonstrated a Normal distribution thus the data was analysed using non-parametric statistics. Friedman's ANOVA was used to determine whether there was a difference in volume and signal intensity between the right ventral, right dorsal, left ventral and left dorsal synovial folds. If there was a significant difference, Wilcoxon's signed-rank test was used for *post hoc* analysis with *Bonferroni correction*. Wilcoxon's signed-rank test with *Bonferroni correction* was used to determine whether there was a difference in volume and signal intensity between the right and left ventral and right and left dorsal synovial folds; and between the ventral and dorsal synovial folds of the left and ventral and dorsal synovial folds of the right lateral atlanto-axial joints. The relationships between age and synovial fold volume and age and synovial fold signal intensity were estimated using Spearman's correlation coefficient (r_s).

Statistical analysis was performed using SPSS version 14.0 for Windows (SPSS Inc., Chicago, Illinois, USA) and Microsoft Excel 2000 (Microsoft Corporation, Redmond, WA, USA). A probability level of P=.05 was set as the minimum criterion of statistical significance for all tests.

5.2.4 Measurement precision

The precision of the MRI acquisition and image analysis for the measurement of synovial fold volume and signal intensity was assessed by re-scanning six subjects using Sequence 5 and three subjects using Sequence 2. Three subjects were re-scanned one month after the initial scan (1 month test-retest precision) using Sequence 5 and three subjects were re-scanned eighteen months following the initial scan (18 month test-retest precision) using Sequences 5 and 2 (Figure 5.5). To assess the inter-observer precision for the measurement of synovial fold volume and signal intensity, a second inexperienced examiner was trained to quantify the synovial fold volume and signal intensity of the initial test scans of three randomly selected subjects (Figure 5.5). Subjects were not re-scanned for the assessment of inter-observer precision.

The limits of agreement method with single measures (Section 4.2.3iii, Chapter 4) was used to estimate the precision of the MRI acquisition and image analysis for the measurement of synovial fold volume and signal intensity.
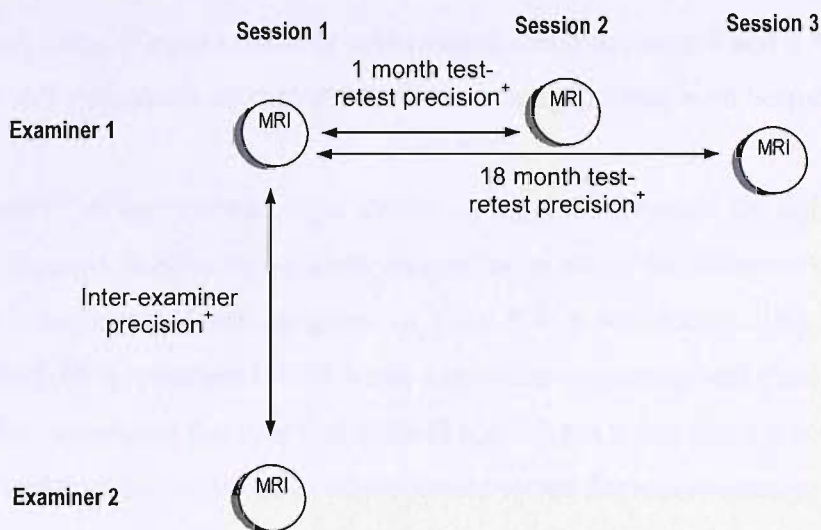
Figure 5.5. Diagrammatic representation of precision data collected and analysed in this study.
[+]Intermediate conditions of precision with the following factors selected as the variable:
Examiner – inter-examiner precision (subjects not re-scanned)
Time – 3 month test-retest precision (subjects re-scanned)
Time – 18 month test-retest precision (subjects re-scanned)

5.2.5 Measurement accuracy

To determine the accuracy of this method of MRI acquisition and image analysis for the measurement of volume, a phantom model was developed. Six cubes of Chorizo sausage (representing the synovial folds) that ranged in volume from 60mm^3 to 174 mm^3 were embedded in plastic test tubes of gelatine (representing the synovial fluid)

140

and scanned using Sequence 5. The scanning parameters were exactly the same as those used for the acquisition of the synovial fold images. The sausage volume was determined from the MRI images using the same method employed for the measurement of synovial fold volume (Section 5.2.3).

The limits of agreement method with single measures (see Section 4.2.3iii) was used to estimate the accuracy of the MRI acquisition and measurement of volume.

5.3   Results

5.3.1 Subjects
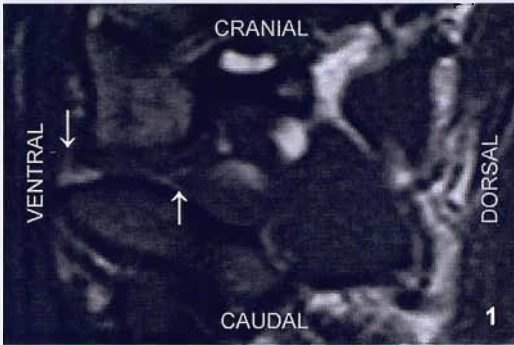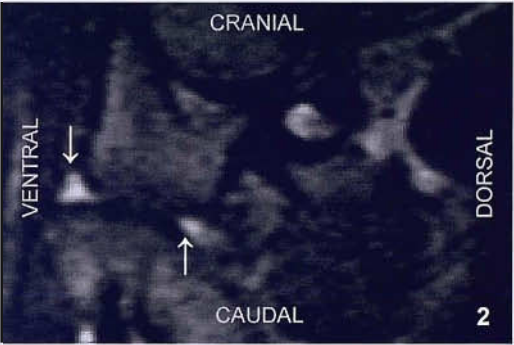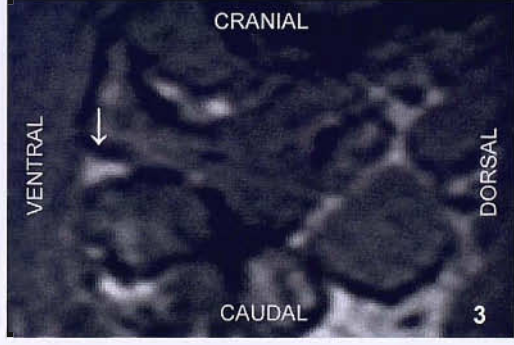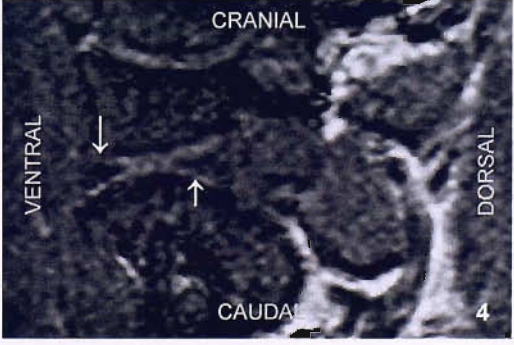
10 subjects aged from 22 to 47 years (mean 32.25 years, SD 8.15 years) participated in this study. There was an equal gender split with 5 female (mean 31.4 years, SD 9.66 years) and 5 male (mean 33.67 years, SD 6.43 years) volunteers.

5.3.2 Image acquisition

The cervical spine of each volunteer was imaged using between 4 and 8 different MRI sequences. All volunteers, except the first, were imaged using both Sequences 5 and 2.

The appearance of the synovial folds shown on sagittal section of the right lateral atlanto-axial joints (medial view) from images taken using the different MRI acquisition sequences is summarised and compared in Table 5.4. It was decided that Sequence 5 (T2-weighted 3D-acquisition DESS water-excitation sequence) was the optimal sequence for visualising the synovial folds (Figure 5.8.A). Sequence 5 was a 3D sequence, and thus was selected as the sequence to use for reconstructing 3D models of the synovial folds and determining their volume. Of the T1-weighted sequences, Sequence 2 produced the best resolution of the synovial folds. Sequence 5 and Sequence 2 were used for the determination of synovial fold signal intensity from T2-weighted and T1-weighted images, respectively.

Table 5.4. Visualisation and resolution of the synovial folds of the right lateral atlanto-axial joints (medial view) of Volunteers imaged using T1-weighted, T2-weighted and proton density-weighted MR sequences .

MR image	Synovial fold appearance
	Sequence 1 On this T1-weighted sequence, the ventral synovial fold (↓) was visualised as a medium-high signal intensity triangle. The dorsal synovial fold (↑) appeared as a low-medium signal intensity triangular-shaped structure.
	Sequence 2 Both the ventral (↓) and dorsal (↑) synovial folds appeared as high signal intensity triangular-shaped structures on this T1-weighted image. Out of the three T1-weighted sequences (Sequences 1, 2 and 3), the synovial folds were best delineated using Sequence 2.
	Sequence 3 The high signal intensity ventral synovial fold (↓) of this volunteer was clearly evident on this T1-weighted image, however, it was not possible to distinguish the dorsal synovial fold.
	Sequence 4 Homogeneous low signal intensity throughout the triangular-shaped ventral (↓) and dorsal (↑) synovial folds surrounded by synovial fluid of comparatively higher signal intensity. This 3D T1-weighted sequence produced better resolution of the synovial folds compared to the equivalent 2D sequence (Sequence 9). The contrast between the synovial folds and synovial fluid was improved with Sequence 5.

142
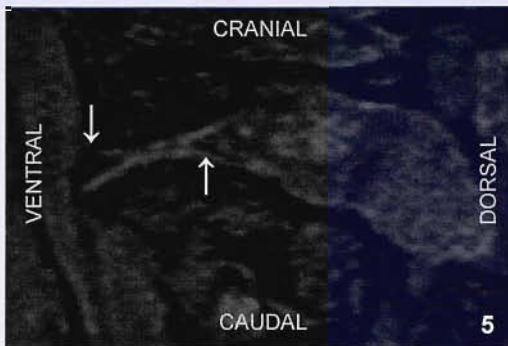
Sequence 5
The synovial folds were clearly demarcated as low to medium signal intensity triangular shaped structures delimited by synovial fluid of high signal intensity. In this image, the ventral synovial fold (↓) has uniform low signal intensity whilst the dorsal synovial fold (↑) has a speckled appearance. Optimal resolution of the synovial folds was obtained with this sequence.
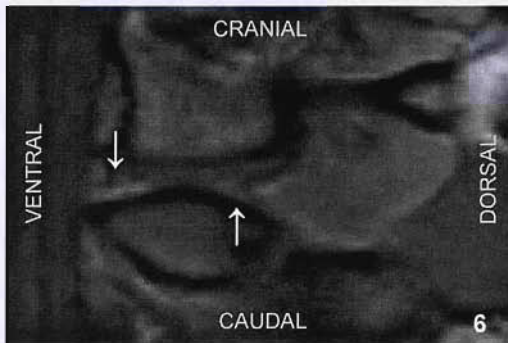
Sequence 6
On this proton density sequence, the triangular shaped synovial folds appeared as varying combinations of low, medium and high signal intensity but were difficult to clearly visualise. In this volunteer, the ventral (↓) and dorsal (↑) synovial folds appeared as regions of medium to high signal intensity.
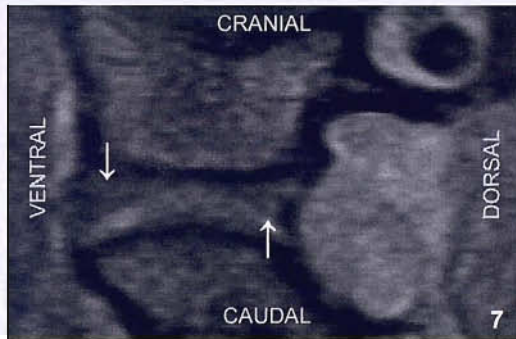
Sequence 7
Both the ventral (↓) and dorsal synovial folds (↑) appeared as triangular-shaped structures composed of low signal intensity on this proton-density sequence (with fat saturation). The synovial folds were easier to identify compared to Sequence 6.
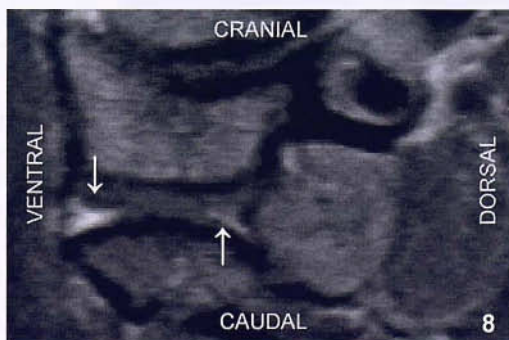
Sequence 8
The triangular-shaped synovial folds were visible as low to medium signal intensity structures using this proton-density sequence (without fat saturation). The ventral synovial fold (↓) of this volunteer was visualised as a high signal intensity triangular-shaped structure whilst the dorsal synovial fold (↑) appeared as a base of low signal intensity and a middle portion and apex of medium-high signal intensity.
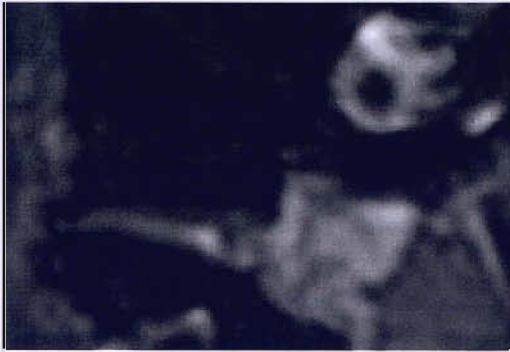
Sequence 9
The synovial folds were very difficult to visualise and differentiate from surrounding structures and appeared as low signal intensity triangular-shaped structures. The resolution of the synovial folds on this T1-weighted 2D sequence was poor in comparison to the equivalent 3D sequence (Sequence 4).

5.3.3 Image analysis

5.3.3i Prevalence and gross morphology

Intra-articular synovial folds were identified in 100% of the lateral atlanto-axial joints imaged using Sequence 5, located at both the ventral and dorsal poles of the right and left joints. Synovial folds were visible on an average of eight sagittal slices per joint from the 64 slice Sequence 5. The morphology of the synovial folds visualised using Sequence 5 is shown in Figure 5.6.
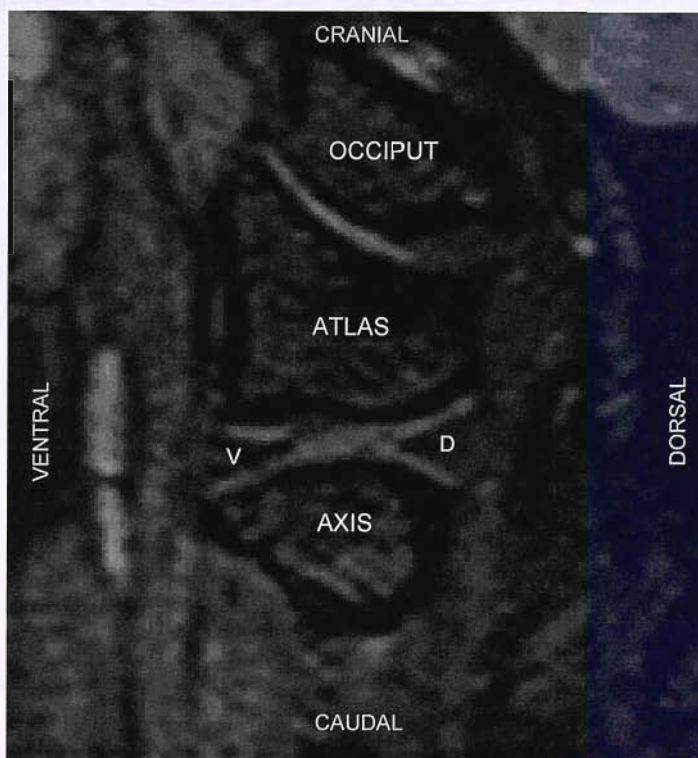
Figure 5.6. Sagittal section of the right lateral atlanto-axial joint (medial view) of Volunteer 7 showing ventral (V) and dorsal (D) synovial folds imaged using Sequence 5.

On sagittal images, the synovial folds typically appeared triangular in shape. The thick base of the synovial folds was continuous with the internal aspect of the fibrous capsule and tapered to form the thin free apex which projected varying distances between the articular surfaces of the atlas and axis.

5.3.3ii Synovial fold volume

The shape and disposition of the 3D models of the synovial folds, reconstructed from the MR images of the volunteers, correlated positively with the synovial folds removed by dissection from the cadaver. Peripherally the 3D model and cadaver synovial folds consisted of a thick base attached to the fibrous capsule. The base tapered to a thin apex that projected into the joint cavity between the articular facets of the atlas and the axis. From a superior view the synovial folds were crescent (semilunar) shaped.

Figure 5.7 is an illustration of the ventral and dorsal synovial folds as they appear *in situ*, drawn to illustrate the 3D morphology of the synovial folds and to assist in the orientation of the superolateral, superior and anterior views of the 3D models and dissections of the synovial folds in Figures 5.8 to 5.10. Figure 5.8.A demonstrates the 3D reconstructed models of the ventral and dorsal synovial folds of the left lateral atlanto-axial joint of Volunteer 7 *in situ* on the reconstructed model of the axis vertebra. Figure 5.8.B shows the ventral and dorsal synovial folds *in situ* on the superior articular facet of the axis of the cadaver following dissection and removal of the atlas vertebra.
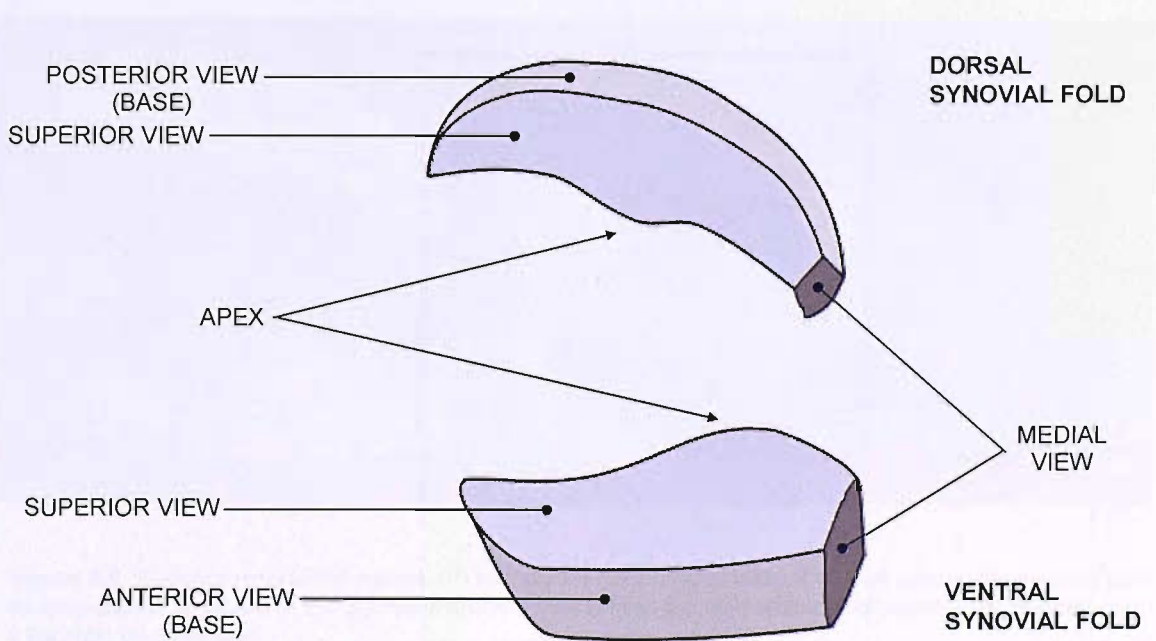
Figure 5.7. 3D illustration of the morphology of the ventral and dorsal synovial folds as they appear *in situ*.
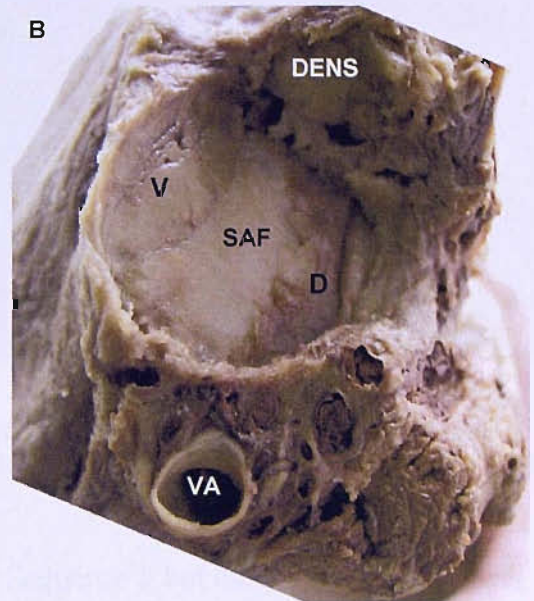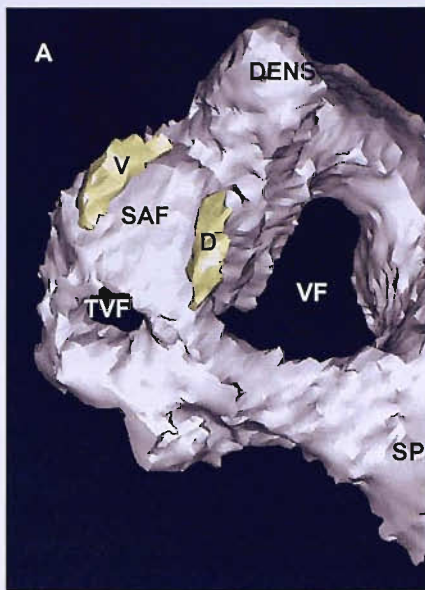
Figure 5.8.A. Superolateral view of the 3D reconstructed model of the axis vertebra and ventral (V) and dorsal (D) synovial folds of the left lateral atlanto-axial joint from an MRI scan of Volunteer 7. The synovial folds can be seen *in situ* on the superior articular facet (SAF) of the axis. **B.** Superolateral view of the dissected left lateral atlanto-axial joint of a cadaver showing the ventral (V) and dorsal (D) synovial folds covering the hyaline articular cartilage of the superior articular facet (SAF) of the axis. TVF-transverse foramen for the vertebral artery (VA); SP-spinous process; VF-vertebral foramen for the spinal cord.

Figures 5.9.A and 5.10.A show the 3D reconstructed models of the ventral and dorsal synovial folds from a superior view and anterior view, respectively. Figures 5.9.B and 5.10.B show superior and anterior views, respectively, of the synovial folds of the cadaver following their removal from the fibrous joint capsule by dissection.
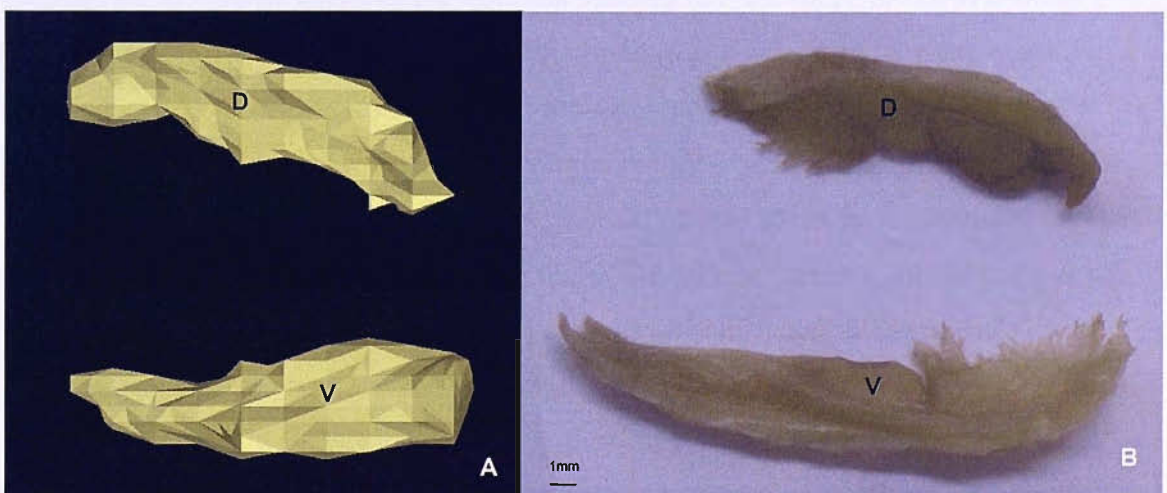
Figure 5.9. Superior view of the ventral (V) and dorsal (D) synovial folds of the left lateral atlanto-axial joint as they appear *in situ* **A.** of the 3D reconstructed model from the MRI scan of Volunteer 7. **B.** isolated from a cadaver by dissection.

146
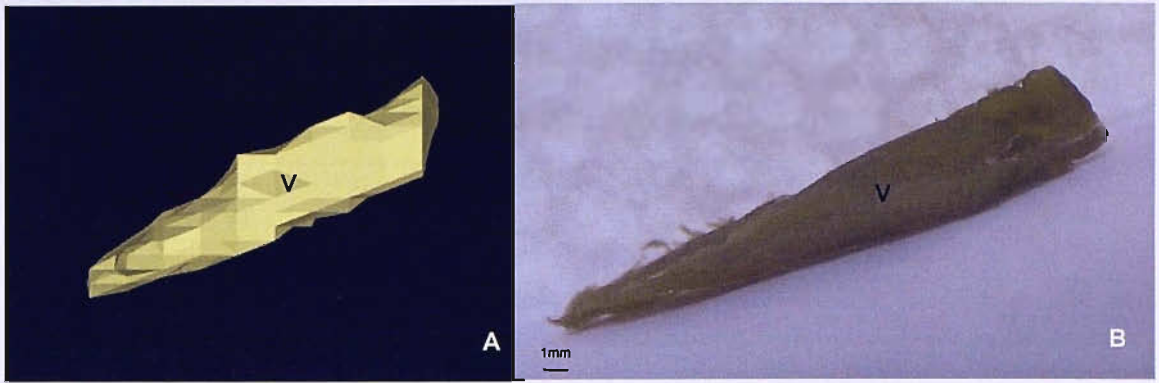
Figure 5.10. Anterior view of the ventral (V) and dorsal (D) synovial folds of the left lateral atlanto-axial joint as they appear *in situ* **A.** of the 3D reconstructed model from the MRI scan of Volunteer 7. **B.** isolated from a cadaver by dissection.

Nine of the ten volunteers were scanned using Sequence 5 but the images of Volunteer 5 were excluded due to poor resolution caused by the absence of the head coil during scanning. Thus eight volunteers provided data on 16 lateral atlanto-axial joints. 32 synovial fold 3D models were reconstructed from the resulting MR images of the ventral and dorsal synovial folds of each joint. The age and gender of each volunteer is summarised in Table 5.5. The volume of the individual 3D synovial fold models ranged from a minimum value of 30.29mm^3 to a maximum value of 175.99mm^3 and the median was 80.15 mm^3 (mean 83.59mm^3, standard deviation 28.67mm^3) (Figure 5.11).

The volume of the ventral and dorsal synovial folds of the right and left lateral atlanto-axial joints are presented in Table 5.5 and Figure 5.11. There was a significant difference in volume between the synovial folds ($\chi^2(3)=14.70$, P=.001). Wilcoxon's signed-rank test was used to follow up this finding. A *Bonferroni correction* was applied and so all effects are reported at a .0125 level of significance. Right ventral was greater than right dorsal synovial fold volume but there was no significant difference (Z=-1.96, P=.06). Left ventral was larger than left dorsal synovial fold volume and the difference was significant (Z=-2.52, P=.008). The volume of the right ventral and left ventral synovial folds was similar and there was no significant difference (Z=-0.70, P=.55). Right dorsal was greater than left dorsal synovial fold volume (Z=-2.24, P=.02) but the difference was not significant.

Table 5.5. The volume (mm^3) of the synovial folds at the lateral atlanto-axial joints of 8 subjects.

Subjects	Age	Gender	Synovial fold volume (mm^3)			
			Right ventral synovial fold	Right dorsal synovial fold	Left ventral synovial fold	Left dorsal synovial fold
Female subjects						
Volunteer 2	47	Female	129.06	86.11	115.55	89.82
Volunteer 4	32	Female	100.18	96.94	115.85	66.49
Volunteer 7	31	Female	86.18	66.66	79.26	47.31
Volunteer 8	25	Female	113.37	92.04	81.04	63.03
Mean (SD)	33.75 (9.36)		107.20 (18.32)	85.44 (13.28)	97.93 (20.54)	66.66 (17.55)
Male subjects						
Volunteer 3	29	Male	69.15	70.40	76.21	50.30
Volunteer 6	31	Male	65.15	83.55	51.50	48.16
Volunteer 9	36	Male	175.99	69.57	102.10	66.24
Volunteer 10	26	Male	97.16	76.44	113.86	30.29
Mean (SD)	30.50 (4.20)		101.86 (51.43)	74.99 (6.48)	85.92 (27.82)	48.75 (14.71)
Mean (SD)	**32.13 (6.94)**		**104.53 (35.85)**	**80.21 (11.17)**	**91.92 (23.53)**	**57.71 (17.79)**
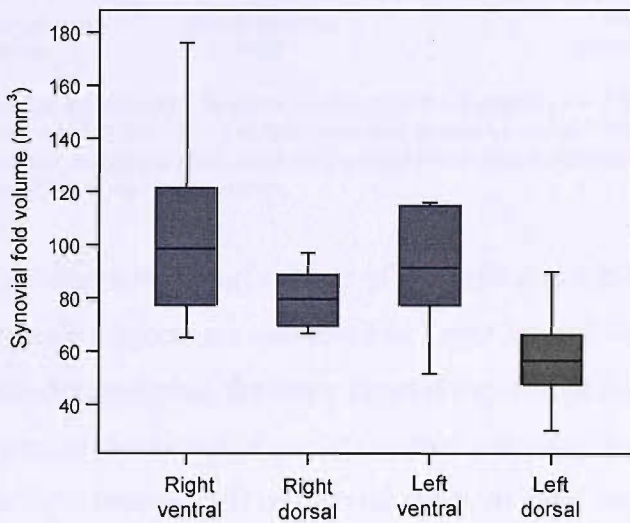
Figure 5.11. Boxplot of ventral and dorsal synovial fold volume (mm^3) at the right and left lateral atlanto-axial joints of 8 subjects showing the range of values and the median (——).

Further analysis was undertaken to compare the volume of the ventral synovial folds of the right and left lateral atlanto-axial joints and the volume of the dorsal synovial folds of the right and left lateral atlanto-axial joints (Table 5.6 and Figure 5.12). The volume of the ventral and dorsal synovial folds of the right joints were compared to the ventral and dorsal synovial folds of the left joints (Table 5.6 and Figure 5.12). The Wilcoxon signed-rank test was used and a *Bonferroni correction* applied, so all effects are reported at a .025 level of significance. Right and left ventral synovial fold volume was significantly greater than right and left dorsal synovial fold volume (Z=-3.21, P=.00). The ventral and dorsal synovial folds of the right lateral atlanto-axial joints were significantly larger than the ventral and dorsal synovial folds of the left lateral atlanto-axial joints (Z=-2.43, P=.01).

Table 5.6. Ventral and dorsal and right and left synovial fold volume (mm^3) at 16 lateral atlanto-axial joints.

Synovial fold volume (mm^3)	Ventral synovial folds	Dorsal synovial folds	Right synovial folds	Left synovial folds
Mean	98.23	68.96	92.37	74.81
SD	30.01	18.47	28.56	26.80
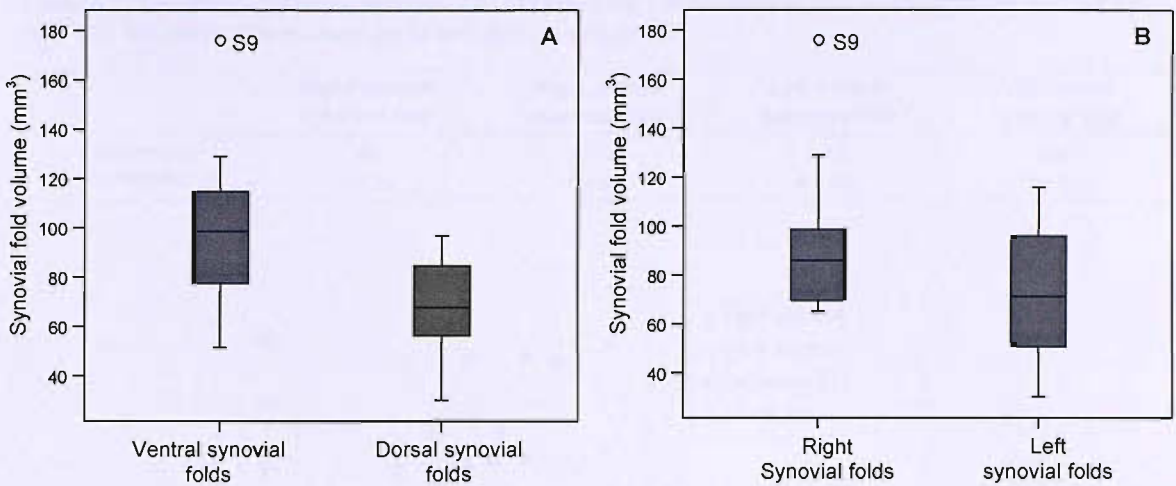
Figure 5.12. Boxplot showing the range of values and the median (——) for the volume (mm^3) of the **A.** ventral synovial folds of the right and left joints and dorsal synovial folds of the right and left joints (n=16) **B.** ventral and dorsal synovial folds of the right joints and ventral and dorsal synovial folds of the left joints (n=16). o=outlier; S=subject number.

Ventral and dorsal synovial fold volume of the right and left lateral atlanto-axial joints of male and female subjects are compared in Table 5.5 and Figure 5.13. Male and female subjects demonstrated the same general trend of larger right ventral compared to right dorsal synovial folds and larger left ventral compared to left dorsal synovial folds. Typically, the right ventral and right dorsal synovial folds were larger than the left ventral and left dorsal synovial folds, respectively, for both males and females. The mean synovial fold volume of the female subjects was greater than that of the male subjects.
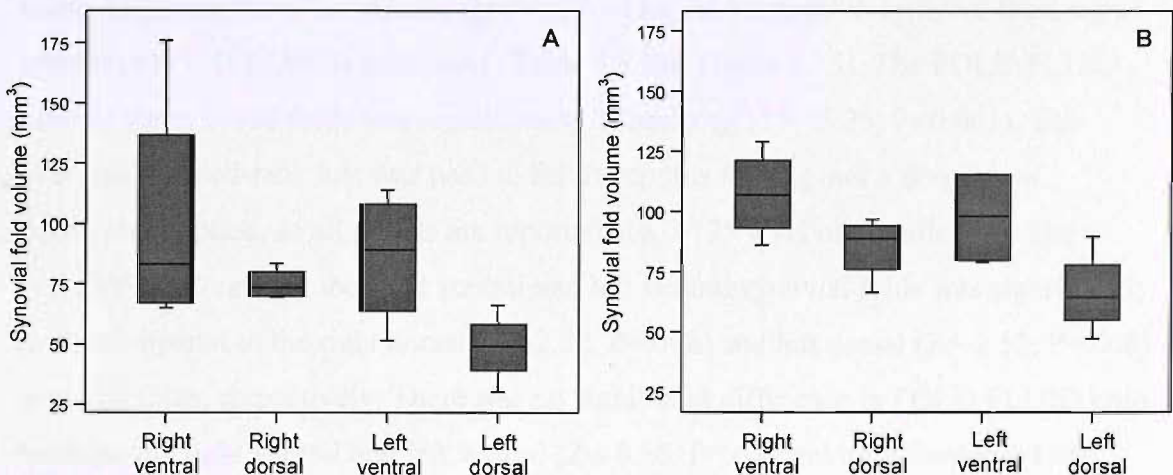
Figure 5.13. Boxplot of ventral and dorsal synovial fold volume (mm^3) at the right and left lateral atlanto-axial joints of **A.** males (n=4) and **B.** females (n=4) showing the range of values and median (——).

149

There was a positive correlation between right ventral and left dorsal synovial fold volume and age. Left ventral synovial fold volume was negatively correlated with age. (Table 5.7 and Figure 5.14).

Table 5.7. Correlation between synovial fold volume (mm^3) of the ventral and dorsal synovial folds of the right and left lateral atlanto-axial joints with age (years) (n=8).

	Right ventral synovial fold	Right dorsal synovial fold	Left ventral synovial fold	Left dorsal synovial fold
Spearman's correlation	.43 P=.29	-.02 P=.96	-.41 P=.32	.66 P=.08
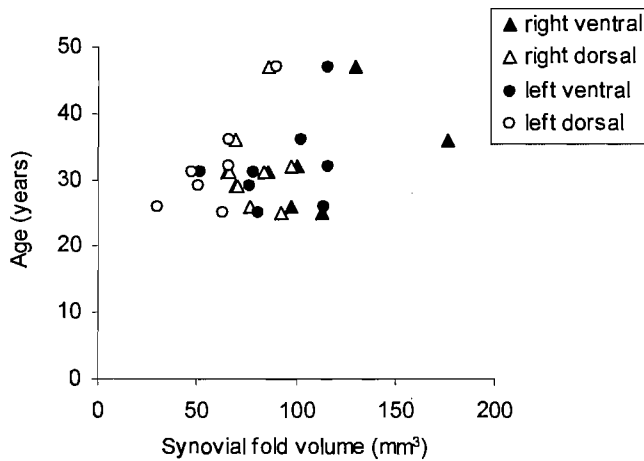
Figure 5.14. Scatter diagram of ventral and dorsal synovial fold volume (mm^3) at the right and left lateral atlanto-axial joints plotted against age (years) (n=8).

5.3.3iii Signal intensity

FOLD/FLUID ratio

Eight subjects (32 synovial folds from 16 lateral atlanto-axial joints) were scanned using Sequence 5 and the ratio of synovial fold signal intensity to synovial fluid signal intensity (FOLD/FLUID) calculated (Table 5.8 and Figure 5.15). The FOLD/FLUID ratio of the synovial folds was significantly different ($\chi^2(3)=13.35$, P=0.001). The Wilcoxon signed-rank test was used to follow up this finding and a *Bonferroni correction* applied, so all effects are reported at a .0125 level of significance. The FOLD/FLUID ratio of the right ventral and left ventral synovial folds was significantly lower compared to the right dorsal (Z=-2.52, P=.008) and left dorsal (Z=-2.52, P=.008) synovial folds, respectively. There was no significant difference in FOLD/FLUID ratio between the right ventral and left ventral (Z=-0.56, P=.64) and right dorsal and left dorsal (Z=-0.42, P=.74) synovial folds.

Table 5.8. Standardised FOLD/FLUID signal intensity ratio of the ventral and dorsal synovial folds of the right and left lateral atlanto-axial joints of 8 subjects imaged using Sequence 5.

	Age	Gender	Right ventral synovial fold	Right dorsal synovial fold	Left ventral synovial fold	Left dorsal synovial fold
			Synovial fold volume (mm^3)			
Female subjects						
Volunteer 2	47	Female	0.95	0.97	0.97	0.98
Volunteer 4	32	Female	0.95	0.96	0.93	0.94
Volunteer 7	31	Female	0.94	0.95	0.95	0.96
Volunteer 8	25	Female	0.96	0.96	0.94	0.94
Mean (SD)	33.75 (9.36)		0.95 (0.01)	0.96 (0.01)	0.94 (0.02)	0.96 (0.02)
Male subjects						
Volunteer 3	29	Male	0.98	0.99	0.98	0.98
Volunteer 6	31	Male	0.92	0.94	0.93	0.95
Volunteer 9	36	Male	0.85	0.93	0.78	0.83
Volunteer 10	26	Male	0.85	0.88	0.86	0.92
Mean (SD)	30.5 (4.20)		0.90 (0.06)	0.93 (0.05)	0.89 (0.09)	0.92 (0.07)
Mean (SD)	**32.13 (6.94)**		**0.92 (0.06)**	**0.95 (0.04)**	**0.92 (0.07)**	**0.94 (0.05)**
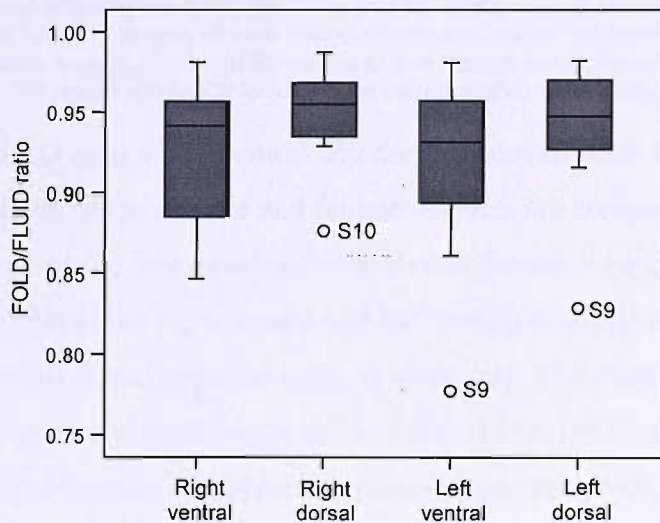
Figure 5.15. Boxplot of standardised FOLD/FLUID signal intensity ratio of the ventral and dorsal synovial folds of the right and left lateral atlanto-axial joints of 8 subjects showing the range of values and the median (——). o=outlier; S=subject number

Additional analysis was undertaken to compare the FOLD/FLUID ratio of the ventral synovial folds of the right and left joints and the dorsal synovial folds of the right and left joints (Table 5.9 and Figure 5.16). The FOLD/FLUID ratio of the ventral and dorsal synovial folds of the right joints and ventral and dorsal synovial folds of the left joints was compared. Wilcoxon's signed-rank test was used and a *Bonferroni correction* applied, so all effects are reported at a .025 level of significance. The FOLD/FLUID ratio of the ventral synovial folds was significantly lower than the dorsal synovial folds (Z=-3.52, P=.000). The FOLD/FLUID ratio was not significantly different between the synovial folds of the right and left lateral atlanto-axial joints (Z=-0.62, P=.56).

151

Table 5.9. Ventral and dorsal and right and left FOLD/FLUID ratio at 16 lateral atlanto-axial joints.

Synovial fold volume (mm^3)	Ventral synovial folds	Dorsal synovial folds	Right synovial folds	Left synovial folds
Mean	0.92	0.94	0.94	0.93
SD	0.06	0.04	0.04	0.06
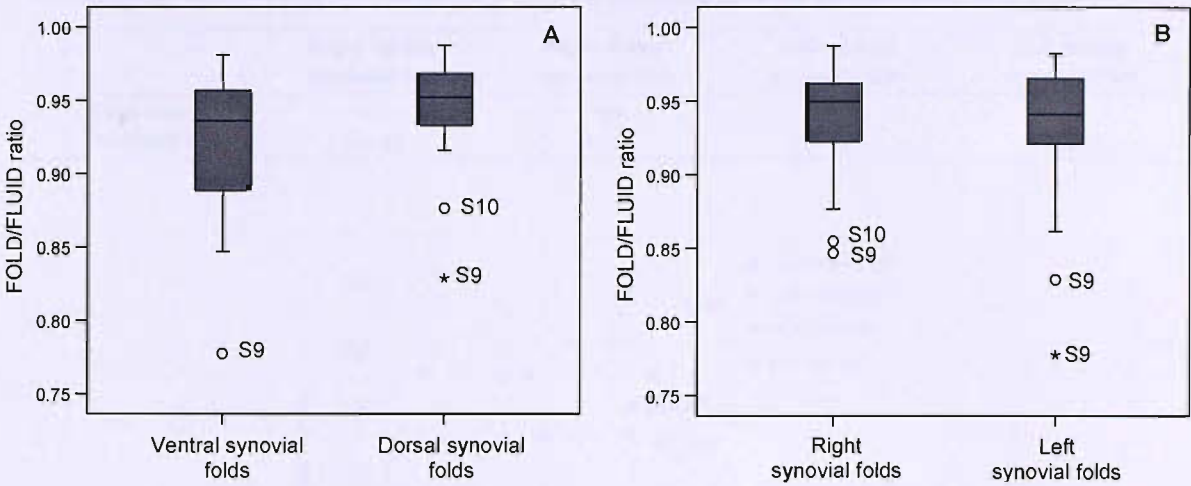
Figure 5.16. Boxplot showing the range of values and the median (——) for the FOLD/FLUID ratio of the **A.** ventral synovial folds of the right and left lateral atlanto-axial joints and dorsal synovial folds of the right and left lateral atlanto-axial joints (n=16) **B.** ventral and dorsal synovial folds of the right lateral atlanto-axial joints and ventral and dorsal synovial folds of the left lateral atlanto-axial joints (n=16). o=outlier; S=subject

The FOLD/FLUID ratio of the ventral and dorsal synovial folds of the right and left lateral atlanto-axial joints of male and female subjects are compared in Table 5.8 and Figure 5.17. Both males and females demonstrated the same general trend of lower FOLD/FLUID ratio at the right ventral and left ventral synovial folds compared to the right dorsal and left dorsal synovial folds, respectively. The right ventral and left ventral FOLD/FLUID ratios and right dorsal and left dorsal FOLD/FLUID ratios were similar for both males and females. Compared to females, the mean FOLD/FLUID ratio of males was lower and the range of values wider.
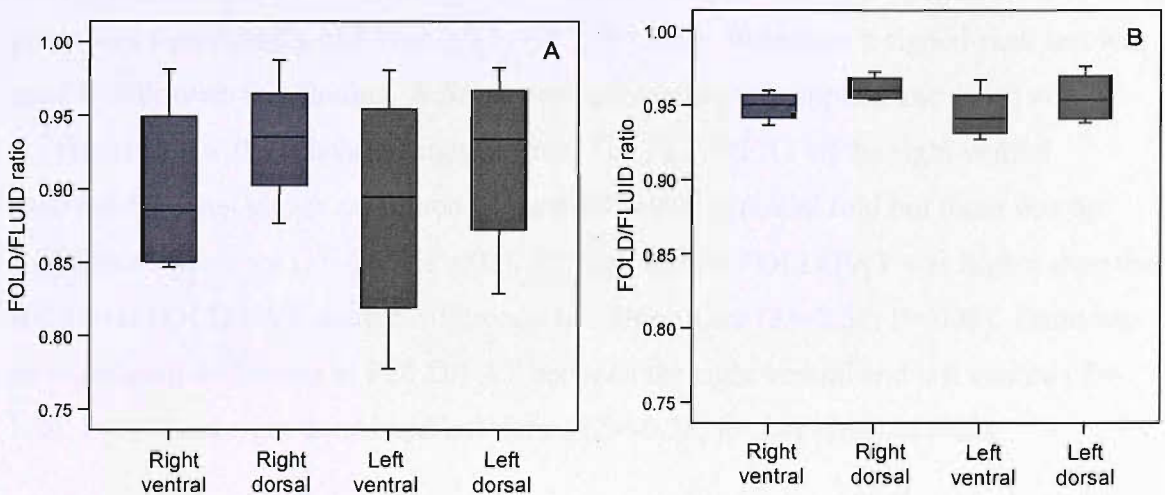
Figure 5.17. Boxplot of standardised FOLD/FLUID signal intensity ratio of the ventral and dorsal synovial folds of the right and left lateral atlanto-axial joints of **A.** male (n=4) and **B.** female (n=4) subjects showing the range of values and the median (——).

A relationship between subject age and FOLD/FLUID signal intensity ratio was not evident (Table 5.10 and Figure 5.18).

Table 5.10. Correlation between age (years) and standardised FOLD/FLUID signal intensity ratio of the synovial folds of the ventral and dorsal synovial folds of the right and left lateral atlanto-axial joints (n=8).

	Right ventral synovial fold	Right dorsal synovial fold	Left ventral synovial fold	Left dorsal synovial fold
Spearman's correlation	-.25 P=.55	.04 P=.93	-.07 P=.87	.13 P=.76

Figure 5.18. Scatter diagram of standardised FOLD/FLUID signal intensity ratio of the ventral and dorsal synovial folds at the right and left lateral atlanto-axial joints (n=8) plotted against age (years).

FOLD/FAT ratio

Eight subjects (32 synovial folds from 16 lateral atlanto-axial joints) were scanned using Sequence 2 and the ratio of synovial fold signal intensity to subcutaneous fat signal intensity (FOLD/FAT) calculated (Table 5.11 and Figure 5.19). The FOLD/FAT ratio of the ventral and dorsal synovial folds of the left and right lateral atlanto-axial joints was significantly different ($\chi^2(3)=15.3$, P=.000). Wilcoxon's signed-rank test was used to follow up this finding. A *Bonferroni correction* was applied and so all effects are reported at a .0125 level of significance. The FOLD/FAT of the right ventral synovial fold was higher compared to the right dorsal synovial fold but there was no significant difference (Z=-2.24, P=.02). The left ventral FOLD/FAT was higher than the left dorsal FOLD/FAT and the difference was significant (Z=-2.52, P=.008). There was no significant difference in FOLD/FAT between the right ventral and left ventral (Z=-1.26, P=.13) and right dorsal and left dorsal (Z=-0.28, P=.84) synovial folds.

Table 5.11. Standardised FOLD/FAT signal intensity ratio of the ventral and dorsal synovial folds of the right and left lateral atlanto-axial joints of 8 subjects imaged using Sequence 2.

	Age	Gender	Right ventral synovial fold	Right dorsal synovial fold	Left ventral synovial fold	Left dorsal synovial fold
			Synovial fold volume (mm³)			
Female subjects						
Volunteer 2	47	Female	0.64	0.58	0.64	0.61
Volunteer 4	32	Female	0.68	0.66	0.71	0.66
Volunteer 7	31	Female	0.81	0.73	0.84	0.76
Volunteer 8	25	Female	0.80	0.72	0.84	0.70
Volunteer 16	29	Female	0.85	0.74	0.83	0.72
Mean (SD)	33.40 (8.14)		0.76 (0.09)	0.68 (0.07)	0.75 (0.10)	0.68 (0.07)
Male subjects						
Volunteer 6	31	Male	0.84	0.79	0.83	0.80
Volunteer 9	36	Male	0.80	0.71	0.80	0.73
Volunteer 10	26	Male	0.88	0.91	0.89	0.82
Mean (SD)	31 (5)		0.84 (0.04)	0.80 (0.10)	0.84 (0.04	0.78(0.05)
Mean (SD)	**32.13 (6.94)**		**0.79 (0.09)**	**0.73 (0.10)**	**0.80 (0.08)**	**0.72 (0.07)**
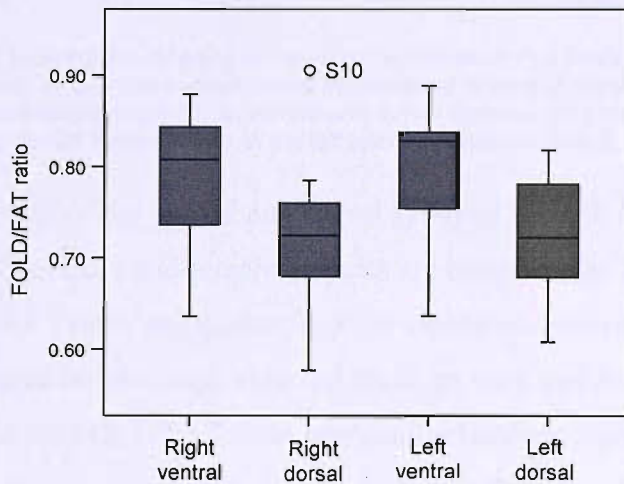
Figure 5.19. Boxplot of standardised FOLD/FAT signal intensity ratio of the ventral and dorsal synovial folds of the right and left lateral atlanto-axial joints of 8 subjects showing the range of values and the median (——); o=outlier; S=subject number

Additional analysis was undertaken to compare the FOLD/FAT ratio of the ventral synovial folds of the right and left joints and the dorsal synovial folds of the right and left joints (Table 5.12 and Figure 5.20). The FOLD/FAT ratio of the ventral and dorsal synovial folds of the right joints was compared to the FOLD/FAT ratio of the ventral and dorsal synovial folds of the left joints. Wilcoxon's signed-rank test was used and a *Bonferroni correction* applied, so all effects are reported at a .025 level of significance. Ventral synovial fold FOLD/FAT ratio was significantly higher than dorsal synovial fold FOLD/FAT ratio (Z=-3.36, P=.000). The FOLD/FAT ratio was not significantly different between the synovial folds of the right and left lateral atlanto-axial joints (Z=-1.14, P=.27).

Table 5.12. Ventral and dorsal and right and left FOLD/FAT ratio at 16 lateral atlanto-axial joints.

Synovial fold volume (mm³)	Ventral synovial folds	Dorsal synovial folds	Right synovial folds	Left synovial folds
Mean	0.79	0.73	0.76	0.76
SD	0.08	0.08	0.09	0.08
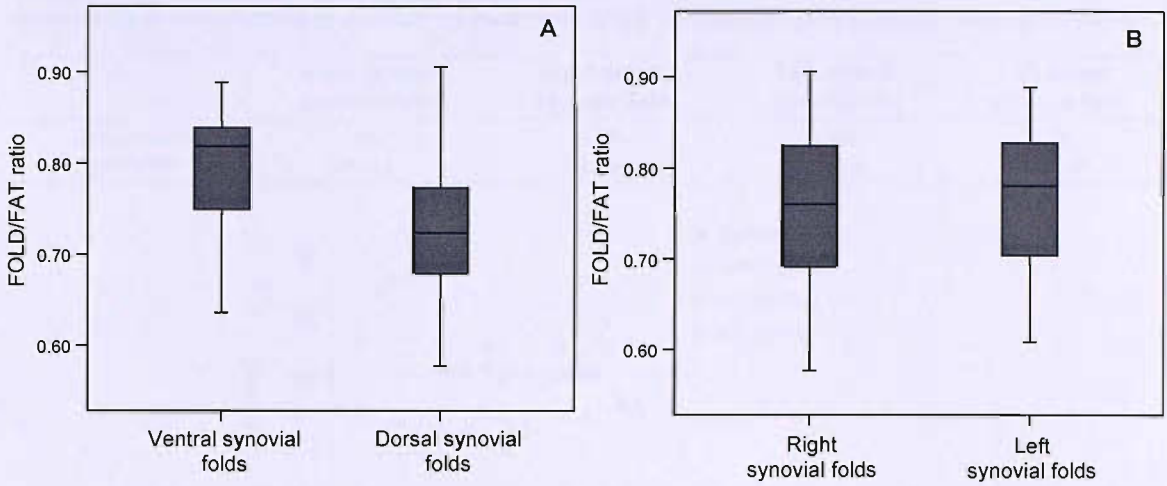
Figure 5.20. Boxplot showing the range of values and the median (——) for the FOLD/FAT ratio of the **A.** ventral synovial folds of the right and left lateral atlanto-axial joints and dorsal synovial folds of the right and left lateral atlanto-axial joints (n=16) **B.** ventral and dorsal synovial folds of the right lateral atlanto-axial joints and ventral and dorsal synovial folds of the left lateral atlanto-axial joints (n=16).

The FOLD/FAT ratio of the ventral and dorsal synovial folds of the right and left lateral atlanto-axial joints of male and female subjects are compared in Table 5.11 and Figure 5.21. The FOLD/FAT ratio was higher for right ventral compared to right dorsal and left ventral compared to left dorsal synovial folds for both males and females. For both males and females the FOLD/FAT ratio was similar between right ventral and left ventral and right dorsal and left dorsal synovial folds. The mean FOLD/FAT ratio of males was higher compared to females.
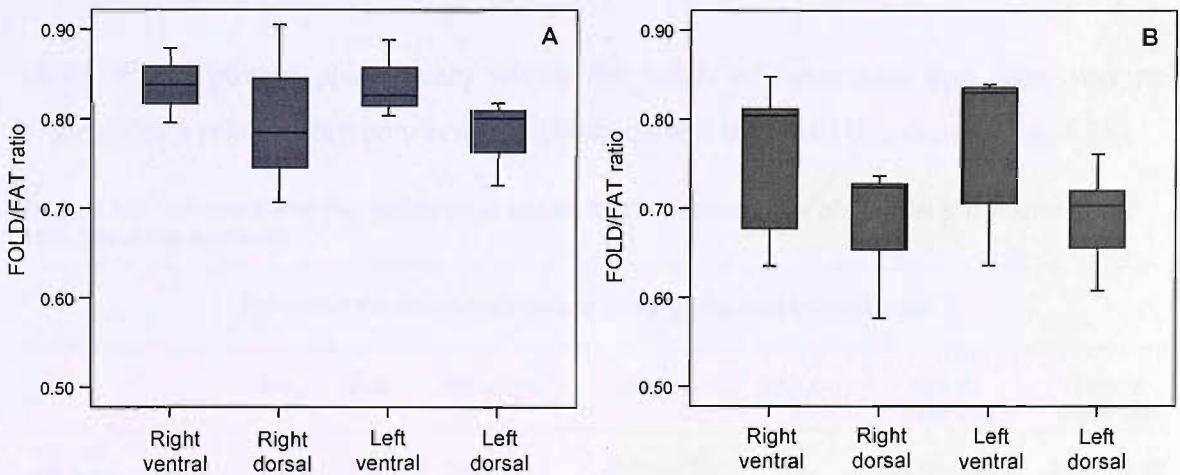
Figure 5.21. Boxplot of standardised FOLD/FAT signal intensity ratio of the ventral and dorsal synovial folds of the right and left lateral atlanto-axial joints of **A.** male (n=3) and **B.** female (n=5) subjects showing the range of values and the median (——).

For all synovial folds there was a negative relationship between age and FOLD/FAT signal intensity ratio (Table 5.13 and Figure 5.22) which was significant for the left ventral synovial fold.

Table 5.13. Correlation between age (years) and standardised FOLD/FAT signal intensity ratio of the synovial folds of the ventral and dorsal synovial folds of the right and left lateral atlanto-axial joints (n=8).

	Right ventral synovial fold	Right dorsal synovial fold	Left ventral synovial fold	Left dorsal synovial fold
Spearman's correlation	-.60 P=.11	-.65 P=.08	-.88 P=.004	-.52 P=.19

Figure 5.22. Scatter diagram of standardised FOLD/FAT signal intensity ratio of the ventral and dorsal synovial folds at the right and left lateral atlanto-axial joints (n=8) plotted against age (years).

5.3.4 Measurement precision

5.3.4i Synovial fold volume

The results of the limits of agreement analysis of 1-month test-retest (n=12), 18-month test-retest (n=12) and inter-examiner (n=12) precision, for the measurement of synovial fold volume are shown in Table 5.14.

100% of the plotted points were within the limits of agreement and there was no evidence of a relationship between the difference and the mean (Figures 5.23 to 5.25).

Table 5.14. Test-retest and inter-examiner precision for the measurement of synovial fold volume (mm^3) from Sequence 5 images.

	Precision for the measurement of synovial fold volume (mm^3)							
	d	$1.96s_d$	SE(d)	95%CI(d)	95%LoA	SE(LoA)	95% CI lower LoA	95% CI upper LoA
1 month test-retest	-0.63	8.39	1.24	-3.35→2.08	-9.02→7.75	2.11	-13.16→-4.88	3.61→11.90
18 month test-retest	-2.53	14.93	2.20	-7.36→2.31	-17.46→12.40	3.76	-24.83→-10.09	5.03→19.78
Inter-examiner	-20.36	48.06	7.08	-35.94→-4.78	-68.44→27.72	12.11	-92.17→-44.70	3.99→51.45

156
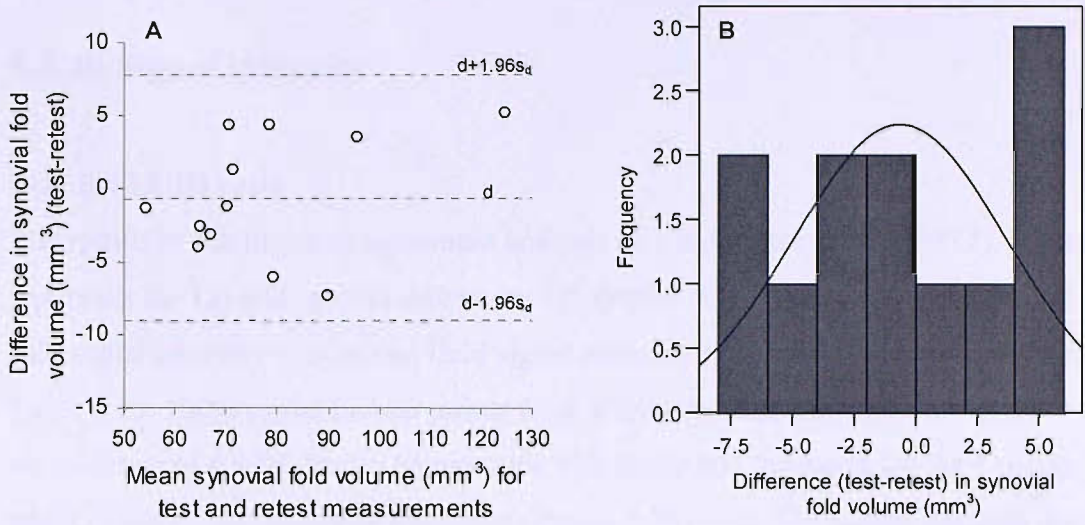
Figure 5.23.A. Difference against mean for repeat measures of synovial fold volume (1-month test-retest precision) (*r* =.38; P=.23). **B.** Histogram of differences for synovial fold volume between test-retest measurements (1-month test-retest precision) (KS test P=.20).
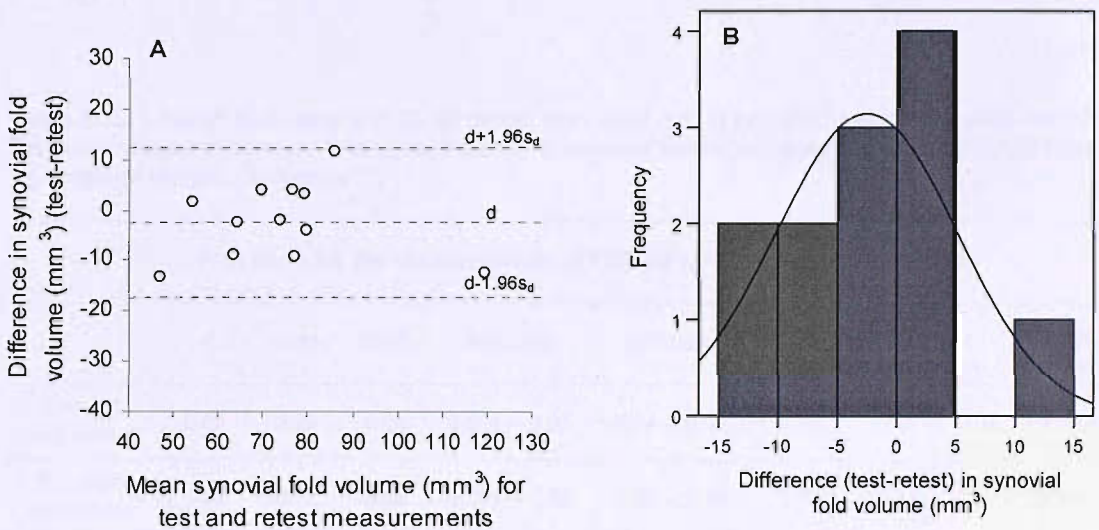
Figure 5.24.A. Difference against mean for repeat measures of synovial fold volume (18-month test-retest precision) (*r*=-.01; P=.97). **B.** Histogram of differences for synovial fold volume between test-retest measurements (18-month test-retest precision) (KS test P=.20).
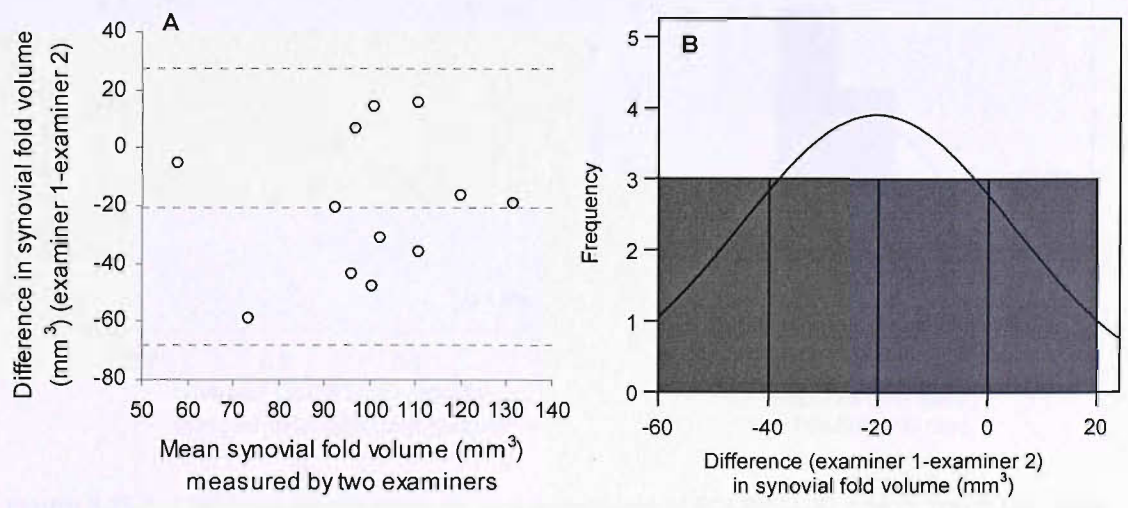
Figure 5.25.A. Difference against mean for inter-examiner measurements of synovial fold volume (inter-examiner precision) (*r*=-.04; P=.23). **B.** Histogram of differences for synovial fold volume between inter-examiner measurements (KS test P=.20).

157

5.3.4ii Signal intensity

FOLD/FLUID ratio

The results of the limits of agreement analysis of 1 month test-retest (n=12), 18 month test-retest (n=12) and inter-examiner (n=12) precision, for the measurement of synovial fold signal intensity to synovial fluid signal intensity (FOLD/FLUID) ratio are shown in Table 5.15. 100% of the plotted points were within the limits of agreement. There was no evidence of a relationship between the difference and the mean for the 1 month test-retest (Figure 5.26) and inter-examiner (Figure 5.28) data. The scatter diagram and Pearson's correlation coefficient of the 18 month test-retest data indicated the presence of proportional bias thus the modified regression approach was performed (Figure 5.27).

Table 5.15. 1 month test-retest (n=12), 18 month test-retest (n=12) and inter-examiner (n=12) precision for the measurement of synovial fold signal intensity to synovial fluid signal intensity (FOLD/FLUID) ratio from T2-weighted images (Sequence 5).

	d	$1.96s_d$	SE(d)	95%CI(d)	95%LoA	SE(LoA)	95% CI lower LoA	95% CI upper LoA
Precision for the measurement of FOLD/FLUID signal intensity ratio								
1 month test-retest	0.03	0.06	0.01	0.004→ 0.05	-0.04→ 0.09	0.02	-0.07→ -0.01	0.06→ 0.13
18 month test-retest	0.03	0.12	0.02	0.004→ 0.05	-0.09→ 0.16	0.02	-0.15→ -0.03	0.10→ 0.22
Inter-examiner	-0.005	0.02	0.002	-0.004→ 0.07	-0.02→ 0.01	0.03	-0.03→ -0.01	0.003→ 0.02
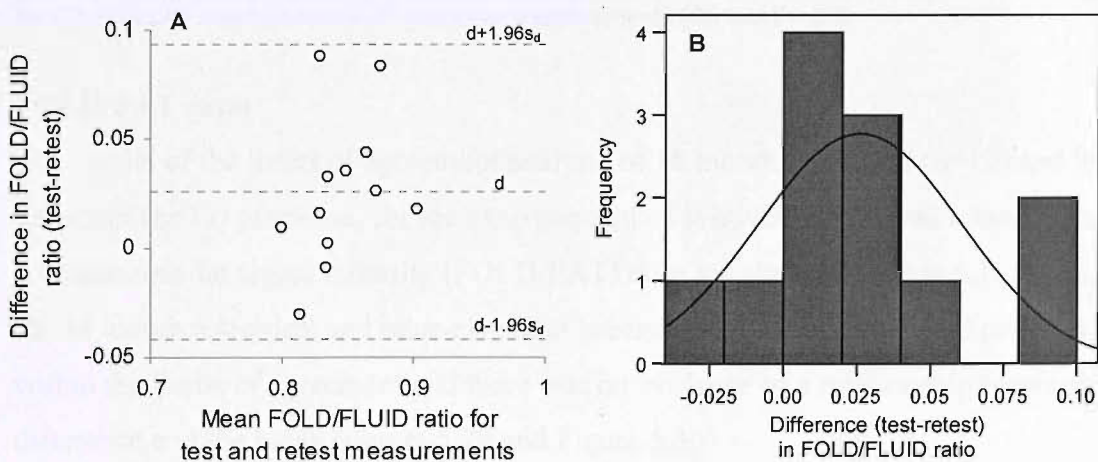
Figure 5.26.A. Difference against mean for repeat measures of FOLD/FLUID ratio (1 month test-retest precision) from T2-weighted Sequence 5 images (r =.36; P=.25). **B.** Histogram of differences for FOLD/FLUID ratio between test-retest measurements (1 month test-retest precision) (KS test P=.20).
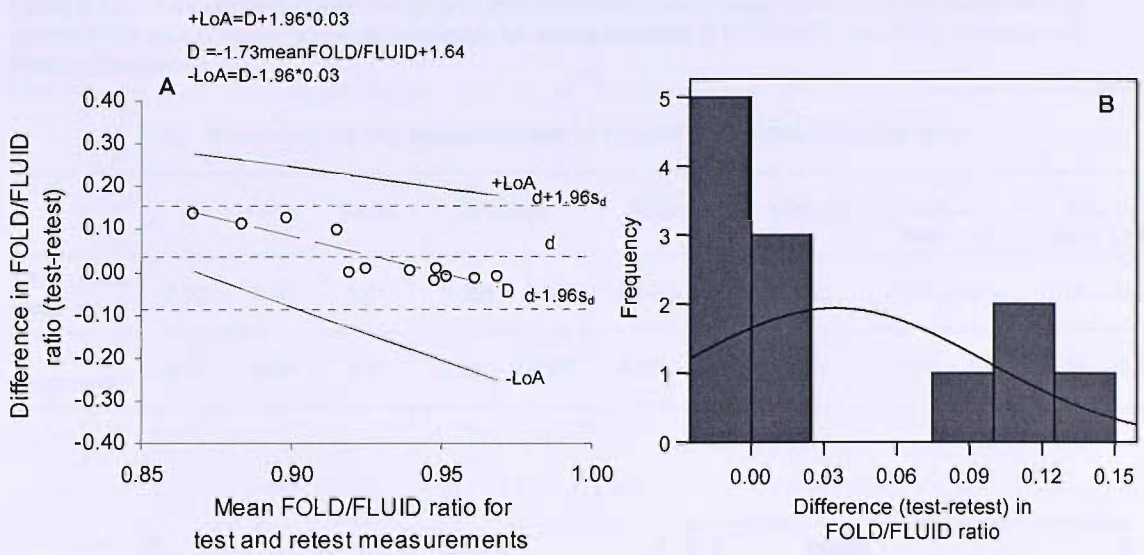
Figure 5.27.A. Difference against mean for repeat measures of FOLD/FLUID ratio (18 month test-retest precision) from T2-weighted Sequence 5 images ($r=-.46$; $P=.13$). **B.** Histogram of differences for FOLD/FLUID ratio between test-retest measurements (18 month test-retest precision) (KS test $P=.19$).
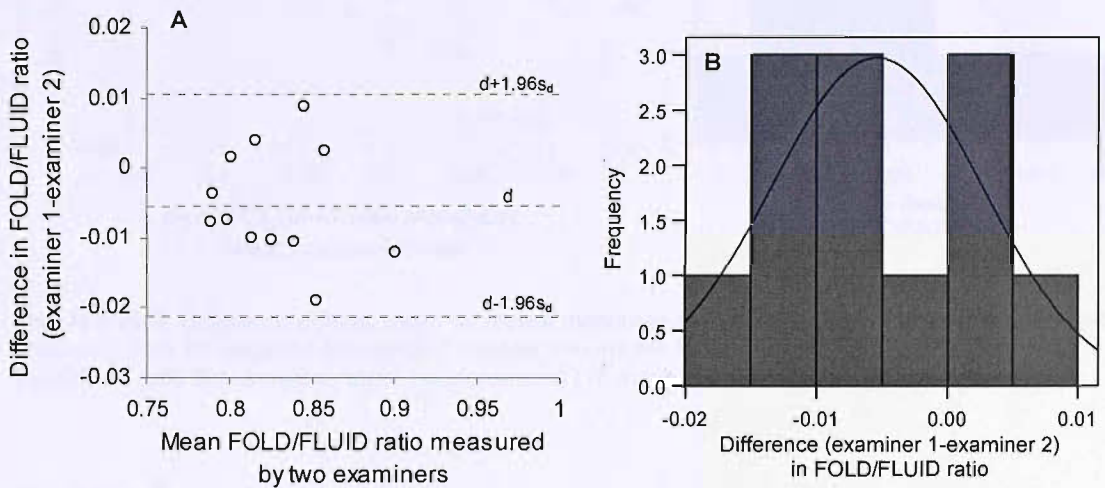
Figure 5.28.A. Difference against mean for inter-examiner measurements of FOLD/FLUID ratio (inter-examiner precision) from T2-weighted Sequence 5 images ($r=-.19$; $P=.55$). **B.** Histogram of differences for FOLD/FLUID ratio between inter-examiner measurements (KS test $P=.20$).

FOLD/FAT ratio

The results of the limits of agreement analysis of 18 month test-retest (n=12) and inter-examiner (n=12) precision, for the measurement of synovial fold signal intensity to subcutaneous fat signal intensity (FOLD/FAT) ratio are shown in Table 5.16. For both the 18 month test-retest and inter-examiner precision, 100% of the plotted points were within the limits of agreement and there was no evidence of a relationship between the difference and the mean (Figure 5.29 and Figure 5.30).

Table 5.16. 18 month test-retest (n=12) and inter-examiner (n=12) precision for the measurement of synovial fold signal intensity to subcutaneous fat signal intensity (FOLD/FAT) ratio from T1-weighted images (Sequence 2).

Precision for the measurement of FOLD/FAT signal intensity ratio								
	d	$1.96s_d$	SE(d)	95%CI(d)	95%LoA	SE(LoA)	95% CI lower LoA	95% CI upper LoA
18 month test-retest	0.02	0.06	0.01	0.001→ 0.04	-0.04→ 0.09	0.02	-0.07→ -0.01	0.06→ 0.12
Inter-examiner	-0.01	0.04	0.01	-0.03→ 0.0005	-0.06→ 0.03	0.01	-0.07→ -0.04	0.05→ 0.01
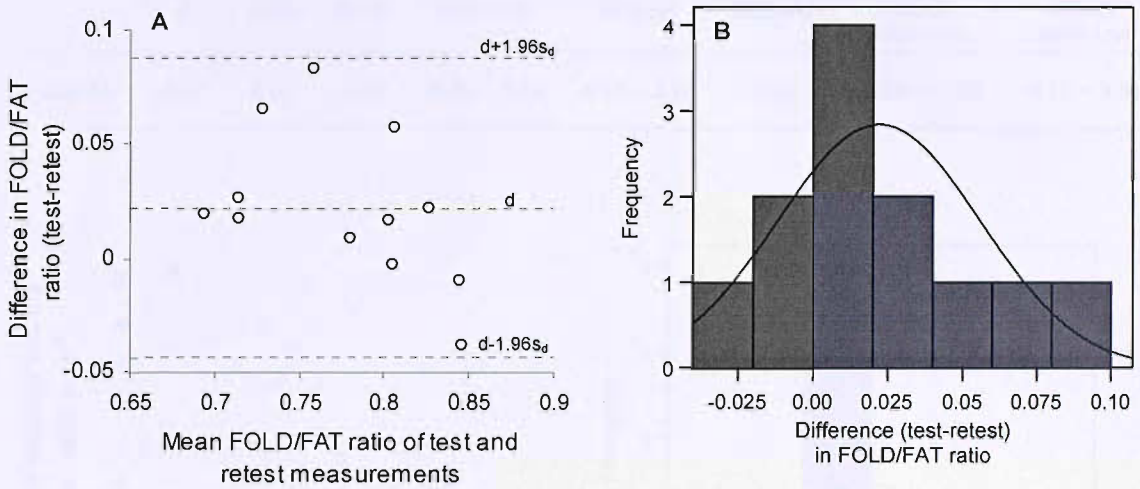
Figure 5.29.A. Difference against mean for repeat measures of FOLD/FAT ratio (18 month test-retest precision) from T1-weighted Sequence 2 images (r =-.46; P=.13). **B.** Histogram of differences for FOLD/FAT ratio between test-retest measurements (18 month test-retest precision) (KS test P=.19).
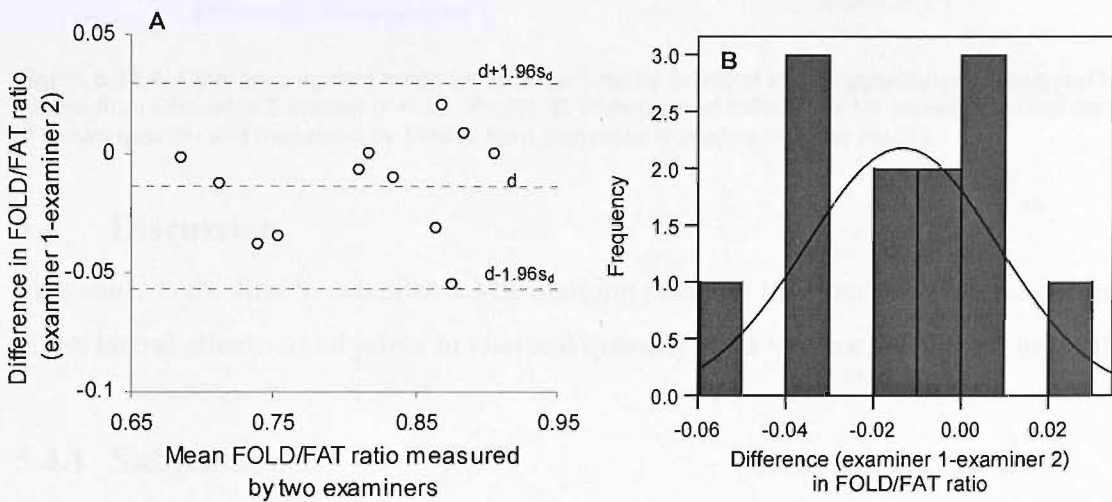
Figure 5.30.A. Difference against mean for inter-examiner measurements of FOLD/FAT ratio (inter-examiner precision) from T1-weighted Sequence 2 images (r = .16; P=.63). **B.** Histogram of differences for FOLD/FAT ratio between inter-examiner measurements (KS test P=.20).

160

5.3.5 Measurement accuracy

The results of the limits of agreement analysis of measurement accuracy (n=6) for the measurement of volume from MR images is shown in Table 5.17. 100% of the plotted points were within the limits of agreement and there was no evidence of a relationship between the difference and the mean (Figures 5.31).

Table 5.17. Measurement accuracy for the determination of volume (mm^3) from Sequence 5 MR images using Mimics.

	Measurement accuracy for the determination of volume (mm^3)							
	d	$1.96s_d$	SE(d)	95%CI(d)	95%LoA	SE(LoA)	95% CI lower LoA	95% CI upper LoA
Accuracy	-2.21	6.57	1.37	-5.26→ 0.84	-8.78→ 4.35	2.34	-13.36→ -4.20	-0.23→ 8.94
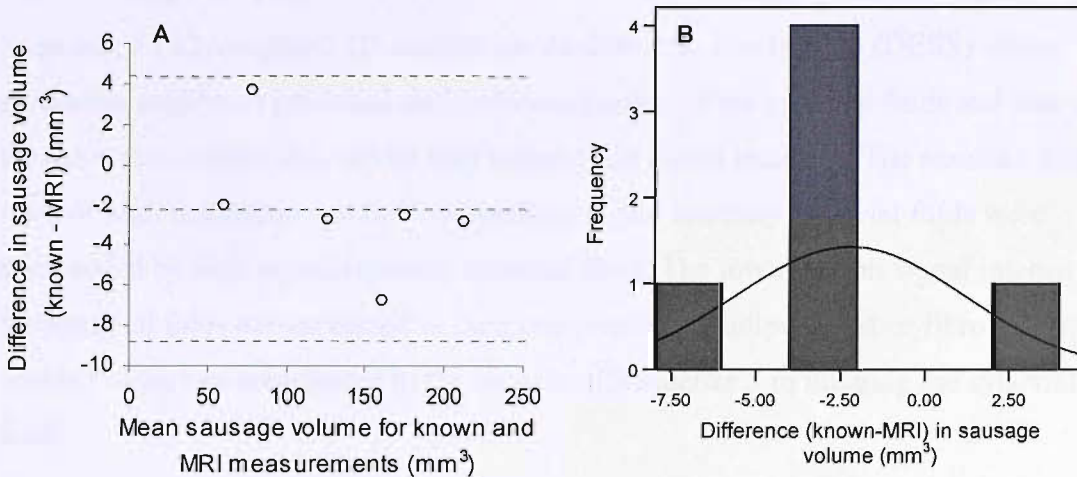
Figure 5.31.A. Difference against mean for sausage volume (mm^3) of known quantity and measured by Mimics from Sequence 5 images (r =-.53, P=.28). B. Histogram of differences for sausage volume (mm^3) of known quantity and measured by Mimics from Sequence 5 images (KS test P=.07).

5.4 Discussion

This study is the first to establish a MR imaging protocol to visualise the synovial folds of the lateral atlanto-axial joints *in vivo* and quantify their volume and signal intensity.

5.4.1 Subjects

The advantage of using an *in vivo* imaging technique was that it enabled the synovial folds of a younger age range to be studied. Previous studies performed on cadavers have been limited to studying subjects predominantly aged greater than 50 years (Yu et al., 1987; Kawabe et al., 1989; Chang et al., 1992; Mercer and Bogduk, 1993; Schonstrom

et al., 1993; Kos et al., 2002; Friedrich et al., 2007). Infant, children and young adult cadavers have been included in some previous studies but typically in small numbers (Yu et al., 1987; Kawabe et al., 1989; Schonstrom et al., 1993; Kos et al., 2002) with the exception of Tang et al. (2007) who studied the synovial folds of 30 embalmed cadavers of children (aged 2 to 11 years). The present study is the first to examine the normal morphology of synovial folds in a sample of adults aged less than 50 years.

The subjects that volunteered for this study were questioned with regard to their suitability for MRI scanning. No inclusion/exclusion criteria regarding current or previous neck pain, trauma or disease were applied in the present study as the primary goal was to develop a protocol for imaging the synovial folds *in vivo* and to establish methods of quantifying their morphometry.

5.4.2 Image acquisition

Sequence 5 (T2-weighted 3D-acquisition double-echo steady-state (DESS) water-excitation sequence) produced optimal visualisation of the synovial folds and was used for the measurement of synovial fold volume and signal intensity. The resultant images were of high resolution and the low-medium signal intensity synovial folds were surrounded by high signal intensity synovial fluid. The low-medium signal intensity of the synovial folds corresponded to their composition of adipose and/or fibrous tissue. A number of factors contributed to the success of Sequence 5 in imaging the synovial folds.

Sequence 5 is well suited to high resolution 3D orthopaedic scanning as it has spatial resolution to submillimetre dimensions (Dufour et al., 1993; McRobbie et al., 2007). It is a specialised dual echo gradient echo sequence unique to Siemens in which the dephase and rephase portions are arranged so that the FISP (fast imaging with steady precession) gradient echo appears ahead of the time-reversed PSIF (an acronym that does not stand for anything but is FISP backwards with respect to spelling and function) echo (McRobbie et al., 2007). In the resultant image, the two echoes are combined to give high resolution images (FISP component) that are strongly T2-weighted (PSIF part) giving strong fluid signals (McRobbie et al., 2007), hence the high signal intensity of the synovial fluid. The voxel size of Sequence 5 measured 0.72mm^3 (0.8x0.6x1.5mm) making it sufficiently sensitive to identify small structures such as the synovial folds. In comparison the larger voxel size of Sequences 2 and 6, 1.65mm^3

(1.10x0.50x3.0mm) and 0.96mm^3 (0.70x0.70x4.0mm), respectively, reduced the resolution of the images.

In the present study, the use of a 3D sequence rather than a 2D multiple slice acquisition had many advantages. Using a 3D acquisition enabled a greater number of thinner contiguous slices to be obtained with a higher resolution than an equivalent 2D acquisition. The T2-weighted Sequence 5 was a 64 slice 3D acquisition with 1.5mm slice thickness and no inter-slice gap and synovial folds were evident on an average of 8 slices per lateral atlanto-axial joint. In comparison, synovial folds were visualised on 3-4 slices per joint using the 2D T1-weighted Sequence 2 (13 slices with 3.0mm slice thickness and 0.3mm inter-slice gap) and 2-3 slices per joint using the 2D proton density-weighted Sequence 6 (15 slices, 4.0mm slice thickness and 0.2mm inter-slice gap). Minimising slice thickness and maximising the number of slices increased the spatial resolution of the resultant image and ensured that as much of each synovial fold as possible was captured on the images. This was especially important for the identification and quantification of the synovial folds which are small structures with a width of approximately 12mm. Minimising slice thickness also lessens the influence of the partial volume effect (see Section 5.4.4) that may otherwise obscure structures that are in close proximity (McRobbie et al., 2007).

In 2D multiple slice imaging, the scanner excites and collects echoes from many slices at the same time. Consequently, gaps (inter-slice gaps) are introduced to separate the slices to prevent the signals of different slices interfering with each other during the acquisition. The inter-slice gap is generally kept to a minimum because tissues in the gap are not imaged at all. If the inter-slice gap is too big there is the possibility of completely missing small structures such as the synovial folds. 3D sequences have no inter-slice gaps (i.e. contiguous slices). In the present study, the use of contiguous slices ensured that the entire synovial fold was imaged and parts were not 'missed' in inter-slice gaps. This was essential for the reconstruction of accurate 3D models and would not have been possible with a 2D acquisition with inter-slice gaps.

Images acquired using a 3D sequence can also be re-formatted on a workstation to produce images in any orientation giving more options for displaying and analysing the images. For example, Sequence 5 was acquired in the sagittal plane but the images could also be viewed in the coronal and axial planes on the workstation and when using

the image analysis software. Furthermore 3D reconstructions of anatomical and pathological structures can be generated through the application of post-acquisition image analysis techniques such as segmentation.

The disadvantages of using 3D imaging sequences are longer acquisition times, and aliasing/phase wrap-around effects (McRobbie et al., 2007). The acquisition time of Sequence 5 was 6 minutes and 32 seconds. This was the longest acquisition time of all of the sequences examined in the present study and was between 30 seconds and 2 minutes longer than the other sequences (Table 5.3). The high resolution, thin contiguous slices and optimal visualisation of the synovial folds afforded by Sequence 5 out-weighed the increased time required for each volunteer to spend in the scanner. The acquisition time of Sequence 5 should not limit its clinical application as the scan time was not much more than that required for routine cervical spine scans in current use.

The phase wrap-around effect is a type of phase sampling artefact where images of the anatomy continue outside of the field of view (FOV) and appear at the opposite edge of the scan in the slice direction (McRobbie et al., 2007). The wrapped-in image has the potential to overlay and interfere with the anatomical structures of interest. In this study, the phase wrap-around effect was an artefact that affected some images but it did not interfere with the visualisation and measurement of the synovial folds.

5.4.3 Comparisons with previous studies

Yu et al. (1987) and more recently Friedrich et al. (2007) successfully imaged the synovial folds of the cervical spine in cadavers using MR imaging. The present study is the first to apply and evaluate MRI techniques *in vivo*. The resolution of the synovial folds achieved in this study (voxel size $0.72mm^3$ [0.8x0.6x1.5mm]) was greatly improved compared to the MRI study undertaken by Yu et al. (1987) (voxel size $3.0mm^3$ [1.0x1.0x3.0mm]). This is likely to reflect continued advancements in MRI technology over the last 20 years, which have resulted in the improved resolution of small anatomic structures.

Friedrich et al. (2007) used a 3.0Tesla (T) scanner whilst in the present study and the study by Yu et al. (1987) the more readily available 1.5T scanner was employed. Most conventional MRI is performed using a magnet with field strength of 1.5T. Magnets with field strengths of 3.0T and higher are increasingly being used in research but are

not widely or commonly used in clinical settings at the present time. The use of a higher magnetic field strength is expected to afford higher spatial resolution and possibly reduced scan times (Frayne et al., 2003; Takahashi et al., 2003). However, 3.0T scanners are associated with substantially higher costs, the need for extended safety boundaries around the magnet, the design and development of new imaging coils, greater acoustic noise, increased power deposition and issues surrounding the safety and compatibility of implanted devices (Frayne et al., 2003; Takahashi et al., 2003). Several magnetic field dependent factors cause the same set of imaging parameters to produce different signal intensities and different image quality at 3.0T compared to 1.5T (Takahashi et al., 2003). Therefore direct comparisons between the images obtained using a 1.5T magnet in the present study and the 3.0T magnet used by Friedrich et al. (2007) are not possible. Suffice to say Friedrich et al. (2007) produced high resolution images of the synovial folds using a 3.0T scanner, however, the acquisition time of 24.3 minutes prevents the *in vivo* application of this sequence at the present time.

Yu et al. (1987) scanned the whole cervical spine and found that a 2D proton density-weighted sequence (TR 2500 ms, TE 20 ms, slice thickness 3mm, acquisition matrix of 256x256, acquisition time 30-42 minutes) produced optimal resolution of the lateral atlanto-axial synovial folds and enlarged cervical zygapopysial synovial folds. Friedrich et al. (2007) imaged just one cervical motion segment (i.e. two articulated cervical vertebrae) and noted that a 2D proton density weighted image sequence (TR 1507.5ms, TE 15.1ms, slice thickness 1.1mm, FOV 5.0x2.5cm, acquisition matrix of 256x192, acquisition time 24.3 minutes) was best for visualisation of the cervical zygapophysial synovial folds. Sequence 5 (T2-weighted 3D DESS water-excitation sequence) utilised in the present study is unique to Siemens and would not have been available for use in the studies of Yu et al. (1987) and Freidrich et al. (2007) as their scanners were manufactured by General Electric (Milwaukee, USA) and Bruker (Ettlingen, Germany), respectively.

The use of a 3D sequence in the present study compared to the 2D sequences of previous studies enabled 3D models of the synovial folds to be generated and their dimensions quantified. Although Friedrich et al. (2007) achieved comparable slice thickness, their field of view was very small and only allowed imaging of one cervical motion segment whilst in the present study thin contiguous slices of the whole cervical spine were possible. In both the present and previous studies (Yu et al., 1987; Friedrich

et al., 2007) the synovial folds were depicted best in the sagittal slice orientation. The acquisition time achieved in the present study was 80-85% less than the acquisition times used to image the whole cadaver cervical spine (Yu et al., 1987) and 75% less than the acquisition time required to image one cadaver cervical motion segment (Friedrich et al., 2007). The short acquisition time utilised in the present study makes it a viable method for continued studies of the synovial folds *in vivo*, in volunteers and patients, for research and clinical purposes. Potential limitations include the expense and relatively limited availability of equipment in the United Kingdom.

Despite the paucity of imaging studies published on the MR appearance of the synovial folds of the vertebral column, the synovial folds (plicae) of the peripheral joints (e.g. knee and elbow) have received greater interest in the radiological literature. The optimal MR imaging sequences and MR appearance of the synovial folds reported in the present study corresponded with previous studies of the peripheral synovial folds. In the knee joint, the synovial folds appear as bands of low signal intensity within the high signal intensity synovial fluid and optimal imaging sequences include gradient echo T2-weighted, fat-suppressed T2-weighted and proton density-weighted sequences (Jee et al., 1998; Kosarek and Helms, 1999; Garcia-Valtuille et al., 2002).

5.4.4 Image analysis

5.4.4i Prevalence and gross morphology

In this *in vivo* study, synovial folds were identified at all lateral atlanto-axial joints imaged using Sequence 5. This is in agreement with previous cadaveric studies that reported 100% prevalence of synovial folds at the lateral atlanto-axial joints (Yu et al., 1987; Mercer and Bogduk, 1993; Schonstrom et al., 1993) and the results of Chapter 4 in this thesis.

The morphology of the synovial folds on sagittal MR images corresponded with their appearance on sagittal sections of cadaver cervical spines reported in Chapter 4 and in previous studies (Yu et al., 1987; Schonstrom et al., 1993). The shape and disposition of the 3D reconstructed models of the synovial folds corresponded with the morphology of the synovial folds in dissected cadavers observed in the present study and described in previous studies (Chang et al., 1992; Mercer and Bogduk, 1993; Kos et al., 2002).

5.4.4ii Quantification of synovial fold morphology

This is the first study to quantify the morphometry of the synovial folds of the lateral atlanto-axial joints using MR scanning *in vivo*, thus comparisons to other studies are not possible. The use of radiological techniques combined with image processing to describe and quantify vertebral column morphology is increasing in research pertaining to abnormalities in patients with neck pain and those interested in developing biomechanical models of the spine. Thus the results of the present study will be compared to imaging studies investigating cervical spine morphology in relation to neck pain and disability.

There is ongoing debate regarding the role of MR imaging in patients with neck pain. In studies of patients with neck pain, of both traumatic and non-traumatic origin, few structural changes have been reported and the images have typically failed to identify potential sources of pain (Ronnen et al., 1996; Karlsborg et al., 1997; Pettersson et al., 1997; Coskun et al., 2003). As the initiation of clinical treatment is not dependant on the outcome of MRI, such imaging is generally regarded as having no role in the routine management of patients with neck pain of mechanical origin. Despite this, research into MR imaging parameters and techniques that may assist in the diagnosis of neck pain has continued unabated. This persistence appears to be paying off as in recent years there have been a number of preliminary observations that have the potential to assist in the diagnosis, treatment and management of patients with neck disorders.

The majority of research to date has centred on the development of MR sequences that enable the ligaments and muscles of the cervical spine to be visualised and their normal morphology assessed (Krakenes et al., 2001; Pfirrmann et al., 2001; Elliott et al., 2005; Elliott et al., 2007). This has subsequently been used as a basis for the identification of abnormal morphology in patients with neck pain. In early studies, the identification of changes in ligament and muscle morphology was based on subjective observations that included the use of a visual grading system of MR images to assess differences in size and signal intensity (McPartland et al., 1997; Andary et al., 1998; Krakenes et al., 2002; 2003). However, the results of published studies have not been consistent, raising doubts over the use of a subjective grading system for the detection of abnormality (Kwan, 2003; Roy et al., 2004; Goradia et al., 2007). A fundamental limitation to the use of a qualitative grading system is its poor test-retest and inter-observer precision (Wilmink and Patijn, 2001; Krakenes et al., 2002; Krakenes et al., 2003; Roy et al.,

2004). Even with the use of experienced observers, estimating the extent of changes in size and signal intensity by simply 'eyeballing' the images does not appear to be sufficiently precise for classification into multiple grades that have impractically fine distinctions between them (Krakenes et al., 2002; Roy et al., 2004). In the present study, an objective system of quantifying synovial fold morphology was developed in order to overcome the limitations of a visual inspection and grading system caused by observer subjectivity.

5.4.5 Measurement precision and accuracy

5.4.5i Precision of synovial fold volume measurements

In the present study, the quantification of synovial fold volume *in vivo* was predominantly affected by random error, a small amount of fixed bias (that was not significant) and no proportional bias. The limits of agreement were wider for 18-month test-retest precision (between 17.46 mm^3 overestimation and 12.40mm^3 underestimation) compared to 1-month test-retest precision (between 9.02mm^3 overestimation and 7.75mm^3 underestimation) as a result of increased random error. The limits of agreement for inter-examiner precision were very wide (between 68.44mm^3 overestimation and 27.72mm^3 underestimation). The limits of agreement for test-retest and inter-examiner precision are summarised in Figure 5.32.
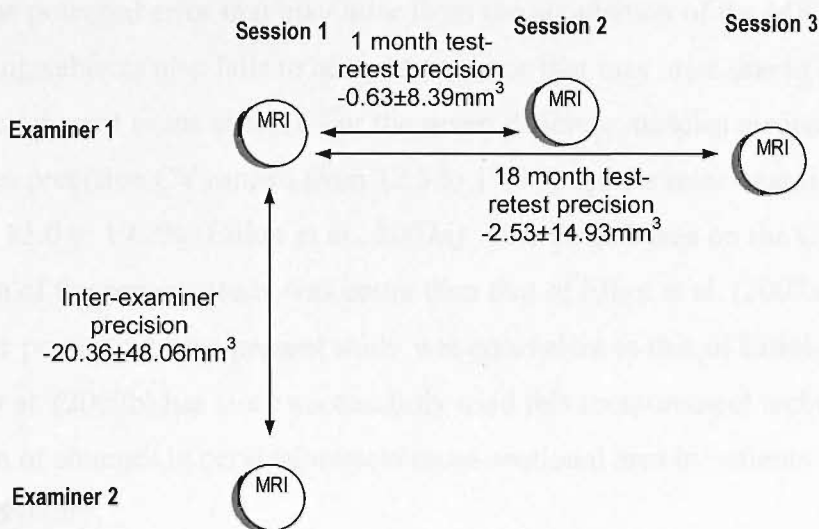
Figure 5.32. Summary of limits of agreement for the precision of synovial fold volume image acquisition and measurement from Sequence 5 images.

Factors that may have contributed to the increased error in the 18-month test-retest precision are inherent biological changes within the subject over the 18 month period between scans, changes inherent to the MR scanner that occur over time and factors that affect the manual segmentation technique, including the partial volume effect, tissue heterogeneity and the fallibility of the examiner performing the measurements (see Section 5.4.5iv). The wide limits of agreement for inter-examiner precision reflect the inexperience of the second examiner in magnetic resonance imaging and quantification techniques. Three synovial folds were over-estimated in excess of $40mm^3$ by the second examiner. All were dorsal synovial folds which were more difficult to differentiate from surrounding structures than the ventral synovial folds.

Previous studies that have assessed the precision of quantifying the cross-sectional area of the cervical musculature (Elliott et al., 2007a) and spinal cord (Tench et al., 2005) and the volume of knee cartilage (Inglis et al., 2007) have reported good to excellent precision. To overcome differences in statistical methods and enable comparison between the present study and previous studies, the precision data collected in the present study was recalculated using the coefficient of variation (CV) (see Appendix 4). For 1-month test-retest precision the CV was 3.77% and for 18-month test-retest and inter-examiner precision, the CV was 7.34% and 22%, respectively.

Elliott et al. (2007a) determined the 1-day test-retest precision for the measurement of cervical muscle cross-sectional area but did not re-scan subjects and so neglected to assess the potential error that may arise from the acquisition of the MR image. Not rescanning subjects also fails to account for error that may arise due to biological variation inherent to the subject. For the seven different muscles measured, the 1-day test-retest precision CV ranged from 12.5 to 17.3% and for inter-examiner precision the CV was 15.0 to 19.2% (Elliott et al., 2007a). Therefore, based on the CV, the test-retest precision of the present study was better than that of Elliot et al. (2007a) and the inter-examiner precision of the present study was equivalent to that of Elliott et al. (2007a). Elliott et al. (2007b) has since successfully used this measurement technique for the detection of changes in cervical muscle cross-sectional area in patients with chronic whiplash injury.

Tench et al. (2005) rescanned subjects for the determination of same-day test-retest precision for the measurement of cervical spinal cord cross-sectional area and calculated

a CV of approximately 1%. For the determination of knee cartilage volume, Inglis et al. (2007) calculated a CV of 1.6 to 3.4% for same-day test-retest precision that included the rescanning of subjects. The greater amount of error reported in the present study compared to Tench et al. (2005) and Inglis et al. (2007) is most likely due to the different time interval between rescans, 1 month and 18 months in the present study compared to same day rescanning in the previous studies. In addition, Tench et al. (2005) used an automated method in contrast to the manual method employed in the present study.

In the present study, the 1-month test-retest precision of the measurement method was adequate for the detection of differences in volume between the right ventral and right dorsal and left ventral and left dorsal synovial folds. The 1-month and 18-month test-retest precision for the MRI method of acquisition and measurement, developed in the present study, was satisfactory for the determination of synovial fold enlargement caused by rheumatoid arthritis (based on the results of Chapter 4). The limits of agreement indicated that the inter-examiner precision was not adequate for the detection of differences in synovial fold volume due to right-left, ventral-dorsal symmetry or rheumatoid change.

5.4.5ii Accuracy of volume measurements

A number of different 'phantom models' were tried and tested in order to devise a model that was suitable for determining the accuracy of the MRI method of volume measurement using Sequence 5. The sausage embedded in gelatine model was found to best simulate the MR appearance of synovial fold surrounded by synovial fluid. Different sizes of sausage phantom model were used in order to approximate the range of synovial fold dimensions in the present study of male and female volunteers aged between 20 and 50 years. The measurement method was affected by random error but not systematic bias. The limits of agreement indicated that the measurement method could at the very worst over-estimate the true volume by $4mm^3$ and under-estimate the true volume by approximately $9mm^3$, which represents approximately 5% over-estimation and 10% under-estimation based upon mean synovial fold volume.

Using plastic cylinders (to simulate the spinal cord) surrounded by water (to represent cerebrospinal fluid) as a phantom model to simulate the measurement of spinal cord cross-sectional area, Tench et al. (2005) calculated a systematic over-estimation of

between 3.15 and 4.6% using an automated segmentation method. Marshall et al. (1995) used a phantom model similar to Tench et al. (2005) to replicate the cartilage of the knee (plastic models of varying volumes) surrounded by synovial fluid (water). Using a manual segmentation method from MR images of 1.5mm thickness, the error for the measurement of knee cartilage volume ranged from 1% to 6% (Marshall et al., 1995).

5.4.5iii Precision of synovial fold signal intensity measurements

Due to acquisition-to-acquisition variations inherent in MR images, the same tissue may have a different signal intensity value even when the same sequence of the same body region of the same patient is imaged in the same scanner (Duncan et al., 1997; Madabhushi et al., 2006a; Witzani et al., 2006). This inhibits direct comparisons between images, studies and subjects/patients (Luoma et al., 1997). To overcome this, signal intensity values are standardised with respect to the signal intensity of a neighbouring tissue, typically one with consistently high signal intensity (Duncan et al., 1997; Luoma et al., 1997; Madabhushi et al., 2006b). The standardisation of signal intensity values has been shown to minimise variations in signal intensity within the same tissue region across different MR images obtained on the same or different scanners (Nyul and Udupa, 1999; Ge et al., 2000).

Fat is frequently used as the tissue of reference in the standardisation of signal intensity values on T1-weighted images (Dooms et al., 1986). On T1-weighted images, fat has a high signal intensity value that is not influenced by factors such as age, gender, obesity and weight loss (Dooms et al., 1986). In the present study, subcutaneous fat was selected for the standardisation of synovial fold signal intensity values from T1-weighted images (Sequence 2). Intermuscular fat was initially selected due to its proximity to the synovial folds but it was not consistently visualised at the midsagittal slice of the lateral atlanto-axial joint. In contrast, subcutaneous fat was visible on all subjects and was present in sufficient quantities to enable the consistent selection of a rectangular-shaped ROI of 35 pixels for each subject. An additional advantage of using adipose tissue for standardisation in the present study was that it could be used to give an estimation of the proportion of adipose tissue content in the synovial folds. Although it is not possible with MRI to determine absolute fat concentration, the signal intensity ratio can provide an indication of the amount of fat in the synovial fold (Elliott et al., 2005).

Like fat, synovial fluid was chosen as the tissue of reference because it consistently demonstrated high signal intensity on T2-weighted images (Sequence 5). Cerebrospinal fluid (CSF) also has inherent MRI properties of high signal intensity on T2-weighted images (Lisanti et al., 2007) and has been used as a signal intensity reference in studies of the lumbar spine (Luoma et al., 1997). Synovial fluid instead of CSF was selected in the present study due to its close proximity to the synovial folds which minimises any effects on signal intensity caused by lack of homogeneity across the image (Duncan et al., 1997).

The precision of the FOLD/FLUID and FOLD/FAT measurements are summarised in Figure 5.33.
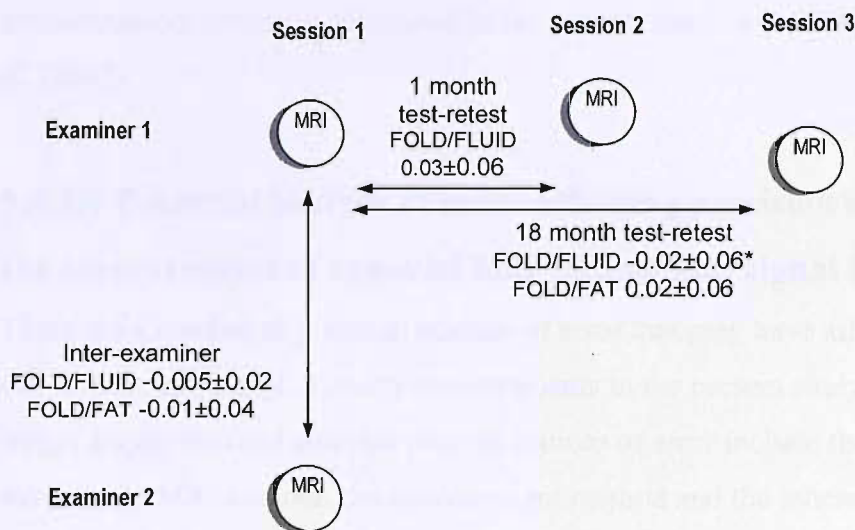
Figure 5.33. Summary of limits of agreement for the precision of signal intensity image acquisition and measurement from Sequence 5 (FOLD/FLUID ratio) and Sequence 2 (FOLD/FAT ratio) images.
* - regressed limits of agreement based on mean FOLD/FLUID ratio.

The test-retest precision of the standardised FOLD/FLUID and FOLD/FAT ratios were affected by small amounts of fixed bias and random error and, with the exception of the FOLD/FLUID 18 month test-retest precision, no proportional bias. The inter-examiner precision was affected by a small amount of random error and no systematic bias. In the present study, the inter-examiner precision but not the test-retest precision of the FOLD/FLUID and FOLD/FAT ratios was sufficient to detect differences in signal intensity between the right ventral and right dorsal and left ventral and left dorsal synovial folds. The difference in measurement error between the test-retest and inter-examiner precision may be primarily due to the biological variation of the subjects

rather than the fallibility of the examiner as subjects were re-scanned for the determination of test-retest precision but not inter-examiner precision.

Elliott et al. (2005) calculated a coefficient of variation (CV) of 0.2 to 0.6% for between day test-retest precision and CV of 7.3 to 10.4% for inter-examiner precision for the measurement of cervical muscle to intermuscular fat signal intensity ratio. Subjects were not re-scanned. Elliott et al. (2006) has since used this method to identify signal intensity changes in the cervical spine musculature of chronic whiplash patients. In the present study the CV of the FOLD/FAT ratio was calculated as 3.4% (18-month test-retest precision) and 2.2% (inter-examiner precision). As previously discussed, the greater measurement error for test-retest precision in the present study is most likely due to re-scanning subjects and the increased time interval between measurements. The inter-examiner precision calculated in the present study was better than that of Elliott et al. (2005).

5.4.5iv Potential sources of error affecting precision and accuracy of the measurement of synovial fold volume and signal intensity

There are a number of potential sources of error that may have affected the precision of the volume and signal intensity measurements in the present study. During the MR image acquisition and analysis process sources of error include the position of the subject, the MRI scanner, the measurement method and the inherent biological variations of the subjects.

When using a 2D sequence it is important to align the subject so that the scan slice is positioned parallel to the structure of interest. This is because any deviation (θ) from the plane of the scan increases the cross-sectional area of measurement by approximately $1/\cos(\theta)$ (Tench et al., 2005). The use of a 3D imaging sequence in the present study removed the need for positioning the synovial folds parallel to the sagittal plane. Thus a standard clinical protocol for positioning each subject in the MR scanner was used to ensure that the method developed was practical for future use in a clinical setting.

To minimise potential sources of error arising from the MRI scanner, the scanner undergoes a regular quality assurance (QA) and maintenance programme. The QA programme involves the measurement of specific image quality parameters using

specially designed test objects and phantoms. The results of the QA analysis during the period of scanning in the present study, revealed that the scanner and process of image acquisition accounted for between $0.15mm^3$ and $0.45mm^3$ of the measurement error for the determination of synovial fold volume. This indicates that the scanner and image acquisition process accounted for some of the measurement error but the majority of the error was from the manual image analysis method and the biological variation of the volunteers.

The measurement method employed in this study utilised segmentation techniques. Segmentation is the process whereby different tissues visible on the MR image can be distinguished by the signal intensity they emit. A grey scale value is assigned to each tissue type on the basis of its emitted signal intensity (Hoad and Martel, 2002; Ranson et al., 2006). In this study, segmentation (or tissue classification) was undertaken manually using the image analysis software Mimics. Limitations that affect both manual and automated segmentation techniques in quantitative MR imaging applications include the partial volume effect and the heterogeneous signal intensities of different tissues (Hoad and Martel, 2002; Meier and Guttmann, 2003; Ranson et al., 2006).

In MR images of the lateral atlanto-axial joints, most of the voxels will exclusively contain synovial fold, bone, cartilage, synovial fluid, fibrous capsule, and synovial membrane. But at the boundaries where the synovial fold lies next to the synovial fluid, cartilage or fibrous capsule, there will be some voxels which contain a mixture of tissues. The signal intensity of the voxels that contain more than one tissue type is the average of the included tissues. This is known as the partial volume effect and introduces errors into the images (Ranson et al., 2006; McRobbie et al., 2007). In the present study, the partial volume effect is likely to have affected both the quantification of synovial fold volume and signal intensity. The partial volume effect cannot be completely avoided but can be minimised by reducing the slice thickness (Krakenes et al., 2001) and the voxel size. Typical voxels measure 1x1x5mm and will contain a mixture of tissues in any given slice (McRobbie et al., 2007). Small voxels measure 0.25x0.25x3.00mm and will typically contain just one tissue (McRobbie et al., 2007). Thus the small voxel size (0.8x0.6x1.5mm) of Sequence 5 minimised the influence of the partial volume effect on the precision and accuracy of the synovial fold volume measurements in the present study. The disadvantage of using a thin slice thickness and small voxel size is the increase in acquisition time and potential reduction in signal-to-

noise ratio. As previously discussed, the 6.32 minute acquisition time of Sequence 5 was not an inconvenience for the volunteers in the present study. However, the acquisition time requires careful consideration in future studies involving patients who may be in pain and discomfort.

The second factor that affects MR segmentation techniques is the heterogeneity of signal intensities of adjacent tissues (Ranson et al., 2006). Although care was taken to exclude surrounding articular structures such as synovial fluid, fibrous capsule, cartilage and bone from the synovial fold ROI, the synovial fold segmentation mask would almost certainly have contained small areas of other tissues including blood vessels and nerves which are known to course through the synovial folds plus elements of the surrounding articular tissues. Like the partial volume effect, signal intensity heterogeneity cannot be completely avoided and is likely to have contributed to the measurement errors affecting the precision and accuracy of synovial fold volume measurements.

Biological effects inherent to human subjects may also have affected the quantification of synovial fold volume and signal intensity. Due to the nature of MR, the signal intensity of the same tissue type can vary between subjects, within subjects, between scan levels and even within the same scan slice, despite the use of identical MR systems and scanning parameters (Ranson et al., 2006). The MR signal intensity of a tissue will also depend upon its vascularity during MRI scanning (Boos and Boesch, 1995; Hoad and Martel, 2002). The synovial folds are thought to be dynamic structures and there are reports in the literature that suggest they undergo changes in size and tissue composition over time and during spinal motion (Mercer and Bogduk, 2001; Schonstrom et al., 1993; Tang et al., 2007). Such time-dependent changes would account for some of the additional random error present in the 18-month test-retest compared to the 1-month test-retest precision.

5.4.6 Synovial fold morphology

5.4.6i Synovial fold volume

Although the primary aim of this study was to determine a method of imaging and quantifying the morphology of the synovial folds of the lateral atlanto-axial joints *in vivo*, a preliminary analysis of the effects of location (ventral/dorsal and right/left),

175

gender and age upon synovial fold volume and signal intensity properties of the synovial folds was undertaken.

In agreement with the findings of the cadaveric study presented in Chapter 4, the right ventral and left ventral synovial folds were typically larger than the right dorsal and left dorsal synovial folds, respectively. Furthermore, the ventral synovial folds of the right and left lateral atlanto-axial joints were larger than the dorsal synovial folds of the right and left lateral atlanto-axial joints both in the present study and in Chapter 4. In contrast, the ventral and dorsal synovial folds of the right lateral atlanto-axial joints were larger than the ventral and dorsal synovial folds of the left lateral atlanto-axial joints in the present study but there was no difference in the cadaveric study reported in Chapter 4.

Male and female synovial folds demonstrated the same general trend – i.e. right ventral larger than right dorsal synovial folds and left ventral larger than left dorsal synovial folds. This same pattern was observed in the cadaver-based study described in Chapter 4. In the present study, female synovial folds were larger than male synovial folds. This is in contrast to the cadaver study in Chapter 4 where female synovial folds were smaller than male synovial folds. The differences due to gender between the MRI and anatomic study may be due to the different age groups studied, the different techniques used and the use of *in vivo* compared to embalmed tissues. Differences due to gender may be accounted for by differences in physical anthropometrics (e.g. height, body mass index, neck circumference) and levels of physical activity (Faber et al., 2001). The influence of physical anthropometrics and physical activity upon the dimensions of the synovial folds will be investigated in Chapter 6.

Females have an increased incidence of neck pain (Makela et al., 1991; Webb et al., 2003; Leroux et al., 2005; Poussa et al., 2005) and whiplash injury (Radanov et al., 1995; Cassidy et al., 2000) compared to males despite males being involved in a greater number of motor vehicle collisions (Cassidy et al., 2000; Temming and Zobel, 2000; Sapir and Gorup, 2001). Reasons for this disparity are not well understood, however, gender-based differences in the geometry and morphologic characteristics of the cervical spine are suggested factors (Vasavada et al., 2007).

The spinal structures of males are typically greater in size than those of females. The

vertebrae, hyaline articular cartilage, musculature and spinal cord of the cervical spine have all been documented to be significantly larger in males compared to females (Schaffler, 1992; Wescott, 2000; Yoganandan et al., 2003; Rankin et al., 2005; Takeuchi et al., 2005; Cassinelli et al., 2006; Yanase et al., 2006; Kjaer et al., 2007). The biomechanical properties of the cervical articulations have also been shown to be different between genders. The male upper cervical spine has been shown to be significantly stiffer and stronger than the female and following the application of whiplash-type forces, female cervical articulations have been shown to undergo significantly greater shear and distraction motions compared to male cervical spines thus supporting the higher incidence of whiplash-related complaints in females compared to males following motor vehicle impact (Pintar et al., 1998; Stemper et al., 2003; Stemper et al., 2004; Nightingale et al., 2007).

Female necks are weaker than male necks (Nightingale et al., 2007; Vasavada et al., 2007) and respond differently in response to the application of whiplash-type forces. When subject to whiplash-type forces, females experience greater and earlier horizontal head and cervico-thoracic spine accelerations compared to males (Siegmund et al., 1997; van den Kroonenberg et al., 1998) and the female cervical articulations undergo significantly greater shear and distraction motions compared to males (Pintar et al., 1998; Stemper et al., 2003; Stemper et al., 2004;). It has been hypothesised that these observed differences between male and female subjects could be explained by the smaller, less resisting necks of female occupants (van den Kroonenberg et al., 1998).

5.4.6ii Synovial fold signal intensity

Both the FOLD/FLUID and FOLD/FAT signal intensity ratios indicated that the signal intensity of the synovial folds varies between the ventral and dorsal synovial folds of the left and right lateral atlanto-axial joints. The FOLD/FLUID and FOLD/FAT signal intensity ratios of the right and left ventral synovial folds were significantly different to the right and left dorsal synovial folds, respectively. There was no significant difference in FOLD/FLUID and FOLD/FAT ratio between right ventral and left ventral and right dorsal and left dorsal synovial folds. The data collected in the present study provides preliminary normative data regarding the standardised signal intensity values of the synovial folds. The normal variations in synovial fold signal intensity documented in the present study need to be taken into account when comparing symptomatic and asymptomatic subjects and assessing changes in signal intensity.

On T1-weighted images such as Sequence 2, adipose tissue has higher signal intensity than fibrous tissue therefore the closer the FOLD/FAT ratio is to 1, the higher the adipose composition of the synovial fold. In the present study, the FOLD/FAT ratio indicated that the right and left ventral synovial folds are composed of more adipose tissue than the right and left dorsal synovial folds. This corresponded to the findings of Inami et al. (2001) who noted a greater number of fibrous synovial folds at the dorsal compared to the ventral aspect of the cervical zygapophysial joints. When the FOLD/FAT ratio of the synovial folds was compared between males and females, the same trend was evident i.e. the FOLD/FAT ratio was higher for right and left ventral synovial folds compared to right and left dorsal synovial folds.

The FOLD/FAT ratio of male synovial folds was higher compared to female synovial folds. This suggests that male synovial folds contain a higher proportion of adipose tissue compared to female synovial folds. Histological differences in the synovial folds as a result of gender have not previously been explored in cadaver studies of either the spinal or peripheral articulations. Synovial folds composed of predominantly adipose tissue have been observed to move more freely compared to synovial folds composed mainly of fibrous tissue (Schonstrom et al., 1993). Therefore adipose synovial folds may be more likely to escape compression between the articular surfaces when subjected to whiplash loading compared to fibrous synovial folds. This may be a factor that contributes to the lower incidence of whiplash injuries in males compared to females.

There was a relationship between subject age and FOLD/FAT ratio. The FOLD/FAT ratio decreased with increasing age which implies that the adipose content of the synovial folds decreases with increasing age. This result is supported by the cadaveric studies of Schonstrom et al. (1993) and Tang et al. (2007) who noted that the synovial folds of older subjects contained less adipose tissue than the synovial folds of younger subjects. The moderate to high negative correlation between FOLD/FAT ratio and subject age was evident for all synovial folds in the present study but only reached significance for the left ventral synovial fold.

5.5   Conclusion

MR imaging is a useful non-invasive imaging modality for the visualisation and evaluation of the synovial folds of the lateral atlanto-axial joints. The ability to visualise and precisely quantify the morphology of the synovial folds of the lateral atlanto-axial joints using MRI makes is possible, for the first time, to assess the normal structure and function of the synovial folds *in vivo*. The use of radiological techniques combined with image processing software to measure the dimensions of spinal structures is becoming increasingly prevalent in research pertaining to spinal abnormalities in patients with neck pain, disability or disease and is of interest to those involved in developing biomechanical models of the neck. Thus the method presented in this chapter has a variety of practical applications in areas such as diagnostic imaging and biomechanical modelling and may serve as an outcome measure in the treatment and rehabilitation of neck pain. Prior to utilising the MR imaging technique, developed in the present study, in patient groups the normal structure and function of the synovial folds needs to be ascertained. Thus the magnetic resonance image acquisition and method for quantifying the dimensions of the synovial folds *in vivo* will be used in the next study to determine the normal structure and function of the synovial folds as a basis for determining the clinical significance of the synovial folds in patient groups affected by neck pain and disability.

Chapter 6

Magnetic resonance imaging study of volume of the intra-articular synovial folds of the lateral atlanto-axial joints in an asymptomatic cohort

6.1 Introduction

Historically, data pertaining to the morphology and geometry of spinal structures has been derived from osseous collections and cadavers. Whilst providing valuable information for clinical use and the development of biomechanical models, the use of osseous and cadaveric material has some limitations. Information regarding factors that may affect normal morphometry (e.g. handedness, occupation, level of physical activity, physical anthropometrics) are typically not available and the age range is frequently limited to older individuals. The effect that cadaveric preservation has upon the normal morphometry is often not known or impossible to quantify.

The advent of new technologies utilising non-invasive imaging methods such as magnetic resonance imaging (MRI) and ultrasound has enabled the spinal structures to be quantified *in vivo* in both asymptomatic and symptomatic populations (Kristjansson, 2004; Elliott et al., 2007a; 2007b; Rankin et al., 2005; Fernandez-de-las-Penas et al., 2007). This has resulted in renewed interest in the comprehensive and detailed analysis of variations in the morphology of the spine to determine 'normal' values that could form the basis for the diagnosis and management of spinal disorders. As this is a recent development, there are few studies available for comparison.

Normative data have been established for cross-sectional area (Elliott et al., 2007a) of the muscles of the posterior cervical spine in adult females. The normal morphology of

the spinal synovial folds *in vivo* is currently not known and normative values for the dimensions of the synovial folds are yet to be established.

The purpose of this study was to establish the normal morphology of the synovial folds of the lateral atlanto-axial joints *in vivo* using MRI in a group of asymptomatic female subjects aged 20-40 years and to gain preliminary normative data. This gender and age range was chosen in this first instance as a basis for a future study of whiplash associated disorder (WAD) and rheumatoid arthritis. Females within this age range tend to have a higher prevalence of symptoms following a whiplash injury (Larsen and Holm, 2000) and a higher incidence of rheumatoid arthritis (Symmons et al., 1994; Kvien et al., 2006). This study will investigate how synovial fold volume varies normally as a factor of age, body size, levels of physical activity, dimensions of the head and neck and cervical range of motion in persons with no history of a neck complaint. Such knowledge is essential to be able to recognise and interpret synovial fold abnormalities in patients with neck pain and disorders of the cervical spine.

The aims of the present study were to determine whether the volume of the synovial folds varies in relation to:

1. age
2. height, body mass and body mass index
3. the dimensions of the head and neck
4. cervical range of motion
5. levels of physical activity
6. visual impairment

6.2   Methods

6.2.1 Subjects

Ten healthy volunteers with no neck pain were recruited from the Departments of Radiology and Medical Physics and Engineering. All subjects were females within the age range of 20 to 40 years. Subjects were excluded if they had a previous history of neck pain, injury or trauma (e.g. motor vehicle accident), history of spinal surgery or spinal anomalies, had been previously diagnosed with a connective tissue disorder (e.g Ehlers-Dahlos), a neurologic disorder (e.g. multiple sclerosis), inflammatory conditions (e.g. rheumatoid arthritis), were pregnant or breast-feeding or did not meet the

inclusion/exclusion criteria to have an MRI scan. In relation to the measurement of the physical characteristics of the cervical spine, volunteers were excluded if they had known contraindications to performing active cervical range of motion in all planes of movement (e.g. dizziness, light-headedness, vertigo). Approval for the study was obtained from the Local Research Ethics Committee. All subjects provided written informed consent prior to inclusion in the study.

6.2.2 Image acquisition and analysis

MRI of the cervical spine was performed with a 1.5-Tesla scanner (Siemens MAGNETOM Symphony, Siemens AG Medical Solutions, Erlangen Germany) (Figure 5.1.A, Chapter 5). Each volunteer was positioned supine on the scanner table and their external auditory meatus was used as a landmark to align their head and neck with respect to the table. The subject's head and neck were placed in a comfortable neutral position. Circularly polarised head and neck array coils (Siemens AG Medical Solutions, Erlangen, Germany) were fitted to each subject to obtain optimal resolution of the upper cervical spine (Figure 5.1.B, Chapter 5).

With the aid of a T1-weighted sagittal locator image, the cervical spine of each volunteer was scanned using Sequence 5, a T2-weighted 3D-acquisition double-echo steady-state (DESS) water-excitation sequence in the sagittal plane (6.63ms TE, 23.68ms TR, 64 slices, 1.50mm slice thickness, no inter-slice gap, 256x192 acquisition matrix, 150mm field of view, 25 degree flip angle, 6 minutes 32 seconds acquisition time). All scans were anonymised and stored as DICOM format files on computer and CD-ROM.

The MR images of each volunteer were visualised and examined using OSIRIS (Version 4.18, University Hospital of Geneva, Geneva, Switzerland) to determine the prevalence of the intra-articular synovial folds at the lateral atlanto-axial joints in this subject sample.

The volume of each synovial fold was determined using Materialise's Interactive Medical Image Control System (Mimics) version 8.11 (Materialise NV, Leuven, Belgium). The volume of each synovial fold was quantified using the manual segmentation technique described in Chapter 5 (Section 5.2.3.ii).

6.2.3 Data collection

6.2.3i Demographic data

On the day of the MRI scan, subjects completed a questionnaire that included details of age, occupation, handedness, visual impairment and regular sports and recreational activities. A checklist of exclusion criteria for the study and contraindications to MRI scanning was completed. Handedness, levels of physical activity and visual impairment were based on subjects' self-report. On the basis of self-reported levels of physical activity, subjects were classified as being physically active (performed regular physical activity) or not physically active (undertook no physical activity).

6.2.3ii Physical anthropometrics

Within a week of the MRI scan, the height, body mass and dimensions of the head and neck were measured on each subject as follows:

Height, body mass and body mass index (BMI)

Standing height was measured in centimetres using a stadiometer (Model 424, Weylux, England; accurate to 1cm) that consisted of a vertical ruler attached to a stable base with a sliding horizontal arm attached to the vertical ruler. Each subject stood barefoot against the stadiometer and was asked to stand "as tall as possible" with their head vertically aligned with the stadiometer and their eyes focused on a point on the wall level with the "straight ahead gaze". Three measurements were made in succession, with the subject moving away from the stadiometer between readings, and the average reading calculated.

Body mass was measured in kilograms with subjects standing barefoot on a beam balance scale (Model 424, Weylux, England; accurate to 50g). Three successive measurements were made, with the subject standing off the beam balance in between measurements, and the average body mass value calculated for each subject.

Body mass index (BMI = weight (kg)/height squared (m^2)) was calculated from the average height and body mass measures. Based on BMI measurements, each subject was classified as normal weight ($\leq$24.99 kg/m^2) or overweight ($\geq$25.00 kg/m^2) (World Health Organization, 2007).

Dimensions of the head and neck

The dimensions of the head and neck were measured with the subject seated and sitting straight with hips, knees and ankles at right angles and arms by their sides. Subjects were instructed to look straight ahead and focus their eyes on a point on a wall chart level with their "straight ahead gaze". A flexible non-stretch tape measure was used to measure the following physical dimensions of the head and neck:

a. Anterior neck length was measured from the gnathion (tip of the chin) to the suprasternal notch. The tape measure was placed on the skin to conform to the contours of the neck.

b. Posterior neck length was measured from the inion (prominence of the external occipital protuberance) to the tip of the 7th cervical spinous process. The tape measure was placed on the skin to conform to the contours of the neck.

c. Cranial circumference was measured from the median point on the glabella horizontally around the cranium to the most prominent point on the back of the cranium.

d. Neck circumference was measured around the cervical column at the level of the 5th cervical spinous process and just below the cricoid cartilage. The tape measure was held firmly against the skin, while allowing the subject to swallow comfortably.

Each bony landmark described above was carefully palpated and demarcated using a skin pencil. All measurements were repeated three times and an average value for each dimension calculated.

6.2.3iii Cervical range of motion (ROM)

The cervical range of motion of each subject was measured within a week of the MRI scan, at the same time as the collection of the physical anthropometric data. The cervical range of motion (CROM) instrument (Performance Attainment Associates, St. Paul, USA) was used to determine the active cervical range of motion of each subject in all planes using the manufacturer's protocol (University of Minnesota, 1988). The CROM instrument is a goniometer that consists of a plastic headpiece and a magnetic neck brace. The plastic frame is placed over the subject's nose and ears and secured by fastening a velcro strap at the back of the subject's head. There are three dials located on the plastic frame in order to measure cervical range of motion. The dials for flexion/extension and lateral flexion are gravity goniometers which respond to gravity, whilst the dial for left and right rotation is a compass goniometer which responds to the magnetic neck brace placed over the subject's shoulder.

Cervical flexion-extension, lateral flexion and rotation were measured with the subject sitting straight, with hips, knees and ankles at right angles and arms resting freely on their thighs. Suboccipital flexion and extension was measured with the subject erect and standing straight against a door frame with the sacrum, thoracic spine and occiput in contact with the door frame and their arms resting freely at their sides. All planes of motion were measured as follows. Each subject was instructed on how to perform each movement and three practise movements in each plane were performed prior to data collection. Participants were instructed to move the head and neck only in order to avoid any compensatory movements in the shoulder girdle and thoracic region and this was visually checked by the examiner. In both seated and standing positions, subjects were instructed to look straight ahead and focus their eyes on a point on a wall chart level with their "straight ahead gaze" and this was recorded as the subject's starting/neutral position. From the neutral position, the ROM in each plane was measured and manually recorded by reading from the relevant dials on the CROM instrument. Each ROM test consisted of flexion-extension, lateral flexion and rotation which were recorded as total ROM (i.e. flexion-extension, lateral flexion, rotation) and half-cycle ROM, meaning motion in a single direction (i.e. flexion or extension, right or left lateral flexion, right or left rotation) from the neutral position. Three repeat measurements were taken for each movement in each plane and the data was entered into a spreadsheet (Excel, Microsoft Corporation, Redmond, WA, USA). The average total and half-cycle ranges of motion were calculated from the three repeat movements.

6.2.4 Statistical analysis

Synovial fold volume data was presented as means and standard deviations and boxplots were used to display the medians and ranges. Age, physical anthropometrics and range of motion data were presented as means with standard deviations and medians with ranges. The data was explored and examined for normality using histograms with Normal curves, quantile-quantile plots and the Kolmogorov-Smirnov (KS) test.

The sample sizes were small and not all data demonstrated a Normal distribution thus the data was analysed using non-parametric statistics. Friedman's ANOVA was used to determine whether there was a difference in volume between the right ventral, right dorsal, left ventral and left dorsal synovial folds. If there was a significant difference, Wilcoxon's signed-rank test was used for *post hoc* analysis with *Bonferroni correction.*

Wilcoxon's signed-rank test with *Bonferroni correction* was used to determine whether there was a difference in volume between the right and left ventral and right and left dorsal synovial folds; and between the ventral and dorsal synovial folds of the left and the ventral and dorsal synovial folds of the right lateral atlanto-axial joints. Spearman's correlation coefficient (r_s) was used to determine the relationship between synovial fold volume and subject age, physical anthropometrics and cervical range of motion.

Statistical analysis was performed using SPSS version 14.0 for Windows (SPSS Inc., Chicago, Illinois, USA) and Microsoft Excel 2000 (Microsoft Corporation, Redmond, WA, USA). A probability level of P=.05 was set as the minimum criterion of statistical significance for all tests.

6.3   Results

6.3.1 Subjects

The ten female subjects ranged in age from 24 to 38 years (mean 29.2 years, SD 4.69 years). The subjects included four radiographers, three radiographic assistants, two medical physicists and one biomedical engineer. All subjects were right-handed including one subject who was ambidextrous. Four subjects wore glasses and/or contact lenses to correct visual impairments. Five subjects were classified as physically active and five subjects as not physically active.

6.3.2 Synovial fold volume

All ten volunteers were scanned using Sequence 5 and provided data on 20 lateral atlanto-axial joints. Intra-articular synovial folds were identified in all of the lateral atlanto-axial joints imaged using Sequence 5, located at both the ventral and dorsal poles of the right and left joints. 40 synovial fold 3D models were reconstructed from the resulting MR images of the ventral and dorsal synovial folds of each joint. The volume of the individual 3D synovial fold models ranged from a minimum value of 23.85mm^3 to a maximum value of 152.27mm^3 and the median was 66.70 mm^3 (mean 76.20mm^3, standard deviation 30.28m^3).

The volume of the ventral and dorsal synovial folds of the right and left lateral atlanto-axial joints are presented in Table 6.1 and Figure 6.1. The volume of the synovial folds

was significantly different ($\chi^2(3)=8.76$, P=.03) between subjects (n=10). Wilcoxon's signed-rank tests were used to follow up this finding. A *Bonferroni correction* was applied and so all effects are reported at a .0125 level of significance. The synovial fold volume of the right ventral and left ventral synovial folds was greater than the right dorsal and left dorsal synovial folds, respectively, but the differences were not significant (Z=-2.09, P=.037 and Z=-1.58, P=.13, respectively). Right ventral synovial fold volume was larger than left ventral synovial fold volume but the difference was not significant (Z=-1.89, P=.06). Right dorsal synovial fold volume was greater than left dorsal synovial fold volume but the difference did not quite reach significance (Z=-2.40, P=.014).

Table 6.1. The volume (mm^3) of the synovial folds at the lateral atlanto-axial joints of the 10 female subjects.

Subjects	Age	Glasses/ contacts*	Phys. active**	Synovial fold volume (mm^3)			
				Right ventral synovial fold	Right dorsal synovial fold	Left ventral synovial fold	Left dorsal synovial fold
Volunteer 11	26	Yes	Yes	126.15	80.35	78.02	65.71
Volunteer 12	29	No	No	57.94	61.07	60.30	60.80
Volunteer 13	25	Yes	Yes	145.41	107.79	83.1	87.13
Volunteer 14	26	No	Yes	66.35	85.94	67.05	87.88
Volunteer 16	32	Yes	No	127.46	80.77	76.25	53.83
Volunteer 17	31	No	No	50.81	49.97	34.90	23.85
Volunteer 18	24	Yes	Yes	92.01	65.93	91.83	38.74
Volunteer 19	35	No	No	64.35	57.57	49.57	56.44
Volunteer 20	38	No	Yes	139.18	98.42	152.27	97.51
Volunteer 21	26	No	No	73.54	60.05	60.09	31.79
Mean	**29.20**	**4 Yes**	**5 Yes**	**94.32**	**74.79**	**75.34**	**60.37**
(SD)	**(4.69)**	**6 No**	**5 No**	**(36.62)**	**(18.96)**	**(31.77)**	**(24.85)**

* wears glasses and/or contact lenses as a result of visual impairment; **physically active
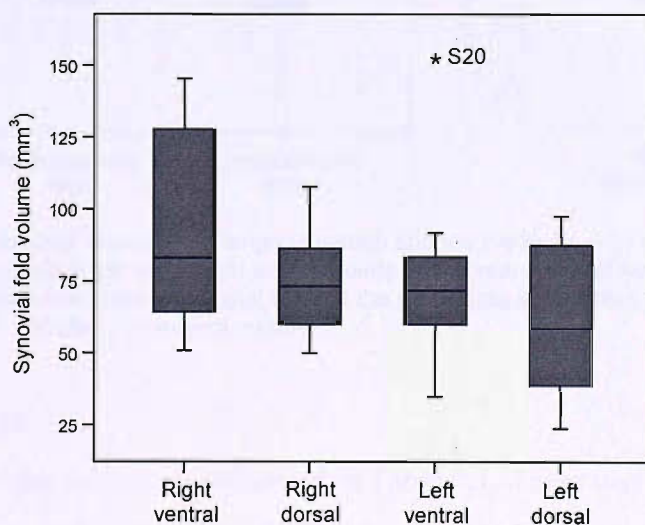
Figure 6.1. Boxplot of ventral and dorsal synovial fold volume (mm^3) at the right and left lateral atlanto-axial joints of 10 female subjects showing the range of values and the median (——). *=extreme outlier S=subject number.

Additional analysis was undertaken to compare the volume of the ventral synovial folds of the right and left lateral atlanto-axial joints and the volume of the dorsal synovial folds of the right and left lateral atlanto-axial joints (Table 6.2 and Figure 6.2). The volume of the ventral and dorsal synovial folds of the right joints were compared to the ventral and dorsal synovial folds of the left joints (Table 6.2 and Figure 6.2). Wilcoxon's signed-rank test was used and a *Bonferroni correction* applied, so all effects are reported at a .025 level of significance. Left and right ventral synovial fold volume was significantly greater than left and right dorsal synovial fold volume ($Z=-2.61$, $P=.007$) and the ventral and dorsal synovial folds of the right lateral atlanto-axial joints were significantly larger than the ventral and dorsal synovial folds of the left lateral atlanto-axial joints ($Z=-3.02$, $P=.001$).

Table 6.2. Ventral and dorsal and right and left synovial fold volume (mm^3) at 20 lateral atlanto-axial joints.

Synovial fold volume (mm^3)	Ventral synovial folds	Dorsal synovial folds	Right synovial folds	Left synovial folds
Mean	84.83	67.58	84.55	67.85
SD	34.76	22.75	30.10	28.80
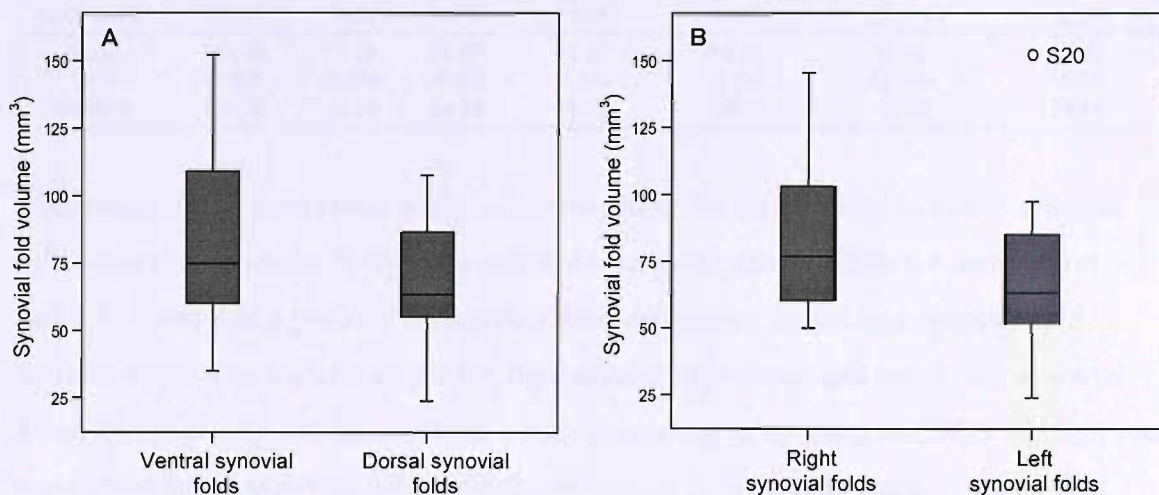
Figure 6.2. Boxplot showing the range of values and the median (———) for the volume (mm^3) of the **A.** ventral synovial folds of the right and left joints and dorsal synovial folds of the right and left joints (n=20) **B.** ventral and dorsal synovial folds of the right joints and ventral and dorsal synovial folds of the left joints (n=20). o=outlier; S=subject number.

6.3.3 Age

The age of the subjects is presented in Table 6.1. There was a negative correlation between age and the volume of the right ventral, right dorsal and left ventral synovial folds (Table 6.4, Figure 6.3). The volume of the left dorsal synovial folds was positively correlated to age (Table 6.4, Figure 6.3).

6.3.4 Height, body mass and body mass index

The height, body mass and body mass index (BMI) of the subjects are presented in Table 6.3. On the basis of BMI score, five subjects were allocated to the normal weight group (BMI $\leq$24.99 kg/m^2) and five subjects to the overweight group (BMI $\geq$25.00 kg/m^2). The five subjects who were physically active and the five subjects who were not physically active were the same subjects classified as normal weight and overweight, respectively (Table 6.5).

Table 6.3. Physical anthropometrics of the 10 female subjects.

	Physical anthropometrics						
Subjects	Height (cm)	Body mass (kg)	Body mass index	Anterior neck length (cm)	Posterior neck length (cm)	Neck circumference (cm)	Head circumference (cm)
Volunteer 11	165.90	59.18	21.50	16.50	14.23	31.70	55.60
Volunteer 12	167.67	71.25	25.34	16.50	13.53	32.90	58.60
Volunteer 13	172.00	62.87	21.25	16.77	16.03	32.03	54.07
Volunteer 14	170.00	58.97	20.40	18.73	19.17	30.43	54.67
Volunteer 16	156.75	78.03	31.76	14.00	10.67	35.73	55.37
Volunteer 17	162.67	91.89	34.73	13.63	12.93	38.60	58.03
Volunteer 18	170.00	67.04	23.20	16.77	12.67	31.67	55.77
Volunteer 19	162.00	75.41	28.73	16.13	14.87	32.77	55.93
Volunteer 20	170.75	70.45	24.16	15.73	15.53	32.63	55.87
Volunteer 21	159.85	75.59	29.58	14.97	13.80	32.73	55.10
Mean	**165.76**	**71.07**	**26.07**	**15.97**	**14.34**	**33.12**	**55.90**
(SD)	**(5.20)**	**(5.20)**	**(4.89)**	**(1.49)**	**(2.29)**	**(2.36)**	**(4.89)**
Median	**166.78**	**70.85**	**24.75**	**16.32**	**14.02**	**32.68**	**55.68**

The results of the correlation analysis investigating the relationship between synovial fold volume and height, body mass and BMI are presented in Table 6.4 and Figures 6.3 and 6.4. There was a positive correlation between subject height and synovial fold volume which was significant for the right dorsal, left ventral and left dorsal synovial folds. Synovial fold volume decreased with increasing body mass and BMI and this was significant for all synovial folds with the exception of the right ventral synovial fold.

Table 6.4. Correlation between ventral and dorsal synovial fold volume (mm^3) at the right and left lateral atlanto-axial joints of 10 female subjects with subject age (years), height (cm), body mass (kg) and BMI (kg/m^2).

Spearman's r_s P-Value	Right ventral synovial fold	Right dorsal synovial fold	Left ventral synovial fold	Left dorsal synovial fold
Age (years)	-.15 P=.67	-.18 P=.62	-.25 P=.48	.10 P=.77
Height (cm)	.27 P=.28	.64 P=.04	.65 P=.04	.68 P=.03
Body mass (kg)	-.24 P=.33	-.64 P=.048	-.58 P=.08	-.73 P=.02
BMI (kg/m^2)	-.29 P=.25	-.69 P=.03	-.59 P=.07	-.75 P=.01
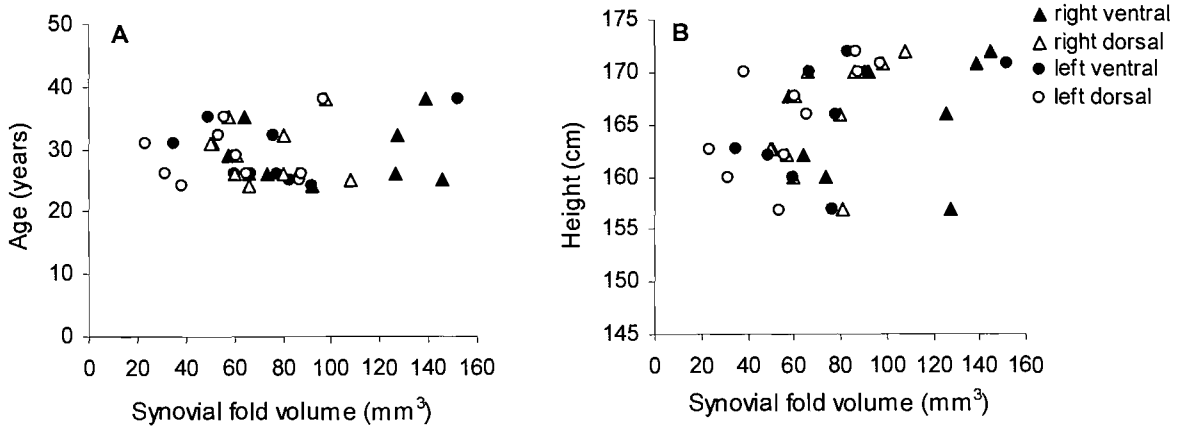
Figure 6.3.A. Scatter diagram of ventral and dorsal synovial fold volume (mm^3) at the right and left lateral atlanto-axial joints (n=10) plotted against age (years). **B.** Scatter diagram of ventral and dorsal synovial fold volume (mm^3) at the right and left lateral atlanto-axial joints (n=10) plotted against height (cm).
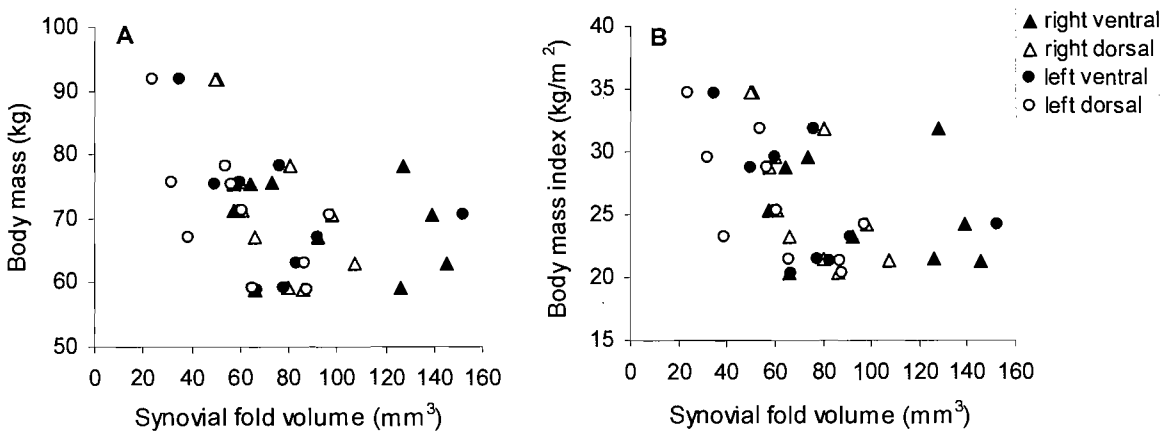
Figure 6.4.A. Scatter diagram of ventral and dorsal synovial fold volume (mm^3) at the right and left lateral atlanto-axial joints (n=10) plotted against body mass (kg). **B.** Scatter diagram of ventral and dorsal synovial fold volume (mm^3) at the right and left lateral atlanto-axial joints (n=10) plotted against body mass index (kg/m^2).

The volume of the ventral and dorsal synovial folds of the right and left lateral atlanto-axial joints of normal weight and overweight subjects are compared in Table 6.5 and Figure 6.5. For all synovial folds, the synovial fold volume of the normal weight subjects was greater than that of the overweight subjects.

The volume of the ventral and dorsal synovial folds of the right and left lateral atlanto-axial joints of subjects with and without visual impairment are compared in Table 6.5 and Figure 6.5. The right ventral, right dorsal and left ventral synovial folds of the visually impaired group were larger in comparison to the group that did not report visual impairment.

190

Table 6.5. Comparison of synovial fold volume (mm^3) between normal weight (BMI ≤24.99 kg/m^2) (n=5) and overweight (BMI ≥25.00 kg/m^2) (n=5) subjects; and subjects with no visual impairment (n=6) and subjects with a visual impairment requiring correction with glasses and/or contact lenses (n=4).

Mean (SD)	Right ventral synovial fold	Right dorsal synovial fold	Left ventral synovial fold	Left dorsal synovial fold
Normal weight (BMI ≤24.99 kg/m^2)	113.82 (33.62)	87.69 (16.20)	94.45 (33.54)	75.39 (23.56)
Overweight (BMI ≥25.00 kg/m^2)	74.82 (30.59)	61.89 (11.42)	56.22 (15.26)	45.34 (16.43)
No visual impairment	75.36 (32.20)	68.84 (18.91)	70.70 (41.51)	59.71 (29.32)
Visual impairment (wear glasses and/or contact lenses)	122.76 (30.59)	83.71 17.47	82.30 (6.99)	61.35 (20.42)
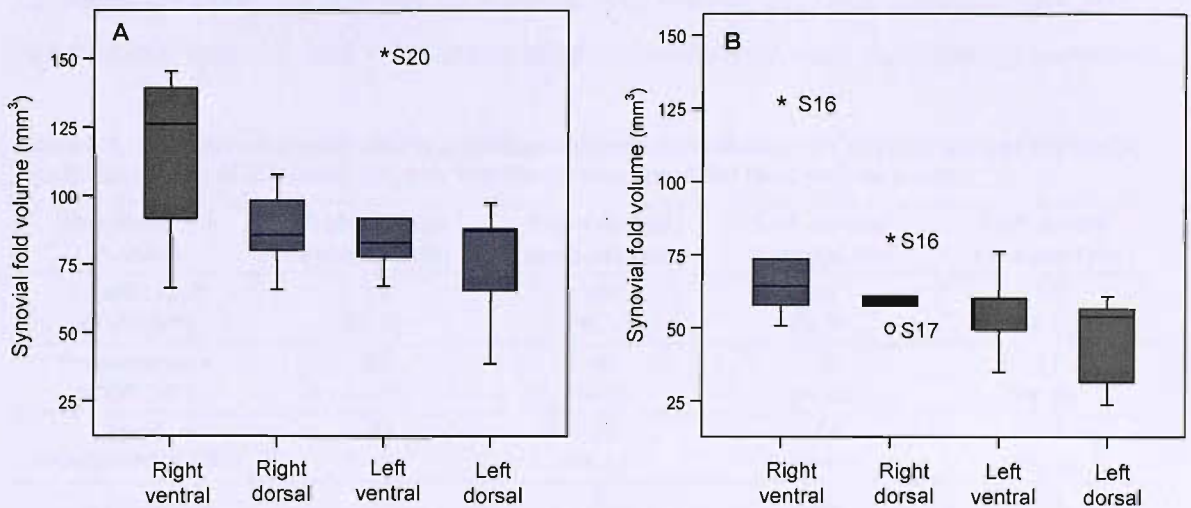
Figure 6.5.A. Boxplot showing the range of values and the median (——) of ventral and dorsal synovial fold volume (mm^3) at the right and left lateral atlanto-axial joints for the **A.** normal weight group (BMI ≤24.99 kg/m^2) (n=5) and the **B.** overweight group (BMI ≥25.00 kg/m^2) (n=5). o=outlier; *=extreme outlier; S=subject number.
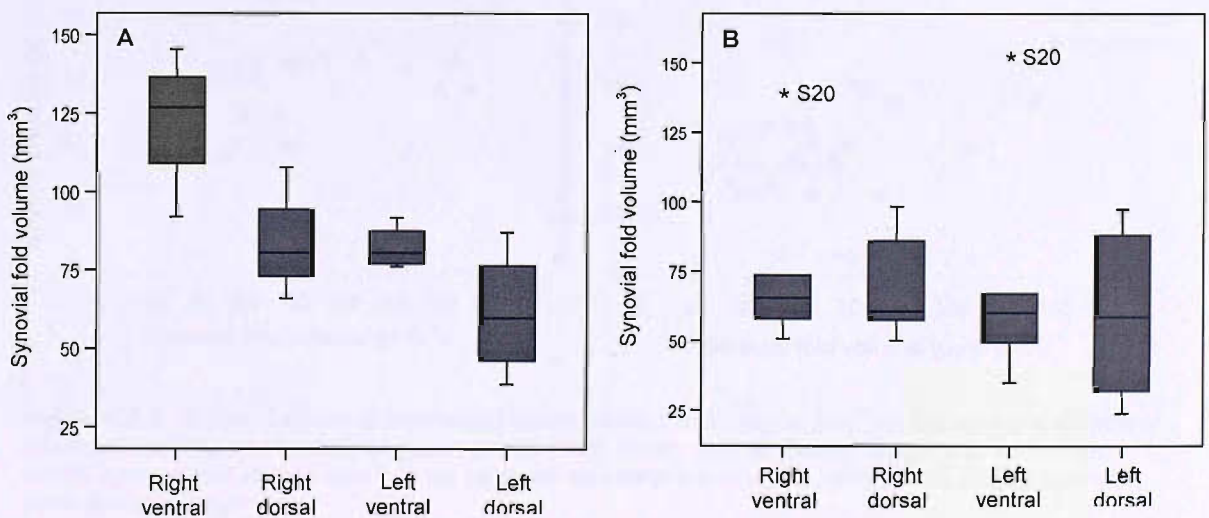
Figure 6.6.A. Boxplot showing the range of values and the median (——) of ventral and dorsal synovial fold volume (mm^3) at the right and left lateral atlanto-axial joints for the **A.** subjects that wear glasses/contact lenses (n=4) and the **B.** subjects that do not wear glasses/contact lenses (n=6). *=extreme outlier; S=subject number.

191

6.3.5 Dimensions of the head and neck

The dimensions of the head and neck for each subject are presented in Table 6.3.

In the main, the dimensions of the head and neck were related to synovial fold volume but were not significantly correlated (Table 6.6 and Figures 6.7 and 6.8). Synovial fold volume increased with increasing anterior and posterior neck length. The correlation between right dorsal and left dorsal synovial fold volume and anterior and posterior neck length was moderate to high, however, only the relationship between left dorsal synovial fold volume and posterior neck length was found to be significant. Generally, synovial fold volume increased with decreasing neck circumference and head circumference but only left ventral synovial fold volume and neck circumference and right ventral synovial fold volume and head circumference were significantly correlated.

Table 6.6. Correlation between ventral and dorsal synovial fold volume (mm^3) at the right and left lateral atlanto-axial joints of 10 female subjects with the dimensions of the head and neck (cm).

Spearman's r_s P-Value	Right ventral synovial fold	Right dorsal synovial fold	Left ventral synovial fold	Left dorsal synovial fold
Anterior neck length (cm)	.18 P=.61	.49 P=.15	.43 P=.21	.56 P=.10
Posterior neck length (cm)	.22 P=.53	.49 P=.15	.16 P=.65	.77 P=.01
Neck circumference (cm)	-.38 P=.28	-.54 P=.11	-.59 P=.07	-.53 P=.12
Head circumference (cm)	-.61 P=.06	-.62 P=.05	-.33 P=.35	-.27 P=.45
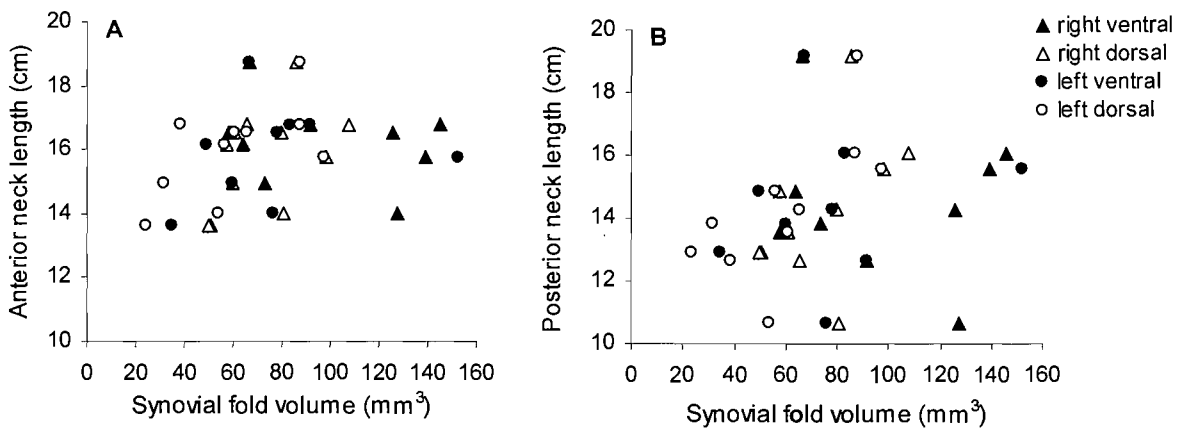
Figure 6.7.A. Scatter diagram of ventral and dorsal synovial fold volume (mm^3) at the right and left lateral atlanto-axial joints (n=10) plotted against anterior neck length (cm). **B.** Scatter diagram of ventral and dorsal synovial fold volume (mm^3) at the right and left lateral atlanto-axial joints (n=10) plotted against posterior neck length (cm).
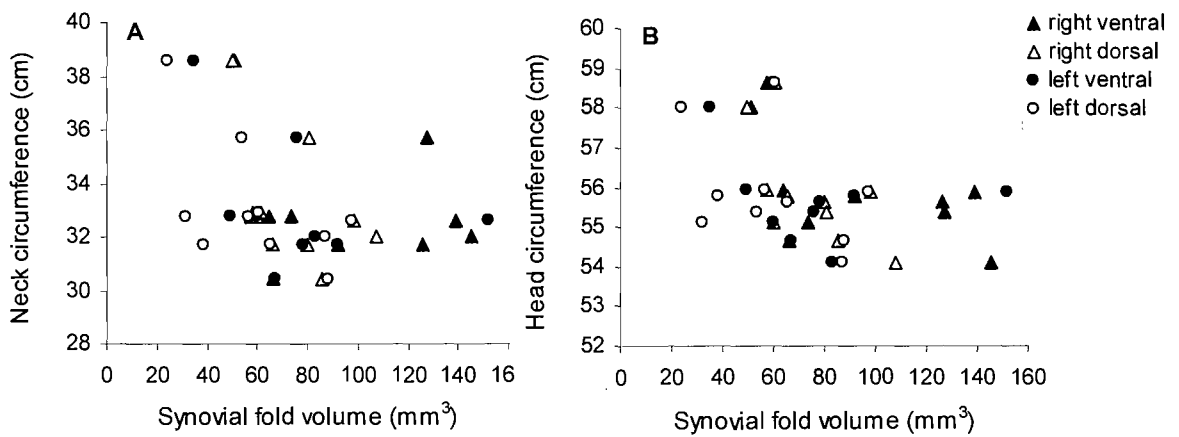
Figure 6.8.A. Scatter diagram of ventral and dorsal synovial fold volume (mm³) at the right and left lateral atlanto-axial joints (n=10) plotted against neck circumference (cm). **B.** Scatter diagram of ventral and dorsal synovial fold volume (mm³) at the right and left lateral atlanto-axial joints (n=10) plotted against head circumference (cm).

6.3.6 Cervical range of motion

Total and half cycle cervical ranges of motion of the volunteer subjects are summarised in Tables 6.7 and 6.8.

Table 6.7. Flexion and extension range of motion (degrees) of the 10 female subjects.

Subjects	Flexion (°)	Extension (°)	Flexion-extension (°)	Suboccipital flexion (°)	Suboccipital extension (°)	Suboccipital flexion-extension (°)
Volunteer 11	62.33	56.67	119.00	14.33	13.67	28.00
Volunteer 12	66.33	63.67	130.00	12.00	16.67	28.67
Volunteer 13	60.00	83.67	143.67	15.33	16.00	31.33
Volunteer 14	68.33	82.00	150.33	10.67	24.00	34.67
Volunteer 16	53.33	54.67	108.00	14.00	22.67	36.67
Volunteer 17	47.33	55.00	102.33	10.33	15.00	25.33
Volunteer 18	69.67	63.00	132.67	9.33	15.00	24.33
Volunteer 19	48.00	66.67	114.67	13.67	23.67	37.33
Volunteer 20	62.00	67.33	129.33	10.33	20.00	30.33
Volunteer 21	60.00	52.67	112.67	10.67	17.00	27.67
Mean (SD)	**59.73 (7.89)**	**64.5 (10.94)**	**124.27 (15.58)**	**12.07 (2.10)**	**18.37 (3.89)**	**30.43 (4.54)**
Median	**61.00**	**63.33**	**124.17**	**11.33**	**16.83**	**29.50**

The volume of the synovial folds was related to the range of flexion, extension and flexion-extension, with synovial fold volume generally increasing in association with a greater range of motion in the sagittal plane (Figures 6.9.A to 6.11.A). The exception to this trend was the negative correlation between right ventral and left ventral synovial fold volume and the range of flexion-extension. There were significant correlations between the right dorsal and left dorsal synovial fold volume and the range of extension and flexion-extension; and between left ventral synovial fold volume and flexion (Table 6.8). There was a positive relationship between right dorsal and left dorsal synovial fold

193

volume and the range of suboccipital flexion, suboccipital extension and suboccipital flexion-extension (Figures 6.9.B to 6.11.B) which was not significant (Table 6.8).

Table 6.8. Correlation between ventral and dorsal synovial fold volume (mm³) at the right and left lateral atlanto-axial joints of 10 female subjects with the range of flexion and extension (degrees) of the cervical spine and the suboccipital region.

Spearman's r_s P-Value	Right ventral synovial fold	Right dorsal synovial fold	Left ventral synovial fold	Left dorsal synovial fold
Flexion	.13 P=.74	.39 P=.27	.56 P=.09	.41 P=.24
Extension	.25 P=.49	.59 P=.07	.38 P=.28	.79 P=.01
Flexion-extension	.27 P=.45	.62 P=.05	.54 P=.11	.67 P=.03
Suboccipital flexion	.35 P=.32	.31 P=.15	-.01 P=.97	.29 P=.42
Suboccipital extension	-.05 P=.89	.16 P=.65	-.18 P=.63	.31 P=.38
Suboccipital flexion-extension	.20 P=.58	.35 P=.33	-.06 P=.88	.49 P=.15
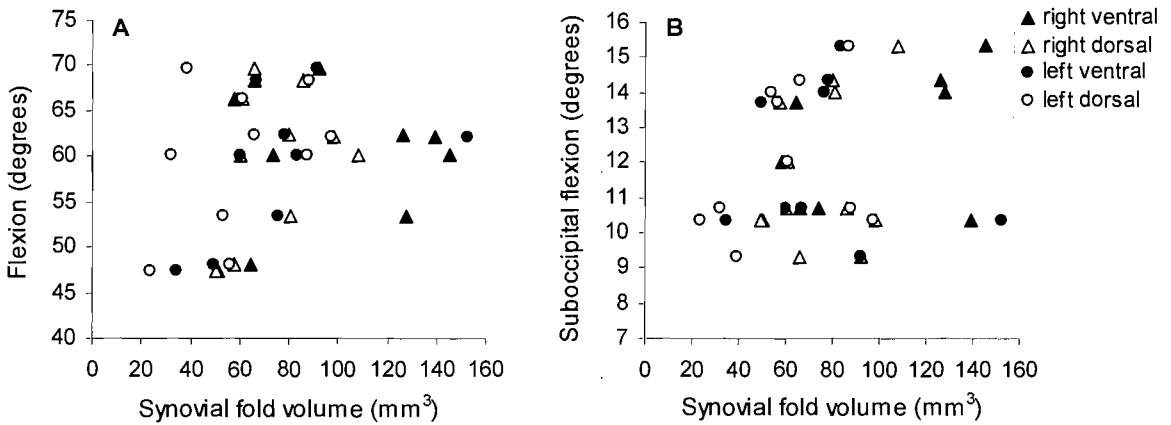
Figure 6.9. Scatter diagram of ventral and dorsal synovial fold volume (mm³) at the right and left lateral atlanto-axial joints (n=10) plotted against **A.** cervical flexion (degrees) **B.** suboccipital flexion (degrees).
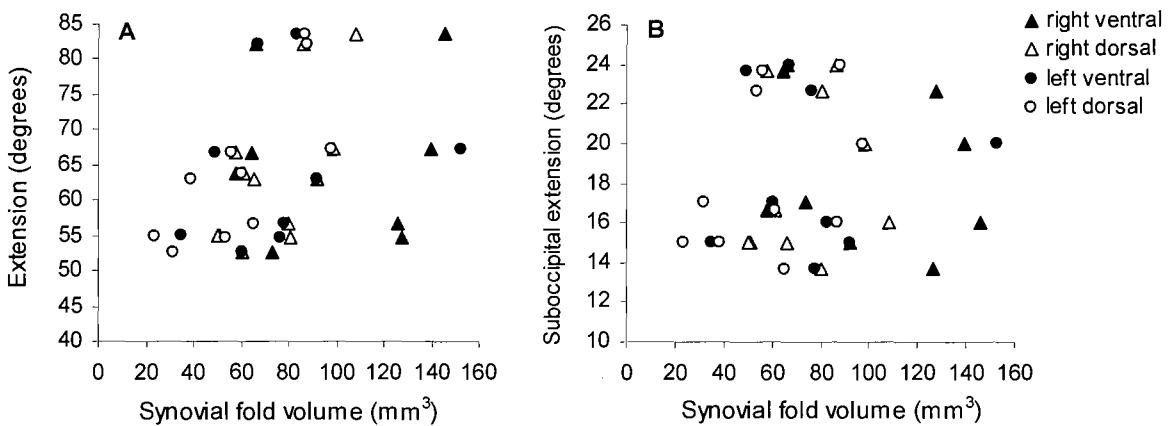
Figure 6.10. Scatter diagram of ventral and dorsal synovial fold volume (mm³) at the right and left lateral atlanto-axial joints (n=10) plotted against **A.** cervical extension (degrees) **B.** suboccipital extension (degrees).

194
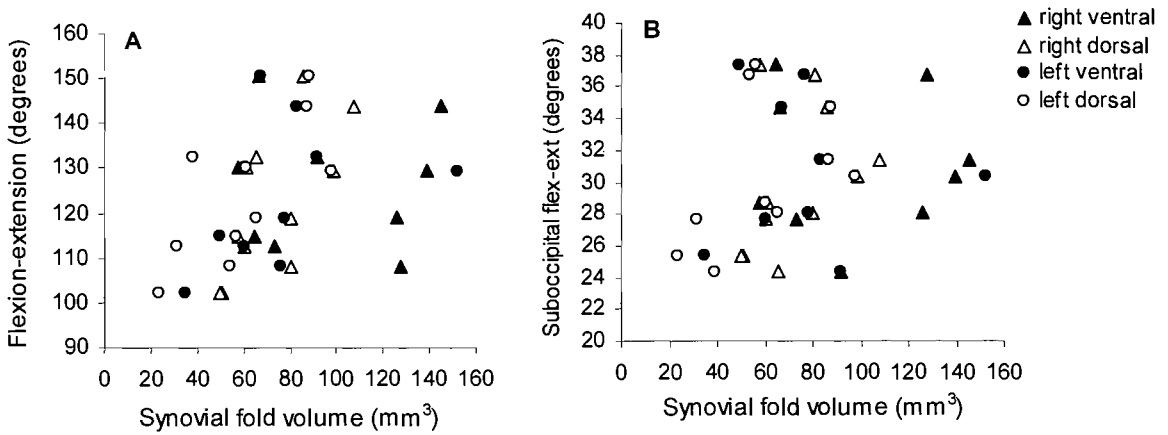
Figure 6.11. Scatter diagram of ventral and dorsal synovial fold volume (mm³) at the right and left lateral atlanto-axial joints (n=10) plotted against **A.** cervical flexion-extension (degrees) **B.** suboccipital flexion-extension (degrees).

Generally, there was a negative correlation between right ventral and left ventral synovial fold volume and range of lateral flexion and a positive correlation between right dorsal and left dorsal synovial fold volume and the range of lateral flexion. None of these relationships were found to be significant (Table 6.10 and Figures 6.12.A to 6.14.A). Synovial fold volume was observed to increase in association with increasing range of rotation (Figures 6.12.B to 6.14.B). With the exception of left ventral synovial fold volume and left rotation these relationships were not significant (Table 6.10).

Table 6.9. Lateral flexion and rotation range of motion (degrees) of the 10 female subjects.

| Subjects	Right rotation (°)	Left rotation (°)	Rotation (°)	Right lateral flexion (°)	Left lateral flexion (°)	Lateral flexion (°)
Volunteer 11	69.33	60.33	129.67	26.33	29.00	55.33
Volunteer 12	78.00	70.00	148.00	43.67	42.67	86.33
Volunteer 13	71.33	73.00	144.33	37.00	45.00	82.00
Volunteer 14	49.00	64.67	113.67	49.00	42.67	91.67
Volunteer 16	44.33	55.00	99.33	27.00	29.33	56.33
Volunteer 17	55.00	51.67	106.67	30.00	29.33	59.33
Volunteer 18	55.33	73.00	128.33	29.00	34.00	63.00
Volunteer 19	51.00	52.33	103.33	30.33	35.00	65.33
Volunteer 20	62.67	65.00	127.67	36.33	37.33	73.37
Volunteer 21	54.67	61.67	116.33	41.67	52.00	93.67
Mean (SD)	**59.07 (10.86)**	**62.67 (7.96)**	**121.73 (16.68)**	**35.03 (7.77)**	**37.63 (7.77)**	**72.67 (14.79)**
Median	**55.17**	**63.17**	**122.00**	**33.33**	**36.17**	**69.50**

Table 6.10. Correlation between ventral and dorsal synovial fold volume (mm^3) at the right and left lateral atlanto-axial joints of 10 female subjects with the range of lateral flexion (degrees) and rotation (degrees) of the cervical spine.

Spearman's r_s P-Value	Right ventral synovial fold	Right dorsal synovial fold	Left ventral synovial fold	Left dorsal synovial fold
Right lateral flexion	.13 P=.74	.13 P=.73	-.20 P=.58	.32 P=.37
Left lateral flexion	.06 P=.87	.21 P=.55	-.03 P=.93	.23 P=.53
Lateral flexion	-.14 P=.70	.10 P=.77	-.14 P=.70	.21 P=.56
Right rotation	.15 P=.68	.18 P=.63	.35 P=.33	.29 P=.43
Left rotation	.44 P=.20	.58 P=.08	.69 P=.03	.43 P=.22
Rotation	.21 P=.56	.31 P=.39	.44 P=.20	.36 P=.31
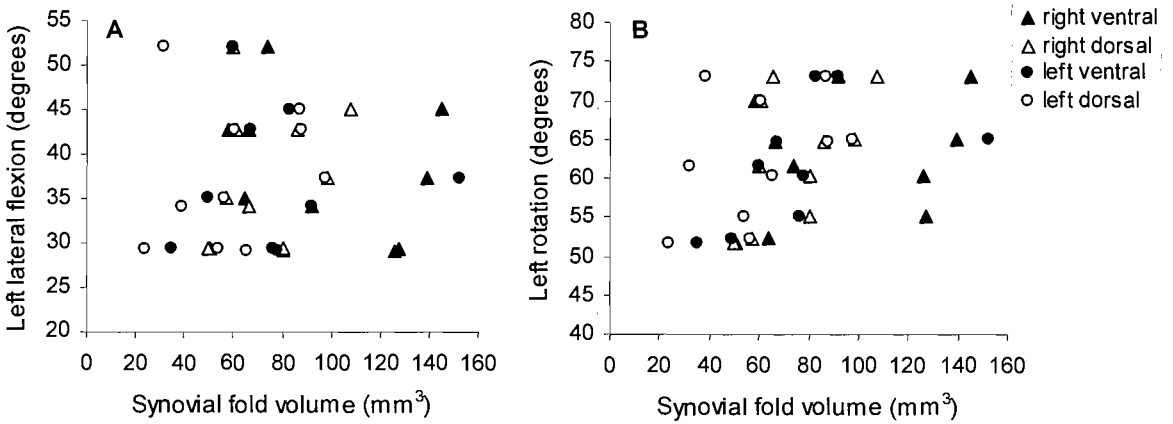
Figure 6.12. Scatter diagram of ventral and dorsal synovial fold volume (mm^3) at the right and left lateral atlanto-axial joints (n=10) plotted against **A.** left lateral flexion (degrees) **B.** left rotation (degrees)
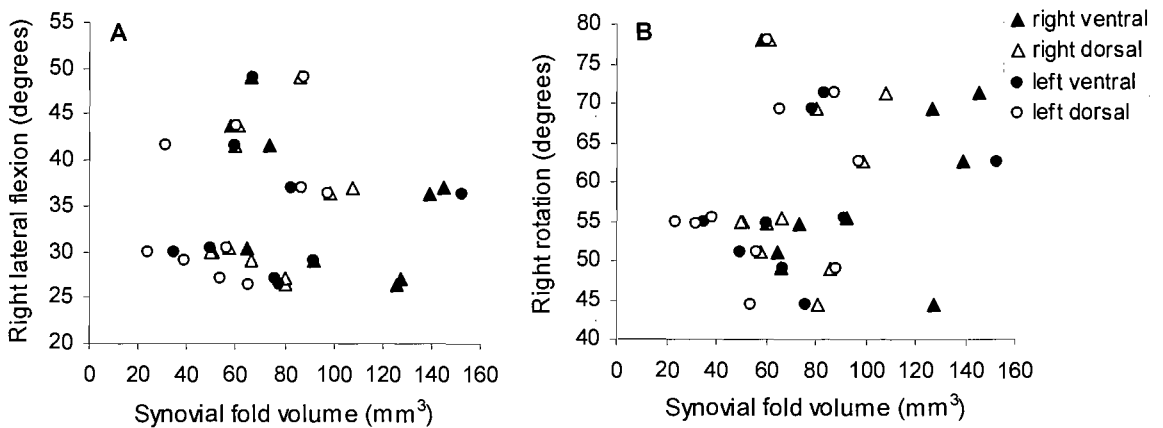
Figure 6.13. Scatter diagram of ventral and dorsal synovial fold volume (mm^3) at the right and left lateral atlanto-axial joints (n=10) plotted against **A.** right lateral flexion (degrees) **B.** right rotation (degrees).

196
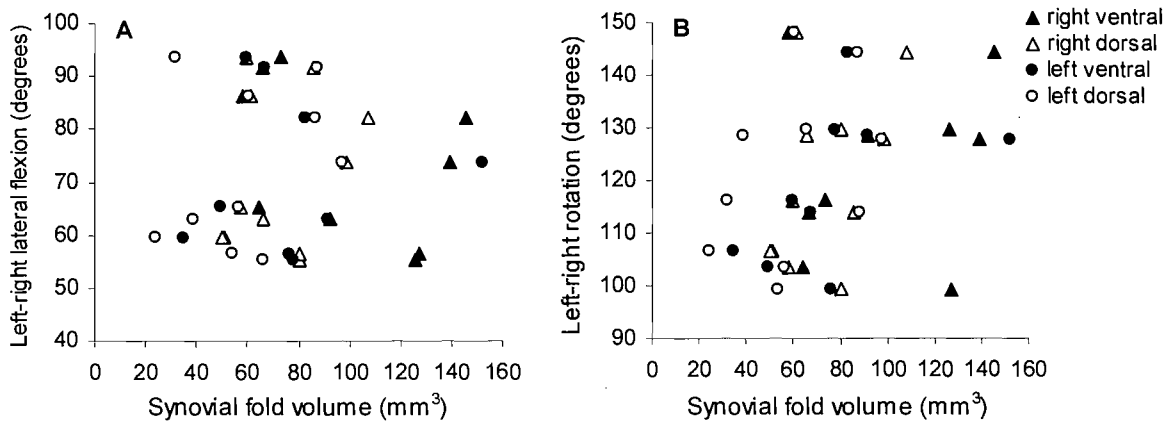
Figure 6.14. Scatter diagram of ventral and dorsal synovial fold volume (mm^3) at the right and left lateral atlanto-axial joints (n=10) plotted against **A.** lateral flexion (degrees) **B.** rotation (degrees).

6.4 Discussion

The present study is the first to determine the normal *in vivo* morphology of the synovial folds of the lateral atlanto-axial joints as a basis for understanding their potential role in the generation of neck pain and disability.

6.4.1 Synovial fold volume

In the present study, the ventral-dorsal asymmetry of the synovial folds followed the same general trend as the synovial folds studied in Chapters 4 and 5. The right ventral and left ventral synovial folds were typically larger compared to the right dorsal and left dorsal synovial folds, respectively. Furthermore the left and right ventral synovial fold volume was significantly greater than left and right dorsal synovial fold volume.

Cervical spine posture and curvature are factors that may potentially contribute to the asymmetry of the synovial folds. Forward head posture has been found to increase with advancing age and it has been hypothesised that increased forward head posture is associated with an increase in upper cervical extension in order to realign the bipupillary plane with the horizontal to compensate for the prolonged and habitual use of flexed postures (Dalton and Coutts, 1994). The adoption of a forward head posture and resultant increase in extension of the upper cervical spine would potentially increase the biomechanical stress in the dorsal region of the joint and thus may lead to a reduction in the size and adipose content of the dorsal synovial folds. The relationship between advancing age and increased forward head posture has been confirmed but the proposed association with increased extension of the upper cervical spine has been

197

disputed (Raine and Twomey, 1997). Nonetheless, the load-bearing capacity of the ventral and dorsal elements of the cervical spine has been found to change with different cervical spine postures and may be one factor that affects the ventral-dorsal morphology of the synovial folds (Oktenoglu et al., 2001; Bonney and Corlett, 2002).

Posture of the head and neck can be affected by wearing glasses and eye dominance (Pradham et al., 2001; Basrai and Aghazadeh, 2004). In the present study, four subjects reported visual impairments that required correction by wearing glasses and/or contact lenses. There was a larger difference in volume between the right ventral and right dorsal and left ventral and left dorsal synovial folds in the group with visual impairment compared to the group without visual impairment. The difference between right ventral and left ventral synovial folds and right dorsal and left dorsal synovial folds, was also larger in the group with visual impairment. The wearing of glasses and contact lenses to correct for visual impairments may result in postural changes that alter the biomechanical load upon the synovial folds causing an accentuation of the 'normal' ventral-dorsal and left-right asymmetry between the synovial folds.

In contrast to the results of Chapter 4 but in agreement with the results of Chapter 5, the right ventral and right dorsal synovial folds were significantly larger than the left ventral and left dorsal synovial folds, respectively. All subjects were right hand dominant (with one subject ambidextrous) therefore the side-to-side differences may be the result of a dominance effect. Studies of skeletal muscle size frequently assess side-to-side symmetry and investigate its association with hand (or foot) dominance. The results of such studies in the cervical spine have failed to demonstrate a consistent pattern of asymmetry associated with handedness. In a study of predominantly right hand dominant subjects, Elliott et al. (2007) found that all of the cervical extensor muscles on the right side were slightly greater than those on the left and the same right-left difference was also apparent in the small number of subjects who were left hand dominant. In contrast, Rankin et al. (2005) reported that all but one cervical extensor muscle demonstrated symmetry between left and right sides whilst Soltani et al. (1996) noted that splenius capitis was larger on the side of hand dominance. With respect to the results of the present study, further research with samples that include left hand dominant subjects are needed to clarify this issue.

Raine and Twomey (1997) examined the coronal head tilt of 160 asymptomatic subjects. Although the mean of the sample was 180.10° (SD 2.6°), indicating that subjects generally stood with their head symmetrical in the coronal plane, the degree of coronal head tilt ranged from 9° to the left to 6° to the right. Thus the degree of an individual's coronal head tilt may be related to the size of their synovial folds when comparing the right and left lateral atlanto-axial joints.

The asymmetry of the synovial folds documented in the present study may be the result of structural asymmetry inherent to the individual. Anatomic asymmetry affecting cervical spine structures such as the osseous vertebrae, cartilage, ligaments, muscles, blood vessels and nerves is well documented (Gottlieb, 1994; Inami et al., 2000; Pfirrmann et al., 2001; Yoganandan et al., 2003; Bilge, 2004; Bruneau et al., 2006; Cagnie et al., 2006; Elliott et al., 2007).

Up to 50% of atlanto-axial joints have been found to be asymmetric and affected by variations in the size and shape of the articular surfaces and differences in the angle of the joints (Van Roy et al., 1997; Ross et al., 1999; Pfirrmann et al., 2001). The shape and size of the synovial folds is likely to reflect, to some extent, the shape and size of the articular surfaces. The articular facets of the atlas are larger on the right compared to the left (Mysorekar and Nandedkar, 1986), which is in agreement with the right-left asymmetry of the synovial folds reported in the present study. Size comparisons between the ventral and dorsal aspects of the atlanto-axial articular surfaces have not been reported to date. From observations of atlas and axis vertebrae, it was noted that the width of the ventral aspect of the articular surface was frequently wider than the dorsal aspect of the articular surface (Figure 6.15). Thus if synovial fold size is a reflection of articular surface shape and size then it would follow that a larger ventral articular surface would be associated with large ventral synovial folds. Like the synovial folds, the hyaline articular cartilage of the atlanto-axial joint surfaces is asymmetric between ventral and dorsal regions, with less cartilage present dorsally compared to ventrally (Yoganandan et al., 2003).
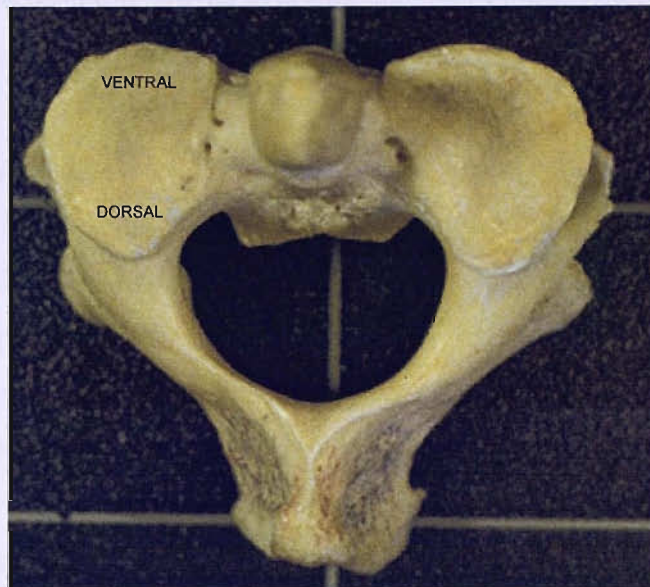
Figure 6.15. Superior view of the axis vertebra.

6.4.2 Age

In agreement with the results of Chapter 5, there was no evidence of a consistent relationship between synovial fold volume and age in the present study of female subjects aged 24 to 38 years.

Many spinal structures have been reported to undergo regressive changes with increasing age (Fletcher et al., 1990; Yanase et al., 2006; Kettler et al., 2007). Whilst the size of the articular facets appears to be age-independent, the thickness/cross-sectional area of the hyaline articular cartilage covering the spinal articular surfaces decreases with increasing age and in association with osteoarthritic change (Fletcher et al., 1990; Singer et al., 1990; Masharawi et al., 2005; Kettler et al., 2007). Based upon observations from cadaver studies it has been suggested that the morphology of the synovial folds also changes in association with increasing age and/or articular degeneration (Yu et al., 1987; Inami et al., 2000; Kos et al., 2002; Tang et al., 2007). Fletcher et al. (1990), Inami et al. (2000) and Tang et al. (2007) reported that the synovial folds appear to undergo attrition in association with increasing age, and/or degenerative change, becoming smaller, thinner and more ragged. In contrast, Yu et al. (1987) and Kos et al. (2002) reported synovial folds of increased size with an irregular form in older subjects. Neither of these age-related observations was verified by the results of the present study involving asymptomatic individuals with no evidence of lateral atlanto-axial degenerative change. The age range of volunteers in the present

study may have been too narrow to appreciate a relationship between age and synovial fold dimensions.

Despite no evidence of a relationship between age and synovial fold volume in the present study, changes in synovial fold morphometry related to increasing age and degeneration should not be ignored as a potential source of asymmetry that may affect the morphology of the synovial folds. Clinically, osteoarthritis affecting the lateral atlanto-axial joints is reported to be relatively uncommon (Halla and Hardin, 1987; Zapletal and de Valois, 1997; Schaeren and Jeanneret, 2005), however, cadaveric studies have demonstrated that degenerative changes affecting the cartilage covering the superior articular facets of the axis is common, affecting adults of all ages (Harata et al., 1981; Konig et al., 2005;).

Based on the grading system of degenerative changes published by Petersson in 1983, the cartilage of the superior articular facets of the axis has been found to be most commonly affected by Grade 1 (superficial degeneration with several fragmentations) and Grade 2 (deep degeneration with cartilaginous disintegration and penetrating ulceration) degenerative changes (Petersson, 1983; Konig et al., 2005). The degenerative changes were found to be most significant at the dorsal aspect of the articular surfaces (Konig et al., 2005). The results of the present study in which the dorsal synovial folds were found to be smaller than the ventral synovial folds supports the suggestion that the synovial folds undergo attrition in association with increasing degenerative change at the dorsal aspect of the articulation. Although the subjects investigated in the present study were aged less than 40 years and did not have any signs of osteoarthritis, thinning of the cartilage of the cervical articulations has been observed in cadavers aged less than 40 years (Fletcher et al., 1990).

6.4.3 Physical anthropometrics

The size of the synovial folds was found to be related to physical anthropometrics. The dimensions of the subject's body as a whole rather than the regional dimensions of the head and neck were significantly linked to synovial fold volume. A larger synovial fold volume was associated with taller subjects and subjects who weighed less. These results were consistent with the finding that subjects who had a BMI value within the normal weight range had larger synovial folds compared to subjects with a BMI value in the overweight range. Although, in the main, synovial fold volume was not significantly

related to the dimensions of the head and neck there was a general trend for synovial fold volume to increase with increasing neck length and to increase with decreasing head and neck circumference, i.e. larger synovial folds were generally associated with long slender necks and smaller heads.

The existing evidence on the association between cervical spine morphology and height, body mass and body mass index is conflicting. Based on measurements from lateral radiographs of the cervical spine, Katz et al. (1975) found that subject height had a minimal effect upon the dimensions of the cervical vertebral bodies whilst for some cervical vertebrae, the vertebral body dimensions were correlated to ponderal index (weight/length^3, similar to the body mass index but typically calculated for newborns and infants) and head weight. In the thoracic and lumbar regions, height has been found to be significantly correlated with the dimensions of the thoracolumbar articular facets and the angle of the facet joints (Karacan et al., 2004; Masharawi et al., 2005). The finding that height is positively correlated with articular facet dimensions is in agreement with the findings of the present study.

Body mass has also been found to be positively correlated with thoracolumbar facet dimensions whilst lumbar facet joint angles do not appear to be related to body mass or BMI (Karacan et al., 2004; Masharawi et al., 2005). In contrast, in the present study, body mass and BMI were negatively correlated to synovial fold volume which may be the result of regional differences between the cervical compared to the thoracic and lumbar spines. In the knee joints of subjects without knee pain, cartilage volume has been found to be related to height, body mass, BMI, physical activity and regional dimensions including leg length and foot size (Nishimura et al., 2005; Hanna et al., 2007).

In addition to articular structures, the cervical spinal cord and musculature have been found to be related to physical anthropometrics. Like synovial fold volume, the cervical spinal cord volume has been found to increase in association with height but unlike synovial fold volume, the spinal cord volume increases with increasing body mass (Yanase et al., 2006). As the dimensions of the vertebral canal are also correlated with subject height and body mass, the dimensions of the spinal cord may reflect the dimensions of the vertebral canal (Karantanas et al., 1998).

In agreement with the present study of synovial fold dimensions, the size of the cervical spine musculature has been found to be related to BMI values. However, the size of the cervical muscles has been found to be significantly larger in subjects with a BMI greater than $25.0 kg/m^2$ (Elliott et al., 2007a) whilst synovial fold volume was found to be greater in subjects with a BMI value less than $24.9 kg/m^2$. The relationship between BMI and synovial fold volume was consistently observed for all synovial folds but has been found to be extremely variable between different cervical muscles (Soltani et al., 1996; Elliott et al., 2007a; 2007b). This variable pattern of relationship between cervical muscle cross-sectional area and BMI has to date defied explanation (Elliott et al., 2007a) and similarly, it is not possible to explain why synovial folds are larger in subjects with lower BMI values.

Subjects with low physical activity levels have larger muscle cross-sectional areas in the cervical spine (Elliott et al., 2007a). In contrast the synovial folds in the present study were larger in subjects that were physically active. The cross-sectional area of cervical musculature has been found to decrease as a result of specific resistance training effects (Conley et al., 1997). It is generally accepted that motor unit recruitment of muscles becomes more efficient in trained individuals which may explain this relationship between level of physical activity and muscle size (Conley et al., 1997). Whilst a relationship between physical activity/training effects and muscle size appears conceivable such a link between synovial fold size and physical activity is not so obvious. In the present study, the subjects with a BMI less than $24.9 kg/m^2$ were the exactly the same subjects that were physically active. Thus it is not possible to ascertain whether it was BMI and/or physical activity that influenced the dimensions of the synovial folds.

Thus there appears to be a general pattern of relationship between height, body mass and BMI and the dimensions of the cervical spine but it does not appear to be consistent for all structures. Generally, structures are larger in association with greater height but the relationship with body mass and BMI is more variable. It would seem plausible that an increase in body mass and BMI would be associated with structures of larger size. What is intriguing is that this appears to be the case for the dimensions of the thoracolumbar articular facets and cervical spinal cord and some of the cervical musculature but for the synovial folds there is an inverse relationship between atlanto-axial synovial fold dimensions and body mass and BMI. It is not known why the

synovial folds and not other structures of the cervical spine have demonstrated this inverse relationship. The findings, although spurious, indicate that body mass and BMI may be an important consideration in future studies of patients with neck pain and/or disorders of the cervical spine.

A linear negative correlation has been found between forward head acceleration and neck circumference in low speed motor vehicle collisions with occupants with thinner necks experiencing significantly greater head acceleration compared to occupants with thicker necks (van den Kroonenberg et al., 1998; Hell et al., 2002). A significant negative correlation was similarly found between body mass index (BMI) and head acceleration (van den Kroonenberg et al., 1998). Freeman et al. (2006) found an increased risk of association between BMI and chronic neck pain following a motor vehicle collision but did not find an increased risk in the female population. Thus Freeman et al. (2006) have suggested that body mass and neck circumference rather than female gender are most likely to result in the development of neck pain following a whiplash trauma. Females generally have smaller necks and less body mass compared to males which may explain why this relationship is thought to have been attributed to gender (Harty et al., 2004; Freeman et al., 2006). If this is the case then it would be expected that males with thin necks and low BMI values are just as likely as females to sustain an injury following motor vehicle trauma and may be just as likely as females to develop chronic symptoms. The finding in the present study that taller individuals with less body mass and lower BMI, and longer more slender necks, had larger synovial folds is of potential relevance to the understanding of the biomechanics and pathoanatomy of whiplash injury.

Larger synovial folds may be more vulnerable to being pinched and bruised between the articular surfaces following the application of a traumatic force. Contusions of the synovial folds and occult fractures of the articular processes are two of the most common injuries observed to affect the cervical articulations at post-mortem following motor vehicle trauma (Jonsson et al., 1991; Taylor and Taylor, 1996). Taller individuals with less body mass, lower BMI and long slender necks that have larger synovial folds may be more prone to bruising of the synovial folds following whiplash trauma but less vulnerable to damage affecting the hyaline articular cartilage and articular facets. In contrast, shorter individuals with greater body mass and BMI and shorter thicker necks

that have smaller synovial folds may be more prone to articular cartilage and subchondral bone damage following motor vehicle trauma.

Freeman et al. (2006) and Hooper et al. (2007) found that BMI was an important variable in subjects with neck pain. Yang et al. (2007) hypothesised that overweight and obese individuals would have a slower recovery from whiplash injury compared with those of normal weight but instead found that underweight subjects had the slowest recovery whilst normal weight, overweight and obese individuals had similar rates of recovery. Grimmer et al. (1999), in agreement with the findings of Yang et al. (2007), found no evidence of significant association of headache with body mass or BMI but did note a correlation in the direction of greater risk of headache for less body mass.

Although the findings of Grimmer et al. (1999) and Yang et al. (2007) were not significant the association between headache and chronic WAD with body mass and BMI are of interest to the present study where low body mass and BMI were associated with large synovial folds. The possibility that individuals with low BMI and body mass have large synovial folds may increase the likelihood of synovial fold injury resulting in neck pain and headache in this population and should be a consideration for future clinical studies.

6.4.4 Cervical range of motion

The function of the synovial folds is not known. Based on cadaveric studies of synovial fold morphology it has been suggested that the synovial folds may facilitate movement between the articular surfaces (Lewin et al., 1962; Bogduk and Engel, 1984; Mercer and Bogduk, 1993). Alternatively the synovial fold 'space-fillers' may enhance joint congruity and stability, promote stress dissipation or even assist in weight-bearing (Lewin et al., 1962; Engel and Bogduk, 1982; Bogduk and Engel, 1984; Chang et al., 1992; Mercer and Bogduk, 1993).

The atlanto-axial joints have the greatest range of rotation in the cervical spine and account for 50% of the total range of cervical rotation (Dvorak et al., 1987; Penning and Wilmink, 1987; Panjabi et al., 1988). In the cadaveric study (Chapter 4) it was observed that the synovial folds of the lateral atlanto-axial joints are larger than the synovial folds of the cervical zygapophysial joints. Therefore larger synovial folds may be associated with a greater range of axial rotation. The measurement of cervical range of motion

(ROM) is interpreted as an indication of the state of the anatomic structures within or around the joints (Walmsley et al., 1996) and the function of the cervical spine is evaluated by assessing its ROM. The presence of a relationship between cervical ROM and the dimensions of the synovial folds would suggest that the synovial folds are involved in the facilitation of mobility rather than stability.

There is considerable literature available to quantify what constitutes normal motion of the cervical spine. There is generally consensus that normal cervical range of motion varies depending on both gender and age. Cervical range of motion decreases with increasing age and females typically have a greater ROM compared to males (Hole et al., 1995; Castro et al., 2000). For this reason, the volunteers in the present study were restricted to females aged between 20 and 40 years of age to eliminate the confounding effects of age and gender.

There was a positive relationship between synovial fold volume and the degree of rotation (left, right and left-right rotation) for all of the synovial folds, i.e. larger synovial folds were associated with a greater ROM. The correlation with left rotation was moderate and the correlation with left rotation and left-right rotation was low. These results indirectly suggest that the synovial folds contribute to motion in the axial plane at the lateral atlanto-axial joints.

Generally, there was a negative correlation between ventral synovial fold volume and range of lateral flexion and a positive correlation between dorsal synovial fold volume and range of lateral flexion. These results suggested that the ventral synovial folds do not facilitate lateral flexion whilst the dorsal synovial folds do. However, the correlation was low for all synovial folds which indicated that the synovial folds make a minimal contribution to lateral flexion at the lateral atlanto-axial joints. This is supported by the small range of segmental lateral flexion reported to occur at the lateral atlanto-axial joints (Dvorak et al., 1987; Panjabi et al., 1988).

There was a positive relationship between the range of cervical flexion-extension and ventral and dorsal synovial fold volume. Furthermore, both cervical flexion and extension were positively correlated with synovial fold volume. All of the correlations were moderate to high with the exception of the right ventral synovial fold which demonstrated small correlations. Therefore large synovial folds were associated with

206

increased motion in the sagittal plane. This indirectly implies that both the ventral and dorsal synovial folds may facilitate flexion and extension movements. However, these findings were not entirely supported by the results of the correlation analysis between suboccipital flexion and extension and synovial fold volume.

Suboccipital flexion and extension isolates sagittal motion of the upper cervical spine (atlanto-occipital and atlanto-axial joints) from the lower cervical spine. The range of suboccipital flexion, extension and flexion-extension were positively related to the volume of all synovial folds with the exception of the left ventral synovial fold and the negative relationship between the right ventral synovial fold and suboccipital extension. On the whole these results supported the relationship between cervical flexion and extension motion and synovial fold volume. However, the correlation between suboccipital sagittal motion and synovial fold volume was not as strong as the correlation between whole cervical sagittal motion and synovial fold volume. The reason for this disparity between results is not clear.

When flexing and extending the cervical spine it is possible to omit upper cervical motion. Suboccipital flexion and extension must be performed before the remainder of the cervical spine is flexed and extended, respectively, to ensure that motion of the upper cervical spine occurs and is included in the ROM measurement. In the present study subjects were instructed first to perform suboccipital flexion and extension prior to moving their head and neck into flexion and extension, respectively. Therefore the cervical flexion and extension measurements, like the suboccipital flexion and extension measurements, included full upper cervical flexion and extension. Consequently, the measurement technique does not account for the different results obtained for suboccipital compared to whole cervical flexion and extension.

To date there have been no biomechanical studies investigating the function of the synovial folds of the spine. Biomechanical studies of the fat pads and synovial folds of the knee, ankle and foot joints have been studied using cadavers. Resection of the infrapatellar fat pad of the knee joint has been found to decrease motion at the knee joint but increase motion at the patellofemoral joint (Bohnsack et al., 2004). The synovial folds of the first metatarsophalangeal and ankle joints have been found to produce a significantly stiffer joint which is consistent with greater joint congruency and stability (Lidtke and George, 2004). The role of the synovial folds may vary between different

synovial articulations depending on whether the joint is designed for mobility or stability. This would explain the different results obtained to date in the present study and previous investigations of synovial fold function.

Whilst cadaveric biomechanical studies provide some insight into the function of the synovial folds they are limited by differences in the material properties of tissues *in vitro* compared to *in vivo*. Furthermore, in order to access the synovial folds, an incision through the fibrous joint capsule is required. Because the fibrous joint capsule contributes to the stability of a synovial joint, disruption of its fibres will reduce the stability of the articulation. This highlights the need for the development of an *in vivo* method of imaging the synovial folds, as was achieved in the present study, in order to determine the function of the synovial folds.

Cervical range of motion forms an integral component of spinal evaluation and is the principal criterion in the quantification of musculoskeletal impairment (Andersson and Cocchiarella, 2000; Mannion et al., 2000; Malmstrom et al., 2003; Tousignant et al., 2006). It is particularly useful as a diagnostic aid in patients with neck pain and headache and is also used to assess the efficacy of therapeutic interventions (Mannion et al., 2000; Dall'Alba et al., 2001; Malmstrom et al., 2003; Strimpakos et al., 2005; Dvir et al., 2006; Zito et al., 2006).

In patients with whiplash associated disorder all planes of motion are reduced with the sagittal plane movements the most affected (Dall'Alba et al., 2001; Dvir et al., 2006; Prushansky et al., 2006; Kaale et al., 2007). Patients with headache also demonstrate decreased motion (Amiri et al., 2003; Ogince et al., 2007; Fernandez-de-Las-Penas et al., 2007). The cause of the reduced range of motion associated with neck pain and headache is not known but suggested reasons include mechanical changes in the tissues or pain inhibition (Dall'Alba et al., 2001; Kaale et al., 2007). Because the measurement of cervical range of motion is interpreted as an indication of the state of the anatomic structures within or around the joint complex, abnormal results may indicate abnormalities affecting the cervical articular structures (Walmsley et al., 1996). What these abnormalities may be is currently not known, however, injuries to the synovial folds in patients with neck pain and/or headache may be related to the reduction in cervical range of motion observed in these patient groups.

6.5. Conclusion

Ventral-dorsal and left-right differences in synovial fold volume were found in an asymptomatic sample of female subjects. Physical anthropometrics and cervical range of motion were found to be related to synovial fold volume in this subject sample.

The results of the present study go some way toward accounting for the variability observed in the dimensions of the synovial folds of the lateral atlanto-axial joints. The results highlight the importance of considering normal variations in synovial fold dimensions for optimal discrimination between asymptomatic individuals and those suffering from neck pain and/or headache in future studies.

This preliminary work provides a basis for further study of a symptomatic population to determine the presence and significance of changes in the dimensions of the synovial folds in patients with neck pain and disorders of the cervical spine.

Thus the development of a novel method in the present study for quantitatively assessing the morphology of the synovial folds of the lateral atlanto-axial joints *in vivo* using high resolution MR imaging has the potential to enable the diagnosis of disorders affecting the cervical spine, the pathoanatomical basis of which have proven elusive to date.

Chapter 7

Conclusions

One of the major problems in understanding the pathogenesis of neck pain has been the lack of detectable morphologic alterations.

Biomechanical models provide a versatile tool for determining the behaviour of spinal structures during different loading conditions. The models can be controlled and repeated and can evaluate external and internal mechanical responses that cannot be measured directly in experiments. Due to the location of the synovial folds within the fibrous capsule, it is very difficult to access the synovial folds without disrupting the integrity of the articulation.

To date the synovial folds have not been incorporated into biomechanical models of the upper cervical spine (Brolin et al., 2004). Because anatomic structure and geometry affect model output, it is important to obtain and input quantified information on every component of the cervical spine, including the synovial folds, to better predict the biomechanical behaviour of the cervical spine in response to normal physiologic and traumatic loading conditions (Yoganandan et al., 1996).

A biomechanical model of the cervical spine, using accurate normative data that includes the synovial folds, would provide an opportunity to determine the behaviour of the synovial folds during normal cervical motion. Because it is possible to vary the parameters within a biomechanical model, the responses of synovial folds of different size and tissue content could be examined.

The 3D models of the synovial folds produced in the present study would be suitable for such applications. Knowledge of normal variations affecting the synovial folds caused

by age, gender and physical anthropometrics would ensure that such factors that may affect the cervical biomechanics are accounted for. Furthermore, the behaviour of the synovial folds during traumatic loading such as whiplash could be modelled.

Following traumatic injury, such as whiplash, the synovial folds are likely to become inflamed which may be associated with enlargement of the folds. In the knee joint, following traumatic injury, symptomatic plicae usually appear thickened with synovitis on MR images (Jee et al., 1998; Garcia-Valtuille et al., 2002). Thus synovial fold inflammation caused by trauma may be detectable on MR images as an increase in synovial fold volume.

Haematomas can be identified on MR images by the signal patterns of haemoglobin breakdown products (Bush, 2000). Therefore the synovial fold bruising observed following whiplash trauma (Taylor and Taylor, 1996) may result in signal intensity changes on MR images. A spectrum of signal patterns is encountered in the various stages of an evolving haematoma enabling the distinction between acute and chronic injuries (Bush, 2000). In the weeks to months following the trauma, the synovial folds are likely to undergo fat necrosis and the formation of a fibrous 'scar' tissue which will also contribute to changes in signal intensity (Sampson, 2007). In the months to years post-trauma, it may be possible to demonstrate the presence of a hemosiderin artefact using MR imaging (Bush, 2000; Sampson, 2007). The FOLD/FAT and FOLD/FLUID signal intensity ratios provide an objective method of detecting signal intensity changes caused by synovial fold bruising following traumatic injury.

Synovial fold volume and the relative measures of adipose tissue (FOLD/FAT ratio) using T1-weighted images and fluid (FOLD/FLUID ratio) using T2-weighted images have the potential to make an original and significant contribution to identifying injuries to the synovial folds, particularly those that result from trauma such as whiplash. The ability to identify a pathoanatomical lesion following whiplash injury could lend itself to the development of diagnostic criteria that could ensure appropriate treatment and management and facilitate the identification of patients who are most susceptible to chronicity.

Rheumatoid arthritis of the upper cervical spine can cause debilitating neck pain and headache (Fujiwara et al., 2000). Currently pain relief can be obtained with anaesthetic

211

injections performed under fluoroscopic guidance (Sampson, 2007). In the future it may be possible to perform MRI-guided injections into the synovial folds, which may be the pain source, and/or joint cavity. Therefore the investigation of changes in synovial fold volume in patients with rheumatoid arthritis using MRI may facilitate the early detection of this disease and may be useful in monitoring disease progression and responses to therapy.

The quantification of synovitis using MRI has been used for the diagnosis of rheumatoid arthritis affecting the peripheral joints (Ostergaard et al., 1996; Tehranzadeh et al., 2003; Farrant et al., 2007). The ability to detect rheumatoid arthritis affecting the lateral atlanto-axial joints using the quantification of synovial fold volume from MR images may be useful in the early detection of rheumatoid arthritis affecting the cervical spine. One of the consequences of rheumatoid arthritis affecting the upper cervical spine is instability of the median atlanto-axial joint. Correlation between the rheumatoid changes affecting the lateral atlanto-axial synovial folds and the median atlanto-axial joint may be useful for detecting and/or monitoring the progression of atlanto-axial instability.

The ability to visualise directly the synovial folds *in vivo* also provides an opportunity to investigate the potential role of the synovial folds in torticollis and non-traumatic neck pain. The hypothesised mechanisms of synovial fold involvement in torticollis and neck pain (i.e. ENtrapment, EXtrapment, adhesion formation and tears) could be tested for the first time by non-invasive means. Knowledge of the normal disposition, shape and size of the synovial folds determined in the present study could be used as a basis for identifying changes in the synovial folds of patients with torticollis and neck pain. Furthermore the hypothesised effects of spinal manipulation upon the synovial folds in patients with torticollis and neck pain could be investigated.

This study presents normative values for the morphometry of the synovial folds, obtained from a range of methods, that can be used in future studies as baseline anatomical data against which the role of the synovial folds in patients with neck pain and disability can be investigated. Future research on a range of asymptomatic volunteers, using the techniques established in the present study, should follow to provide further anatomical data on age- and gender-related variations across the whole population, and further work is required to determine whether these same relationships

between physical and synovial fold dimensions exist in male subjects and subjects of more advanced age. It may be possible with results from future studies to estimate the dimensions of the synovial fold from factors of physical size. Future study of cervical pathology using these normative values may also enable the development of a grading system that could be used clinically for the diagnosis of synovial fold disorders.

The results of the present study indicate that synovial fold volume is related to physical anthropometrics. In female subjects aged 24 to 38 years, the synovial fold volume decreased in association with increasing body mass and body mass index, decreasing height and shorter and thicker necks. Larger synovial folds were associated with a greater range of cervical spine rotation and flexion-extension

Table 7.1 presents the synthesis of normative data of cervical spines collected in this study through anatomical and MRI techniques. Scrutinisation of the table enables the common variation of normative morphometry to be seen.

Table 7.1. Summary of ventral and dorsal synovial fold volume (mm^3) at the right and left lateral atlanto-axial joints quantified using *in vitro* anatomic and *in vivo* MRI techniques in the present study.

Median (range) Mean (SD)	Synovial fold volume (mm^3)			
	Right ventral synovial fold	Right dorsal synovial fold	Left ventral synovial fold	Left dorsal synovial fold
Cadavers aged 75-102 years (mean 84.44 years, SD 9.22 years)				
Females (n=6)	40.90 (26.68-82.75) 48.68 (22.28)	16.28 (8.49-29.38) 18.24 (9.05)	49.68 (30.03-105.07) 54.11 (27.41)	32.30 (11.32-65.60) 33.94 (17.72)
Males (n=3)	58.58 (33.12-114.91) 68.87 (41.85)	34.16 (25.88-64.48) 41.51 (20.32)	61.29 (46.90-64.38) 57.53 (9.33)	42.12 (35.98-50.68) 42.93 (7.38)
All subjects (n=9)	46.67 (26.68-114.91) 55.41 (29.16)	25.88 (8.49-64.48) 26.00 (17.02)	52.36 (30.03-105.07) 55.25 (22.23)	35.15 (11.32-65.60) 36.94 (15.17)
Volunteers aged 25 to 47 years (mean 32.13 years, SD 6.94 years)				
Females (n=4)	106.78 (86.18-129.06) 107.20 (18.32)	89.08 (66.66-96.94) 85.44 (13.28)	98.30 (79.26-115.85) 97.93 (20.54)	64.76 (47.31-89.82) 66.66 (17.55)
Males (n=4)	83.16 (65.15-175.99) 101.86 (51.43)	73.42 (69.57-83.55) 74.99 (6.48)	89.16 (51.50-113.86) 85.92 (27.82)	49.23 (30.29-66.24) 48.75 (14.71)
All subjects (n=8)	98.67 (65.15-175.99) 104.53 (35.85)	80.00 (66.66-96.94) 80.21 (11.17)	91.57 (51.50-115.85) 91.92 (23.53)	56.67 (30.29-89.82) 57.71 (17.79)
Female volunteers aged 24 to 38 years (mean 29.2, SD 4.69 years)				
All subjects (n=10)	82.78 (50.81-145.51) 94.32 (36.62)	73.14 (49.97-107.79) 74.79 (18.96)	71.65 (34.90-152.27) 75.34 (31.77)	58.62 (23.85-97.51) 60.37 (24.85)

There was considerable variation in the dimensions of the synovial folds of the lateral atlanto-axial joints between individuals in this study. Asymmetry affecting the synovial folds was common but followed a general trend with right and left ventral synovial folds typically larger in size and composed of more adipose tissue than right and left dorsal synovial folds, respectively.

In the defined age ranges studied, no correlation between age and synovial fold volume was evident. The adipose content of the synovial folds decreased in association with increasing age. The differences in synovial fold volume between male and female subjects were not consistent. However, the same pattern of synovial fold asymmetry was consistently observed in males and females, i.e. right and left ventral synovial folds were larger than right and left dorsal synovial folds, respectively. The synovial folds of male subjects contained a higher proportion of adipose tissue compared to female subjects.

In conclusion the techniques developed and verified in the present study provide, for the first time, a methodology by which the normal morphology of the synovial folds both *in vivo* and *in vitro* can be quantified precisely and objectively.

The techniques developed have been shown to be suitably precise for the determination of normal variations affecting the synovial folds and changes in synovial fold size caused by rheumatoid arthritis. The accuracy and precision offered by the MRI technique is suitable for the investigation of potential changes in morphology affecting the synovial folds in patients with neck pain and disability. The anatomical technique is suitable for investigating changes in the synovial fold morphometry of cadavers with a history of cervical spine disorders.

APPENDIX 1

Table A1.1 A summary of published experimental studies that have studied the intra-articular synovial folds of the cervical spine.

Study	Specimens (number of specimens)	Spinal levels	Investigative techniques				Age [mean] (years)	Gender male ♂ female♀
			Gross	Histology	Neural	Imaging		
Bland and Boushey, 1990	Fixed (171)	O/C1-C7/T1	√	√	X	X	-	-
Chang et al., 1992	Fresh (9)	C1/C2	√	√	X	X	64-96 [77]	4♂ 5♀
*De Marchi, 1963	Fixed (20)	Whole spine	√	√	X	X	Fetus Adult	ND
*Dorr, 1958	ND (6)	Whole spine	√	√	X	X	1-56	ND
Giles, 1986	Embalmed (4)	Cervical	X	√	X	X	40-60	ND
Fletcher et al., 1990	Embalmed (20)	C2/C3-C6/C7	√	√	X	√	10-86	12♂ 8♀
Friedrich et al., 2007	Fresh (1)	C3/C4 C4/C5 C6/C7	X	√	X	√	63	1♂
*Ibatullin et al., 1987	ND (35)	O/C1-C1/C2	√	√	X	X	Fetus Child Adult	ND
Inami et al., 2000	Embalmed (20)	C2/C3-C6/C7	√	√	X	X	42-94	ND
Inami et al., 2001	Surgical (10 SF)	ND	-	√	√	X	32-64	ND
Kawabe et al., 1989	ND (29)	C1/C2 O/C1	ND	√	X	X	0-3.4 50-91	ND
*Kos et al., 2002	ND (20)	O/C1-L5/S1	√	√	X	X	20-80	ND
Mercer and Bogduk, 1993	Embalmed (15)	O/C1-C7/T1	√	√	X	X	≥65	ND
*Schmincke and Santo, 1932	ND	Cervical	√	√	X	X	Fetus Child Adult	ND
Schonstrom et al., 1993	Fresh (41[+]) Embalmed (10)	C1/C2	√	X	X	X	2-82	39♂ 12♀
Tang et al., 2007	Embalmed (30 child, 20 adult)	O/C1 C1/C2	√	√	X	X	2-11 42-80	13♂17♀ 11♂9♀
Taylor and Taylor, 1996	Fresh 180 (109[+])	O/C1-C7/T1	√	X	X	Xray	0-89	74♂[+] 35♀[+]
*Tondury, 1940	ND (13)	Whole spine	√	√	X	X	22-45 + Fetus + Child	ND
Yu et al., 1987	Fresh (8) Embalmed (2)	C1/C2-C6/C7	√	√	X	MRI	10-69	ND
*Zaccheo and Reale, 1956	(20)	Whole spine	√	√	X	X	Fetus Child Adult	ND

ND – not described; * non-English literature; SF – synovial fold; [+]blunt trauma fatalities; Gross – study of the gross morphology; Neural – study of the innervation.

APPENDIX 2

Table A2.1. Synovial fold cross-sectional area measurements (n=143) made using two different measurement methods, the automated computer-assisted technique (auto-CAT) and the manual computer-assisted technique (manual-CAT) from 10.5 cervical spines (22 lateral atlanto-axial joints). Known quantities of systematic bias (+2mm^2 fixed bias, x2mm^2 proportional bias and +2x2mm^2 fixed and proportional bias), random error (RE) and heteroscedasticity/proportional error (PE) have been added to the data sets.

Section	Auto-CAT	Manual-CAT	Systematic Bias			Random Error		Heteroscedasticity[†]	
			Manual-CAT	Manual-CAT	Manual-CAT	Auto-CAT	Manual-CAT	Auto-CAT	Manual-CAT
			+2	x2	+2x2	+RE	+RE		+PE
1	6.60	6.97	8.97	13.93	15.93	6.29	6.84	0.16	-0.82
2	5.72	6.05	8.05	12.10	14.10	3.93	9.46	0.22	0.21
3	4.54	4.72	6.72	9.43	11.43	2.79	5.90	0.37	-0.65
4	2.68	2.59	4.59	5.18	7.18	3.93	-0.29	0.39	0.40
5	8.15	8.32	10.32	16.65	18.65	7.68	10.47	0.40	0.40
6	3.42	3.62	5.62	7.23	9.23	4.10	1.80	0.47	-0.54
7	3.59	3.63	5.63	7.26	9.26	3.31	3.43	0.52	0.53
8	0.47	0.46	2.46	0.91	2.91	-1.07	0.89	0.52	-0.44
9	2.65	2.66	4.66	5.32	7.32	1.99	2.30	0.62	0.64
10	4.83	4.88	6.88	9.76	11.76	5.61	6.06	0.63	0.61
11	1.69	1.74	3.74	3.49	5.49	1.35	4.21	0.66	-0.37
12	3.07	3.21	5.21	6.42	8.42	0.45	2.26	0.71	0.72
13	4.86	4.96	6.96	9.91	11.91	5.14	7.64	0.81	-0.15
14	3.12	3.21	5.21	6.42	8.42	3.70	3.68	0.82	0.90
15	5.64	5.67	7.67	11.34	13.34	5.60	8.04	0.84	0.86
16	9.17	9.20	11.20	18.41	20.41	12.72	11.92	0.90	3.00
17	5.62	5.95	7.95	11.89	13.89	4.12	6.68	1.10	-0.81
18	21.94	22.15	24.15	44.30	46.30	22.03	21.07	1.11	3.21
19	21.53	22.00	24.00	44.00	46.00	21.94	21.76	1.13	3.16
20	2.87	2.97	4.97	5.94	7.94	4.10	1.65	1.14	-0.75
21	3.77	3.63	5.63	7.26	9.26	1.81	3.13	1.20	3.18
22	5.32	5.36	7.36	10.73	12.73	5.41	5.27	1.22	-0.72
23	1.13	1.16	3.16	2.33	4.33	3.38	2.34	1.29	3.32
24	0.71	0.72	2.72	1.44	3.44	2.93	-1.48	1.32	3.41
25	10.96	11.28	13.28	22.55	24.55	8.96	13.50	1.37	-0.55
26	5.78	5.78	7.78	11.55	13.55	7.00	7.08	1.43	3.41
27	6.05	6.07	8.07	12.14	14.14	6.42	5.59	1.45	-0.45
28	1.45	1.55	3.55	3.10	5.10	-0.34	4.01	1.63	3.67
29	5.54	5.93	7.93	11.85	13.85	6.13	4.36	1.69	3.74
30	8.68	8.77	10.77	17.53	19.53	4.91	7.93	1.76	-0.17
31	2.47	2.57	4.57	5.14	7.14	2.40	5.09	1.76	5.83
32	9.91	10.07	12.07	20.15	22.15	8.23	12.18	1.85	4.92
33	15.21	15.41	17.41	30.83	32.83	11.32	14.76	1.88	2.95
34	9.63	9.51	11.51	19.02	21.02	8.21	9.69	1.94	6.00
35	9.34	9.66	11.66	19.33	21.33	11.24	8.25	1.95	-1.96
36	11.06	11.00	13.00	22.00	24.00	8.04	12.73	2.08	6.06
37	5.00	4.92	6.92	9.83	11.83	3.97	6.10	2.10	5.15
38	2.37	2.42	4.42	4.84	6.84	-0.05	0.03	2.15	3.20
39	8.82	9.05	11.05	18.10	20.10	10.34	10.38	2.17	6.17
40	4.37	4.53	6.53	9.05	11.05	4.37	5.08	2.24	-1.66
41	2.15	2.20	4.20	4.40	6.40	-3.33	3.14	2.35	6.45
42	5.20	5.31	7.31	10.62	12.62	5.93	3.99	2.37	5.42
43	12.18	12.33	14.33	24.67	26.67	10.20	13.47	2.40	3.50
44	4.83	4.69	6.69	9.38	11.38	6.36	4.86	2.43	6.39
45	3.16	3.16	5.16	6.32	8.32	0.42	1.72	2.47	-1.43
46	0.90	1.00	3.00	1.99	3.99	2.17	3.62	2.50	2.50
47	3.82	4.11	6.11	8.21	10.21	0.04	2.13	2.55	6.65

			Systematic Bias			Random Error		Heteroscedasticity[†]	
Section	Auto-CAT	Manual-CAT	Manual-CAT +2	Manual-CAT x2	Manual-CAT +2x2	Auto-CAT +RE	Manual-CAT +RE	Auto-CAT	Manual-CAT +PE
48	4.99	5.62	7.62	11.25	13.25	5.10	7.98	2.58	5.72
49	8.64	9.17	11.17	18.33	20.33	9.95	11.10	2.62	0.73
50	6.89	6.98	8.98	13.97	15.97	4.10	6.45	2.65	-5.34
51	7.00	6.67	8.67	13.35	15.35	9.56	6.42	2.68	2.59
52	9.35	9.60	11.60	19.19	21.19	7.75	9.10	2.68	6.54
53	15.06	15.05	17.05	30.10	32.10	13.11	15.16	2.76	5.95
54	8.81	8.67	10.67	17.35	19.35	9.26	9.61	2.77	0.87
55	4.18	3.97	5.97	7.94	9.94	4.33	4.98	2.80	-5.12
56	3.08	3.10	5.10	6.21	8.21	5.11	7.24	2.82	2.78
57	5.38	5.35	7.35	10.69	12.69	6.75	6.71	2.86	6.94
58	3.17	3.20	5.20	6.40	8.40	4.16	2.40	2.87	5.97
59	4.02	3.95	5.95	7.91	9.91	6.69	2.71	3.04	1.07
60	2.82	2.78	4.78	5.56	7.56	3.44	3.76	3.07	-4.79
61	0.82	0.90	2.90	1.79	3.79	4.24	2.44	3.08	-0.90
62	3.27	3.31	5.31	6.62	8.62	0.64	5.63	3.08	10.39
63	2.40	2.50	4.50	5.01	7.01	2.48	5.05	3.12	4.21
64	4.35	4.45	6.45	8.90	10.90	3.87	4.38	3.16	13.16
65	0.22	0.21	2.21	0.42	2.42	-0.84	-0.66	3.17	20.20
66	2.86	2.94	4.94	5.89	7.89	3.32	1.35	3.23	-0.68
67	2.55	2.65	4.65	5.29	7.29	3.05	2.19	3.27	10.31
68	1.88	1.95	3.95	3.91	5.91	-0.23	0.81	3.36	4.22
69	4.19	4.36	6.36	8.72	10.72	4.62	7.67	3.38	13.40
70	3.04	3.07	5.07	6.14	8.14	1.70	2.05	3.42	20.46
71	3.36	3.22	5.22	6.44	8.44	2.31	1.61	3.42	-0.38
72	4.14	4.14	6.14	8.28	10.28	-0.10	2.73	3.42	10.62
73	3.71	3.75	5.75	7.50	9.50	2.85	2.57	3.54	4.64
74	6.76	6.95	8.95	13.91	15.91	6.29	6.91	3.59	13.63
75	2.68	2.54	4.54	5.09	7.09	4.57	0.38	3.61	20.58
76	8.34	8.51	10.51	17.02	19.02	5.82	7.26	3.71	11.75
77	3.54	3.64	5.64	7.29	9.29	5.06	7.53	3.77	11.63
78	4.47	4.53	6.53	9.05	11.05	3.59	5.26	3.82	-0.89
79	2.76	2.95	4.95	5.90	7.90	3.70	2.74	3.86	17.06
80	1.22	1.28	3.28	2.56	4.56	1.02	1.36	3.99	5.15
81	2.17	2.17	4.17	4.34	6.34	2.61	2.52	4.02	11.95
82	5.05	5.22	7.22	10.44	12.44	3.76	4.88	4.14	12.14
83	3.23	3.32	5.32	6.64	8.64	3.93	-0.66	4.16	-0.74
84	1.76	1.83	3.83	3.66	5.66	0.69	0.99	4.18	16.97
85	2.77	2.87	4.87	5.75	7.75	4.44	0.39	4.19	5.36
86	6.86	6.90	8.90	13.80	15.80	5.85	3.90	4.35	12.45
87	3.42	3.46	5.46	6.93	8.93	3.91	3.20	4.37	12.53
88	6.37	6.68	8.68	13.37	15.37	8.00	9.44	4.47	-0.47
89	7.11	7.26	9.26	14.53	16.53	3.72	6.78	4.54	17.72
90	9.18	9.71	11.71	19.42	21.42	10.13	10.42	4.79	6.05
91	21.63	22.32	24.32	44.64	46.64	19.86	22.34	4.83	1.88
92	6.98	7.15	9.15	14.29	16.29	5.92	5.74	4.83	-14.31
93	17.79	17.37	19.37	34.73	36.73	18.91	18.51	4.86	10.96
94	9.66	9.81	11.81	19.62	21.62	13.65	8.14	4.99	-9.38
95	3.99	4.15	6.15	8.30	10.30	3.11	0.30	5.00	7.92
96	2.80	2.88	4.88	5.76	7.76	2.26	2.31	5.05	2.22
97	0.81	0.85	2.85	1.69	3.69	-0.46	0.31	5.19	-14.09
98	0.39	0.40	2.40	0.80	2.80	-0.41	-2.62	5.20	11.31
99	1.63	1.67	3.67	3.34	5.34	-0.13	2.51	5.32	-9.64
100	3.42	3.62	5.62	7.25	9.25	5.54	3.48	5.37	8.34

Section	Auto-CAT	Manual-CAT	Systematic Bias			Random Error		Heteroscedasticity†	
			Manual-CAT +2	Manual-CAT x2	Manual-CAT +2x2	Auto-CAT +RE	Manual-CAT +RE	Auto-CAT	Manual-CAT +PE
101	1.95	2.04	4.04	4.07	6.07	0.63	-1.44	5.38	2.35
102	5.19	4.91	6.91	9.81	11.81	5.49	4.80	5.54	-13.07
103	2.58	2.72	4.72	5.44	7.44	0.64	0.65	5.57	11.85
104	2.62	2.73	4.73	5.46	7.46	0.59	1.36	5.62	-9.05
105	4.16	4.26	6.26	8.52	10.52	0.30	7.28	5.64	8.67
106	3.38	3.40	5.40	6.81	8.81	3.59	0.98	5.72	12.05
107	5.37	5.34	7.34	10.69	12.69	3.75	7.59	5.78	4.78
108	2.35	2.45	4.45	4.90	6.90	0.83	1.44	6.05	3.07
109	0.62	0.64	2.64	1.28	3.28	2.23	-0.10	6.37	12.68
110	2.08	2.06	4.06	4.12	6.12	2.40	2.60	6.60	20.97
111	1.20	1.18	3.18	2.37	4.37	-4.27	0.71	6.74	12.60
112	0.37	0.35	2.35	0.70	2.70	-0.91	-2.07	6.76	5.95
113	2.50	2.50	4.50	5.00	7.00	1.06	4.47	6.86	3.90
114	1.32	1.41	3.41	2.81	4.81	0.61	2.76	6.89	12.98
115	7.16	7.42	9.42	14.84	16.84	5.04	7.80	6.98	21.15
116	4.79	5.05	7.05	10.11	12.11	5.66	1.26	7.00	12.67
117	3.86	4.06	6.06	8.11	10.11	0.82	1.46	7.11	6.26
118	1.14	1.25	3.25	2.50	4.50	1.53	-3.19	7.16	4.42
119	3.08	3.39	5.39	6.78	8.78	2.22	4.23	7.99	13.72
120	9.76	10.42	12.42	20.83	22.83	6.58	12.58	8.15	22.32
121	9.02	9.19	11.19	18.38	20.38	9.25	9.90	8.34	2.51
122	0.52	0.53	2.53	1.05	3.05	-0.97	2.89	8.64	13.17
123	1.43	1.41	3.41	2.83	4.83	3.96	2.88	8.68	5.77
124	1.10	1.19	3.19	2.38	4.38	5.15	3.92	8.81	-14.33
125	5.57	5.85	7.85	11.71	13.71	3.63	6.62	8.82	4.05
126	2.43	2.39	4.39	4.78	6.78	6.22	4.19	9.02	3.19
127	7.99	7.72	9.72	15.44	17.44	8.51	11.38	9.17	13.20
128	2.24	2.34	4.34	4.68	6.68	2.86	0.10	9.18	6.71
129	1.37	1.45	3.45	2.91	4.91	-0.91	1.37	9.34	-13.34
130	0.66	0.63	2.63	1.25	3.25	0.10	-0.21	9.35	4.60
131	0.84	0.86	2.86	1.71	3.71	-0.95	4.91	9.63	3.51
132	1.94	2.00	4.00	4.01	6.01	4.29	0.21	9.66	13.81
133	0.63	0.61	2.61	1.23	3.23	0.78	-1.11	9.76	7.42
134	3.61	3.58	5.58	7.16	9.16	2.78	0.71	9.91	-12.93
135	0.16	0.18	2.18	0.35	2.35	-2.97	0.57	10.96	6.28
136	0.52	0.56	2.56	1.11	3.11	-0.14	0.10	11.06	9.00
137	2.10	2.15	4.15	4.30	6.30	4.13	3.85	12.18	9.33
138	1.29	1.32	3.32	2.64	4.64	2.22	-0.71	15.06	3.05
139	1.76	1.83	3.83	3.66	5.66	0.67	1.91	15.21	30.41
140	1.11	1.21	3.21	2.42	4.42	0.38	0.72	17.79	-13.63
141	6.74	6.60	8.60	13.20	15.20	9.76	5.20	21.53	20.00
142	1.85	1.92	3.92	3.85	5.85	-1.98	2.45	21.63	19.32
143	0.40	0.40	2.40	0.80	2.80	-0.37	0.91	21.94	10.15
n	143	143	143	143	143	143	143	143	143
Mean	4.68	4.77	6.77	9.54	11.54	4.29	4.81	4.68	4.88
SD	4.09	4.15	4.15	8.29	8.29	4.42	4.70	4.09	7.90
Maximum	21.94	22.32	24.32	44.64	46.64	22.03	22.34	21.94	30.41
Minimum	0.16	0.18	2.18	0.35	2.35	-4.27	-3.19	0.16	-14.33

†Data arranged in ascending order (minimum value to maximum value) based on auto-CAT values

Table A2.2. Synovial fold cross-sectional area measurements made using two different measurement methods, the automated computer-assisted technique (auto-CAT) and the manual computer-assisted technique (manual-CAT). The data set auto-CAT+random error (RE) and manual-CAT+random error (RE) measured from 143 sections (Table A2.1) was split into two ranges using the auto-CAT+RE values (2 to 8.5mm^2 and 0 to 22mm^2) to form two new data sets of equal size (n=54).

Section	Range: 2 to 8.5mm^2		Range: 0 to 22mm^2	
	Auto-CAT +RE	Manual-CAT +RE	Auto-CAT +RE	Manual-CAT +PE
1	3.79	5.90	0.38	1.72
2	3.59	5.26	10.45	12.26
3	4.63	6.62	0.59	2.36
4	3.72	7.78	12.61	12.76
5	3.75	7.59	10.64	12.63
6	5.76	4.88	0.69	0.99
7	3.87	4.38	0.83	2.44
8	2.00	8.46	1.02	2.36
9	3.97	6.10	1.70	3.05
10	4.10	6.45	2.17	3.62
11	4.12	6.68	2.26	4.31
12	4.13	3.85	2.40	2.60
13	4.33	4.98	2.78	1.71
14	5.37	5.08	2.86	0.10
15	4.62	7.67	13.32	11.35
16	4.91	7.93	3.44	3.76
17	5.04	7.80	13.59	15.26
18	5.06	7.53	3.59	0.98
19	5.10	7.98	3.70	3.68
20	5.11	7.24	3.76	4.88
21	4.17	3.62	3.87	4.38
22	6.41	5.27	7.93	9.46
23	5.49	4.80	14.10	16.45
24	5.60	8.04	4.10	3.80
25	5.61	6.06	4.10	1.65
26	5.82	7.26	4.16	2.40
27	5.85	3.90	12.29	11.21
28	6.92	5.74	14.37	15.08
29	6.13	4.36	14.91	17.93
30	6.22	4.19	5.10	7.98
31	6.59	6.91	5.11	7.24
32	7.29	6.84	15.15	13.92
33	6.36	4.86	5.41	5.27
34	7.42	5.59	5.49	4.80
35	5.58	7.58	15.54	13.48
36	6.69	2.71	5.61	6.06
37	6.75	6.71	5.66	1.26
38	8.00	7.08	5.82	7.26
39	3.48	5.05	5.92	5.74
40	3.70	3.68	5.93	3.99
41	4.44	3.76	6.22	4.19
42	4.61	2.52	16.29	16.91
43	2.22	4.23	6.36	4.86
44	5.10	2.00	6.58	12.58
45	4.24	2.44	7.00	7.08
46	4.16	2.40	7.75	9.10
47	3.96	2.88	18.00	19.44
48	4.70	2.74	9.04	12.73
49	3.85	2.57	8.23	12.18

	Range: 2 to 8.5mm^2		Range: 0 to 22mm^2	
Section	Auto-CAT +RE	Manual-CAT +RE	Auto-CAT	Manual-CAT +PE
50	3.38	2.34	9.26	9.61
51	4.05	2.19	10.13	10.42
52	4.31	3.43	12.72	11.92
53	3.26	2.31	13.65	8.14
54	2.40	5.09	22.03	22.07
n	54	54	54	54
Mean	4.85	5.21	7.53	7.84
SD	1.32	1.94	5.18	5.50
Maximum	8.00	8.46	22.03	22.07
Minimum	2.00	2.00	0.38	0.10

APPENDIX 3

Limits of agreement method with repeated measures and equal numbers of replicates

The method agreement data was combined with the repeatability and test-retest precision data to calculate the method agreement with repeated measures between the auto-CAT and manual-CAT, for synovial fold cross-sectional area and volume, using the Bland and Altman limits of agreement method, with repeated measures.

A3.1 Data analysis for limits of agreement with repeated measures and equal numbers of replicates

The limits of agreement for method agreement (between the auto-CAT and the manual-CAT) was calculated with repeated measures (repeatability and test-retest precision) for synovial fold cross-sectional area and volume. The mean of the replicate measurements (i.e. original measurement and replicate measurement) by each method on each section (synovial fold cross-sectional area) and each articulation (synovial fold volume) were calculated. These pairs of means (auto-CAT mean and manual-CAT mean) were then used to compare the measurement methods using the limits of agreement method.

The difference (i.e. auto-CAT mean – manual-CAT mean) and the mean ([auto-CAT mean + manual-CAT mean]/2) of the auto-CAT and manual-CAT measurements were calculated for each section (synovial fold cross-sectional area) and for each articulation (synovial fold volume). The mean difference (d) and the standard deviation of the differences (s_d) were then determined. The assumptions of the limits of agreement method were verified (Section 4.2.3iii, Chapter 4) and if there was a relationship between the difference and the mean the modified regression approach was performed (Section 4.2.3iii, Chapter 4).

Repeated, instead of single, measurements does not affect the estimate of the bias (i.e. the mean difference, d) but the standard deviation of the differences (i.e. s_d) will be too small because some of the effect of repeated measurement error has been removed. To correct for this, the adjusted (or corrected) standard deviation of the differences (s_c) was calculated as follows:

$$s_c = \sqrt{s_d^2 + (s_{Aw}^2/2) + (s_{Mw}^2/2)}$$

(A3.1)

where s_d^2 (the square of the standard deviation of the differences) represents the observed variance of the differences between the within-subject means. s_w^2 represents the within-subject variance of repeated measurements for each measurement method, thus s_{Aw}^2 is the within-subject variance of the auto-CAT measurement method and s_{Mw}^2 is the within-subject variance of the manual-CAT measurement method. s_w^2 is the mean of the variances (i.e. the squares of the standard deviations) of the original and replicate measurements for each measurement method

The 95% limits of agreement were calculated from the mean difference $\pm$ 1.96 adjusted standard deviations (i.e. $d \pm 1.96 s_c$).

An approximate standard error and confidence interval for these limits of agreement was calculated as follows. The standard error for the limits of agreement (SE($d \pm$ 1.96s_c)):

$$\text{SE}(d \pm 1.96 s_c) = \sqrt{s_c^2/n + 1.96^2/2 s_c^2 \ (s_d^4/\text{n-1} + s_{Aw}^4/4n + s_{Mw}^4/4n)} \qquad (A3.2)$$

The 95% confidence interval for the upper and lower limits of agreement was given by:
95% confidence interval for the upper limits of agreement

$$d + 1.96 s_c \pm t\text{SE}(d \pm 1.96 s_c) \qquad (A3.3)$$

95% confidence interval for the lower limits of agreement

$$d - 1.96 s_c \pm t\text{SE}(d \pm 1.96 s_c) \qquad (A3.4)$$

where the value for t was determined by finding the appropriate point of the t distribution with n-1 degrees of freedom.

A3.2i Results of method agreement with repeated measures between the auto-CAT and the manual-CAT (repeatability)

The results of the limits of agreement analysis using repeated measurements, for the measurement of synovial fold cross-sectional area (repeatability n=53; test-retest precision n=66) and volume (repeatability n=14; test-retest precision n=10) between the auto-CAT and the manual-CAT are shown in Table A3.1.

94% and 100% of plotted points were within the limits of agreement for the synovial fold cross-sectional area data (Figures A3.1.A) and volume data (Figure A3.3.A), respectively. The scatter diagram and Pearson's correlation coefficient for the cross-

sectional area data (Figure A3.1.A) indicated the presence of heteroscedasticity and proportional bias. For the volume data, an increasing between-measurement difference as the magnitude of the measurement increased, was evident on the scatter diagram and the difference was negatively correlated to the mean thus demonstrating the presence of proportional bias (Figure A3.3.A). Therefore the modified regression approach was performed for both the cross-sectional area and volume data (Figures A3.1.A and A3.3.A).

A3.2ii Results of method agreement with repeated measures between the auto-CAT and the manual-CAT (test-retest precision)

All plotted points were within the limits of agreement (Figures A3.2.A and A3.4.A). The scatter diagrams and Pearson's correlation coefficient indicated the presence of both heteroscedasticity and proportional bias for the cross-sectional area data (Figure A.3.2.A) and proportional bias alone for the volume data (Figure A3.4.A), thus the modified regression approach was performed.

Table A3.1. Results of Bland and Altman analysis for method agreement with repeated measures for the measurement of intra-articular synovial fold (IASF) cross-sectional area (CSA) (mm^2) and volume (mm^3).

Comparison of two measurement methods: auto-CAT and manual-CAT

Method agreement (repeatability)

IASF Geometry	d	1.96s$_c$	SE(d)	95% CI(d)	s$_{EDw}^2$	s$_{MTw}^2$	95% LoA	SE(LoA)	95%CI lower LoA	95%CI upper LoA
CSA (mm^2)	-0.11	0.33	0.02	-0.14→ -0.08	0.006	0.008	-0.44→ 0.21	0.03	-0.50→ -0.38	0.15→ 0.27
Volume (mm^3)	-0.86	1.80	0.23	-1.27→ -0.35	0.17	0.07	-2.55→ 0.83	0.46	-3.36→ -1.73	0.02→ 1.64

Method agreement (test-retest precision)

IASF Geometry	d	1.96s$_c$	SE(d)	95% CI(d)	s$_{EDw}^2$	s$_{MTw}^2$	95% LoA	SE(LoA)	95%CI lower LoA	95%CI upper LoA
CSA (mm^2)	-0.10	0.47	0.02	-0.14→ -0.07	0.04	0.04	-0.58→ 0.38	0.04	-0.67→ -0.49	0.29→ 0.46
Volume (mm^3)	-0.88	1.90	0.31	-1.56→ -0.20	0.58	0.50	-2.78→ 1.02	0.40	-3.67→ -1.88	0.13→ 1.91
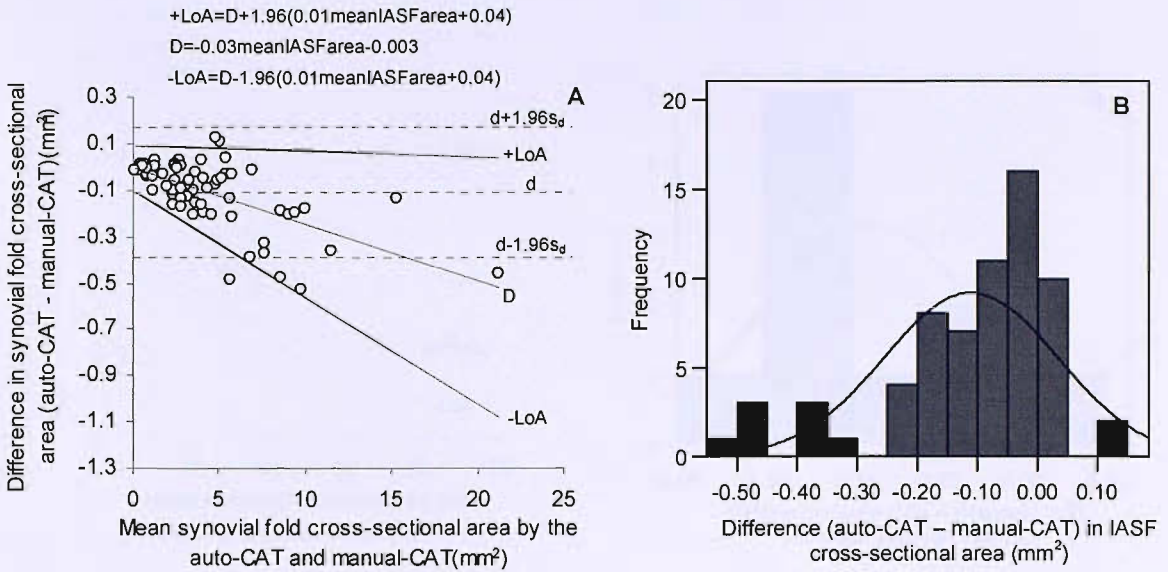
Figure A3.1.A. Difference against mean for intra-articular synovial fold (IASF) cross-sectional area (mm^2) measured by the auto-CAT and the manual-CAT (repeated measures, repeatability) (r =-.63, P=.000). B. Histogram of differences for IASF cross-sectional area (mm^2) measured by the auto-CAT and the manual-CAT (repeated measures, repeatability) (KS test P=.004).
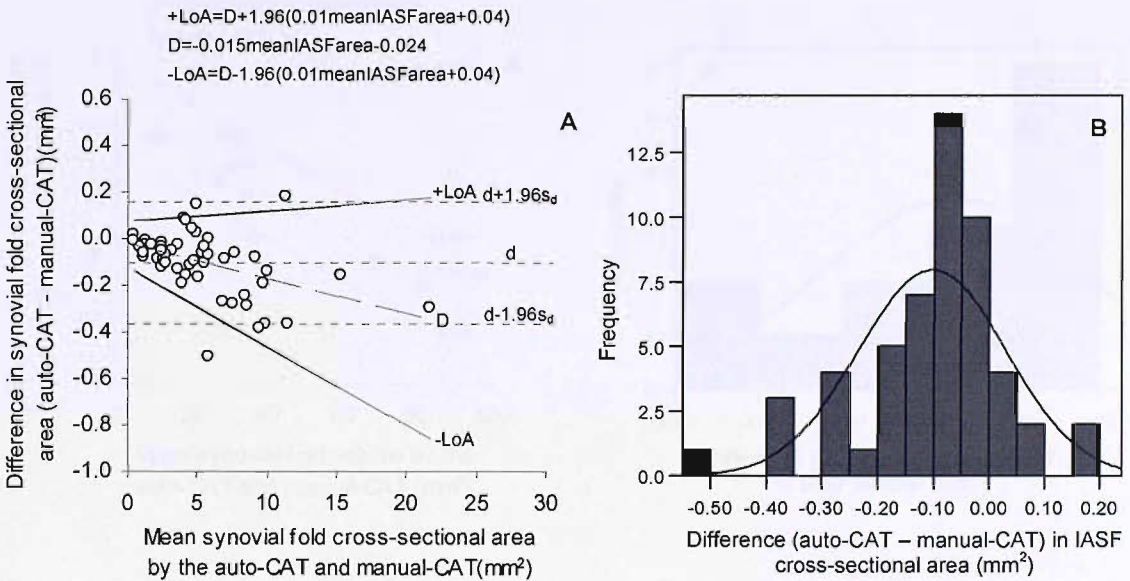
Figure A3.2.A. Difference against mean for intra-articular synovial fold (IASF) cross-sectional area (mm^2) measured by the auto-CAT and the manual-CAT (repeated measures, test-retest precision) (r =-.45, P=.001). B. Histogram of differences for IASF cross-sectional area (mm^2) measured by the auto-CAT and the manual-CAT (repeated measures, test-retest precision) (KS test P=.01).

224

+LoA=D+1.96*0.41

D = -0.02meanIASFvolume+0.01

-LoA=D-1.96*0.41
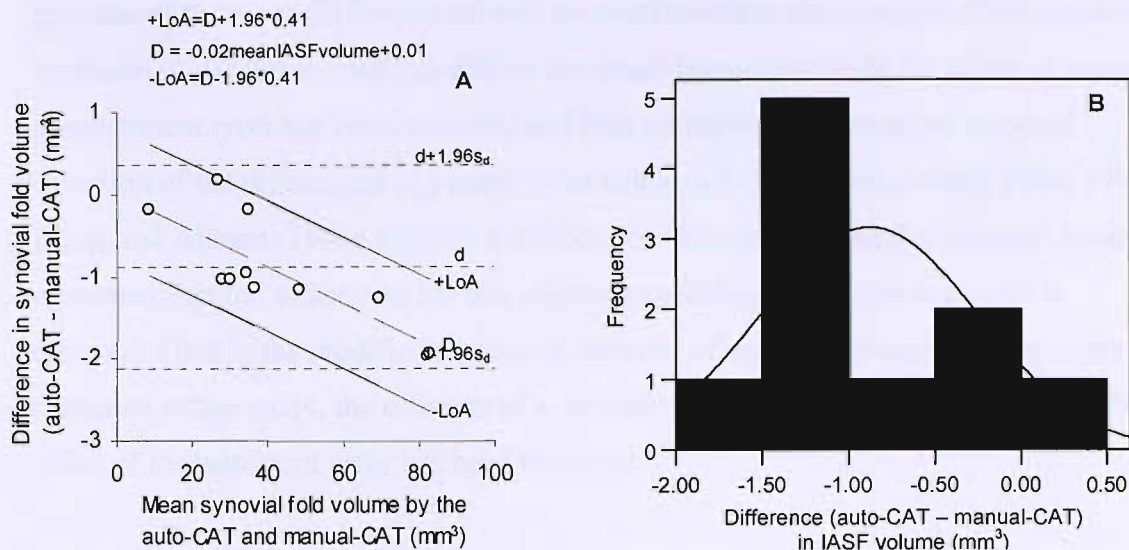
Figure A3.3.A. Difference against mean for intra-articular synovial fold (IASF) volume (mm^3) measured by the auto-CAT and the manual-CAT (repeated measures, repeatability) (r =-.89, P=.000). **B.** Histogram of differences for IASF volume (mm^3) measured by the manual-CAT and the auto-CAT (repeated measures, repeatability) (KS test P=.13).

+LoA=D+1.96*0.36

D = -0.03meanIASFvolume+0.33

-LoA=D-1.96*0.36
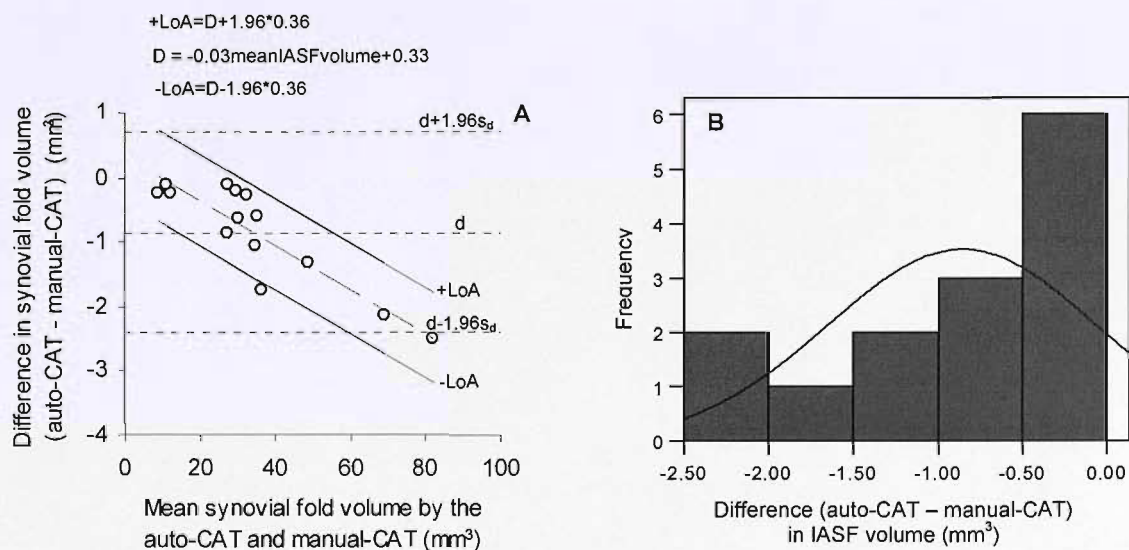
Figure A3.4.A. Difference against mean for intra-articular synovial fold (IASF) volume (mm^3) measured by the auto-CAT and the manual-CAT (repeated measures, test-retest precision) (r =-.76, P=.01). **B.** Histogram of differences for IASF volume (mm^3) measured by the auto-CAT and the manual-CAT (repeated measures, test-retest precision) (KS test P=.09).

A3.3 Discussion

Limits of agreement with repeated measures are more robust than those calculated with single measures because the precision of the method itself will affect its agreement with other measurement methods e.g. if one method has poor repeatability its agreement with another method is bound to be poor (Bland and Altman, 1999). As described in the methods section, when calculating limits of agreement with repeated measures the

estimate of the mean difference (d) will be unaffected but the estimate of the standard deviation of the differences (s_d) will be too small because some of the effect of repeated measurement error has been removed and thus an adjusted or corrected standard deviation of the differences (s_c) needs to be calculated (Bland and Altman 1986; 1999). Bland and Altman (1999) describe a method for calculating s_c for the 'normal' limits of agreement but fail to account for this when the modified regression approach is required. Thus in the modified regression analysis of method agreement using repeated measures in this study, the estimate of s_d is likely to be too small because some of the effect of measurement error has been removed.

APPENDIX 4

Coefficient of variation

The coefficient of variation is another often-quoted estimate of measurement precision. The (within subjects) coefficient of variation is the within subjects deviation (s_w) divided by the mean (of the two measurement methods or repeat measures) and is often multiplied by 100 to give a percentage. Using the method agreement data (auto-CAT and manual-CAT) for the measurement of synovial fold cross-sectional area (Table A1.1), the coefficient of variation is 0.13/4.73 = 0.028 or 2.8%. The problem with quoting the error as a percentage is that 2.8% of the smallest observation ($0.005mm^2$) will differ markedly from 2.8% of the largest observation ($0.625mm^2$) (Bruton et al., 2000; Bland, 2005). Therefore it has been suggested that this method of analysis should not be used to estimate precision if the interval is great compared to the size of the smallest observations and the error does not depend on the value of the measurement (Bruton et al., 2000; Bland, 2005). However, if the difference is proportional to the mean, this method is an appropriate method to determine precision following a logarithmic transformation of the data (Bland, 2005; Chinn, 1990).

References

AIRAKSINEN, O., BROX, J. I., CEDRASCHI, C., HILDEBRANDT, J., KLABER-MOFFETT, J., KOVACS, F., MANNION, A. F., REIS, S., STAAL, J. B., URSIN, H. & ZANOLI, G. (2006) Chapter 4. European guidelines for the management of chronic nonspecific low back pain. *Eur Spine J,* 15 Suppl 2, S192-300.

AKESON, W. H., AMIEL, D. & WOO, S. L. Y. (1980) Immobility effects on synovial joints. The pathomechanics of joint contracture. *Biorheology,* 17, 95-110.

ALTMAN, D. G. & BLAND, J. M. (1983) Measurement in medicine: the analysis of method comparison studies. *The Statistician,* 32, 307-317.

ALTMAN, D. G. & BLAND, J. M. (1995) Statistics notes: the normal distribution. *BMJ,* 310, 298.

AMIRI, M., JULL, G. & BULLOCK-SAXTON, J. (2003) Measuring range of active cervical rotation in a position of full head flexion using the 3D Fastrak measurement system: an intra-tester reliability study. *Man Ther,* 8, 176-9.

ANDARY, M. T., HALLGREN, R. C., GREENMAN, P. E. & RECHTIEN, J. J. (1998) Neurogenic atrophy of suboccipital muscles after a cervical injury: a case study. *Am J Phys Med Rehabil,* 77, 545-9.

ANDERSSON, G.B.J. & COCCHIARELLA (2000) *Guides to the Evaluation of Permanent Impairment 3rd ed.* Chicago: AMA Press.

ANDERSSON, H. I., EJLERTSSON, G., LEDEN, I. & ROSENBERG, C. (1993) Chronic pain in a geographically defined general population: studies of differences in age, gender, social class, and pain localization. *Clin J Pain,* 9, 174-82.

APRILL, C., AXINN, M. J. & BOGDUK, N. (2002) Occipital headaches stemming from the lateral atlanto-axial (C1-2) joint. *Cephalalgia,* 22, 15-22.

APRILL, C., DWYER, A. & BOGDUK, N. (1990) Cervical zygapophyseal joint pain patterns. II: A clinical evaluation. *Spine,* 15, 458-61.

ATKINSON, G. & NEVILL, A. M. (1998) Statistical methods for assessing measurement error (reliability) in variables relevant to sports medicine. *Sports Med,* 26, 217-38.

AVRAMOV, A. I., CAVANAUGH, J. M., OZAKTAY, C. A., GETCHELL, T. V. & KING, A. I. (1992) The effects of controlled mechanical loading on group-II, III, and IV afferent units from the lumbar facet joint and surrounding tissue. An in vitro study. *J Bone Joint Surg Am,* 74, 1464-71.

AWAYA, H., SCHWEITZER, M. E., FENG, S. A., KAMISHIMA, T., MARONE, P. J., FAROOKI, S., TRUDELL, D. J., HAGHIGHI, P. & RESNICK, D. L. (2001) Elbow synovial fold syndrome: MR imaging findings. *American Journal of Roentgenology,* 177, 1377-81.

BAKER WDE, C., THOMAS, T. G. & KIRKALDY-WILLIS, W. H. (1969) Changes in the cartilage of the posterior intervertebral joints after anterior fusion. *J Bone Joint Surg Br,* 51, 736-46.

BARNETT, C. H., DAVIES, D. V. & MACCONAILL, M. A. (1961) *Synovial Joints: Their Structure and Mechanics,* London, Longmans.

BARNSLEY, L., LORD, S. & BOGDUK, N. (1994) Whiplash injury. *Pain,* 58, 283-307.

BARNSLEY, L., LORD, S. M., WALLIS, B. J. & BOGDUK, N. (1995) The prevalence of chronic cervical zygapophysial joint pain after whiplash. *Spine,* 20, 20-5.

BASRAI, F. & AGHAZADEH, F. (2004) Effects of VDT monitor placement and single versus bifocal glasses on somatic discomfort and postural profiles in data entry tasks. *J Hum Ergol (Tokyo),* 33, 29-43.

BEAMAN, D. N., GRAZIANO, G. P., GLOVER, R. A., WOJTYS, E. M. & CHANG, V. (1993) Substance P innervation of lumbar spine facet joints. *Spine,* 18, 1044-9.

BENINI, A. (1979) Das kleine gelenk der lendenwirbelsaule. *Fortschr Med,* 97, 2103-2106.

BENJAMIN, M. & RALPHS, J. R. (1998) Fibrocartilage in tendons and ligaments--an adaptation to compressive load. *J Anat,* 193 (Pt 4), 481-94.

BENJAMIN, M., REDMAN, S., MILZ, S., BUTTNER, A., AMIN, A., MORIGGL, B., BRENNER, E., EMERY, P., MCGONAGLE, D. & BYDDER, G. (2004) Adipose tissue at entheses: the rheumatological implications of its distribution. A potential site of pain and stress. *Ann Rheum Dis,* 63, 1549-55.

BIEDERT, R.M., & SANCHIS-ALFONSO, V. (2002) Sources of anterior knee pain. *Clin Sports Med,* 21, 335-47.

BILGE, O. (2004) An anatomic and morphometric study of C2 nerve root ganglion and its corresponding foramen. *Spine,* 29, 495-9.

BINET, E.F., MORO, J.J., MARANGOLA, J.P., & HODGE, C.J. (1977) Cervical spine tomography in trauma. *Spine,* 2, 163-72.

BLAND, J. H. & BOUSHEY, D. R. (1990) Anatomy and physiology of the cervical spine. *Seminars in Arthritis and Rheumatism,* 20, 1-20.

BLAND, J. M. & ALTMAN, D. G. (1986) Statistical methods for assessing agreement between two methods of clinical measurement. *Lancet,* 1, 307-10.

BLAND, J. M. & ALTMAN, D. G. (1986) Statistical methods for assessing agreement between two methods of clinical measurement. *Lancet,* i, 307-310.

BLAND, J. M. & ALTMAN, D. G. (1990) A note on the use of the intraclass correlation coefficient in the evaluation of agreement between two methods of measurement. *Computers in Biology and Medicine,* 20, 337-40.

BLAND, J. M. & ALTMAN, D. G. (1995) Comparing methods of measurement: why plotting difference against standard method is misleading. *Lancet.,* 346, 1085-87.

BLAND, J. M. & ALTMAN, D. G. (1999) Measuring agreement in method comparison studies. *Stat Methods Med Res,* 8, 135-60.

BLAND, J. M. & ALTMAN, D. G. (2003) Applying the right statistics: analyses of measurement studies. *Ultrasound in Obstetrics and Gynecology,* 22, 85-93.

BLAND, M. (2005) *An introduction to medical statistics,* Oxford, Oxford University Press.

BLAND, J. M. (2005) *Frequently asked questions on the design and analysis of measurement studies.* Available from: http://www-users.york.ac.uk/~mb55/meas/comfaq.htm [Accessed 2005]

BOGDAN, R.J. (1985) Plicae syndrome of the knee. *J Am Podiatr Med Assoc,* 75, 377-81.

BOGDUK, N. (1982) The clinical anatomy of the cervical dorsal rami. *Spine,* 7, 319-30.

BOGDUK, N. (1992) The anatomical basis for cervicogenic headache. *J Manipulative Physiol Ther,* 15, 67-70.

BOGDUK, N. (1999) The neck. *Baillieres Best Pract Res Clin Rheumatol,* 13, 261-285.

BOGDUK, N. (2001) Cervicogenic headache: anatomic basis and pathophysiologic mechanisms. *Curr Pain Headache Rep,* 5, 382-6.

BOGDUK, N. (2003) The anatomy and pathophysiology of neck pain. *Phys Med Rehabil Clin N Am,* 14, 455-72, v.

BOGDUK, N., CORRIGAN, B., KELLY, P., SCHNEIDER, G. & FARR, R. (1985) Cervical headache. *Med J Aust,* 143, 202-7.

BOGDUK, N. & ENGEL, R. (1984) The menisci of the lumbar zygapophyseal joints. A review of their anatomy and clinical significance. *Spine,* 9, 454-60.

BOGDUK, N. & JULL, G. (1985) The theoretical pathology of acute locked back: a basis for manipulative therapy. *Manual Medicine,* 1, 78-82.

BOGDUK, N. & MARSLAND, A. (1988) The cervical zygapophysial joints as a source of neck pain. *Spine,* 13, 610-7.

BOGDUK, N. & YOGANANDAN, N. (2001) Biomechanics of the cervical spine Part 3: minor injuries. *Clinical Biomechanics,* 16, 267-75.

BOHNSACK, M., WILHARM, A., HURSCHLER, C., RUHMANN, O., STUKENBORG-COLSMAN, C. & WIRTH, C. J. (2004) Biomechanical and kinematic influences of a total infrapatellar fat pad resection on the knee. *Am J Sports Med,* 32, 1873-80.

BONNEY, R. A. & CORLETT, E. N. (2002) Head posture and loading of the cervical spine. *Appl Ergon,* 33, 415-7.

BOOS, N. & BOESCH, C. (1995) Quantitative magnetic resonance imaging of the lumbar spine. Potential for investigations of water content and biochemical composition. *Spine,* 20, 2358-65.

BORCHGREVINK, G. E., SMEVIK, O., NORDBY, A., RINCK, P. A., STILES, T. C. & LEREIM, I. (1995) MR imaging and radiography of patients with cervical hyperextension-flexion injuries after car accidents. *Acta Radiol,* 36, 425-8.

BORGHOUTS, J. A., KOES, B. W., VONDELING, H. & BOUTER, L. M. (1999) Cost-of-illness of neck pain in The Netherlands in 1996. *Pain,* 80, 629-36.

BOSZCZYK, A. A., BOSZCZYK, B. M., PUTZ, R., BENJAMIN, M. & MILZ, S. (2003) Expression of a wide range of fibrocartilage molecules at the entheses of the alar ligaments - possible antigenic targets for rheumatoid arthritis? *J Rheumatol,* 30, 1420-5.

BOVIM, G., BERG, R. & DALE, L. G. (1992) Cervicogenic headache: anesthetic blockades of cervical nerves (C2-C5) and facet joint (C2/C3). *Pain,* 49, 315-20.

BRITISH STANDARDS INSTITUTE (1994) ISO 5725-1 *Accuracy (trueness and precision) of measurement methods and results.* Available from: http://www.bsonline.bsi-global.com/server/index.jsp

BROLIN, K. & HALLDIN, P. (2004) Development of a finite element model of the upper cervical spine and a parameter study of ligament characteristics. *Spine,* 29, 376-85.

BRUNEAU, M., CORNELIUS, J. F., MARNEFFE, V., TRIFFAUX, M. & GEORGE, B. (2006) Anatomical variations of the V2 segment of the vertebral artery. *Neurosurgery,* 59, ONS20-4.

BRUTON, A., CONWAY, J. H. & HOLGATE, S. T. (2000) Reliability: what is it, and how is it measured? *Physiotherapy,* 86, 94-99.

BURKITT, H. G., YOUNG, B. & HEATH, J. W. (1993) Wheater's Functional Histology. A Text and Colour Atlas. 3rd edition ed. Edinburgh, Churchill Livingstone.

BUSCH, E. H. & WILSON, P. R. (1989) Atlanto-occipital and atlanto-axial injections in the treatment of headache and neck pain. *Proceedings of the American Society Regional Anaesthesia.* Boston, Massachusetts, USA.

BUSH, C. H. (2000) The magnetic resonance imaging of musculoskeletal hemorrhage. *Skeletal Radiol,* 29, 1-9.

CAGNIE, B., PETROVIC, M., VOET, D., BARBAIX, E. & CAMBIER, D. (2006) Vertebral artery dominance and hand preference: is there a correlation? *Man Ther,* 11, 153-6.

CASSIDY, J. D., CARROLL, L. J. & COTE, P. (1998) The Saskatchewan health and back pain survey. The prevalence of low back pain and related disability in Saskatchewan adults. *Spine,* 23, 1860-6; discussion 1867.

CASSIDY, J. D., CARROLL, L. J., COTE, P., LEMSTRA, M., BERGLUND, A. & NYGREN, A. (2000) Effect of eliminating compensation for pain and suffering on the outcome of insurance claims for whiplash injury. *N Engl J Med,* 342, 1179-86.

CASSINELLI, E. H., LEE, M., SKALAK, A., AHN, N. U. & WRIGHT, N. M. (2006) Anatomic considerations for the placement of C2 laminar screws. *Spine,* 31, 2767-71.

CASTRO, W. H., SAUTMANN, A., SCHILGEN, M. & SAUTMANN, M. (2000) Noninvasive three-dimensional analysis of cervical spine motion in normal subjects in relation to age and sex. An experimental examination. *Spine,* 25, 443-9.

CATAN, H., BULUC, L., ANIK, Y., AYYILDIZ, E. & SARLAK, A. Y. (2007) Pedicle morphology of the thoracic spine in preadolescent idiopathic scoliosis: magnetic resonance supported analysis. *Eur Spine J,* 16, 1203-8.

CHANG, H., FOUND, E. M., CLARK, C. R., GOEL, V. K. & GANG, C. S. (1992) Meniscus-like synovial fold in the atlanto-axial (C1-C2) joint. *Journal of Spinal Disorders,* 5, 227-231.

CHEVROT, A., CERMAKOVA, E., VALLEE, C., CHANCELIER, M. D., CHEMLA, N., ROUSSELIN, B. & LANGER-CHERBIT, A. (1995) C1-2 arthrography. *Skeletal Radiol,* 24, 425-9.

CHINN, S. (1991) Statistics in respiratory medicine. 2. Repeatability and method comparison. *Thorax,* 46, 454-6.

CHRISTENSEN, D. M., EASTLACK, R. K., LYNCH, J. J., YASZEMSKI, M. J. & CURRIER, B. L. (2007) C1 anatomy and dimensions relative to lateral mass screw placement. *Spine,* 32, 844-8.

CLINICAL KNOWLEDGE SUMMARIES (2005) *National Library for Health Neck Pain Guidelines.* Available from: http://www.library.nhs.uk/guidelinesfinder/ViewResource.aspx?resID=29954 [Accessed 2006]

CLOWARD, R. B. (1959) Cervical discography: a contribution to the etiology and mechanism of neck, shoulder, arm pain. *Ann Surg,* 150, 1052-1064.

COCHRANE, W., DAVIES, D. V. & PALFREY, A. J. (1965) Absorptive functions of the synovial membrane. *Ann Rheum Dis,* 24, 2-15.

COLLINS, P. (1999) Early concepts and terminology. IN RODECK, C. H. & WHITTLE, M. J. (Eds.) *Fetal medicine. Basic science and clinical practice.* London, Churchill Livingstone.

CONLEY, M. S., STONE, M. H., NIMMONS, M. & DUDLEY, G. A. (1997) Specificity of resistance training responses in neck muscle size and strength. *Eur J Appl Physiol Occup Physiol,* 75, 443-8.

COSKUN, O., UCLER, S., KARAKURUM, B., ATASOY, H. T., YILDIRIM, T., OZKAN, S. & INAN, L. E. (2003) Magnetic resonance imaging of patients with cervicogenic headache. *Cephalalgia,* 23, 842-5.

COTE, P., CASSIDY, J. D. & CARROLL, L. (1998) The Saskatchewan Health and Back Pain Survey. The prevalence of neck pain and related disability in Saskatchewan adults. *Spine*, 23, 1689-98.

CRAMER, G. D., FOURNIER, J. T., HENDERSON, C. N. & WOLCOTT, C. C. (2004) Degenerative changes following spinal fixation in a small animal model. *Journal of Manipulative and Physiological Therapeutics*, 27, 141-54.

CRAMER, G. D., GREGERSON, D. M., KNUDSEN, J. T., HUBBARD, B. B., USTAS, L. M. & CANTU, J. A. (2002) The effects of side-posture positioning and spinal adjusting on the lumbar Z joints: a randomized controlled trial with sixty-four subjects. *Spine*, 27, 2459-66.

CUSICK, J. F., PINTAR, F. A. & YOGANANDAN, N. (2001) Whiplash syndrome: kinematic factors influencing pain patterns. *Spine*, 26, 1252-8.

CUTTS, A. (1988) Shrinkage of muscle fibres during the fixation of cadaveric tissue. *J Anat*, 160, 75-8.

CYRIAX, J. (1938) Rheumatic headache. *Br Med J*, 2, 1367-68.

DALL'ALBA, P. T., STERLING, M. M., TRELEAVEN, J. M., EDWARDS, S. L. & JULL, G. A. (2001) Cervical range of motion discriminates between asymptomatic persons and those with whiplash. *Spine*, 26, 2090-4.

DALTON, M. & COUTTS, A. (1994) The effect of age on cervical posture in a normal population. IN BOYLING, J. D., PALASTANGA, N., JULL, G. A. & LEE, D. G. (Eds.) *Grieve's Modern Manual Therapy. The Vertebral Column.* Churchill Livingstone, Edinburgh.

DAVIES, D. V. (1946) Synovial membrane and synovial fluid of joints. *Lancet*, 2, 815-818.

DAVIES, D. V. (1950) Structure and function of synovial membrane. *Br Med J*, 1, 92-95.

DAVIES, D. V. & EDWARDS (1948) The blood supply of the synovial membrane and intra-articular structures. *Am R Coll Surg*, 1, 142-156.

DE CARVALHO, A., VIALLE, R., THOMSEN, L., AMZALLAG, J., CLUZEL, G., POINTE, H. D. & MARY, P. (2007) Reliability analysis for manual measurement of coronal plane deformity in adolescent scoliosis. Are 30 x 90 cm plain films better than digitized small films? *Eur Spine J*.

DE MARCHI, G. F. (1963) Le articolazioni intervertebrali. *La Clinica Ortopedica*, 15, 26-33.

DEUTSCH, A. L., RESNICK, D., DALINKA, M. K., GILULA, L., DANZIG, L., GUERRA, J., JR. & DUNN, F. H. (1981) Synovial plicae of the knee. *Radiology*, 141, 627-34.

DIRHEIMER, Y., RAMSHEYI, A. & REOLON, M. (1977) Positive arthrography of the craniocervical joints. *Neuroradiology*, 12, 257-60.

DOOMS, G. C., HRICAK, H., MARGULIS, A. R. & DE GEER, G. (1986) MR imaging of fat. *Radiology*, 158, 51-4.

DORR, W. (1958) Uber die anatomie der wirbelgelenke. *Archiv fur Orthopadische und Unfallchirurgie*, 50, 222-234.

DORY, M. A. (1981) Arthrography of the lumbar facet joints. *Radiology*, 140, 23-7.

DORY, M. A. (1983) Arthrography of the cervical facet joints. *Radiology*, 148, 379-82.

DREYFUSS, P., MICHAELSEN, M. & FLETCHER, D. (1994a) Atlanto-occipital and lateral atlanto-axial joint pain patterns. *Spine*, 19, 1125-31.

DREYFUSS, P., TIBILETTI, C. & DREYER, S. J. (1994b) Thoracic zygapophyseal joint pain patterns. A study in normal volunteers. *Spine*, 19, 807-11.

DUFOUR, I., BITTOUN, J., IDY-PERETTI, I., JOLIVET, O., DARRASSE, L. & DI PAOLA, R. (1993) Implementation and optimization by the simplex method of a 3D double echo sequence in steady-state free precession. *Magn Reson Imaging,* 11, 87-93.

DUNCAN, K. R., BAKER, P. N., GOWLAND, P. A., ISSA, B., MOORE, R., WORTHINGTON, B. & JOHNSON, I. R. (1997) Demonstration of changes in fetal liver erythropoiesis using echo-planar magnetic resonance imaging. *Am J Physiol,* 273, G965-7.

DUPARC, F., PUTZ, R., MICHOT, C., MULLER, J. M. & FREGER, P. (2002) The synovial fold of the humeroradial joint: anatomical and histological features, and clinical relevance in lateral epicondylalgia of the elbow. *Surg Radiol Anat,* 24, 302-7.

DUPONT, J. Y. (1997) Synovial plicae of the knee. Controversies and review. *Clin Sports Med,* 16, 87-122.

DUTIA, M. B. (1991) The muscles and joints of the neck: their specialisation and role in head movement. *Prog Neurobiol,* 37, 165-78.

DVIR, Z., GAL-ESHEL, N., SHAMIR, B., PRUSHANSKY, T., PEVZNER, E. & PERETZ, C. (2006) Cervical motion in patients with chronic disorders of the cervical spine: a reproducibility study. *Spine,* 31, E394-9.

DVORAK, J., PANJABI, M., GERBER, M. & WICHMANN, W. (1987) CT-functional diagnostics of the rotatory instability of upper cervical spine. 1. An experimental study on cadavers. *Spine,* 12, 197-205.

DWYER, A., APRILL, C. N. & BOGDUK, N. (1990) Cervical zygapophyseal joint pain patterns I: a study in normal volunteers. *Spine,* 15, 453-457.

ELLIOTT, J., JULL, G., NOTEBOOM, J. T., DARNELL, R., GALLOWAY, G. & GIBBON, W. W. (2006) Fatty infiltration in the cervical extensor muscles in persistent whiplash-associated disorders: a magnetic resonance imaging analysis. *Spine,* 31, E847-55.

ELLIOTT, J., JULL, G., NOTEBOOM, J. T. & GALLOWAY, G. (2007b) MRI study of the cross-sectional area for the cervical extensor musculature in patients with persistent whiplash associated disorders (WAD). *Man Ther.*

ELLIOTT, J. M., GALLOWAY, G. J., JULL, G. A., NOTEBOOM, J. T., CENTENO, C. J. & GIBBON, W. W. (2005) Magnetic resonance imaging analysis of the upper cervical spine extensor musculature in an asymptomatic cohort: an index of fat within muscle. *Clin Radiol,* 60, 355-63.

ELLIOTT, J. M., JULL, G. A., NOTEBOOM, J. T., DURBRIDGE, G. L. & GIBBON, W. W. (2007a) Magnetic resonance imaging study of cross-sectional area of the cervical extensor musculature in an asymptomatic cohort. *Clin Anat,* 20, 35-40.

EMMINGER, E. (1972) Les articulations interapophysaires et leurs structures meniscoides vues sous l'angle de la pathologie. *Ann Med Physique,* 15, 219-238.

ENERSEN, O.D. (2003) *Nikolai Ivanovich Pirogov, Who Named It?* Available from: http://www.whonamedit.com/doctor.cfm/2627.html [Accessed November 2003]

ENGEL, R. & BOGDUK, N. (1982) The menisci of the lumbar zygapophysial joints. *Journal of Anatomy,* 135, 795-809.

ENNEKING, W. & HOROWITZ, M. (1972) The intra-articular effects of immobilisation of the human knee. *Journal of Bone and Joint Surgery (Am),* 54, 973-985.

ERWIN, W. M., JACKSON, P. C. & HOMONKO, D. A. (2000) Innervation of the human costovertebral joint: implications for clinical back pain syndromes. *Journal of Manipulative and Physiological Therapeutics,* 23, 395-403.

ESCOLAR, J. (1948) The afferent connections of the 1st, 2nd and 3rd cervical nerves in the cat. *J Comp. Neurol.,* 89, 79-92.

EVANS, D. W. (2002a) Mechanisms and effects of spinal high-velocity, low-amplitude thrust manipulation: previous theories. *J Manipulative Physiol Ther,* 25, 251-62.

EVANS, D. W. (2002b) Mechanisms and effects of spinal high-velocity, low-amplitude thrust manipulation: previous theories. *Journal of Manipulative and Physiological Therapeutics,* 25, 251-62.

EVANS, R. W. (1992) Some observations on whiplash injuries. *Neurol Clin,* 10, 975-97.

FABER, S. C., ECKSTEIN, F., LUKASZ, S., MUHLBAUER, R., HOHE, J., ENGLMEIER, K. H. & REISER, M. (2001) Gender differences in knee joint cartilage thickness, volume and articular surface areas: assessment with quantitative three-dimensional MR imaging. *Skeletal Radiol,* 30, 144-50.

FARRANT, J. M., O'CONNOR, P. J. & GRAINGER, A. J. (2007) Advanced imaging in rheumatoid arthritis. Part 1: synovitis. *Skeletal Radiol,* 36, 269-79.

FEHLINGS, M. G., FURLAN, J. C., MASSICOTTE, E. M., ARNOLD, P., AARABI, B., HARROP, J., ANDERSON, D. G., BONO, C. M., DVORAK, M., FISHER, C., FRANCE, J., HEDLUND, R., MADRAZO, I., NOCKELS, R., RAMPERSAUD, R., RECHTINE, G. & VACCARO, A. R. (2006) Interobserver and intraobserver reliability of maximum canal compromise and spinal cord compression for evaluation of acute traumatic cervical spinal cord injury. *Spine,* 31, 1719-25.

FERNANDEZ-DE-LAS-PENAS, C., ALONSO-BLANCO, C., CUADRADO, M. L. & PAREJA, J. A. (2007a) Neck mobility and forward head posture are not related to headache parameters in chronic tension-type headache. *Cephalalgia,* 27, 158-64.

FERNANDEZ-DE-LAS-PENAS, C., BUENO, A., FERRANDO, J., ELLIOTT, J. M., CUADRADO, M. L. & PAREJA, J. A. (2007b) Magnetic resonance imaging study of the morphometry of cervical extensor muscles in chronic tension-type headache. *Cephalalgia,* 27, 355-62.

FERRARI, R. & RUSSELL, A. S. (2003) Regional musculoskeletal conditions: neck pain. *Best Pract Res Clin Rheumatol,* 17, 57-70.

FICK, R. (1904) Handbuch der Anatomie und Mechanik der Gelenke. IN VON BARDELEBEN, K. (Ed.) *Handbuch der Anatomie des Menschen.* Jena, Verlag G. Fischer.

FIELD, A. (2005) *Discovering statistics using SPSS,* London, SAGE Publications.

FLETCHER, G., HAUGHTON, V. M., HO, K. C. & YU, S. W. (1990) Age-related changes in the cervical facet joints: studies with cryomicrotomy, MR, and CT. *AJR Am J Roentgenol,* 154, 817-20.

FRAYNE, R., GOODYEAR, B. G., DICKHOFF, P., LAUZON, M. L. & SEVICK, R. J. (2003) Magnetic resonance imaging at 3.0 Tesla: challenges and advantages in clinical neurological imaging. *Invest Radiol,* 38, 385-402.

FREEMAN, M.D., CROFT, A.C., ROSSIGNOL, A.M., CENTENO, C.J., & ELKINS, W.L. (2006) Chronic neck pain and whiplash: a case-control study of the relationship between acute whiplash injuries and chronic neck pain. *Pain Res Manag,* 11, 79-83.

FRIEDRICH, K. M., TRATTNIG, S., MILLINGTON, S. A., FRIEDRICH, M., GROSCHMIDT, K. & PRETTERKLIEBER, M. L. (2007) High-field magnetic resonance imaging of meniscoids in the zygapophyseal joints of the human cervical spine. *Spine,* 32, 244-8.

FUJIWARA, K., OWAKI, H., FUJIMOTO, M., YONENOBU, K. & OCHI, T. (2000) A long-term follow-up study of cervical lesions in rheumatoid arthritis. *J Spinal Disord,* 13, 519-26.

FUKUI, S., OHSETO, K., SHIOTANI, M., OHNO, K., KARASAWA, H., NAGANUMA, Y. & YUDA, Y. (1996) Referred pain distribution of the cervical zygapophyseal joints and cervical dorsal rami. *Pain, 68,* 79-83.

GAFFNEY, K., COOKSON, J., BLAKE, D., COUMBE, A. & BLADES, S. (1995) Quantification of rheumatoid synovitis by magnetic resonance imaging. *Arthritis Rheum, 38,* 1610-7.

GALIANO, K., OBWEGESER, A. A., BODNER, G., FREUND, M. C., GRUBER, H., MAURER, H., SCHATZER, R., FIEGELE, T. & PLONER, F. (2006) Ultrasound-guided facet joint injections in the middle to lower cervical spine: a CT-controlled sonoanatomic study. *Clin J Pain, 22,* 538-43.

GARCIA-VALTUILLE, R., ABASCAL, F., CEREZAL, L., GARCIA-VALTUILLE, A., PEREDA, T., CANGA, A. & CRUZ, A. (2002) Anatomy and MR imaging appearances of synovial plicae of the knee. *Radiographics, 22,* 775-84.

GARGAN, M. F. & BANNISTER, G. C. (1990) Long-term prognosis of soft-tissue injuries of the neck. *J Bone Joint Surg Br, 72,* 901-3.

GE, Y., UDUPA, J. K., NYUL, L. G., WEI, L. & GROSSMAN, R. I. (2000) Numerical tissue characterization in MS via standardization of the MR image intensity scale. *J Magn Reson Imaging, 12,* 715-21.

GHADIALLY, F. N. & ROY, S. (1969) Ultrastructure of Synovial Joints in Health and Disease. London, Butterworths.

GILES, L. G. (1984) Lumbar apophyseal joint arthrography. *Journal of Manipulative and Physiological Therapeutics, 7,* 21-4.

GILES, L. G. (1986) Lumbo-sacral and cervical zygapophyseal joint inclusions. *Manual Medicine, 2,* 89-92.

GILES, L. G. & HARVEY, A. R. (1987) Immunohistochemical demonstration of nociceptors in the capsule and synovial folds of human zygapophyseal joints. *British Journal of Rheumatology, 26,* 362-364.

GILES, L. G. & TAYLOR, J. R. (1982) Intra-articular synovial protrusions in the lower lumbar apophyseal joints. *Bulletin of the Hospital for Joint Diseases Orthopaedic Institute, 42,* 248-55.

GILES, L. G. & TAYLOR, J. R. (1987a) Innervation of lumbar zygapophyseal joint synovial folds. *Acta Orthopaedica Scandinavica, 58,* 43-6.

GILES, L. G. F. (1988) Human lumbar zygapophyseal joint inferior recess synovial folds: a light microscope examination. *The Anatomical Record, 220,* 118-124.

GILES, L. G. F. (1989) Anatomical Basis of Low Back Pain. Baltimore, Williams and Wilkins.

GILES, L. G. F. & TAYLOR, J. R. (1987b) Human zygapophyseal joint capsule and synovial fold innervation. *British Journal of Rheumatology, 26,* 93-98.

GILLE, O., CHAMPAIN, N., BENCHIKH-EL-FEGOUN, A., VITAL, J. M. & SKALLI, W. (2007) Reliability of 3D reconstruction of the spine of mild scoliotic patients. *Spine, 32,* 568-73.

GINSBURG, C. D., DALEY, C. L., CRAMER, G. D. & HENDERSON, C. N. (2000) Light microscopic changes of the z joints following spinal fixation. *Proceedings of the International Conference of Spinal Manipulation.* Bloomington, Minnesota, USA, Northwestern College of Chiropractic.

GORADIA, D., LINNAU, K. F., COHEN, W. A., MIRZA, S., HALLAM, D. K. & BLACKMORE, C. C. (2007) Correlation of MR imaging findings with intraoperative findings after cervical spine trauma. *AJNR Am J Neuroradiol, 28,* 209-15.

GOTTLIEB, M. S. (1994) Absence of symmetry in superior articular facets on the first cervical vertebra in humans: implications for diagnosis and treatment. *J Manipulative Physiol Ther, 17,* 314-20.

GRAICHEN, H., JAKOB, J., VON EISENHART-ROTHE, R., ENGLMEIER, K. H., REISER, M. & ECKSTEIN, F. (2003) Validation of cartilage volume and thickness measurements in the human shoulder with quantitative magnetic resonance imaging. *Osteoarthritis Cartilage,* 11, 475-82.

GRAUER, J. N., PANJABI, M. M., CHOLEWICKI, J., NIBU, K. & DVORAK, J. (1997) Whiplash produces an S-shaped curvature of the neck with hyperextension at lower levels. *Spine,* 22, 2489-94.

GREENFIELD, B. H., DONATELLI, R., WOODEN, M. J. & WILKES, J. (1990) Isokinetic evaluation of shoulder rotational strength between the plane of scapula and the frontal plane. *Am J Sports Med,* 18, 124-8.

GRIMMER, K., BLIZZARD, L. & DWYER, T. (1999) Frequency of headaches associated with the cervical spine and relationships with anthropometric, muscle performance, and recreational factors. *Arch Phys Med Rehabil,* 80, 512-21.

GRONBLAD, M., KORKALA, O., KONTTINEN, Y. T., NEDERSTROM, A., HUKKANEN, M., TOLVANEN, E. & POLAK, J. M. (1991) Silver impregnation and immunohistochemical study of nerves in lumbar facet joint plical tissue. *Spine,* 16, 34-8.

GROSS, A. R., HOVING, J. L., HAINES, T. A., GOLDSMITH, C. H., KAY, T., AKER, P. & BRONFORT, G. (2004) A Cochrane review of manipulation and mobilization for mechanical neck disorders. *Spine,* 29, 1541-8.

GRUBB, S. A. & KELLY, C. K. (2000) Cervical discography: clinical implications from 12 years of experience. *Spine,* 25, 1382-9.

GUPTA, M. C., WIJESEKERA, S., SOSSAN, A., MARTIN, L., VOGEL, L. C., BOAKES, J. L., LERMAN, J. A., MCDONALD, C. M. & BETZ, R. R. (2007) Reliability of radiographic parameters in neuromuscular scoliosis. *Spine,* 32, 691-5.

GUYTON, A. C. & HALL, J. E. (2006) *Textbook of Medical Physiology,* Philadelphia, Elsevier.

HAAS, M. (1991) The reliability of reliability. *Journal of Manipulative and Physiological Therapeutics,* 14, 199-208.

HADLEY, L. A. (1961) Anatomico-roentgenographic studies of the posterior spinal articulations. *American Journal of Roentgenology,* 86, 270-276.

HALLA, J. T. & HARDIN, J. G., JR. (1987) Atlantoaxial (C1-C2) facet joint osteoarthritis: a distinctive clinical syndrome. *Arthritis Rheum,* 30, 577-82.

HAM, A. W. & CORMACK, D. H. (1979) Histology. 8th edition ed. Philadelphia, J.B. Lippincott Company.

HANNA, F. S., BELL, R. J., DAVIS, S. R., WLUKA, A. E., TEICHTAHL, A. J., O'SULLIVAN, R. & CICUTTINI, F. M. (2007) Factors affecting patella cartilage and bone in middle-aged women. *Arthritis Rheum,* 57, 272-8.

HARATA, S., TOHNO, S. & KAWAGISHI, T. (1981) Osteoarthritis of the Atlanto-Axial Joint. *International Orthopaedics,* 5, 277-282.

HARTY, J.A., QUINLAN, J.F., KENNEDY, J.G., WALSH, M., & O'BYRNE, J.M. (2004) Anthropometrical analysis of cervical spine injuries. *Injury,* 35, 249-52.

HARVEY, E., BURTON, A. K., MOFFETT, J. K. & BREEN, A. (2003) Spinal manipulation for low-back pain: a treatment package agreed to by the UK chiropractic, osteopathy and physiotherapy professional associations. *Man Ther,* 8, 46-51.

HASSELBACHER, P. (1981) Structure of the synovial membrane. *Clinics in Rheumatic Diseases,* 7, 57-69.

HEARN, A. & RIVETT, D. A. (2002) Cervical SNAGs: a biomechanical analysis. *Man Ther,* 7, 71-9.

HELL, W., SCHICK, S., LANGWIEDER, K., & ZELLMER, H. (2002) Biomechanics of cervical spine injuries in rear end car impacts: influence of car seats and possible evaluation criteria. *Traffic Inj. Prev.,* 3, 127-40.

HELLER, C. A., STANLEY, P., LEWIS-JONES, B. & HELLER, R. F. (1983) Value of x ray examinations of the cervical spine. *Br Med J (Clin Res Ed),* 287, 1276-8.

HERMANN, K. G. & BOLLOW, M. (2004) Magnetic resonance imaging of the axial skeleton in rheumatoid disease. *Best Pract Res Clin Rheumatol,* 18, 881-907.

HERZOG, W., KATS, M. & SYMONS, B. (2001) The effective forces transmitted by high-speed, low-amplitude thoracic manipulation. *Spine,* 26, 2105-10.

HILDINGSSON, C. & TOOLANEN, G. (1990) Outcome after soft-tissue injury of the cervical spine. A prospective study of 93 car-accident victims. *Acta Orthop Scand,* 61, 357-9.

HIRASAWA, Y., BASHIR, W. A., SMITH, F. W., MAGNUSSON, M. L., POPE, M. H. & TAKAHASHI, K. (2007) Postural changes of the dural sac in the lumbar spines of asymptomatic individuals using positional stand-up magnetic resonance imaging. *Spine,* 32, E136-40.

HOAD, C. L. & MARTEL, A. L. (2002) Segmentation of MR images for computer-assisted surgery of the lumbar spine. *Phys Med Biol,* 47, 3503-17.

HOLE, D. E., COOK, J. M. & BOLTON, J. E. (2000) Reliability and concurrent validity of two instruments for measuring cervical range of motion: effects of age and gender. *Man Ther,* 1, 36-42.

HOOPER, R. A., FRIZZELL, J. B. & FARIS, P. (2007) Case series on chronic whiplash related neck pain treated with intraarticular zygapophysial joint regeneration injection therapy. *Pain Physician,* 10, 313-8.

IBATULLIN, I. A., ZAITSEVA, R. L., CHUDNOVSKII, N. A. & CHUDNOVSKAIA, M. N. (1987) [Structure and histo-topography of meniscoid structures of the atlanto-occipital and atlanto-axial joints]. *Arkhiv Anatomii, Gistologii i Embriologii,* 92, 30-8.

INAMI, S., KANEOKA, K., HAYASHI, K. & OCHIAI, N. (2000) Types of synovial fold in the cervical facet joint. *Journal of Orthopaedic Science,* 5, 475-80.

INAMI, S., SHIGA, T., TSUJINO, A., YABUKI, T., OKADO, N. & OCHIAI, N. (2001) Immunohistochemical demonstration of nerve fibers in the synovial fold of the human cervical facet joint. *Journal of Orthopaedic Research,* 19, 593-6.

INGLIS, D., PUI, M., IOANNIDIS, G., BEATTIE, K., BOULOS, P., ADACHI, J. D., WEBBER, C. E. & ECKSTEIN, F. (2007) Accuracy and test-retest precision of quantitative cartilage morphology on a 1.0 T peripheral magnetic resonance imaging system. *Osteoarthritis Cartilage,* 15, 110-5.

ISOGAI, S., MURAKAMI, G., WADA, T. & ISHII, S. (2001) Which morphologies of synovial folds result from degeneration and/or aging of the radiohumeral joint: an anatomic study with cadavers and embryos. *J Shoulder Elbow Surg,* 10, 169-81.

JACOBSEN, E. A. & RIISE, T. (2000) MRI of cervical spine with flexion and extension used in patients with rheumatoid arthritis. *Scand J Rheumatol,* 29, 249-54.

JEE, W. H., CHOE, B. Y., KIM, J. M., SONG, H. H. & CHOI, K. H. (1998) The plica syndrome: diagnostic value of MRI with arthroscopic correlation. *J Comput Assist Tomogr,* 22, 814-8.

JEE, W. S. S. (1988) Cell and Tissue Biology. A Textbook of Histology. IN WEISS, L. (Ed.) Baltimore, Urban and Schwarzenberg Inc.

JOHANSSON, B. H. (2006) Whiplash injuries can be visible by functional magnetic resonance imaging. *Pain Res Manag,* 11, 197-9.

JONES, T. R., JAMES, J. E., ADAMS, J. W., GARCIA, J., WALKER, S. L. & ELLIS, J. P. (1989) Lumbar zygapophyseal joint meniscoids: evidence of their role in chronic intersegmental hypomobility. *Journal of Manipulative and Physiological Therapeutics*, 12, 374-85.

JONSSON, H., JR., BRING, G., RAUSCHNING, W. & SAHLSTEDT, B. (1991) Hidden cervical spine injuries in traffic accident victims with skull fractures. *Journal of Spinal Disorders*, 4, 251-63.

JULL, G., ZITO, G., TROTT, P., POTTER, H. & SHIRLEY, D. (1997) Inter-examiner reliability to detect painful upper cervical joint dysfunction. *The Australian Journal of Physiotherapy*, 43, 125-129.

JULL, G. A. (1986) Clinical observations of upper cervical mobility. IN GRIEVE, G. P. (Ed.) *Modern manual therapy of the vertebral column*. Edinburgh, Churchill Livingstone.

JULL, G.A., & NIERE, K.R. (2004) The cervical spine and headache IN: BOYLING, J.D. & JULL, G.A., eds. *Grieve's Modern Manual Therapy. The Vertebral Column* Edinburgh: Churchill Livingstone.

KAALE, B. R., KRAKENES, J., ALBREKTSEN, G. & WESTER, K. (2005) Whiplash-associated disorders impairment rating: neck disability index score according to severity of MRI findings of ligaments and membranes in the upper cervical spine. *J Neurotrauma*, 22, 466-75.

KAALE, B. R., KRAKENES, J., ALBREKTSEN, G. & WESTER, K. (2007) Active range of motion as an indicator for ligament and membrane lesions in the upper cervical spine after a whiplash trauma. *J Neurotrauma*, 24, 713-21.

KALLAKURI, S., SINGH, A., CHEN, C. & CAVANAUGH, J. M. (2004) Demonstration of substance P, calcitonin gene-related peptide, and protein gene product 9.5 containing nerve fibers in human cervical facet joint capsules. *Spine*, 29, 1182-6.

KANEOKA, K., ONO, K., INAMI, S. & HAYASHI, K. (1999) Motion analysis of cervical vertebrae during whiplash loading. *Spine*, 24, 763-9; discussion 770.

KARACAN, I., AYDIN, T., SAHIN, Z., CIDEM, M., KOYUNCU, H., AKTAS, I. & ULUDAG, M. (2004) Facet angles in lumbar disc herniation: their relation to anthropometric features. *Spine*, 29, 1132-6.

KARANTANAS, A. H., ZIBIS, A. H., PAPALIAGA, M., GEORGIOU, E. & ROUSOGIANNIS, S. (1998) Dimensions of the lumbar spinal canal: variations and correlations with somatometric parameters using CT. *Eur Radiol*, 8, 1581-5.

KARLSBORG, M., SMED, A., JESPERSEN, H., STEPHENSEN, S., CORTSEN, M., JENNUM, P., HERNING, M., KORFITSEN, E. & WERDELIN, L. (1997) A prospective study of 39 patients with whiplash injury. *Acta Neurol Scand*, 95, 65-72.

KATZ, P. R., REYNOLDS, H. M., FOUST, D. R. & BAUM, J. K. (1975) Mid-sagittal dimensions of cervical vertebral bodies. *Am J Phys Anthropol*, 43, 319-26.

KAWABE, N., HIROTANI, H. & TANAKA, O. (1989) Pathomechanism of atlantoaxial rotatory fixation in children. *Journal of Pediatric Orthopaedics.*, 9, 569-574.

KEATING, J. & MATYAS, T. (1998) Unreliable inferences from reliable measurements. *Aust J Physiother*, 44, 5-10.

KERR, F.W.L. (1961) Structural relation of the trigeminal spinal tract to upper cervical roots and the solitary nucleus in the cat. *Exp. Neurol.*, 4, 134-48.

KETTLER, A., WERNER, K. & WILKE, H. J. (2007) Morphological changes of cervical facet joints in elderly individuals. *Eur Spine J*, 16, 987-92.

KIM, S. J. & CHOE, W. S. (1997) Arthroscopic findings of the synovial plicae of the knee. *Arthroscopy*, 13, 33-41.

KITAMURA, H. P., YANASE, H., KITAMURA, H. & IWANAGA, T. (1999) Unique localization of protein gene product 9.5 in type B synoviocytes in the joints of the horse. *J Histochem Cytochem,* 47, 343-52.

KJAER, P., BENDIX, T., SORENSEN, J. S., KORSHOLM, L. & LEBOEUF-YDE, C. (2007) Are MRI-defined fat infiltrations in the multifidus muscles associated with low back pain? *BMC Med,* 5, 2.

KONIG, S. A., GOLDAMMER, A. & VITZTHUM, H. E. (2005) Anatomical data on the craniocervical junction and their correlation with degenerative changes in 30 cadaveric specimens. *J Neurosurg Spine,* 3, 379-85.

KONTTINEN, Y. T., GRONBLAD, M., KORKALA, O., TOLVANEN, E. & POLAK, J. M. (1990) Immunohistochemical demonstration of subclasses of inflammatory cells and active, collagen-producing fibroblasts in the synovial plicae of lumbar facet joints. *Spine,* 15, 387-90.

KOS, J. (1969) Contribution a l'etude de l'anatomie et de la vascularisation des articulations intervertebrales. *Bulletin de l Association des Anatomistes,* 142, 1088-1105.

KOS, J., HERT, J. & SEVCIK, P. (2002) [Meniscoids of the intervertebral joints]. *Acta Chirurgiae Orthopaedicae et Traumatologiae Cechoslovaca,* 69, 149-57.

KOS, J. & WOLF, J. (1972a) Die "menisci" der zwischenwirbelgelenke und ihre mogliche rolle bei wirbelblockierung. *Man Med,* 10, 105-114.

KOS, J. & WOLF, J. (1972b) Les menisques intervertebraux et leur role possible dans les blocages vertebraux. *Ann Med Phys,* 15, 203-217.

KOS, J. & WOLF, J. (1976) Intervertebral menisci and their possible role in intervertebral blockage. *Bulletin of the Sports Medicine Section,* 1, 8-9, 14.

KOSAREK, F. J. & HELMS, C. A. (1999) The MR appearance of the infrapatellar plica. *AJR Am J Roentgenol,* 172, 481-4.

KRAFT, G. & LEVINTHAL, D. (1951) Facet synovial impingement. *Surgery, Gynecology and Obstetrics,* 93, 439-443.

KRAKENES, J. & KAALE, B. R. (2006) Magnetic resonance imaging assessment of craniovertebral ligaments and membranes after whiplash trauma. *Spine,* 31, 2820-6.

KRAKENES, J., KAALE, B. R., MOEN, G., NORDLI, H., GILHUS, N. E. & RORVIK, J. (2002) MRI assessment of the alar ligaments in the late stage of whiplash injury--a study of structural abnormalities and observer agreement. *Neuroradiology,* 44, 617-24.

KRAKENES, J., KAALE, B. R., NORDLI, H., MOEN, G., RORVIK, J. & GILHUS, N. E. (2003) MR analysis of the transverse ligament in the late stage of whiplash injury. *Acta Radiol,* 44, 637-44.

KRAKENES, J., KAALE, B. R., RORVIK, J. & GILHUS, N. E. (2001) MRI assessment of normal ligamentous structures in the craniovertebral junction. *Neuroradiology,* 43, 1089-97.

KRISTJANSSON, E. (2004) Reliability of ultrasonography for the cervical multifidus muscle in asymptomatic and symptomatic subjects. *Man Ther,* 9, 83-8.

KVIEN, T. K., UHLIG, T., ODEGARD, S. & HEIBERG, M. S. (2006) Epidemiological aspects of rheumatoid arthritis: the sex ratio. *Ann N Y Acad Sci,* 1069, 212-22.

KWAN, O. (2003) MRI assessment of the alar ligaments in the late stage of whiplash injury. *Neuroradiology,* 45, 195-6; author reply 197-8.

LARSEN, L. B. & HOLM, R. (2000) [Prolonged neck pain following automobile accidents. Gender and age related risk calculated on basis of data from an emergency department]. *Ugeskr Laeger,* 162, 178-81.

LAZORTHES, G. & GAUBERT, J. (1956) L'innervation des articulations interapophysaire vertebrales. *Comptes Rendues de l'Association des Anatomistes,* 43, 488-494.

LEE, J. P., TSENG, W. Y., SHAU, Y. W., WANG, C. L., WANG, H. K. & WANG, S. F. (2007) Measurement of segmental cervical multifidus contraction by ultrasonography in asymptomatic adults. *Man Ther,* 12, 286-94.

LEE, R. Y., MCGREGOR, A. H., BULL, A. M. & WRAGG, P. (2005) Dynamic response of the cervical spine to posteroanterior mobilisation. *Clin Biomech,* 20, 228-31.

LEROUX, I., DIONNE, C. E., BOURBONNAIS, R. & BRISSON, C. (2005) Prevalence of musculoskeletal pain and associated factors in the Quebec working population. *Int Arch Occup Environ Health,* 78, 379-86.

LEWIN, T., MOFFETT, B. & VIIDIK, A. (1962) The morphology of the lumbar synovial intervertebral joints. *Acta Morphologica Neerlando-Scandinavica,* 4, 299-319.

LEWIT, K. (1985) The muscular and articular factor in movement restriction. *Manual Medicine,* 1, 83-85.

LEWIT, K. (1987) "The theoretical pathology of acute locked back: a basis for manipulative therapy" by N. Bogduk and G. Jull. *Manual Medicine,* 3, 69.

LIDTKE, R. H. & GEORGE, J. (2004) Anatomy, biomechanics, and surgical approach to synovial folds within the joints of the foot. *J Am Podiatr Med Assoc,* 94, 519-27.

LIEN, S. B., LIOU, N. H. & WU, S. S. (2006) Analysis of anatomic morphometry of the pedicles and the safe zone for through-pedicle procedures in the thoracic and lumbar spine. *Eur Spine J.*

LISANTI, C., CARLIN, C., BANKS, K. P. & WANG, D. (2007) Normal MRI appearance and motion-related phenomena of CSF. *AJR Am J Roentgenol,* 188, 716-25.

LORD, S. M., BARNSLEY, L. & BOGDUK, N. (1995) Percutaneous radiofrequency neurotomy in the treatment of cervical zygapophysial joint pain: a caution. *Neurosurgery,* 36, 732-9.

LORD, S. M., BARNSLEY, L., WALLIS, B. J. & BOGDUK, N. (1996a) Chronic cervical zygapophysial joint pain after whiplash. A placebo- controlled prevalence study [see comments]. *Spine,* 21, 1737-44; discussion 1744-5.

LORD, S. M., BARNSLEY, L., WALLIS, B. J. & BOGDUK, N. (1996b) Chronic cervical zygapophysial joint pain after whiplash. A placebo-controlled prevalence study. *Spine,* 21, 1737-44.

LOVELL, M. E. & GALASKO, C. S. (2002) Whiplash disorders--a review. *Injury,* 33, 97-101.

LUAN, F., YANG, K. H., DENG, B., BEGEMAN, P. C., TASHMAN, S. & KING, A. I. (2000) Qualitative analysis of neck kinematics during low-speed rear-end impact. *Clinical Biomechanics,* 15, 649-57.

LUDBROOK, J. (1997) Comparing methods of measurements. *Clin Exp Pharmacol Physiol,* 24, 193-203.

LUDBROOK, J. (2002) Statistical techniques for comparing measurers and methods of measurement: a critical review. *Clin Exp Pharmacol Physiol,* 29, 527-36.

LUOMA, E. K., RAININKO, R., NUMMI, P. J., LUUKKONEN, R., MANNINEN, H. I. & RIIHIMAKI, H. A. (1997) Suitability of cerebrospinal fluid as a signal-intensity reference on MRI: evaluation of signal-intensity variations in the lumbosacral dural sac. *Neuroradiology,* 39, 728-32.

MACNAB, I. (1971) The "whiplash syndrome". *Orthop Clin North Am,* 2, 389-403.

MADABHUSHI, A. & UDUPA, J. K. (2006) New methods of MR image intensity standardization via generalized scale. *Med Phys*, 33, 3426-34.

MADABHUSHI, A., UDUPA, J. K. & MOONIS, G. (2006) Comparing MR image intensity standardization against tissue characterizability of magnetization transfer ratio imaging. *J Magn Reson Imaging*, 24, 667-75.

MAKELA, M., HELIOVAARA, M., SIEVERS, K., IMPIVAARA, O., KNEKT, P. & AROMAA, A. (1991) Prevalence, determinants, and consequences of chronic neck pain in Finland. *Am J Epidemiol*, 134, 1356-67.

MALMSTROM, E. M., KARLBERG, M., MELANDER, A. & MAGNUSSON, M. (2003) Zebris versus Myrin: a comparative study between a three-dimensional ultrasound movement analysis and an inclinometer/compass method: intradevice reliability, concurrent validity, intertester comparison, intratester reliability, and intraindividual variability. *Spine*, 28, E433-40.

MANNION, A. F., KLEIN, G. N., DVORAK, J. & LANZ, C. (2000) Range of global motion of the cervical spine: intraindividual reliability and the influence of measurement device. *Eur Spine J*, 9, 379-85.

MAPP, P. I. (1995) Innervation of the synovium. *Annals of the Rheumatic Diseases*, 54, 398-403.

MARKENSON, J.A., (1991) Worldwide trends in the socioeconomic impact and long-term prognosis of rheumatoid arthritis *Semin Arthritis Rheum*, 21, 4-12.

MARSHALL, K.W., MIKULIS, D.J., & GUTHRIE, B.M. (1995) Quantitation of articular cartilage using magnetic resonance imaging and three-dimensional reconstruction. *J Orthop Res*, 13, 814-23.

MASHARAWI, Y., ROTHSCHILD, B., SALAME, K., DAR, G., PELEG, S. & HERSHKOVITZ, I. (2005) Facet tropism and interfacet shape in the thoracolumbar vertebrae: characterization and biomechanical interpretation. *Spine*, 30, E281-92.

MASTERS, I.B., EASTBURN, M.M., FRANCIS, P.W., WOOTTON, R., ZIMMERMAN, P.V., WARE, R.S., & CHANG, A.B. (2005) Quantification of the magnification and distortion effects of a pediatric flexible video-bronchoscope. *Respir Res*, 6, 16.

MAYOU, R. & BRYANT, B. (1996) Outcome of 'whiplash' neck injury. *Injury*, 27, 617-23.

MCCALL, I. W., PARK, W. M. & O'BRIEN, J. P. (1979) Induced pain referral from posterior lumbar elements in normal subjects. *Spine*, 4, 441-6.

MCCORMICK, C. C., TAYLOR, J. R. & TWOMEY, L. T. (1989) Facet joint arthrography in lumbar spondylolysis: anatomic basis for spread of contrast medium. *Radiology*, 171, 193-6.

MCFADDEN, K. D. & TAYLOR, J. R. (1990) Axial rotation in the lumbar spine and gaping of the zygapophyseal joints. *Spine*, 15, 295-9.

MCGONAGLE, D., CONAGHAN, P. G., WAKEFIELD, R. & EMERY, P. (2001) Imaging the joints in early rheumatoid arthritis. *Best Pract Res Clin Rheumatol*, 15, 91-104.

MCGRAW, K. O. & WONG, S. P. (1996) Forming inferences about some intraclass correlation coefficients. *Psychological Methods*, 1, 30-46.

MCLAIN, R. F. (1994) Mechanoreceptor endings in human cervical facet joints. *Spine*, 19, 495-501.

MCLAIN, R.F., FERRARA, L., & KABINS, M. (2002) Pedicle morphometry in the upper thoracic spine: limits to safe screw placement in older patients. *Spine*, 27, 2467-71.

MCLAIN, R. F. & PICKAR, J. G. (1998) Mechanoreceptor endings in human thoracic and lumbar facet joints. *Spine*, 23, 168-73.

MCNAMARA, R. M., O'BRIEN, M. C. & DAVIDHEISER, S. (1988) Post-traumatic neck pain: a prospective and follow-up study. *Ann Emerg Med,* 17, 906-11.

MCPARTLAND, J. M., BRODEUR, R. R. & HALLGREN, R. C. (1997) Chronic neck pain, standing balance, and suboccipital muscle atrophy--a pilot study. *J Manipulative Physiol Ther,* 20, 24-9.

MCROBBIE, D. W., MOORE, E. A., GRAVES, M. J. & PRINCE, M. R. (2007) *MRI From Picture to Proton,* Cambridge, Cambridge University Press.

MEIER, D. S. & GUTTMANN, C. R. (2003) Time-series analysis of MRI intensity patterns in multiple sclerosis. *Neuroimage,* 20, 1193-209.

MELLSTROM, A., GREPE, A. & LEVANDER, B. (1980) Atlantoaxial arthrography. A postmortem study. *Neuroradiology,* 20, 135-44.

MERCER, S. & BOGDUK, N. (1993) Intra-articular inclusions of the cervical synovial joints. *British Journal of Rheumatology,* 32, 705-10.

MERCER, S. R. & BOGDUK, N. (2001) Joints of the cervical vertebral column. *Journal of Orthopaedic and Sports Physical Therapy,* 31, 174-82.

MERSKEY, H. & BOGDUK, N. (1994) *Classification of Chronic Pain. Descriptions of Chronic Pain Syndromes and Definition of Pain Terms.,* Seattle, IASP Press.

MILLER-YOUNG, J. E., DUNCAN, N. A. & BAROUD, G. (2002) Material properties of the human calcaneal fat pad in compression: experiment and theory. *J Biomech,* 35, 1523-31.

MILZ, S., SCHLUTER, T., PUTZ, R., MORIGGL, B., RALPHS, J. R. & BENJAMIN, M. (2001) Fibrocartilage in the transverse ligament of the human atlas. *Spine,* 26, 1765-71.

MOCHIZUKI, T., MUNETA, T., SAKAGUCHI, Y., NIMURA, A., YOKOYAMA, A., KOGA, H. & SEKIYA, I. (2006) Higher chondrogenic potential of fibrous synovium- and adipose synovium-derived cells compared with subcutaneous fat-derived cells: distinguishing properties of mesenchymal stem cells in humans. *Arthritis Rheum,* 54, 843-53.

MOHAMED-ALI, V., PINKNEY, J. H. & COPPACK, S. W. (1998) Adipose tissue as an endocrine and paracrine organ. *Int J Obes Relat Metab Disord,* 22, 1145-58.

MONTFOORT, I., KELDERS, W. P., VAN DER GEEST, J. N., SCHIPPER, I. B., FEENSTRA, L., DE ZEEUW, C. I. & FRENS, M. A. (2006) Interaction between ocular stabilization reflexes in patients with whiplash injury. *Invest Ophthalmol Vis Sci,* 47, 2881-4.

MOONEY, V. & ROBERTSON, J. (1976) The facet syndrome. *Clin Orthop Relat Res,* 149-56.

MULLER, R. & BUTTNER, P. (1994) A critical discussion of intraclass correlation coefficients. *Stat Med,* 13, 2465-76.

MYSOREKAR, V. R. & NANDEDKAR, A. N. (1986) Surface area of the atlanto-occipital articulations. *Acta Anat (Basel),* 126, 223-5.

NARVAEZ, J. A., NARVAEZ, J., ROCA, Y. & AGUILERA, C. (2002) MR imaging assessment of clinical problems in rheumatoid arthritis. *Eur Radiol,* 12, 1819-28.

NATIONAL INSTRUMENTS (2004) *Analysis* Available from: http://www.ni.com/analysis/lvaddon_vision.htm. [Accessed 2002, 2003]

NGUYEN, H. V., LUDWIG, S. C., SILBER, J., GELB, D. E., ANDERSON, P. A., FRANK, L. & VACCARO, A. R. (2004) Rheumatoid arthritis of the cervical spine. *Spine J,* 4, 329-34.

NIGHTINGALE, R. W., CAROL CHANCEY, V., OTTAVIANO, D., LUCK, J. F., TRAN, L., PRANGE, M. & MYERS, B. S. (2007) Flexion and extension structural properties and strengths for male cervical spine segments. *J Biomech,* 40, 535-42.

NISHIMURA, K., TANABE, T., KIMURA, M., HARASAWA, A., KARITA, K. & MATSUSHITA, T. (2005) Measurement of articular cartilage volumes in the normal knee by magnetic resonance imaging: can cartilage volumes be estimated from physical characteristics? *J Orthop Sci,* 10, 246-52.

NORRIS, S. H. & WATT, I. (1983) The prognosis of neck injuries resulting from rear-end vehicle collisions. *J Bone Joint Surg Br,* 65, 608-11.

NYUL, L. G. & UDUPA, J. K. (1999) On standardizing the MR image intensity scale. *Magn Reson Med,* 42, 1072-81.

OGATA, S. & UHTHOFF, H. K. (1990) The development of synovial plicae in human knee joints: an embryologic study. *Arthroscopy,* 6, 315-21.

OHARA, A., MIYAMOTO, K., NAGANAWA, T., MATSUMOTO, K. & SHIMIZU, K. (2006) Reliabilities of and correlations among five standard methods of assessing the sagittal alignment of the cervical spine. *Spine,* 31, 2585-91; discussion 2592.

OHTORI, S., TAKAHASHI, K., CHIBA, T., YAMAGATA, M., SAMEDA, H. & MORIYA, H. (2001) Sensory innervation of the cervical facet joints in rats. *Spine,* 26, 147-50.

OKADA, K. (1981) [Studies on the cervical facet joints using arthrography of the cervical facet joint (author's transl)]. *Nippon Seikeigeka Gakkai Zasshi,* 55, 563-80.

OKTENOGLU, T., OZER, A. F., FERRARA, L. A., ANDALKAR, N., SARIOGLU, A. C. & BENZEL, E. C. (2001) Effects of cervical spine posture on axial load bearing ability: a biomechanical study. *J Neurosurg,* 94, 108-14.

ONO, K., YONENOBU, K., FUJI, T. & OKADA, K. (1985) Atlantoaxial rotatory fixation. Radiographic study of its mechanism. *Spine,* 10, 602-8.

OOSTVEEN, J. C. & VAN DE LAAR, M. A. (2000) Magnetic resonance imaging in rheumatic disorders of the spine and sacroiliac joints. *Semin Arthritis Rheum,* 30, 52-69.

ORDWAY, N. R., SEYMOUR, R. J., DONELSON, R. G., HOJNOWSKI, L. S. & EDWARDS, W. T. (1999) Cervical flexion, extension, protrusion, and retraction. A radiographic segmental analysis. *Spine,* 24, 240-7.

OSTERGAARD, M., DUER, A. & HORSLEV-PETERSEN, K. (2005a) Can magnetic resonance imaging differentiate undifferentiated arthritis? *Arthritis Res Ther,* 7, 243-5.

OSTERGAARD, M., HANSEN, M., STOLTENBERG, M. & LORENZEN, I. (1996) Quantitative assessment of the synovial membrane in the rheumatoid wrist: an easily obtained MRI score reflects the synovial volume. *Br J Rheumatol,* 35, 965-71.

OSTERGAARD, M., MCQUEEN, F. M., BIRD, P., EJBJERG, B., LASSERE, M. N., PETERFY, C. G., O'CONNOR, P. J., HAAVARDSHOLM, E., SHNIER, R., GENANT, H. K., EMERY, P., EDMONDS, J. P. & CONAGHAN, P. G. (2005b) Magnetic resonance imaging in rheumatoid arthritis advances and research priorities. *J Rheumatol,* 32, 2462-4.

OSTERGAARD, M., STOLTENBERG, M., LOVGREEN-NIELSEN, P., VOLCK, B., JENSEN, C. H. & LORENZEN, I. (1997) Magnetic resonance imaging-determined synovial membrane and joint effusion volumes in rheumatoid arthritis and osteoarthritis: comparison with the macroscopic and microscopic appearance of the synovium. *Arthritis Rheum,* 40, 1856-67.

PAGET, S. & BULLOUGH, P. G. (1980) Scientific Foundations of Orthopaedics and Traumatology. IN OWEN, R., GOODFELLOW, J. & BULLOUGH, P. (Eds.) London, William Heinemann Medical Books.

PANJABI, M., DVORAK, J., DURANCEAU, J., YAMAMOTO, I., GERGER, M., RAUSCHNING, W., & BUEFF, H.U. (1988) Three-dimension movements of the upper cervical spine. *Spine,* 13, 726-30.

PANJABI, M. M., PEARSON, A. M., ITO, S., IVANCIC, P. C. & WANG, J. L. (2004) Cervical spine curvature during simulated whiplash. *Clinical Biomechanics,* 19, 1-9.

PARMAR, H. V. & RAYMAKERS, R. (1993) Neck injuries from rear impact road traffic accidents: prognosis in persons seeking compensation. *Injury,* 24, 75-8.

PARTIK, B. L., STADLER, A., SCHAMP, S., KOLLER, A., VORACEK, M., HEINZ, G. & HELBICH, T. H. (2002) 3D versus 2D ultrasound: accuracy of volume measurement in human cadaver kidneys. *Invest Radiol,* 37, 489-95.

PENNING, L. & WILMINK, J. T. (1987) Rotation of the cervical spine. A CT study in normal subjects. *Spine,* 12, 732-8.

PETERFY, C. G., VAN DIJKE, C. F., LU, Y., NGUYEN, A., CONNICK, T. J., KNEELAND, J. B., TIRMAN, P. F., LANG, P., DENT, S. & GENANT, H. K. (1995) Quantification of the volume of articular cartilage in the metacarpophalangeal joints of the hand: accuracy and precision of three-dimensional MR imaging. *AJR Am J Roentgenol,* 165, 371-5.

PETERSSON, C. J. (1983) Degeneration of the acromioclavicular joint. A morphological study. *Acta Orthop Scand,* 54, 434-8.

PETTERSSON, K., HILDINGSSON, C., TOOLANEN, G., FAGERLUND, M. & BJORNEBRINK, J. (1997) Disc pathology after whiplash injury. A prospective magnetic resonance imaging and clinical investigation. *Spine,* 22, 283-7.

PFIRRMANN, C. W., BINKERT, C. A., ZANETTI, M., BOOS, N. & HODLER, J. (2001) MR morphology of alar ligaments and occipitoatlantoaxial joints: study in 50 asymptomatic subjects. *Radiology,* 218, 133-7.

PICKAR, J. G. & MCLAIN, R. F. (1995) Responses of mechanosensitive afferents to manipulation of the lumbar facet in the cat. *Spine,* 20, 2379-85.

PINTAR, F. A., YOGANANDAN, N. & VOO, L. (1998) Effect of age and loading rate on human cervical spine injury threshold. *Spine,* 23, 1957-62.

POUSSA, M. S., HELIOVAARA, M. M., SEITSAMO, J. T., KONONEN, M. H., HURMERINTA, K. A. & NISSINEN, M. J. (2005) Predictors of neck pain: a cohort study of children followed up from the age of 11 to 22 years. *Eur Spine J,* 14, 1033-6.

PRADHAM, N. S., WHITE, G. E., MEHTA, N. & FORGIONE, A. (2001) Mandibular deviations in TMD and non-TMD groups related to eye dominance and head posture. *J Clin Pediatr Dent,* 25, 147-55.

PRUSHANSKY, T., PEVZNER, E., GORDON, C. & DVIR, Z. (2006) Performance of cervical motion in chronic whiplash patients and healthy subjects: the case of atypical patients. *Spine,* 31, 37-43.

PUTTLITZ, C. M., GOEL, V. K., CLARK, C. R., TRAYNELIS, V. C., SCIFERT, J. L. & GROSLAND, N. M. (2000) Biomechanical rationale for the pathology of rheumatoid arthritis in the craniovertebral junction. *Spine,* 25, 1607-16.

RADANOV, B. P., STURZENEGGER, M., DE STEFANO, G. & SCHNIDRIG, A. (1994) Relationship between early somatic, radiological, cognitive and psychosocial findings and outcome during a one-year follow-up in 117 patients suffering from common whiplash. *Br J Rheumatol,* 33, 442-8.

RADANOV, B. P., STURZENEGGER, M. & DI STEFANO, G. (1995) Long-term outcome after whiplash injury. A 2-year follow-up considering features of injury mechanism and somatic, radiologic, and psychosocial findings. *Medicine,* 74, 281-97.

RAINE, S. & TWOMEY, L. T. (1997) Head and shoulder posture variations in 160 asymptomatic women and men. *Arch Phys Med Rehabil,* 78, 1215-23.

RANKIN, G. & STOKES, M. (1998) Reliability of assessment tools in rehabilitation: an illustration of appropriate statistical analyses. *Clin Rehabil,* 12, 187-99.

RANKIN, G., STOKES, M. & NEWHAM, D. J. (2005) Size and shape of the posterior neck muscles measured by ultrasound imaging: normal values in males and females of different ages. *Man Ther,* 10, 108-15.

RANSON, C. A., BURNETT, A. F., KERSLAKE, R., BATT, M. E. & O'SULLIVAN, P. B. (2006) An investigation into the use of MR imaging to determine the functional cross sectional area of lumbar paraspinal muscles. *Eur Spine J,* 15, 764-73.

RICHTER, M., OTTE, D., POHLEMANN, T., KRETTEK, C. & BLAUTH, M. (2000) Whiplash-type neck distortion in restrained car drivers: frequency, causes and long-term results. *Eur Spine J,* 9, 109-17.

RONNEN, H. R., DE KORTE, P. J., BRINK, P. R., VAN DER BIJL, H. J., TONINO, A. J. & FRANKE, C. L. (1996) Acute whiplash injury: is there a role for MR imaging?--a prospective study of 100 patients. *Radiology,* 201, 93-6.

ROPPONEN, A., VIDEMAN, T. & BATTIE, M. C. (2007) The reliability of paraspinal muscles composition measurements using routine spine MRI and their association with back function. *Man Ther.*

ROSS, J. K., BEREZNICK, D. E. & MCGILL, S. M. (1999) Atlas-axis facet asymmetry. Implications in manual palpation. *Spine,* 24, 1203-9.

ROTH, C., JACOBSON, J., JAMADAR, D., CAOILI, E., MORAG, Y. & HOUSNER, J. (2004) Quadriceps fat pad signal intensity and enlargement on MRI: prevalence and associated findings. *AJR Am J Roentgenol,* 182, 1383-7.

ROY, S., HOL, P. K., LAERUM, L. T. & TILLUNG, T. (2004) Pitfalls of magnetic resonance imaging of alar ligament. *Neuroradiology,* 46, 392-8.

SABOE, L. A. (1988) Possible clinical significance of intra-articular synoival protrusions: a review of the literature. *Manual Medicine,* 3, 148-151.

SAMPSON, M. (2007) Personal communication.

SAPIR, D., & GROUP, J. (2001) Radiofrequency medial branch neurotomy in litigant and nonlitigant patients with cervical whiplash. *Spine,* 26, E268-73.

SCHAEREN, S. & JEANNERET, B. (2005) Atlantoaxial osteoarthritis: case series and review of the literature. *Eur Spine J,* 14, 501-6.

SCHAFFLER, M. B., ALSON, M. D., HELLER, J. G. & GARFIN, S. R. (1992) Morphology of the dens. A quantitative study. *Spine,* 17, 738-43.

SCHMINCKE, A. & SANTO, E. (1932) Zur normalen und pathologischen anatomie der halswirbelsaule. *Zentralbl Allg Pathol Anat,* 55, 369-372.

SCHONSTROM, N., TWOMEY, L. & TAYLOR, J. (1993) The lateral atlanto-axial joints and their synovial folds: an in vitro study of soft tissue injuries and fractures. *Journal of Trauma,* 35, 886-92.

SCHUCK, P. (2004) Assessing reproducibility for interval data in health-related quality of life questionnaires: which coefficient should be used? *Qual Life Res,* 13, 571-86.

SHEKELLE, P. G. (1994) Spinal manipulation. *Spine,* 19, 858-61.

SHROUT, P. E. & FLEISS, J. L. (1979) Intraclass correlations: uses in assessing rater reliability. *Psychological Bulletin,* 86, 420-428.

SIEGMUND, G.P., KING, D.J., LAWRENCE, J.M., WHEELER, J.B, BRAULT, J.R. & SMITH, T.A. (1997) Head/neck kinematic response of human subjects in low-speed rear-end collisions. *Proceedings of the SAE Conference.*

SINGER, K. P., GILES, L. G. & DAY, R. E. (1990) Intra-articular synovial folds of thoracolumbar junction zygapophyseal joints. *Anat Rec,* 226, 147-52.

SJAASTAD, O., FREDRIKSEN, T. A. & STOLT-NIELSEN, A. (1986) Cervicogenic headache, C2 rhizopathy, and occipital neuralgia: a connection? *Cephalalgia,* 6, 189-95.

SKINNER, H. A. (1961) *The Origin of Medical Terms,* Baltimore: Williams and Wilkins.

SOLTANI, A. R., KALLINEN, M., MALKIA, E. & VIHKO, V. (1996) Ultrasonography of the neck splenius capitis muscle. Investigation in a group of young healthy women. *Acta Radiol,* 37, 647-50.

SOMMER, O. J., KLADOSEK, A., WEILER, V., CZEMBIREK, H., BOECK, M. & STISKAL, M. (2005) Rheumatoid arthritis: a practical guide to state-of-the-art imaging, image interpretation, and clinical implications. *Radiographics,* 25, 381-98.

SPITZER, W. O., SKOVRON, M. L., SALMI, L. R., CASSIDY, J. D., DURANCEAU, J., SUISSA, S. & ZEISS, E. (1995) Scientific monograph of the Quebec Task Force on Whiplash-Associated Disorders: redefining "whiplash" and its management. *Spine,* 20, 1S-73S.

STANDRING, S. (2005) *Gray's anatomy 39th ed.* Edinburgh: Elsevier.

STEMPER, B. D., YOGANANDAN, N., GENNARELLI, T. A. & PINTAR, F. A. (2005) Localized cervical facet joint kinematics under physiological and whiplash loading. *J Neurosurg Spine,* 3, 471-6.

STEMPER, B. D., YOGANANDAN, N. & PINTAR, F. A. (2003) Gender dependent cervical spine segmental kinematics during whiplash. *J Biomech,* 36, 1281-9.

STEMPER, B. D., YOGANANDAN, N. & PINTAR, F. A. (2004) Gender- and region-dependent local facet joint kinematics in rear impact: implications in whiplash injury. *Spine,* 29, 1764-71.

STERLING, M., JULL, G., VICENZINO, B. & KENARDY, J. (2004) Characterization of acute whiplash-associated disorders. *Spine,* 29, 182-8.

STRIMPAKOS, N., SAKELLARI, V., GIOFTSOS, G., PAPATHANASIOU, M., BROUNTZOS, E., KELEKIS, D., KAPRELI, E. & OLDHAM, J. (2005) Cervical spine ROM measurements: optimizing the testing protocol by using a 3D ultrasound-based motion analysis system. *Cephalalgia,* 25, 1133-45.

STURZENEGGER, M., DISTEFANO, G., RADANOV, B. P. & SCHNIDRIG, A. (1994) Presenting symptoms and signs after whiplash injury: the influence of accident mechanisms. *Neurology,* 44, 688-93.

SUISSA, S., HARDER, S. & VEILLEUX, M. (2001) The relation between initial symptoms and signs and the prognosis of whiplash. *Eur Spine J,* 10, 44-9.

SYMMONS, D. P., BARRETT, E. M., BANKHEAD, C. R., SCOTT, D. G. & SILMAN, A. J. (1994) The incidence of rheumatoid arthritis in the United Kingdom: results from the Norfolk Arthritis Register. *Br J Rheumatol,* 33, 735-9.

TAKAHASHI, M., UEMATSU, H. & HATABU, H. (2003) MR imaging at high magnetic fields. *Eur J Radiol,* 46, 45-52.

TAKEUCHI, K., YOKOYAMA, T., ABURAKAWA, S., ITABASHI, T. & TOH, S. (2005) Anatomic study of the semispinalis cervicis for reattachment during laminoplasty. *Clin Orthop Relat Res,* 126-31.

TAMAI, K., YAMATO, M., YAMAGUCHI, T. & OHNO, W. (1994) Dynamic magnetic resonance imaging for the evaluation of synovitis in patients with rheumatoid arthritis. *Arthritis Rheum,* 37, 1151-7.

TANG, X. Y., LIU, L. J., YANG, H. J., PENG, M. X. & LIAO, S. H. (2007) Anatomic study of the synovial folds of the occipito-atlanto-axial joints. *Clin Anat,* 20, 376-81.

TANNO, I., MURAKAMI, G., OGUMA, H., SATO, S., LEE, U. Y., HAN, S. H. & YAMASHITA, T. (2004) Morphometry of the lumbar zygapophyseal facet capsule and cartilage with special reference to degenerative osteoarthritic changes: an anatomical study using fresh cadavers of elderly Japanese and Korean subjects. *J Orthop Sci,* 9, 468-77.

TAYLOR, J. R. (2001) The Spine (CD-ROM).

TAYLOR, J. R. & FINCH, P. (1993a) Acute injury of the neck: anatomical and pathological basis of pain. *Annals of the Academy of Medicine, Singapore,* 22, 187-92.

TAYLOR, J. R. & FINCH, P. M. (1993b) Neck sprain. *Australian Family Physician,* 22, 1623-1629.

TAYLOR, J. R. & MCCORMICK, C. C. (1991) Lumbar facet joint fat pads: their normal anatomy and their appearance when enlarged. *Neuroradiology,* 33, 38-42.

TAYLOR, J. R. & TAYLOR, M. M. (1996) Cervical spine injuries: an autopsy study of 109 blunt injuries. *Journal of Musculoskeletal Pain,* 4, 61-79.

TAYLOR, J. R. & TWOMEY, L. T. (1986) Age changes in lumbar zygapophyseal joints. Observations on structure and function. *Spine,* 11, 739-745.

TAYLOR, J. R. & TWOMEY, L. T. (1993) Acute injuries to cervical joints. An autopsy study of neck sprain. *Spine,* 18, 1115-22.

TEHRANZADEH, J., ASHIKYAN, O. & DASCALOS, J. (2003) Magnetic resonance imaging in early detection of rheumatoid arthritis. *Semin Musculoskelet Radiol,* 7, 79-94.

TEMMING, J., & ZOBEL, R. (2000) Neck distortion injuries in road traffic crashes (Analysis of the Volkswagen database), IN: YOGANANDAN, N. & PINTAR, F., eds. *Frontiers in Whiplash Trauma: Clinical and Biomechanical* The Netherlands: IOS Press.

TENCH, C. R., MORGAN, P. S. & CONSTANTINESCU, C. S. (2005) Measurement of cervical spinal cord cross-sectional area by MRI using edge detection and partial volume correction. *J Magn Reson Imaging,* 21, 197-203.

THE FEDERATIVE COMMITTEE ON ANATOMICAL TERMINOLOGY. (1998) *Terminologia Anatomica. International Anatomical Terminology,* Stuttgart: Thieme Verlag.

TONDURY, G. (1940) Beitrag zur kenntniss der kleinen wirbelgelenke. *Zeitschrift fur Anatomie und Entwicklungsgeschichte,* 110, 568-575.

TONDURY, G. (1972) Anatomie fonctionnelle des petites articulations de rachis. *Annales de medicine physique,* 15, 173-191.

TOUSIGNANT, M., SMEESTERS, C., BRETON, A. M., BRETON, E. & CORRIVEAU, H. (2006) Criterion validity study of the cervical range of motion (CROM) device for rotational range of motion on healthy adults. *J Orthop Sports Phys Ther,* 36, 242-8.

TOUSSIROT, E., STREIT, G. & WENDLING, D. (2007) The contribution of adipose tissue and adipokines to inflammation in joint diseases. *Curr Med Chem,* 14, 1095-100.

TRELEAVEN, J., JULL, G. & STERLING, M. (2003) Dizziness and unsteadiness following whiplash injury: characteristic features and relationship with cervical joint position error. *J Rehabil Med,* 35, 36-43.

UNIVERSITY OF MINNESOTA (1988) CROM Procedure Manual. Procedure for Measuring Neck Motion with the CROM. Minnesota: University of Minnesota.

USHIYAMA, T., CHANO, T., INOUE, K. & MATSUSUE, Y. (2003) Cytokine production in the infrapatellar fat pad: another source of cytokines in knee synovial fluids. *Ann Rheum Dis,* 62, 108-12.

VACCARO, A. R., MADIGAN, L., SCHWEITZER, M. E., FLANDERS, A. E., HILIBRAND, A. S. & ALBERT, T. J. (2001) Magnetic resonance imaging analysis of soft tissue disruption after flexion-distraction injuries of the subaxial cervical spine. *Spine,* 26, 1866-72.

VAN ROY, P., CABOOR, D., DE BOELPAEP, S., BARBAIX, E. & CLARYS, J. P. (1997) Left-right asymmetries and other common anatomical variants of the first cervical vertebra. *Manual Therapy,* 2, 24-36.

VAN TULDER, M. W., KOES, B. W. & BOUTER, L. M. (1997) Conservative treatment of acute and chronic nonspecific low back pain. A systematic review of randomized controlled trials of the most common interventions. *Spine,* 22, 2128-56.

VANDENABEELE, F., LAMBRICHTS, I., LIPPENS, P. & CREEMERS, J. (2001) In vitro loading of human synovial membrane with 5-hydroxydopamine: evidence for dense core secretory granules in type B cells. *Arch Histol Cytol,* 64, 1-16.

VAN DEN KROONENBERG, A., PHILIPPENS, H., CAPPON, J., WISMANS, J., HELL, W. & LANGWEIDER, K. (1998) Human head-neck response during low-speed rear end impacts. *Proceedings of the 42nd Stapp Car Crash Conference.*

VASAVADA, A. N., DANARAJ, J. & SIEGMUND, G. P. (2007) Head and neck anthropometry, vertebral geometry and neck strength in height-matched men and women. *J Biomech.*

VERHAGEN, A. P., SCHOLTEN-PEETERS, G. G., VAN WIJNGAARDEN, S., DE BIE, R. A. & BIERMA-ZEINSTRA, S. M. (2007) Conservative treatments for whiplash. *Cochrane Database Syst Rev,* CD003338.

VERNON, H., HUMPHREYS, K. & HAGINO, C. (2007) Chronic mechanical neck pain in adults treated by manual therapy: a systematic review of change scores in randomized clinical trials. *J Manipulative Physiol Ther,* 30, 215-27.

VESELA, M., STETKAROVA, I. & LISY, J. (2005) Prevalence of C1/C2 involvement in Czech rheumatoid arthritis patients, correlation of pain intensity, and distance of ventral subluxation. *Rheumatol Int,* 26, 12-5.

VIALLE, R., ILHARREBORDE, B., DAUZAC, C. & GUIGUI, P. (2006) Intra and inter-observer reliability of determining degree of pelvic incidence in high-grade spondylolisthesis using a computer assisted method. *Eur Spine J,* 15, 1449-53.

VOGEL, K. G. (1996) The effect of compressive loading on proteoglycan turnover in cultured fetal tendon. *Connect Tissue Res,* 34, 227-37.

WALMSLEY, R. P., KIMBER, P. & CULHAM, E. (1996) The effect of initial head position on active cervical axial rotation range of motion in two age populations. *Spine,* 21, 2435-42.

WEBB, R., BRAMMAH, T., LUNT, M., URWIN, M., ALLISON, T. & SYMMONS, D. (2003) Prevalence and predictors of intense, chronic, and disabling neck and back pain in the UK general population. *Spine,* 28, 1195-202.

WENNERBERG, D. (1991) Reliability of an isokinetic dorsiflexion and plantar flexion apparatus. *Am J Sports Med,* 19, 519-22.

WESCOTT, D. J. (2000) Sex variation in the second cervical vertebra. *J Forensic Sci,* 45, 462-6.

WESTGARD, J. O. & HUNT, M. R. (1973) Use and interpretation of common statistical tests in method-comparison studies. *Clin Chem,* 19, 49-57.

WHITE, S. A. & VAN DEN BROEK, N. R. (2004) Methods for assessing reliability and validity for a measurement tool: a case study and critique using the WHO haemoglobin colour scale. *Statistics in Medicine,* 23, 1603-19.

WILMINK, J. T. & PATIJN, J. (2001) MR imaging of alar ligament in whiplash-associated disorders: an observer study. *Neuroradiology,* 43, 859-63.

WINKELSTEIN, B. A., NIGHTINGALE, R. W., RICHARDSON, W. J. & MYERS, B. S. (2000) The cervical facet capsule and its role in whiplash injury: a biomechanical investigation. *Spine,* 25, 1238-46.

WITZANI, L., BRUGGER, P. C., HORMANN, M., KASPRIAN, G., CSAPONE-BALASSY, C. & PRAYER, D. (2006) Normal renal development investigated with fetal MRI. *Eur J Radiol,* 57, 294-302.

WOODRING, J. H. & GOLDSTEIN, S. J. (1982) Fractures of the articular processes of the cervical spine. *AJR Am J Roentgenol,* 139, 341-4.

WORLD HEALTH ORGANIZATION (2006) *International Classification of adult underweight, overweight and obesity according to BMI.* Available from: http://www.who.int/bmi/index.jsp?introPage=intro_3.html [Accessed 1 February 2007]

WYKE, B. (1979) Neurology of the cervical spinal joints. *Physiotherapy,* 65, 72-6.

WYKE, B. D. (1981) The neurology of joints: a review of general principles. *Clinics in Rheumatic Diseases,* 7, 223-239.

XU, G. L., HAUGHTON, V. M. & CARRERA, G. F. (1990) Lumbar facet joint capsule: appearance at MR imaging and CT. *Radiology,* 177, 415-20.

YANASE, M., MATSUYAMA, Y., HIROSE, K., TAKAGI, H., YAMADA, M., IWATA, H. & ISHIGURO, N. (2006) Measurement of the cervical spinal cord volume on MRI. *J Spinal Disord Tech,* 19, 125-9.

YANG, X., COTE, P., CASSIDY, J.D., & CARROLL, L. (2007) Association between body mass index and recovery from whiplash injuries: a cohort study. *Am J Epidemiol,* 165, 1063-69.

YOGANANDAN, N., CUSICK, J. F., PINTAR, F. A. & RAO, R. D. (2001) Whiplash injury determination with conventional spine imaging and cryomicrotomy. *Spine,* 26, 2443-8.

YOGANANDAN, N., KNOWLES, S. A., MAIMAN, D. J. & PINTAR, F. A. (2003) Anatomic study of the morphology of human cervical facet joint. *Spine,* 28, 2317-23.

YOGANANDAN, N., KUMARESAN, S. & PINTAR, F. A. (2000) Geometric and mechanical properties of human cervical spine ligaments. *Journal of Biomechanical Engineering,* 122, 623-9.

YOGANANDAN, N., KUMARESAN, S., VOO, L. & PINTAR, F. A. (1996) Finite element applications in human cervical spine modeling. *Spine,* 21, 1824-34.

YOGANANDAN, N., PINTAR, F. A. & CUSICK, J. F. (2002) Biomechanical analyses of whiplash injuries using an experimental model. *Accident Analysis and Prevention,* 34, 663-71.

YOGANANDAN, N., PINTAR, F.A. & GENNARELLI, T. A. (2002) Biomechanical mechanisms of whiplash injury. *Traffic Injury Prevention,* 3, 98-104.

YOGANANDAN, N., PINTAR, F. A. & KLEINBERGER, M. (1999) Whiplash injury. Biomechanical experimentation. *Spine,* 24, 83-5.

YU, S. W., SETHER, L. & HAUGHTON, V. M. (1987) Facet joint menisci of the cervical spine: correlative MR imaging and cryomicrotomy study. *Radiology,* 164, 79-82.

ZACCHEO, D. & REALE, E. (1956) Contributo alla conoscenza delle tra i processi articolari delle vertebre dell'uomo. *Archivio Italiano di Anatomia e di Embriologia,* 61, 1-16.

ZAPLETAL, J. & DE VALOIS, J. C. (1997) Radiologic prevalence of advanced lateral C1-C2 osteoarthritis. *Spine,* 22, 2511-3.

ZITO, G., JULL, G. & STORY, I. (2006) Clinical tests of musculoskeletal dysfunction in the diagnosis of cervicogenic headache. *Man Ther,* 11, 118-29.

ZOLI, A., PRIOLO, F., GALOSSI, A., ALTOMONTE, L., DI GREGORIO, F., CERASE, A., MIRONE, L. & MAGARO, M. (2000) Craniocervical junction involvement in rheumatoid arthritis: a clinical and radiological study. *J Rheumatol*, 27, 1178-82.

ZUKSCHWERDT, L., EMMINGER, E., BIEDERMANN, F. & ZETTEL, H. (1955) Wirbelgelenk und Bandscheibe. Stuttgart, Hippokrates.